UNIVERSIDAD D CÓRDOBA

Facultad de Ciencias
Departamento de Genética

Intracellular pH as a new mechanism of signal transduction

Tânia Alícia Ribeiro Fernandes

Córdoba, 2017

TITULO: *Intracellular pH as a new mechanism of signal transduction*

AUTOR: Tânia Alícia *Ribeiro Fernandes*

Campus de Rabanales
Ctra. Nacional IV, Km. 396 A
14071 Córdoba

www.uco.es/publicaciones
publicaciones@uco.es

TÍTULO DE LA TESIS: Intracellular pH as a new mechanism of signal transduction

DOCTORANDO/A: Tânia Alícia Ribeiro Fernandes

INFORME RAZONADO DEL/DE LOS DIRECTOR/ES DE LA TESIS

(se hará mención a la evolución y desarrollo de la tesis, así como a trabajos y publicaciones derivados de la misma).

La Tesis Doctoral de Dña. Tânia Alícia Ribeiro Fernandes se ha llevado a cabo en el Departamento de Genética de la Universidad de Córdoba, en el seno del Grupo "Genética molecular de la patogénesis fúngica" (BIO-3138). Su desarrollo ha permitido a la doctoranda adquirir una sólida formación en Genética y Biología Molecular. Durante la realización de la Tesis, Dña. Tânia ha mostrado tener una gran capacidad de trabajo y aptitud para la investigación científica. En el trabajo se ha identificado el pH intracelular como nuevo mecanismo de regulación de las rutas de señalización MAPKs en hongos. Además, los resultados sugieren que existe una compleja interacción entre dichas rutas y las distintas funciones celulares que intervienen en la regulación de las MAPKs por el pH intracelular. Los resultados obtenidos se han comunicado en varios congresos internacionales, y parte de ellos se ha recogido en un artículo que actualmente está en prensa en la revista PLoS Pathogens.

Por todo ello, se autoriza la presentación de la tesis doctoral.

Córdoba, 26 de Septiembre de 2017

Firma del/de los director/es

Fdo.:Antonio Di Pietro

Fdo.: David Turrà

This work has been conducted in the Department of Genetics of the University of Córdoba and financially supported by the FUNGIBRAIN – EU Marie Curie Research Training Network (ITN) (FP7-ITN-607963).

INDEX

LIST OF FIGURES

LIST OF TABLES

RESUMEN

El pH juega un papel clave en el control de la patogénesis fúngica. En el patógeno del suelo *Fusarium oxysporum*, causante de la marchitez vascular, el pH actúa como regulador maestro de Fmk1, una MAPK altamente conservada, esencial para el crecimiento invasivo y patogénesis en raíces de tomate. Estudios previos demostraron que el pH también regula las MAPKs Mpk1 y Hog1, de manera opuesta a Fmk1. Sin embargo, se desconocen los mecanismos moleculares de la respuesta al pH. En el presente trabajo se ha investigado, si el pH del medio afecta las rutas MAPK a través de un cambio en el pH intracelular (pH_i). Se ha determinado que el pH_i funciona como una señal para la regulación de las rutas MAPK en *F. oxysporum*. El tratamiento de las células con diethylstilbestrol (DES), un inhibidor especifico de Pma1, la principal bomba de protones de la membrana plasmática, conlleva una rápida y sostenida bajada del pH_i, acompañada de una rápida y transitoria activación de las MAPKs Mpk1 y Hog1, y la inactivación de Fmk1. Esta respuesta esta conservada en la levadura panadera *Saccharomyces cerevisiae*, lo que indica que está conservado en hongos. Por ello se ha utilizado la levadura como modelo para investigar el mecanismo de activación de Mpk1 por acidificación del pH_i. Se identificaron: una ruta alternativa de la respuesta a stress de pared, mediada por la quinasa Ypk1/2; la rama Sln1 de la ruta Hog1; y la MAPK fosfatasa Msg5 cuya abundancia es afectada por el pH_i. En segundo lugar, un escrutinio realizado con mutantes knockout sensibles a ácido identificó un gran número de proteínas candidatas implicadas en la activación de Mpk1 inducida por DES. Muchos de ellos poseen ortólogos en *F. oxysporum*. Las funciones celulares más relevantes en este proceso son tráfico celular, homeostasis de iones (principalmente V-ATPase) y metabolismo de lípidos. Los resultados revelan que el pH_i es un nuevo mecanismo de regulación de MAPKs en hongos, y sugieren que existe una compleja interacción entre rutas de señalización y funciones celulares en la regulación de este proceso.

SUMMARY

pH is as a key player in the control of fungal pathogenicity. In the soilborne vascular wilt fungus *Fusarium oxysporum*, ambient pH acts as a master switch for regulation of the conserved Fmk1 MAPK cascade, essential for invasive growth and pathogenicity toward tomato roots. Previous studies indicated that pH also modulates the activity of the two other MAPKs, Mpk1 and Hog1, in an opposite way to Fmk1. The molecular events underlying the pH response are currently unknown. Here we investigated whether ambient pH modulates MAPK signaling by affecting the intracellular pH (pH_i). We found that pH_i acts as a signal regulating MAPK activity in *F. oxysporum*. Diethylstilbestrol (DES), a specific inhibitor of the plasma membrane H^+-ATPase Pma1, induced a rapid and sustained decrease of pH_i accompanied by rapid and transitory phosphorylation of the MAPKs Mpk1 and Hog1, and inactivation of Fmk1. Analogously, pH_i also regulates MAPK signaling in the budding yeast *Saccharomyces cerevisiae*, suggesting that this mechanism is conserved in fungi. We initially investigated the mechanism of pH_i-induced Mpk1 activation in the yeast model, using a candidate gene approach. Our studies revealed three potential mechanisms: an alternative branch of the canonical cell wall integrity pathway mediated by the Ypk1/2 kinase; the Sln1 branch of the Hog1 cascade; and the dual specificity MAPK phosphatase Msg5 whose abundance is affected by pH_i. Moreover, a screen with a subset of acid-sensitive yeast mutants identified a number of candidates affected in DES-triggered Mpk1 activation, many of which have predicted orthologues in *F. oxysporum*. These candidate proteins have conserved cellular functions including cellular trafficking, ion homeostasis (mainly V-ATPase function) and lipid metabolism. Our results discover pH_i as a new mechanism for MAPK signaling in fungi and reveal a complex interplay between signaling pathways and cellular functions in the regulation of this process.

1

INTRODUCTION

PH: A GENERAL REGULATOR OF CELL FUNCTION
FUNGAL PATHOGENS: HOW THEY LIVE AND INFECT
PH AS REGULATOR OF FUNGAL PATHOGENICITY

INTRODUCTION

1.1.PH: A GENERAL REGULATOR OF CELL FUNCTION

pH balance is a key factor determining life or death in all known biological systems. Changes in pH affect the ionization state of all weak acids and weak bases, including a bewildering array of cellular molecules such as peptides, proteins and lipids which regulate fundamental processes in the cell. It is thus not surprising that pH affects a wide array of biological processes. Proton binding or release to the active site of enzymes can interfere with their substrate affinity and consequently with the metabolic route in which they are implicated. Further, protein folding can also be affected by variations in pH, since charged amino acid side chains are modified according to pH. As a consequence, electrostatic interactions between residues of the same protein as well as protein-protein interactions may suffer modifications in response to changes in pH (Orij *et al*., 2011). Besides proteins, some lipids can also sense changes in pH since they exhibit polar head groups that can be protonated or deprotonated depending on the environmental pH. Advances in structural and functional analysis of cell membranes revealed an asymmetric distribution of lipids, with negatively charged phospholipids such as phosphatidylserine (PS) and phosphatidylinositol (PI) located predominantly in the inner leaflet of the plasma membrane (PM) and neutral or positively charged phospholipids being mostly non-cytosolic (Carman and Han, 2011; Orij *et al*., 2011). This asymmetric distribution of charged phospholipids at the PM is highly relevant for targeting of charged proteins (Heo *et al*., 2006).

Because proteins and lipids are dependent on pH to maintain their structure and function, and protonation–deprotonation events dictate the charge of biological surfaces, pH determines cell metabolism and survival. Changes in pH have been shown to trigger cell disorders and serious diseases in animal cells. For instance, in tumor cells a drop of the surrounding pH which occurs apparently as consequence of elevated glycolysis and proton and lactate excretion under hypoxia, determines

tumor malignancy (Webb *et al*., 2011). Although more data are still required to understand how tumor cells respond to pH, recent findings suggest that there are low pH-responsive genes whose activation provides a growth advantage for tumor cells (Kondo *et al*., 2017). On the other hand, pH has also been shown to be a key factor in the control of programmed cell death (apoptosis) (Lagadic-Gossmann *et al*., 2004). Intracellular acidification is an early event in apoptosis and appears to be triggered by an inhibition of NHE1 (sodium-hydrogen antiporter 1) at the PM (Schelling and Abu Jawdeh, 2008). A drop in the intracellular pH (pH_i) regulates the activity of endonucleases and of many proapoptotic proteins such as cytochrome c and caspases promoting cell death (Collins *et al*., 1996; Matsuyama *et al*., 2000).

The finding that pH regulates a broad range of processes including cell development, apoptosis or cancer has given rise to new approaches for the study of pH dynamics and mechanisms of regulation. The genetically encoded pH-sensor pHluorin, a green fluorescent protein (GFP) variant which is sensitive to changes in pH, has been extensively used for determination of pH_i. Although tightly regulated, pH_i is significantly affected by changes in external pH. Therefore, it is likely that pH-driven cell responses are largely regulated by pH_i dynamics.

1.2. FUNGAL PATHOGENS: HOW THEY LIVE AND INFECT

The kingdom of Fungi is evolutionarily distant from the kingdoms Plants and Animals and encompasses a high diversity of taxa with varied habitats, life cycles, morphologies and nutrient requirements. Most fungi are found in rich environments, where they assimilate organic molecules such as proteins, polysaccharides and nucleotides. However, fungi are also found in extreme conditions. *Aspergillus sydowii* inhabits hydrothermal fluids with temperatures that can reach 400ºC (Burgaud *et al*., 2009), while *Penicillium chrysogenum* is found in the Atacama Desert, the driest non-polar desert in the world (Gonçalves *et al*., 2016)

and *Nadsoniella nigra* var. *hesuelica* survives periodic freezing and thawing in Antarctica (Lyakh *et al*., 1983).

Some fungal species are pathogens that can thrive on living organisms. Fungal pathogens face unfavorable conditions during host colonization and thus need to be resilient to the immune defenses and able to obtain nutrients that can be difficult to acquire. Fungal pathogens include plant pathogens that cause crop diseases and have a serious economic impact on global agriculture, as well as human pathogens that cause life-threatening systemic infections in immunocompromised humans. Human pathogenic fungi are hidden killers taking the lives of one and a half million people every year. Although great effort has been made in the last years to reduce the number of people dying from fungal infections, progress has not been rapid and efficient enough to prevent or treat life-threatening fungal diseases. Among the fungal pathogens affecting humans, three pose the most consistent threat worldwide: *Aspergillus fumigatus*, *Candida albicans* and *Cryptococcus neoformans*, which cause aspergillosis, candidiasis and cryptococcosis, respectively. Each fungal pathogen preferentially infects specific sites in the human body, from the lung in pulmonary aspergillosis to the brain in cryptococcal meningoencephalitis and the blood stream in systemic candidiasis (Kim, 2016).

Fungal phytopathogens are by far the most harmful class of plant pathogens. They cause over 70% of all crop diseases and each year destroy 15% of global agricultural production, enough food calories to feed half a billion people. The growing human population will unquestionably require a significant increase in agricultural production, which includes an efficient response to fungal infection. Based on relevance, the five most important fungal plant pathogens are *Magnaporthe oryzae*, *Botrytis cinerea*, *Puccinia* spp., *Fusarium graminearum* and *Fusarium oxysporum* (Dean *et al*., 2012).

The ubiquitous soil-borne ascomycete *F. oxysporum* attacks a wide range of economically important crops as diverse as tomato (*Lycopersicon* spp.), cotton

(*Gossypium* spp.) or banana (*Musa* spp.) (Armstrong and Armstrong, 1981). It is the causal agent of vascular wilt, the major limiting factor in the production of many agricultural crops. Characteristic disease symptoms caused by this fungus include vascular browning, leaf epinasty, stunting, progressive wilting, defoliation and plant death (Agrios, 2005). *F. oxysporum* at the species complex level includes more than 120 different *formae speciales* (ff. spp.) which have been identified according to their specificity for the host plant (Michielse and Rep, 2009). Thus, individual isolates of *F. oxysporum* affect only one or a few plant species. The intriguing host specificity in the different *F. oxysporum* isolates is currently subject to intense investigation. Phylogenetic studies revealed that different isolates of a given *forma specialis* (f. sp.) that infect the same host plant, have originated independently during evolution (O'Donnell *et al*., 2004). Since there is no known sexual stage in the life cycle of *F. oxysporum*, the most likely hypothesis is that horizontal transfer of genetic information between isolates could account for the emergence of new pathogenic lineages. Indeed, complete genome sequence analysis of the tomato pathogenic form *F. oxysporum* f. sp. *lycopersici* demonstrated the existence of certain lineage-specific (LS) genomic regions, including four entire chromosomes that are absent from other *Fusarium* species such as *F. graminearum* and *F. verticillioides* (Ma *et al*., 2010).

Between plant infection, *F. oxysporum* can survive in the soil for long time periods, either as chlamydospores or by growing as a saprophyte on decaying organic matter. When the appropriate conditions for infection are found, spores in the soil germinate and grow towards the plant host. Germinated microconidia adhere to the plant roots and penetrate them directly without requirement of specialized structures such as apressoria which are formed in other fungal plant pathogens. Root penetration occurs mainly through natural openings or wounds in the roots (Pérez-Nadales and Di Pietro, 2011). Infectious hypha grow inter- and intracellularly to invade the cortex and cross the endodermis, until reaching the xylem vessels which they use to colonize the entire plant [Figure 1] (Michielse and Rep, 2009).

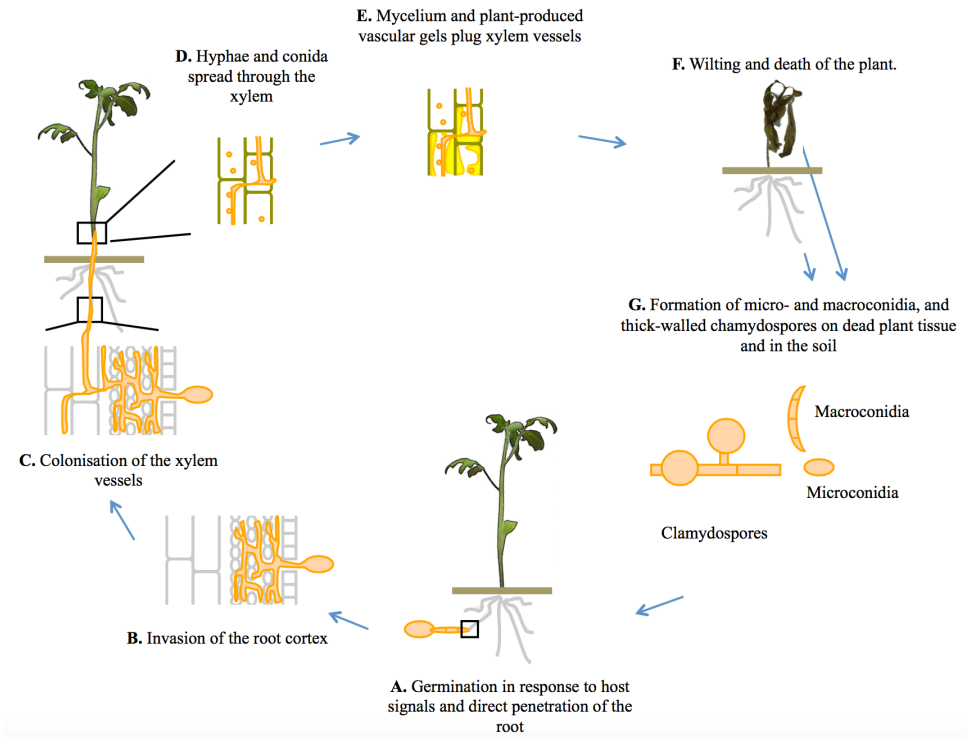

Figure 1 - Life cycle of *F. oxysporum*.
(A) Germination in response to host signals and direct penetration of the root. (B) Invasion of the root cortex. (C) Colonization of the xylem vessels. (D) Hyphae and conidia spread through the xylem. (E) Fungal mycelium and plant-produced vascular gels plug the xylem vessels. (F) Wilting and death of the plant. (G) Formation of micro- and macroconidia, and thick-walled chlamydospores on the dead plant tissue and in the soil (Perez-Nadales *et al*., 2014).

The mechanism by which a fungal plant pathogen grows towards the host root relies on precise signals in the rhizosphere. To fight against root-infecting pathogenic fungi, plant roots exudate a wide range of chemicals with broad-spectrum antifungal properties and defense-related proteins (Bais *et al*., 2006). Among these, peroxidases which reduce hydrogen peroxide to produce reactive oxygen species (ROS), are highly abundant. Therefore, plants can increase oxidative stress at wounded sites and increase toxicity against invading pathogens (Shigeto and Tsutsumi, 2016). Recently, research in the fungal pathogen *F. oxysporum* f. sp. *lycopersici* demonstrated that the catalytic activity of class III peroxidases found in root exudates, mediates the fungal chemotropic response towards tomato roots

(Turrà *et al*., 2015). Thus, apart from being a plant defense mechanism, peroxidases act as signals for *F. oxysporum* to track and colonize tomato roots.

Besides plant infection, *F. oxysporum* is also an opportunistic pathogen of humans (Nucci and Anaissie, 2007). *F. oxysporum* f. sp. *lycopersici* 4287 was the first fungal isolate shown to cause disease both in tomato plants and in immunodepressed mice. The striking ability to infect both plants and mammals makes this fungus a unique multihost pathogen for studying trans-kingdom pathogenicity in fungi (Ortoneda *et al*., 2004).

1.3. PH AS REGULATOR OF FUNGAL PATHOGENICITY

Environmental pH is a critical factor controlling fungal growth and development. To survive and propagate in a dynamic pH environment, fungal pathogens have the capacity to sense and respond to environmental pH changes. Further, fungal pathogens also can change the surrounding pH to increase their infectious potential. Although the mechanism of pH sensing and response is well studied in fungi, how exactly fungus-induced pH change contributes to virulence is not fully understood. Below we provide a brief update of the current knowledge on how pH affects fungal pathogenicity.

1.3.1. How fungi sense and adapt to environmental pH changes

High pH imposes severe stress on the fungal cell, including difficulties in the acquisition of nutrients or reduced availability of essential elements, such as iron or copper (Cyert and Philpott, 2013). The Pal/Rim pathway is the best-studied mechanism of alkaline pH sensing and response in fungi. First described in *Aspergillus nidulans* and *Saccharomyces cerevisiae*, this pathway has been since found throughout the ascomycetes and basidiomycetes (Peñalva *et al*., 2008). Signaling upon a shift to alkaline pH is initiated by the seven transmembrane domain receptor PalH/Rim21. How exactly PalH/Rim21 senses changes in pH is

not fully understood. Recent work in *S. cerevisiae* suggests that the C-terminal cytosolic domain detects altered lipid asymmetry of the PM as a result of alkaline-induced depolarization (Nishino *et al*., 2015). PalH/Rim21 mediates ubiquitination and phosphorylation of its interaction partner, the α-arrestin PalF/Rim8, resulting in endocytosis of the PalH-PalF complex. ESCRT (endosomal sorting complexes required for transport) complex components Vps20 and Snf7, recruits the interacting proteins PalA/Rim20 and the calpain-like protease PalB/Rim13 to the endomembranes. Ultimately, PalB leads to processing and activation of the zinc finger transcription factor PacC/Rim101. PalA binds to the C-terminal inhibitory domain of the inactive full-length PacC and contributes to PalB induced proteolytic activation of PacC. The processed PacC protein functions both as an activator of alkaline-expressed genes and a repressor of acidic-expressed genes, thereby orchestrating the cellular response to alkaline pH [Figure 2] (Peñalva *et al*., 2008).

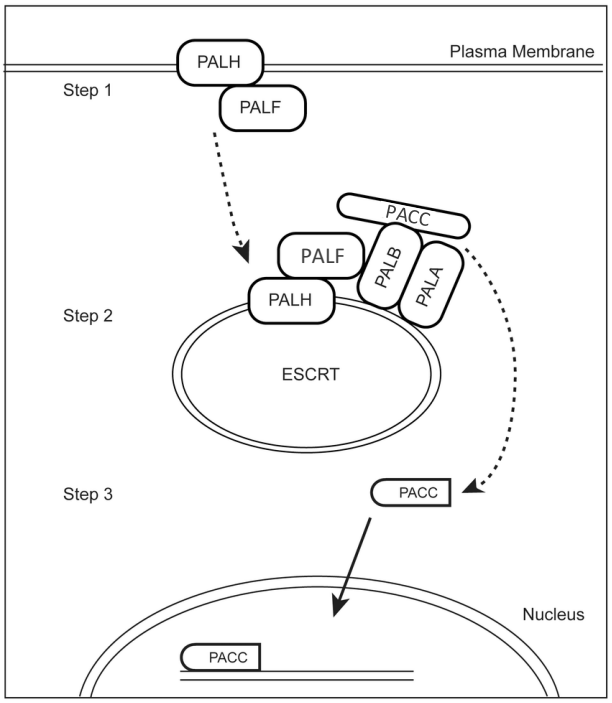

Figure 2 - A model of the Pal/Rim pathway signaling in fungi.
The PalH at the PM senses a shift to alkaline pH and mediates PalF activation. PalH-PalF complex is relocated to the endosomes and activates PalB, that leads to processing and activation of the transcription factor PacC. Activated PacC enters the nucleus and directs the transcription of alkaline-expressed genes (Adapted from (Chinnici *et al*., 2014)).

This is crucial during fungal infection to ensure, for example, the correct deployment of virulence factors that function at a specific pH (Barad *et al*., 2016; Davis, 2009; Prusky and Yakoby, 2003).

The Pal/Rim pathway is essential for infection in a number of fungal pathogens of humans. In *C. albicans*, the major invasive fungal pathogen of humans, Rim101 mutant shown to be defective in yeast to hyphal transition, a key virulence trait in this species, and unable to cause disseminated infection (Davis, 2009). Rim101 was also implicated in regulation of the Als3 adhesin and the secreted aspartyl protease (Sap) Sap5 during the interaction of *C. albicans* with the mucosal surface, which explains the involvement of this pathway in oral pharyngeal candidiasis where filamentous growth is not required (Nobile *et al*., 2008; Villar *et al*., 2007). Similarly, Rim101 is required for virulence of the opportunistic pathogen *A. fumigatus* in a murine model of infection (Bertuzzi *et al*., 2015). The *pacC* null mutant fails to cause infection and constitutively expressed PacC induces earliest tissue invasion (Bignell *et al*., 2005). In *C. neoformans*, a Rim101 mutant presents capsular defects due to alterations in polysaccharide attachment and is hypervirulent in an animal model of cryptococcosis. Interestingly, the defective cell surface of this mutant triggers a dramatic hyper-inflammatory response that accelerates host death (O'Meara *et al*., 2013).

During plant infection, PacC contributes to virulence in necrotrophic or postharvest pathogens such as *Colletotrichum acutatum*, *Colletotrichum gloeosporioides* and *Sclerotinia sclerotiorum* (Miyara *et al*., 2008; Rollins, 2003; You and Chung, 2007), but is dispensable in others such as the hemibiotrophic root-infecting fungus *F. oxysporum* (Caracuel *et al*., 2003). Interestingly, a *F. oxysporum* pacC loss-of-function mutant was more virulent than the wild type towards the plant host, but less virulent in a murine infection model (Caracuel *et al*., 2003; Ortoneda *et al*., 2004).

While necrotrophic pathogens trigger rapid host cell death and extensive tissue

necrosis by secreting toxins and enzymes to rapidly obtain nutrients for growth and reproduction, hemibiotrophic pathogens undergo a latent or biotrophic phase in which they manipulate plant defenses and obtain nutrients from living plant cells, followed by a switch to the necrotrophic phase. Therefore, the contrasting role of PacC is most likely associated with distinct modes of host infection of these different phytopathogens.

1.3.2. How fungi modulate the surrounding pH

Fungal pathogens have been known for decades to adjust the extracellular pH in order to increase their infectious potential (Alkan *et al*., 2013; Jennings, 1989). Therefore, apart from efficient mechanisms to adapt to environmental pH, fungal pathogens have evolved amazing ways to modulate ambient pH. Some mechanisms have been described to explain this ability, including the secretion of acids or alkali during infection. Alkalinization has been described mainly for hemibiotrophic pathogens, such as the tomato root-infecting *F. oxysporum*, during the early biotrophic stages of infection, while acidification happens mostly in necrotrophic pathogens (Alkan *et al*., 2013).

Host acidification by fungal pathogens is achieved by secretion of organic acids. *S. sclerotiorum* and *B. cinerea* secrete significant amounts of oxalic acid, while *Phomopsis magnifera* produces gluconic acid (Cessna *et al*., 2000; Davidzon *et al*., 2010; Manteau *et al*., 2003). Some fungi such as *Penicillium* and *Aspergillus*, secrete a combination of gluconic and citric acids (Shindia *et al*., 2006).

Alkalinization of the plant host was first reported in a number of fruit-infecting species such as *Colletotrichum* spp. and *Alternaria alternata* (Alkan *et al*., 2013; Prusky *et al*., 2001), and more recently in the root-infecting pathogen *F. oxysporum* (Masachis *et al*., 2016). These fungi are able to trigger an increase of more than two units in the pH of the surrounding fruit tissue or the rhizosphere, respectively. Similarly, the human pathogen *C. albicans* raises the pH in host macrophages by several units, resulting in neutralization of the normally acidic phagosome (Vylkova

et al., 2011; Vylkova and Lorenz, 2014). The main mechanism of host alkalinization reported in these fungal species is the release of ammonia that acts as a weak base (Prusky *et al*., 2001; Vylkova *et al*., 2011). Concentrations of up to 5 mM ammonia have been measured in colonized fruit tissue (Miyara *et al*., 2010). The exact mechanism that leads to extracellular accumulation of ammonia remains to be elucidated. Work in *S. cerevisiae*, *C. albicans* and *C. gloeosporioides* showed that this process requires the regulated uptake of amino acids via amino acid permeases or their mobilization from vacuolar stores, followed by catabolism through different routes involving steps of deamination (Bi *et al*., 2016; Miyara *et al*., 2012; Vylkova *et al*., 2011). In *C. gloeosporioides* transformation of glutamate to α-ketoglutarate and ammonium was shown to be carried out by the NAD^+-specific glutamate dehydrogenase Gdh2 (Miyara *et al*., 2012). A second requirement for ammonia-mediated alkalinization is carbon deprivation. Presumably, lack of carbon prevents the efficient use of ammonia for biosynthesis of amino acids and nucleotides, favouring its accumulation (Bi *et al*., 2016; Vylkova *et al*., 2011). To protect the cell from the toxic effects ammonia is released either through passive diffusion or by action of transporters such as the members of the Ato protein family (Danhof and Lorenz, 2015; Palková *et al*., 2002; Vylkova *et al*., 2011). The precise mechanisms of ammonia extrusion during alkalinization remain to be determined.

Phytopathogens have been traditionally classified into acidifiers and alkalinizers, based on their strategy to either decrease or increase the pH of the surrounding host tissue during infection (Alkan *et al*., 2013). However, this distinction might be less clear-cut than previously assumed. A recent study involving different fruit-infecting fungi revealed that each of them could induce either alkalinization or acidification of the environment, depending on the availability of carbon. Carbon limitation triggered extracellular accumulation of ammonia and alkalinization, whereas an excess of carbon induced acidification through the release of gluconic acid (Bi *et al*., 2016). These findings are of biological relevance, because pathogens are likely

to encounter different levels of carbon availability, depending on the host niche or the stage of infection (biotrophic or necrotrophic). For example, a postharvest pathogen will be exposed to gradually increasing sugar levels as the fruit ripens, and therefore may undergo a switch from alkalinization to acidification during the infection process.

To efficiently alkalinize the plant tissue through the release of ammonia, fungal pathogens must first build up a significant amount of hyphal biomass. How then is alkalinization achieved during early stages of infection when only a low number of hyphae is present in the host? To overcome this limitation, some biotrophic and hemibiotrophic pathogens have co-opted a pH regulatory mechanism that is naturally present in the plant host. *F. oxysporum* was recently shown to secrete a functional homologue of RALF (Rapid ALkalinization Factor), a family of conserved plant regulatory peptides (Pearce *et al.*, 2001). Similar to plant RALFs, the *Fusarium* (F-)RALF peptide triggers rapid alkalinization of the apoplast (Masachis *et al.*, 2016). Isogenic *F. oxysporum* mutants lacking functional F-RALF failed to induce root alkalinization and showed markedly reduced virulence in tomato plants. Intriguingly, these strains also provoked a strong host immune response. F-RALF appears to target the plant receptor-like kinase FERONIA, which mediates responses to endogenous plant RALF peptides. An *Arabidopsis* mutant defective in FERONIA failed to respond to fungal F-RALF and displayed enhanced resistance against *F. oxysporum* (Masachis *et al.*, 2016). While the details on the mode of action of F-RALF remain to be elucidated, it was recently shown that endogenous RALF-FERONIA signaling leads to inactivation of the plant PM H^+-ATPase AHA2 and inhibition of plant cell elongation [Figure 4A] (Haruta *et al.*, 2014). Intriguingly, fungal RALF homologues are found in phylogenetically distant species spanning both ascomycetes and basidiomycetes, as well as hemibiotrophs and biotrophs (Masachis *et al.*, 2016; Thynne *et al.*, 2017), This taxonomically discontinuous distribution suggests that co-option of FERONIA by fungal RALF peptides was acquired multiple times during evolution.

In summary, these studies illustrate how fungal pathogens have evolved multiple ways to manipulate host pH during different stages of infection.

1.3.3. How alkalinization drives fungal pathogenicity

One of the key questions is how host pH modulation promotes fungal infection. Different mechanisms have been proposed, based either on the host or the fungal cell machinery. For example, ammonium secretion by *Colletotrichum* was shown to activate plant NADPH oxidase and to enhance host cell death (Alkan *et al*., 2009). On the other hand, alkaline pH triggers PacC/Rim101-mediated expression of genes encoding fungal virulence factors, such as the cell wall-degrading enzymes pectate lyase and endoglucanase from *C. gloeosporioides* that display maximum activity at alkaline pH typically observed in decaying fruit tissue (Prusky and Yakoby, 2003). Similarly, *C. albicans PHR1*, a gene encoding a cell wall remodeling β(1,3)-glucanosyltransferase, is fundamental for host tissue adhesion and invasion and upregulated at alkaline pH via Rim101 (De Bernardis *et al*., 1998).

Furthermore, alkalinization has been associated with infection-related morphogenetic changes. Ammonia release during germination of *C. gloeosporioides* conidia led to formation of specialized infection structures called apressoria. Apressorium formation is hampered by reduction of ammonia levels outside and was reestablished by increasing ammonia. Therefore, fungal-induced pH modulation through ammonia is believed to restrict pathogenicity, at least in part, in situations in which penetration is apressorium-dependent (Miyara *et al*., 2010). In *C. albicans*, an upshift in pH promotes transition from the unicellular yeast to the filamentous hyphal form (Davis, 2009; Vylkova, 2017; Vylkova *et al*., 2011). This morphogenetic switch, which is critical for virulence in the mammalian host, is mediated by a number of cell signaling pathways including the Pal/Rim pathway and the invasive growth (IG) mitogen-activated protein kinase (MAPK) cascade (Davis, 2009; Lengeler *et al*., 2000).

Among the key pathways sensing and responding to external stimuli are the MAPK

cascades, a family of evolutionarily conserved three–tiered protein kinase modules composed of a MAPK kinase kinase (MAPKKK) that phosphorylates the downstream MAPK kinase (MAPKK), which in turn activates the MAPK for downstream transmission of cellular signals (Turrà *et al*., 2014). This module is activated mostly after sensing of external signals by receptors at the PM, and their activation results in a number of substrates phosphorylation including transcription factors that trigger the regulated expression of genes relevant for cell response to the stimuli (Rispail *et al*., 2009). Most of the current understanding of MAPK pathways is largely based on research in the model organism *S. cerevisiae*. Five MAPK signaling pathways have been reported in this fungus. Fus3 controls the response to mating pheromones, Kss1 (the IG MAPK) the morphogenetic switch in response to nutrient conditions, Hog1 regulates cells adaptation to hyperosmotic stress, Slt2/Mpk1 controls cell surface remodeling in response to cell wall integrity (CWI) stress, and Smk1 spore wall assembly (Chen and Thorner, 2007). By contrast, most of ascomycete fungi only possess three MAPK pathways, which are orthologous to yeast Fus3/Kss1, Mpk1 and Hog1 [Figure 3] (Turrà *et al*., 2014). In fungal plant pathogens, Xu and Hamer first reported that the ortholog of *S. cerevisiae* Fus3/Kss1 in the rice blast fungus *M. oryzae*, named Pmk1 (for Pathogenicity MAPK 1), is required for infection (Xu and Hamer, 1996). Subsequently, orthologs of the Fus3/Kss1 MAPK pathway were shown to be broadly conserved and essential for infection-related morphogenesis and IG in a wide range of plant pathogens (Turrà *et al*., 2014). The *F. oxysporum* IG Fmk1 (*Fusarium* MAPK 1) was also found to be essential for virulence on tomato plants (Di Pietro *et al*., 2001). Infection-related processes such as IG, vegetative hyphal fusion, root adhesion and chemotropic sensing of nutrients are dependent on the Fmk1 MAPK pathway (Di Pietro *et al*., 2001; Prados Rosales and Di Pietro, 2008; Turrà *et al*., 2015). In *F. oxysporum*, a major effort was made to identify all key components of this pathway, as well as the mechanism of regulation in pathogenicity control. Thus, the mucin-like transmembrane protein Msb2 functions upstream of the cascade while the transcription factor Ste12 is regulated by the

Fmk1 MAPK (Pérez-Nadales and Di Pietro, 2011; Rispail *et al*., 2009).

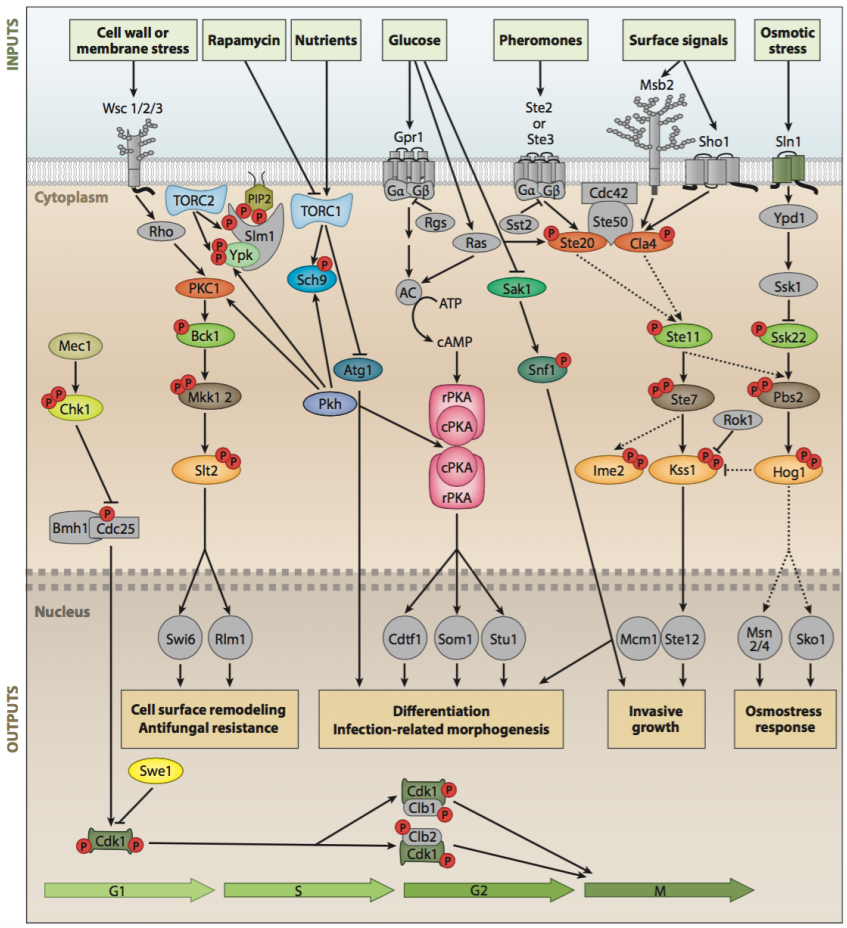

Figure 3 - MAPK signaling in plant pathogenic fungi.
Green boxes at the top represent different inputs that are sensed by surface receptors and translated to the appropriate MAPK module. Arrows and bars denote positive and negative interactions, respectively. Solid arrows and bars refer to direct interactions; dashed arrows and bars refer to indirect and/or potential interactions. Red circles containing the letter p denote phosphorylated amino acid residues (Turrà *et al*., 2014).

In addition to the Fmk1 MAPK, orthologs of the *S. cerevisiae* CWI Mpk1/Slt2 and the high osmolarity Hog1 MAPK signaling cascades were identified and characterized in fungal plant pathogens. The Mpk1 MAPK is involved in cell wall remodeling and maintenance of integrity. Activation of this pathway is fundamental during cell cycle progression and in response to compounds that imply a stress for

the cell wall. Not surprisingly, Mpk1 is fundamental for fungal pathogen development and virulence, especially during interaction with the host (Brown *et al*., 2014; Levin, 2011). Mpk1 orthologs of different fungal pathogens showed to be essential for resistance to heat stress and cell wall-damaging agents such as Congo Red (CR) or Calcofluor White (CFW), as well as to plant defense compounds such as chitinases, glucanases or antimicrobial peptides (Mehrabi *et al*., 2006; Ramamoorthy *et al*., 2007; Segorbe *et al*., 2017; Turrà *et al*., 2014). Further, *mpk1* mutants have serious defects in host sensing, penetration and colonization, leading to decreased fungal pathogenicity (Kojima *et al*., 2002; Kraus *et al*., 2003; Mey *et al*., 2002; Segorbe *et al*., 2017; Turrà *et al*., 2014). The high osmolarity glycerol (Hog1) MAPK is activated in response to hyperosmotic stress and its activation leads to adaptive responses such as temporary arrest of the cell-cycle, adjustment of transcription and translation patterns, and the synthesis of the compatible osmolyte glycerol (Saito and Posas, 2012). Fungal mutants lacking *hog1* exhibit increased sensitivity to hyperosmotic stress due to defects in the synthesis and accumulation of compatible solutes. In some fungal pathogens, Hog1 is required for host penetration and virulence (Igbaria *et al*., 2008; Turrà *et al*., 2014). In summary, MAPK cascades are among the major signaling pathways controlling fungal pathogenicity [Figure 3] (Turrà *et al*., 2014).

Although pH and MAPK signaling both act as master regulators of fungal pathogenicity, a link between pH and MAPK in fungal pathogenicity was not considered for many years. Recently, a study in *F. oxysporum* revealed that pH regulates fungal pathogenicity by modulating the phosphorylation status of the IG MAPK Fmk1, with alkalinization leading to enhanced IG and virulence through activation of this MAPK cascade [Figure 4A]. A series of experiments demonstrated that adjusting the pH to 7 or 5, respectively, activates or prevents cellophane penetration and other infection-related processes, as well as tomato root infection (Masachis *et al*., 2016). In addition, the two other MAPKs Mpk1 and Hog1 are also regulated by pH in an opposite way to Fmk1 (Segorbe, 2014) [Figure

4B]. These findings are of relevance, because although pH has been known for a long time to act as a master switch for fungal pathogenicity, most previous studies have focused on the Pal/Rim pathway. In fungus-host interactions where this pathway is not relevant for pathogenicity, the IG MAPK regulation could explain the effect of ambient pH on pathogenicity.

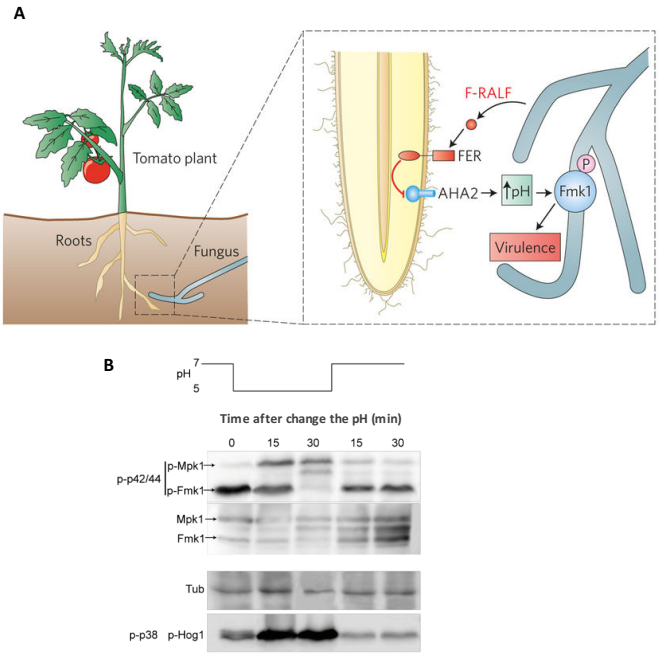

Figure 4 – Fungus-triggered alkalinization modulates MAPK signaling.
(A) Schematic illustration of the effect of *F. oxysporum*-secreted F-RALF peptide. F-RALF induced alkalinization triggers IG Fmk1 MAPK activation promoting virulence (adapted from (Kamoun and Zipfel, 2016)). (B) pH effect on MAPK phosphorylation status. Fmk1 MAPK is activated at pH 7, and inactivated at pH 5. By contrast, Mpk1 and Hog1 MAPK phosphorylation is induced at pH 5 and inhibited at pH 7 (adapted from (Segorbe, 2014)).

1.3.3.1. How ambient pH and pH_i regulate cell signaling and pathogenicity: a hypothesis

In contrast to ambient pH, pH_i tends to be constant and tightly regulated in all organisms (Kane, 2016). Nevertheless, rapid changes in pH_i can occur in response to different stimuli such as shifts in extracellular pH or nutrient status (Orij *et al.*, 2011). Two major mechanisms of pH_i regulation have been reported in fungi, both

based on conserved proton-pumping ATPases. The primary determinant of cytosolic pH is the PM H^+-ATPase 1 (Pma1), an essential H^+-ATPase and the most abundant PM protein in *S. cerevisiae*. The second mechanism is the vacuolar H^+-ATPase (V-ATPase), a multiprotein complex, which mediates acidification of organelles, such as vacuoles, endosomes or the Golgi (Kane, 2016).

Pma1 mediates ATP-dependent H^+ extrusion from the cell, creating the driving force for nutrient uptake. Plants and fungi contain at least one isoform of this H^+-ATPase. Structurally, it consists of a single large catalytic subunit of around 100 kDa, embedded in the lipid bilayer by 10 hydrophobic α -helices (Kane, 2016; Scarborough, 2000). Because of the abundance of Pma1 in the PM and its relative long half-life, Pma1 regulation occurs mainly at the post-translational level. An auto-inhibitory regulatory domain at the C-terminus reduces the hydrolysis of ATP under starvation conditions. By contrast, glucose-triggered phosphorylation releases the inhibitory effect of the C-terminus, causing increased affinity for ATP (Portillo *et al*., 1991). Mass spectrometry studies identified S899, S911 and Thr912 in the C-terminal tail as the key phosphorylation sites required for Pma1 activation in response to glucose (Lecchi *et al*., 2007).

Although the PM H^+-ATPase Pma1 is the primary contributor to pH_i regulation, the activity of the V-ATPase is also highly relevant. In contrast to the single-subunit P-type H^+-ATPase, the V-ATPases consist of fourteen subunits arranged in two subcomplexes. The peripheral subcomplex V1 harbors the sites for ATP hydrolysis, while the V0 subcomplex is embedded in the organellar membrane and contains the proton pore. V-ATPases are involved in pH_i regulation by pumping protons out of the cytosol, keeping the organelles in which they are present more acidic than the surrounding cytosol (Martínez-Muñoz and Kane, 2008).

Pma1 and V-ATPase are often co-regulated, for example in response to sudden shifts in ambient pH or glucose levels. In *S. cerevisiae*, high glucose levels lead to activation of Pma1 via phosphorylation of conserved C-terminal residues, and also

promote assembly of the V-ATPase complex. By contrast, glucose depletion results in Pma1 autoinhibition and disassembly of the V-ATPase complex, concomitant with an acidification of the cytosol (Dechant *et al*., 2010; Kane, 2016). As a general rule, activation of these proton-pumping ATPases leads to a pH_i increase due to increased proton export, whereas their inhibition triggers intracellular acidification.

It is increasingly appreciated that pH_i acts as a general regulator of cellular functions, such as growth and proliferation (Reshkin *et al*., 2014), life span (Hughes and Gottschling, 2012) and nutrient response (Dechant *et al*., 2010). So far, the role of pH_i in fungal infection has not been examined in detail. However, changes on extracellular pH had been showed to affects pH_i dynamics in some fungi (Bagar *et al*., 2009). Therefore, it is conceivable that pH_i could act as a signal linking fungal-triggered extracellular pH change to activation of important signaling pathways governing fungal pathogenicity [Figure 5].

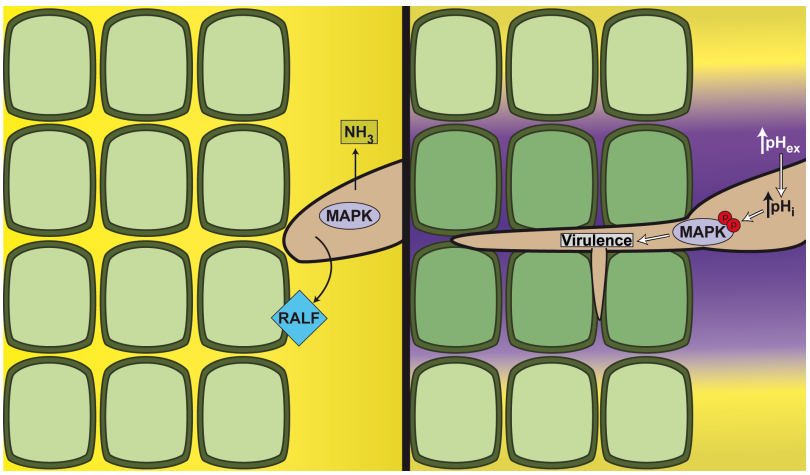

Figure 5 – Schematic illustration of how host alkalinization drives virulence in fungal pathogens.
During infection, fungal pathogens induce alkalinization of the surrounding host tissue through regulated release of ammonia and, in certain phytopathogens, such as *F. oxysporum*, by secreting small regulatory peptides that mimick plant RALF (Rapid ALkalinization Factor) (left panel). The resulting increase in extracellular pH activates the fungal invasive growth (IG) MAPK cascade, likely via modulation of intracellular pH (pH_i), to trigger phosphorylation of the IG MAPK and morphogenetic transition towards infectious growth (right panel). Yellow color denotes acidic pH while purple neutral to alkaline pH (Fernandes *et al*., 2017).

2

AIMS OF THE STUDY

AIMS OF THE STUDY

pH is as a key player in the control of fungal pathogenicity. Fungus-induced ambient pH modulation contributes to virulence, but the underlying mechanisms are not fully understood. Recent studies have revealed new and unexpected ways by which fungi induce host alkalinization to increase their infectious potential. In the root-infecting pathogen *F. oxysporum*, pH functions as a master switch for regulation of the conserved Fmk1 MAPK cascade, essential for IG and pathogenicity toward tomato roots (Masachis *et al.*, 2016). Previous studies indicated that pH also modulates the phosphorylation status of the two other MAPKs, Mpk1 and Hog1, in an opposite way to Fmk1 (Segorbe, 2014). Moreover, Mpk1 activation at acidic pH appears to be required for Fmk1 dephosphorylation (Segorbe, 2014), suggesting a crosstalk between the MAPK cascades in mediating the pH response.

Although the knowledge of how alkalinization affects fungal pathogenicity has advanced considerably, the pH sensing process that links extracellular alkalinization to pathogenicity signaling modules as the IG MAPK cascade remains unknown. pH_i has been shown to act as a major regulator of cellular function and to be transitorily affected by changes in external pH (Orij *et al.*, 2011). Therefore, the aim of this work was to understand whether ambient pH modulates MAPK signaling in fungi by affecting pH_i homeostasis. To achieve this goal, we set out to: 1) measure pH_i and monitor its effect on the three distinct MAPKs, 2) construct isogenic mutants defective in pH_i homeostasis and ambient pH sensing, and 3) identify cellular processes that affect pH_i-mediated MAPK signaling.

3

MATERIALS AND METHODS

BACTERIAL AND FUNGAL STRAINS. PLANT MATERIALS
PLASMIDS
MEDIA AND BUFFER SOLUTIONS
GROWTH CONDITIONS
MOLECULAR METHODOLOGY
GENETIC TRANSFORMATION
WESTERN BLOT
IN VIVO DETERMINATION OF INTRACELLULAR PH THROUGH THE GENETICALLY ENCODED PH SENSOR PHLUORIN
EXTRACELLULAR PH MEASUREMENTS
MEMBRANE ISOLATION FOR MEASUREMENT OF PMA1 ACTIVITY IN *F. OXYSPORUM*
VEGETATIVE GROWTH ASSAY
CELLOPHANE PENETRATION
TOMATO ROOT INFECTION
CELL STAINING WITH FLUORESCENT DYES
FLUORESCENCE MICROCOPY
BIOINFORMATIC ANALYSIS
SOFTWARE AND ONLINE TOOLS

MATERIALS AND METHODS

3.1.BACTERIAL AND FUNGAL STRAINS. PLANT MATERIALS

3.1.1. Bacterial strains

The strain of *Escherichia coli* used in this study is described in [Table 1].

Table 1 – Bacteria strain used in this study

STRAIN	GENOTYPE	REFERENCE
DH5α	*sup*E44, Δ*lac*U169 (Φ80*lac*ZΔM15), *hsd*R17, *rec*A1 *end*A1, *gyr*A96, *thi*-1, *rel*A1	Invitrogen™

3.1.2. Yeast strains

The *S. cerevisiae* strains used in this study are described in detail in [Table 2] and were kindly provided by Professor María Molina, Universidad Complutense de Madrid, Spain. Most of the yeast strains used in this work are derived from the wild type strain BY4741 from Euroscarf (Frankfurt, Germany).

Table 2 – Yeast strains used in this study

STRAIN	ORF	GENOTYPE	REF.
BY4741	-	*MAT*a *his3*Δ1 *leu2*Δ0 *met15*Δ0 *ura3*Δ0	Euroscarf
Δ*alg5*	YPL227C	*MAT*a *his3*Δ1 *leu2*Δ0 *met15*Δ0 *ura3*Δ0 *alg5::KanMX4*	Euroscarf
Δ*alg6*	YOR002W	*MAT*a *his3*Δ1 *leu2*Δ0 *met15*Δ0 *ura3*Δ0 *alg6::KanMX4*	Euroscarf
Δ*alg8*	YOR067C	*MAT*a *his3*Δ1 *leu2*Δ0 *met15*Δ0 *ura3*Δ0 *alg8::KanMX4*	Euroscarf
Δ*arg82*	YDR173C	*MAT*a *his3*Δ1 *leu2*Δ0 *met15*Δ0 *ura3*Δ0 *arg82::KanMX4*	Euroscarf
Δ*aro1*	YDR127W	*MAT*a *his3*Δ1 *leu2*Δ0 *met15*Δ0 *ura3*Δ0 *aro1::KanMX4*	Euroscarf
Δ*aro2*	YGL148W	*MAT*a *his3*Δ1 *leu2*Δ0 *met15*Δ0 *ura3*Δ0 *aro2::KanMX4*	Euroscarf
Δ*asc1*	YMR116C	*MAT*a *his3*Δ1 *leu2*Δ0 *met15*Δ0 *ura3*Δ0 *asc1::KanMX4*	Euroscarf
Δ*atg14*	YBR128C	*MAT*a *his3*Δ1 *leu2*Δ0 *met15*Δ0 *ura3*Δ0 *atg14::KanMX4*	Euroscarf
Δ*bck1*	YJL095W	*MAT*a *his3*Δ1 *leu2*Δ0 *met15*Δ0 *ura3*Δ0 *bck1::KanMX4*	Euroscarf
Δ*bem2*	YER155C	*MAT*a *his3*Δ1 *leu2*Δ0 *met15*Δ0 *ura3*Δ0 *bem2::KanMX4*	Euroscarf
Δ*bst1*	YFL025C	*MAT*a *his3*Δ1 *leu2*Δ0 *met15*Δ0 *ura3*Δ0 *bst1::KanMX4*	Euroscarf
Δ*bud32*	YGR262C	*MAT*a *his3*Δ1 *leu2*Δ0 *met15*Δ0 *ura3*Δ0 *bud32::KanMX4*	Euroscarf
Δ*cch1*	YGR217W	*MAT*a *his3*Δ1 *leu2*Δ0 *met15*Δ0 *ura3*Δ0 *cch1::KanMX4*	Euroscarf
Δ*ccs1*	YMR038C	*MAT*a *his3*Δ1 *leu2*Δ0 *met15*Δ0 *ura3*Δ0 *ccs1::KanMX4*	Euroscarf
Δ*cdc10*	YCR002C	*MAT*a *his3*Δ1 *leu2*Δ0 *met15*Δ0 *ura3*Δ0 *cdc10::KanMX4*	Euroscarf
Δ*clc1*	YGR167W	*MAT*a *his3*Δ1 *leu2*Δ0 *met15*Δ0 *ura3*Δ0 *clc1::KanMX4*	Euroscarf
Δ*cnb1*	YKL190W	*MAT*a *his3*Δ1 *leu2*Δ0 *met15*Δ0 *ura3*Δ0 *cnb1::KanMX4*	Euroscarf
Δ*csf1*	YLR087C	*MAT*a *his3*Δ1 *leu2*Δ0 *met15*Δ0 *ura3*Δ0 *csf1::KanMX4*	Euroscarf
Δ*csg2*	YBR036C	*MAT*a *his3*Δ1 *leu2*Δ0 *met15*Δ0 *ura3*Δ0 *csg2::KanMX4*	Euroscarf
Δ*cup5*	YEL027W	*MAT*a *his3*Δ1 *leu2*Δ0 *met15*Δ0 *ura3*Δ0 *cup5::KanMX4*	Euroscarf

Δ*cwh41*	YGL027C	*MAT*a *his3*Δ1 *leu2*Δ0 *met15*Δ0 *ura3*Δ0 *cwh41::KanMX4*	Euroscarf
Δ*dcw1*	YKL046C	*MAT*a *his3*Δ1 *leu2*Δ0 *met15*Δ0 *ura3*Δ0 *dcw1::KanMX4*	Euroscarf
Δ*did4*	YKL002W	*MAT*a *his3*Δ1 *leu2*Δ0 *met15*Δ0 *ura3*Δ0 *did4::KanMX4*	Euroscarf
Δ*die2*	YGR227W	*MAT*a *his3*Δ1 *leu2*Δ0 *met15*Δ0 *ura3*Δ0 *die2::KanMX4*	Euroscarf
Δ*drs2*	YAL026C	*MAT*a *his3*Δ1 *leu2*Δ0 *met15*Δ0 *ura3*Δ0 *drs2::KanMX4*	Euroscarf
Δ*ecm7*	YLR443W	*MAT*a *his3*Δ1 *leu2*Δ0 *met15*Δ0 *ura3*Δ0 *ecm7::KanMX4*	Euroscarf
Δ*erg24*	YNL280C	*MAT*a *his3*Δ1 *leu2*Δ0 *met15*Δ0 *ura3*Δ0 *erg24::KanMX4*	Euroscarf
Δ*erg28*	YER044C	*MAT*a *his3*Δ1 *leu2*Δ0 *met15*Δ0 *ura3*Δ0 *erg28::KanMX4*	Euroscarf
Δ*erg3*	YLR056W	*MAT*a *his3*Δ1 *leu2*Δ0 *met15*Δ0 *ura3*Δ0 *erg3::KanMX4*	Euroscarf
Δ*erg4*	YGL012W	*MAT*a *his3*Δ1 *leu2*Δ0 *met15*Δ0 *ura3*Δ0 *erg4::KanMX4*	Euroscarf
Δ*erg6*	YML008C	*MAT*a *his3*Δ1 *leu2*Δ0 *met15*Δ0 *ura3*Δ0 *erg6::KanMX4*	Euroscarf
Δ*flc1*	YPL221W	*MAT*a *his3*Δ1 *leu2*Δ0 *met15*Δ0 *ura3*Δ0 *flc1::KanMX4*	Euroscarf
Δ*fur4*	YBR021W	*MAT*a *his3*Δ1 *leu2*Δ0 *met15*Δ0 *ura3*Δ0 *fur4::KanMX4*	Euroscarf
Δ*gas1*	YMR307W	*MAT*a *his3*Δ1 *leu2*Δ0 *met15*Δ0 *ura3*Δ0 *gas1::KanMX4*	Euroscarf
Δ*gly1*	YEL046C	*MAT*a *his3*Δ1 *leu2*Δ0 *met15*Δ0 *ura3*Δ0 *gly1::KanMX4*	Euroscarf
Δ*gup1*	YGL084C	*MAT*a *his3*Δ1 *leu2*Δ0 *met15*Δ0 *ura3*Δ0 *gup1::KanMX4*	Euroscarf
Δ*gyp1*	YOR070C	*MAT*a *his3*Δ1 *leu2*Δ0 *met15*Δ0 *ura3*Δ0 *gyp1::KanMX4*	Euroscarf
Δ*hog1*	YLR113W	*MAT*a *his3*Δ1 *leu2*Δ0 *met15*Δ0 *ura3*Δ0 *hog1*::*KanMX4*	Euroscarf
Δ*hom2*	YDR158W	*MAT*a *his3*Δ1 *leu2*Δ0 *met15*Δ0 *ura3*Δ0 *hom2::KanMX4*	Euroscarf
Δ*hom3*	YER052C	*MAT*a *his3*Δ1 *leu2*Δ0 *met15*Δ0 *ura3*Δ0 *hom3::KanMX4*	Euroscarf
Δ*hsl1*	YKL101W	*MAT*a *his3*Δ1 *leu2*Δ0 *met15*Δ0 *ura3*Δ0 *hsl1::KanMX4*	Euroscarf
Δ*hur1*	YGL168W	*MAT*a *his3*Δ1 *leu2*Δ0 *met15*Δ0 *ura3*Δ0 *hur1::KanMX4*	Euroscarf
Δ*ics3*	YJL077C	*MAT*a *his3*Δ1 *leu2*Δ0 *met15*Δ0 *ura3*Δ0 *ics3::KanMX4*	Euroscarf
Δ*ilv1*	YER086W	*MAT*a *his3*Δ1 *leu2*Δ0 *met15*Δ0 *ura3*Δ0 *ilv1::KanMX4*	Euroscarf
Δ*kcs1*	YDR017C	*MAT*a *his3*Δ1 *leu2*Δ0 *met15*Δ0 *ura3*Δ0 *kcs1::KanMX4*	Euroscarf
Δ*kex1*	YGL203C	*MAT*a *his3*Δ1 *leu2*Δ0 *met15*Δ0 *ura3*Δ0 *kex1::KanMX4*	Euroscarf
Δ*kre1*	YNL322C	*MAT*a *his3*Δ1 *leu2*Δ0 *met15*Δ0 *ura3*Δ0 *kre1::KanMX4*	Euroscarf
Δ*kre11*	YGR166W	*MAT*a *his3*Δ1 *leu2*Δ0 *met15*Δ0 *ura3*Δ0 *kre11::KanMX4*	Euroscarf
Δ*kre6*	YPR159W	*MAT*a *his3*Δ1 *leu2*Δ0 *met15*Δ0 *ura3*Δ0 *kre6::KanMX4*	Euroscarf
Δ*mid1*	YNL291C	*MAT*a *his3*Δ1 *leu2*Δ0 *met15*Δ0 *ura3*Δ0 *mid1::KanMX4*	Euroscarf
Δ*mid2*	YLR332W	*MAT*a *his3*Δ1 *leu2*Δ0 *met15*Δ0 *ura3*Δ0 *mid2::KanMX4*	Euroscarf
Δ*mot2*	YER068W	*MAT*a *his3*Δ1 *leu2*Δ0 *met15*Δ0 *ura3*Δ0 *mot2::KanMX4*	Euroscarf
Δ*mpk1*	YHR030C	*MAT*a *his3*Δ1 *leu2*Δ0 *met15*Δ0 *ura3*Δ0 *mpk1::KanMX4*	Euroscarf
Δ*msg5*	YNL053W	*MAT*a *his3*Δ1 *leu2*Δ0 *met15*Δ0 *ura3*Δ0 *msg5::KanMX4*	Euroscarf
Δ*mtl1*	YGR023W	*MAT*a *his3*Δ1 *leu2*Δ0 *met15*Δ0 *ura3*Δ0 *mtl1::KanMX4*	Euroscarf
Δ*mtq2*	YDR140W	*MAT*a *his3*Δ1 *leu2*Δ0 *met15*Δ0 *ura3*Δ0 *mtq2::KanMX4*	Euroscarf
Δ*nbp2*	YDR162C	*MAT*a *his3*Δ1 *leu2*Δ0 *met15*Δ0 *ura3*Δ0 *nbp2::KanMX4*	Euroscarf
Δ*och1*	YGL038C	*MAT*a *his3*Δ1 *leu2*Δ0 *met15*Δ0 *ura3*Δ0 *och1::KanMX4*	Euroscarf
Δ*ost4*	YDL232W	*MAT*a *his3*Δ1 *leu2*Δ0 *met15*Δ0 *ura3*Δ0 *ost4::KanMX4*	Euroscarf
Δ*pbs2*	YJL128C	*MAT*a *his3*Δ1 *leu2*Δ0 *met15*Δ0 *ura3*Δ0 *pbs2::KanMX4*	Euroscarf
Δ*pep3*	YLR148W	*MAT*a *his3*Δ1 *leu2*Δ0 *met15*Δ0 *ura3*Δ0 *pep3::KanMX4*	Euroscarf
Δ*pep5*	YMR231W	*MAT*a *his3*Δ1 *leu2*Δ0 *met15*Δ0 *ura3*Δ0 *pep5::KanMX4*	Euroscarf
Δ*pep7*	YDR323C	*MAT*a *his3*Δ1 *leu2*Δ0 *met15*Δ0 *ura3*Δ0 *pep7::KanMX4*	Euroscarf
Δ*pep8*	YJL053W	*MAT*a *his3*Δ1 *leu2*Δ0 *met15*Δ0 *ura3*Δ0 *pep8::KanMX4*	Euroscarf
Δ*per1*	YCR044C	*MAT*a *his3*Δ1 *leu2*Δ0 *met15*Δ0 *ura3*Δ0 *per1::KanMX4*	Euroscarf
Δ*pkh1*	YDR490C	*MAT*a *his3*Δ1 *leu2*Δ0 *met15*Δ0 *ura3*Δ0 *pkh1::KanMX4*	Euroscarf
Δ*pkh2*	YOL100W	*MAT*a *his3*Δ1 *leu2*Δ0 *met15*Δ0 *ura3*Δ0 *pkh2::KanMX4*	Euroscarf

Δ*ptp1*	YDL230W	*MAT*a *his3*Δ1 *leu2*Δ0 *met15*Δ0 *ura3*Δ0 *ptp1::KanMX4*	Euroscarf
Δ*ptp2*	YOR208W	*MAT*a *his3*Δ1 *leu2*Δ0 *met15*Δ0 *ura3*Δ0 *ptp2::KanMX4*	Euroscarf
Δ*ptp3*	YER075C	*MAT*a *his3*Δ1 *leu2*Δ0 *met15*Δ0 *ura3*Δ0 *ptp3::KanMX4*	Euroscarf
Δ*rbl2*	YOR265W	*MAT*a *his3*Δ1 *leu2*Δ0 *met15*Δ0 *ura3*Δ0 *rbl2::KanMX4*	Euroscarf
Δ*rgd1*	YBR260C	*MAT*a *his3*Δ1 *leu2*Δ0 *met15*Δ0 *ura3*Δ0 *rgd1::KanMX4*	Euroscarf
Δ*rhk1*	YBL082C	*MAT*a *his3*Δ1 *leu2*Δ0 *met15*Δ0 *ura3*Δ0 *rhk1::KanMX4*	Euroscarf
Δ*rmd7*	YER083C	*MAT*a *his3*Δ1 *leu2*Δ0 *met15*Δ0 *ura3*Δ0 *rmd7::KanMX4*	Euroscarf
Δ*rny1*	YPL123C	*MAT*a *his3*Δ1 *leu2*Δ0 *met15*Δ0 *ura3*Δ0 *rny1::KanMX4*	Euroscarf
Δ*rom2*	YLR371W	*MAT*a *his3*Δ1 *leu2*Δ0 *met15*Δ0 *ura3*Δ0 *rom2::KanMX4*	Euroscarf
Δ*rot2*	YBR229C	*MAT*a *his3*Δ1 *leu2*Δ0 *met15*Δ0 *ura3*Δ0 *rot2::KanMX4*	Euroscarf
Δ*sac1*	YKL212W	*MAT*a *his3*Δ1 *leu2*Δ0 *met15*Δ0 *ura3*Δ0 *sac1::KanMX4*	Euroscarf
Δ*scp160*	YJL080C	*MAT*a *his3*Δ1 *leu2*Δ0 *met15*Δ0 *ura3*Δ0 *scp160::KanMX4*	Euroscarf
Δ*sdp1*	YIL113W	*MAT*a *his3*Δ1 *leu2*Δ0 *met15*Δ0 *ura3*Δ0 *sdp1::KanMX4*	Euroscarf
Δ*she4*	YOR035C	*MAT*a *his3*Δ1 *leu2*Δ0 *met15*Δ0 *ura3*Δ0 *she4::KanMX4*	Euroscarf
Δ*sho1*	YER118C	*MAT*a *his3*Δ1 *leu2*Δ0 *met15*Δ0 *ura3*Δ0 *sho1::KanMX4*	Euroscarf
Δ*sit4*	YDL047W	*MAT*a *his3*Δ1 *leu2*Δ0 *met15*Δ0 *ura3*Δ0 *sit4::KanMX4*	Euroscarf
Δ*skm1*	YOL113W	*MAT*a *his3*Δ1 *leu2*Δ0 *met15*Δ0 *ura3*Δ0 *skm1::KanMX4*	Euroscarf
Δ*sla2*	YBL007C	*MAT*a *his3*Δ1 *leu2*Δ0 *met15*Δ0 *ura3*Δ0 *sla2::KanMX4*	Euroscarf
Δ*smi1*	YGR229C	*MAT*a *his3*Δ1 *leu2*Δ0 *met15*Δ0 *ura3*Δ0 *smi1::KanMX4*	Euroscarf
Δ*snf7*	YLR025W	*MAT*a *his3*Δ1 *leu2*Δ0 *met15*Δ0 *ura3*Δ0 *snf7::KanMX4*	Euroscarf
Δ*sod1*	YJR104C	*MAT*a *his3*Δ1 *leu2*Δ0 *met15*Δ0 *ura3*Δ0 *sod1::KanMX4*	Euroscarf
Δ*spc72*	YAL047C	*MAT*a *his3*Δ1 *leu2*Δ0 *met15*Δ0 *ura3*Δ0 *spc72::KanMX4*	Euroscarf
Δ*spt3*	YDR392W	*MAT*a *his3*Δ1 *leu2*Δ0 *met15*Δ0 *ura3*Δ0 *spt3::KanMX4*	Euroscarf
Δ*srv2*	YNL138W	*MAT*a *his3*Δ1 *leu2*Δ0 *met15*Δ0 *ura3*Δ0 *srv2::KanMX4*	Euroscarf
Δ*ssd1*	YDR293C	*MAT*a *his3*Δ1 *leu2*Δ0 *met15*Δ0 *ura3*Δ0 *ssd1::KanMX4*	Euroscarf
Δ*ssk1*	YLR006C	*MAT*a *his3*Δ1 *leu2*Δ0 *met15*Δ0 *ura3*Δ0 *ssk1::KanMX4*	Euroscarf
Δ*sur1*	YPL057C	*MAT*a *his3*Δ1 *leu2*Δ0 *met15*Δ0 *ura3*Δ0 *sur1::KanMX4*	Euroscarf
Δ*thr1*	YHR025W	*MAT*a *his3*Δ1 *leu2*Δ0 *met15*Δ0 *ura3*Δ0 *thr1::KanMX4*	Euroscarf
Δ*tlg2*	YOL018C	*MAT*a *his3*Δ1 *leu2*Δ0 *met15*Δ0 *ura3*Δ0 *tlg2::KanMX4*	Euroscarf
Δ*trk1*	YJL129C	*MAT*a *his3*Δ1 *leu2*Δ0 *met15*Δ0 *ura3*Δ0 *trk1::KanMX4*	Euroscarf
Δ*tyr1*	YBR166C	*MAT*a *his3*Δ1 *leu2*Δ0 *met15*Δ0 *ura3*Δ0 *tyr1::KanMX4*	Euroscarf
Δ*vam10*	YOR068C	*MAT*a *his3*Δ1 *leu2*Δ0 *met15*Δ0 *ura3*Δ0 *vam10::KanMX4*	Euroscarf
Δ*vma1*	YDL185W	*MAT*a *his3*Δ1 *leu2*Δ0 *met15*Δ0 *ura3*Δ0 *vma1::KanMX4*	Euroscarf
Δ*vma11*	YPL234C	*MAT*a *his3*Δ1 *leu2*Δ0 *met15*Δ0 *ura3*Δ0 *vma11::KanMX4*	Euroscarf
Δ*vma13*	YPR036W	*MAT*a *his3*Δ1 *leu2*Δ0 *met15*Δ0 *ura3*Δ0 *vma13::KanMX4*	Euroscarf
Δ*vma16*	YHR026W	*MAT*a *his3*Δ1 *leu2*Δ0 *met15*Δ0 *ura3*Δ0 *vma16::KanMX4*	Euroscarf
Δ*vma2*	YBR127C	*MAT*a *his3*Δ1 *leu2*Δ0 *met15*Δ0 *ura3*Δ0 *vma2::KanMX4*	Euroscarf
Δ*vma21*	YGR105W	*MAT*a *his3*Δ1 *leu2*Δ0 *met15*Δ0 *ura3*Δ0 *vma21::KanMX4*	Euroscarf
Δ*vma4*	YOR332W	*MAT*a *his3*Δ1 *leu2*Δ0 *met15*Δ0 *ura3*Δ0 *vma4::KanMX4*	Euroscarf
Δ*vma5*	YKL080W	*MAT*a *his3*Δ1 *leu2*Δ0 *met15*Δ0 *ura3*Δ0 *vma5::KanMX4*	Euroscarf
Δ*vma7*	YGR020C	*MAT*a *his3*Δ1 *leu2*Δ0 *met15*Δ0 *ura3*Δ0 *vma7::KanMX4*	Euroscarf
Δ*vma8*	YEL051W	*MAT*a *his3*Δ1 *leu2*Δ0 *met15*Δ0 *ura3*Δ0 *vma8::KanMX4*	Euroscarf
Δ*vph2*	YKL119C	*MAT*a *his3*Δ1 *leu2*Δ0 *met15*Δ0 *ura3*Δ0 *vph2::KanMX4*	Euroscarf
Δ*vps1*	YKR001C	*MAT*a *his3*Δ1 *leu2*Δ0 *met15*Δ0 *ura3*Δ0 *vps1::KanMX4*	Euroscarf
Δ*vps15*	YBR097W	*MAT*a *his3*Δ1 *leu2*Δ0 *met15*Δ0 *ura3*Δ0 *vps15::KanMX4*	Euroscarf
Δ*vps17*	YOR132W	*MAT*a *his3*Δ1 *leu2*Δ0 *met15*Δ0 *ura3*Δ0 *vps17::KanMX4*	Euroscarf
Δ*vps20*	YMR077C	*MAT*a *his3*Δ1 *leu2*Δ0 *met15*Δ0 *ura3*Δ0 *vps20::KanMX4*	Euroscarf

Δ*vps24*	YKL041W	*MAT*a *his3*Δ1 *leu2*Δ0 *met15*Δ0 *ura3*Δ0 *vps24::KanMX4*	Euroscarf
Δ*vps25*	YJR102C	*MAT*a *his3*Δ1 *leu2*Δ0 *met15*Δ0 *ura3*Δ0 *vps25::KanMX4*	Euroscarf
Δ*vps29*	YHR012W	*MAT*a *his3*Δ1 *leu2*Δ0 *met15*Δ0 *ura3*Δ0 *vps29::KanMX4*	Euroscarf
Δ*vps3*	YDR495C	*MAT*a *his3*Δ1 *leu2*Δ0 *met15*Δ0 *ura3*Δ0 *vps3::KanMX4*	Euroscarf
Δ*vps45*	YGL095C	*MAT*a *his3*Δ1 *leu2*Δ0 *met15*Δ0 *ura3*Δ0 *vps45::KanMX4*	Euroscarf
Δ*vps5*	YOR069W	*MAT*a *his3*Δ1 *leu2*Δ0 *met15*Δ0 *ura3*Δ0 *vps5::KanMX4*	Euroscarf
Δ*vps51*	YKR020W	*MAT*a *his3*Δ1 *leu2*Δ0 *met15*Δ0 *ura3*Δ0 *vps51::KanMX4*	Euroscarf
Δ*vps9*	YML097C	*MAT*a *his3*Δ1 *leu2*Δ0 *met15*Δ0 *ura3*Δ0 *vps9::KanMX4*	Euroscarf
Δ*wsc1*	YOR008C	*MAT*a *his3*Δ1 *leu2*Δ0 *met15*Δ0 *ura3*Δ0 *wsc1::KanMX4*	Euroscarf
Δ*ypk1*	YKL126W	*MAT*a *his3*Δ1 *leu2*Δ0 *met15*Δ0 *ura3*Δ0 *ypk1::KanMX4*	Euroscarf
Δ*ypk2*	YMR104C	*MAT*a *his3*Δ1 *leu2*Δ0 *met15*Δ0 *ura3*Δ0 *ypk2::KanMX4*	Euroscarf
YMF1	-	1783 isogenic, *msg5*::6*myc*::*leu2*	(Marín *et al*., 2009)
YPH499	-	*MATa ade2-10 trp1-63 leu2-1 ura3-52 his3-*Δ*200 lys2-801*	(Sikorski and Hieter, 1989)
ypk1-ts/ Δ*ypk2*	-	YPH499 *ypk1-ts::HIS3 ypk2::TRP1*	(Casamayor *et al*., 1999)
OHNY	-	*MATa ura3 his3 trp1 leu2 ade2*	(Ozaki *et al*., 1996)
HNY21 (*rho1-ts*)	-	OHNY *rho1–104*	(Ozaki *et al*., 1996)
SEY6221	-	*MATa leu2-3,112 ura3-52 his3*Δ*200 trp1*Δ*901 suc2*Δ*9 ade2-101*	(Paravicini *et al*., 1992)
GPY1115S (*pkc1-ts*)	-	SEY6221 *pkc1*Δ*1::HIS3*	(Paravicini *et al*., 1992)

3.1.3. *Fusarium oxysporum* strains

The *F. oxysporum* strains used in this study are described in detail in [Table 3]. All are derived from the *F. oxysporum* f. sp. *lycopersici* wild type strain 4287.

Table 3 – *F. oxysporum* strains used in this study

STRAIN	GENOTYPE	REFERENCE
4287 (FGS 9935)	Wild type, Race 2	FGS [(1)]
pHluorin expressing strain	*pHluorin*; *HYG*	(Serrano, 2014)
Δ*pacC*	*pacC*::*HYG*	This study
Δ*palH*	*palH*::*HYG*	This study
Δ*pacC* expressing pHluorin	*pacC*::*NEO*; *pHluorin*; *HYG*	This study
Δ*palH* expressing pHluorin	*palH*::*NEO*; *pHluorin*; *HYG*	This study
pacC^{c}	Truncated version of PacC; *HYG*	(Caracuel *et al*., 2003)
Δ*ptk2*	*ptk2*::*HYG*	This study
Δ*msg5*	*msg5*::*HYG*	This study
Δ*bck1*	*bck1*::*HYG*	(Turrà *et al*., 2015)
Δ*rho1*	*rho1*::*HYG*	(Martinez-Rocha *et al*., 2008)

[(1)] Fusarium Genetics Stock Center

3.1.4. Plant cultivars

The tomato cultivar used in this study is described in [Table 4].

Table 4 – Tomato plant used in this study

SPECIES	CULTIVAR	SPECIFICATIONS	SOURCE
Tomato (*Lycopersicon esculentum*)	Monika (seeds)	Susceptible to *F. oxysporum* f. sp. *lycopersici* Race 2	Syngenta, Almeria, Spain

3.2 PLASMIDS

The plasmids used in this study are listed in [Table 5]. They include plasmids used for amplification of resistance cassettes to transform *F. oxysporum* and yeast vectors used for *S. cerevisiae* transformation.

Table 5 – Plasmids used in this study

PLASMID	ORIGIN/FEATURES	REFERENCE
pGEMT®-T	Derived from plasmid pGEM®-5Zf(+), linearized with *Eco*RV and with a T added in both 3' ends	Promega
pAN7-1	Derived from pUC18; *A. nidulans GpdA* promoter; phosphotransferase *hygromycin B* (*hph*) gene from *Streptomyces spp.*; *A. nidulans TrpC* terminator	(Punt *et al.*, 1987)
PGEMT - *hph*BB	Derived from pAN7-1 plasmid with shorter version of *GpdA* and *TrpC*	Our group
P_pHluorin	Derived from pGEMT; *A. nidulans gpdA* promoter; *pHluorin* gene; *S. cerevisiae ADH5* terminator	(Serrano, 2014)
pYEplac181	pYEplac181 plasmid (2µ, ampR, LEU2+) containing the *pHluorin* gene flanked by the *TEF1* promoter and *CYC1* terminator from *S. cerevisiae*	Rajini Rao, Johns Hopkins University

3.3.MEDIA AND BUFFER SOLUTIONS

All media were prepared with RO deionized water and sterilized by autoclaving at 1.2 atm and 120°C for 20 minutes. Buffer solutions were prepared with RO ultrapure water and sterilized by filtration (0.22 μm pore size, Millipore). RO deionized and RO ultrapure water were obtained through the Direct-Q® 8 UV remote water purification system (Merck Millipore). [Table 6] lists the media and buffer solutions used for cell growth. For each experimental protocol, the buffer solutions prepared will be described in the respective section.

Table 6 – Media used for bacteria and fungi growth

Media for *E. Coli* (w/v)	
LB	1% tryptone, 0.5% yeast extract, 1% sodium chloride
LA	1% tryptone, 0.5% yeast extract, 1% sodium chloride and 2% agar
Media for *S. cerevisiae* (w/v)	
YPD	2% tryptone, 2% glucose and 1% yeast extract
YPDA	2% tryptone, 2% glucose, 1% yeast extract and 2% agar
SC	0.17% yeast nitrogen base without amino acids and ammonium sulfate, 0.5% ammonium sulfate, 2% glucose, 0.2% Drop-out mix, plus 0.01% of amino acids
Media for *F. oxysporum* (w/v)	
PDB	Boil 200 g of peeled potatoes in 0.6 L of deionized water for 60 minutes. Stir and add 20 g of glucose and deionized water up to 1 L
PDA	3.9% potato dextrose agar
YPD	1% glucose and 1% yeast extract. Adjust the pH to 8.0 with NaOH 1N
YPDA	1% tryptone, 2% glucose, 0.3% yeast extract and 1.5% agar
Puhalla's MM	0.05% $MgSO_4.7H_2O$, 0.05% KCl, 0.1% KH_2PO_4, 0.22% $NaNO_3$, 3% sucrose and 2% oxoid agar.
Regeneration MM	0.05% $MgSO_4.7H_2O$, 0.05% KCl, 0.1% KH_2PO_4, 0.2% $NaNO_3$, 2% glucose, 20% sucrose and oxoid agar (1.5% for Petri dishes and 0.5% for top agar)
Buffer solutions	
HEPES 1M	Prepared with ultrapure water and adjust the pH to 7.4 with NaOH 10 N
KSU	50 mM K_2HPO_4, 50 mM sodium succinate and 25 mM Urea. Adjust the pH accordingly to the experiment

LB - Luria-Bertoni; LA - Luria-Bertoni with agar; YPD -Yeast Extract Peptone Dextrose; YPDA - Yeast Extract Peptone Dextrose Agar; SC - Synthetic Complete medium; PDB - Potato Dextrose Broth; PDA - Potato Dextrose Agar (BD Difco™); MM - Minimal Medium.

3.4.GROWTH CONDITIONS

3.4.1. Bacteria

The *E. coli* DH5α strain was grown overnight (O.N.) at 37 °C in LA medium. For bacteria transformants, LA medium was supplemented with ampicillin (Sigma Aldrich) at 100 μg/ml. Grown colonies on plate were picked and grown in LB medium O.N. at 37 °C with orbital shaking at 250 rpm. LB medium was supplemented with the same concentration of ampicillin as LA medium, when bacteria transformants were grown. Bacterial cells were preserved at -80 °C in 30% glycerol (v/v).

3.4.2. Yeast

Yeast cells were cultured in YPDA medium at 30°C. Yeast mutant strains were cultured in YPDA supplemented with geneticin (G418; Sigma Aldrich) at 200 μg/ml. Yeast transformants were cultured in solid SC medium lacking the auxotrophic marker, with or without (for wild type transformants) geneticin at 200 μg/ml. For experimental assays, cells were grown O.N. at 30°C or 25°C, for temperature sensitive strains, with orbital shaking at 200 rpm in YPD medium. Gene repression in the temperature strains was induced by transferring the cells to 34°C, 200 rpm for one hour before start the treatment. In all situations, cells were grown O.N. until reach an OD_{640nm} of 0.9 and after that, they were collected at room temperature (RT) by centrifugation at 5000 rpm for 5 minutes and transferred to a new flask with KSU buffer at pH 6.5. Cells were then incubated for 1 hour at 30°C, or 34°C for temperature sensitive strains, with orbital shaking at 200 rpm. After this time of incubation, cells were treated with the respective chemical compound.

Yeast cells were stored at -80°C in 20% glycerol (v/v).

3.4.3. *F. oxysporum*

F. oxysporum strains were cultured in PDB medium at 28°C with orbital shaking at 170 rpm. When needed the following antibiotics were added to the culture medium: hygromicin B (InvivoGen) at 20 µg/ml or geneticin at 10 µg/ml. After 3 to 5 days of culture in liquid medium, microconidia were collected by filtration through a nylon filter (Monodur; mesh size 10 µm) and then by centrifugation at 10000 rpm for 10 minutes. Depending of the experimental condition and design, microconidia were either germinated in rich medium or plated on solid media for phenotypical assays. For transformants selection on solid medium, antibiotics were added at the following concentrations: 55 µg/ml of hygromicin B or 27.5 µg/ml of geneticin.

For long-term storage of the different strains, microconidia collected from 3 to 5 days-old cultures were resuspended in 33% glycerol (v/v) and stored at -80°C. These suspensions were used for later inoculation to obtain fresh microconidia.

3.4.4. Tomato plant culture

Tomato seeds were surface sterilized in 20% bleach (v/v). After 30 minutes, seeds were washed twice for 10 minutes with sterilized ultrapure water. Seeds were planted on wet vermiculite and incubated in plant growth chambers with fluorescent lights (36 W, photoperiod of 14 hours light and 10 hours dark) at 28°C. Infection assays with *F. oxysporum* were performed with 14 days-old tomato plants.

3.5 MOLECULAR METHODOLOGY

Macromolecules were isolated from bacteria, yeast or *F. oxysporum* cultures for subsequent downstream processes, analytical or preparative purposes. The protocols employed in this study will be described in detail in the sections below.

3.5.1. DNA extraction and quantification

3.5.1.1. Plasmid DNA extraction from *E. coli*

For plasmid DNA extraction from bacteria the CTAB method was used as previously described (Murray and Thompson, 1980). Briefly, a single colony of bacteria grown O.N. on a LA plate at 37°C was peaked to liquid LB medium (containing antibiotic if required) and grown O.N. at 37°C with orbital shaking of 250 rpm. The day after, cells were collected by centrifugation 2 minutes at 13400 rpm and resuspended in 200 µl of STET[(2)] solution, supplemented with 4 µl of lysozyme (50 mg/ml; Sigma Aldrich) and 4 µl of RNase (10 mg/ml; Roche Life Science), and incubated 10 minutes at RT. Then, cells were boiled for 45 seconds and centrifuged 10 minutes at 13400 rpm. The obtained pellet was removed using a sterile wood stick and 10 µl of 5% CTAB extraction buffer[(3)] was added to precipitate the plasmid DNA. After 10 minutes of incubation at RT, samples were centrifuged 10 minutes at 13400 rpm. Each pellet was resuspended in 350 µl of 1.2 M NaCl and 750 µl of 100% ice-cold ethanol and centrifuged again for 10 minutes at 13400 rpm. Precipitated plasmid DNA was then washed for two times more with 1 ml of ethanol 70%, dried and resuspended in sterile ultrapure water.

[(2)] STET: 8% sucrose (w/v), 0.1% Triton X-100 (v/v), 50 mM EDTA pH 8.0, 50 mM Tris-HCl pH 8.0.

[(3)] CTAB extraction buffer: 12.1 g/l Trizma base, 7.44 g/l EDTA, 81.8 g/l NaCl and 20 g/l Cetyltrimethylammonium bromide. Heat to 60ºC to dissolve and adjust to pH 8.0 with NaOH 10 N. Store at 37ºC to avoid precipitation.

3.5.1.2. Nucleic acid extraction from *F. oxysporum*

Genomic DNA was extracted from *F. oxysporum* mycelium using the CTAB method (Torres *et al*., 1993). Mycelium from 5-25 ml of 3 to 5 days-old cultures were transferred to a 2 ml Eppendorf centrifuge tube and frozen at –80°C. Completely frozen samples were then lyophilized using a freeze-drying system. Subsequently, a 5 mm diameter glass bead (Sigma Aldrich) was added to each sample, and samples were submitted in a BeadBeater to 3 cycles of 20 seconds of beat and pause, respectively. After that, DNA was extracted from samples following the CTAB method. To each sample, 1 ml of CTAB extraction buffer was added and vigorously vortexed. Next, 4 µl of β-mercaptoethanol (Merck) and 500 µl of a chloroform:octanol 24:1 (v/v) solution were added and the mix was incubated firstly at 65°C for 45 minutes and then, at RT, for 15 minutes more. The Eppendorf tube was centrifuged for 10 minutes at 7000 rpm at RT and 500 µl of the upper part of the supernatant was precipitated with 1 ml of 100 % ice-cold ethanol and incubated at -20°C for at least 30 minutes. Precipitated DNA was centrifuged for 10 minutes at 13400 rpm and washed two times with 1 ml of ethanol 70%. Finally, the pellet was dried and resuspended in 50 µl of sterile ultrapure water with 5 µl de RNase (10 mg/ml; Roche Life Science) and incubated at 37°C for 30 minutes.

3.5.1.3 Nucleic acid quantification

The amount and quality of DNA extracted was monitored either by electrophoresis in a 0.7 % agarose gel (w/v) or in a Nanodrop® ND-1000 spectrophotometer at 260 nm and 280 nm wavelength.

3.5.2. DNA amplification reactions

After extraction and quantification, plasmid and genomic DNA were used to amplify fragments of interest. Standard and Fusion PCR reactions were employed using synthetic oligonucleotides that were designed according to the experimental purpose.

3.5.2.1. Standard PCR

PCR amplification reactions were performed in a thermocycler using the thermostable DNA polymerase of the Expand High Fidelity PCR System (Roche Life Sciences). Each PCR reaction contained 300 nM of each primers, 2.5 mM $MgCl_2$, 0.8 mM of dNTPs mix and 0.05 U/µl of polymerase. Genomic DNA was added at 5-10 ng/µl and plasmid DNA at 1-5 ng/µl final concentration. PCR cycling conditions were defined by an initial step of denaturation (5 minutes, 94°C) followed by 35 cycles of 35 seconds at 94°C, 35 seconds at the calculated primer annealing temperature and 1 minute/1.5 Kb was stablished for DNA amplification at 72°C (or 68°C for templates larger than 3 kb), and a final extension step at 72°C (or 68°C) for 10 minutes. For knockout mutant confirmation, the thermostable BioTaq™ DNA Polymerase (Bioline) was used. PCR cycling conditions were defined by an initial step of denaturation (5 minutes, 94°C) followed by 35 cycles of 35 seconds at 94°C, 35 seconds at the calculated primer annealing temperature and 1 minutes/2 Kb was stablished for DNA amplification at 72°C, and a final extension step at 72°C for 10 minutes.

3.5.2.2. Fusion PCR

Fusion PCR or overlap extension is a method used to fuse two or more PCR products (Yang *et al*., 2004) and is schematically represented in [Figure 6]. Complementary oligonucleotides and the polymerase chain reaction are used to generate two DNA fragments with overlapping ends. In this PCR reaction (PCR I), an approximately 2 Kb fragment upstream (promoter) and downstream (terminator) of the Open Reading Frame (ORF) of the target gene were amplified with oligonucleotides containing a tail homologous to the selectable marker cassette. The amplified fragments are then combined in a 'fusion' reaction without oligonucleotides in which the overlapping ends anneal. In this reaction, the 3' overlap of each strand serves as a primer for the 3' extension of the complementary strand and the promoter and terminator regions are fused with the selectable marker cassette (PCR II). The resulting fusion products are used as template for further

amplification by PCR (PCR III) using the primers of interest. In this work, the main purpose of fusion PCR was the generation of linear DNA consisting of a selectable marker gene conferring hygromycin/neomycin resistance, flanked by 1.5 kb stretches of DNA that target a gene of interest, for application of the "split-marker" deletion strategy for knockout mutant generation [Figure 6].

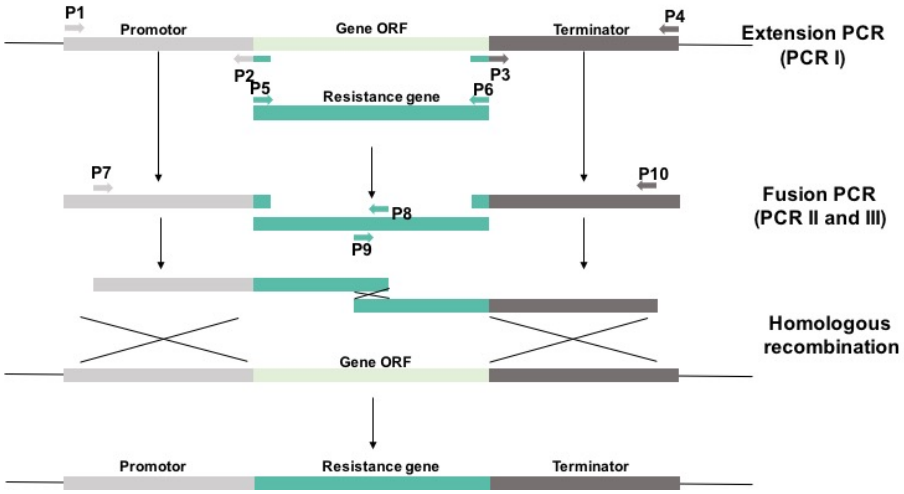

Figure 6 - Schematic representation of the split-marker deletion strategy for gene knockout in *F. oxysporum*.
Amplification of the upstream (promotor; P1-P2) and downstream (terminator; P3-P4) regions of the target gene with primers that contain overlapping ends to the antibiotic resistance cassette. The obtained PCR products are used as templates for the fusion PCR reactions between each flank and overlapping parts of the resistance cassette. Pairs of primers P7-P8 and P9-P10 were used to amplify the fragments which were subsequently used to transform *F. oxysporum* protoplasts for gene ORF replacement by the resistance cassette through homologous recombination.

In all cases, we found that fusion of two PCR products was best achieved by precipitation of the extension PCR products following the protocol described in Section 3.5.2.4, and then using equimolar quantities of the purified products as templates for subsequent PCR reactions.

3.5.2.2.1. Generation of the *neomycin* resistance cassette for targeted gene knockout in *F. oxysporum*

The *neomycin* resistance cassette was generated by fusion PCR. The resistance gene amplified from plasmid pAc5-STABLE2-Neo was placed under control of the *A. nidulans gpdA* promoter and *trpC* terminator, amplified from the PGEMT-*hph*BB and pAN7-1 plasmids, respectively, as shown in [Figure 7].

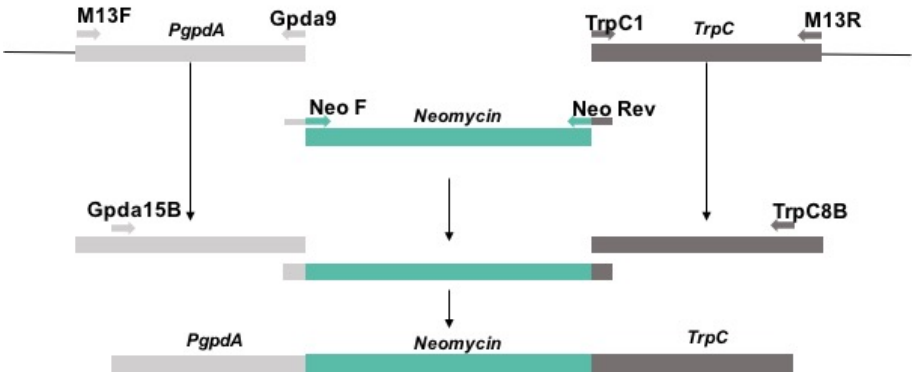

Figure 7 - Schematic representation of the generated *Neomycin* cassette.
The *gpdA* promotor (1200 bp) and the *TrpC* terminator (760 bp) were amplified with the M13F-Gpda9 and TrpC1-M13R primers, respectively. The *Neomycin* resistance gene (804 bp) was amplified with the primers NeoF and NeoR containing ends overlapping with the promotor and terminator. The three fragments were fused by Fusion PCR reactions using the Gpda15B and TrpC8B primers.

3.5.2.3. Synthetic oligonucleotides

The oligonucleotides used in this study are listed in [Table 7] and were designed with the Primer Analysis Software Oligo version 7.0 (Molecular Biology Insights, Inc. – Colorado, USA). Internal stability, duplex and hairpin formation and different physicochemical parameters, such as temperature of melting (Tm; calculated through the [2(A+T)°+4(G+C)°] method) were determined in each case. Oligonucleotides were synthesized by Isogen Life Science, Netherlands.

Table 7 - List of primers used in this study. Lowercase nucleotides do not belong to the original sequence and were introduced to generate overlapping ends for fusion pcr reactions

Gene/ Vector	Name	[Tm]_Sequence 5'-3'
hyg	HygG	[62]_CGTTGCAAGACCTGCCTGAA
	HygY	[62]_GGATGCCTCCGCTCGAAGTA
hyg/*neo* cassettes	gpdA15B	[62]_GGATCCCGAGACCTAATACAGCCCCT
	gpdA16B	[62]_AGGGGCTGTATTAGGTCTCG
	gpdA9B	[62]_GTGATGTCTGCTCAAGCGG
	TrpC1	[64]_AGTAGATGCCGACCGCGGG
	TrpC8B	[62]_GGATCCAAACAAGTGTACCTGTGCATTC
	TrpC4B	[62]_CCTGGGTTCGCAAAGATAATT
msg5	Msg5_P_Fwd	[62]_CACGAGGTCTATATTTAGGATC
	Msg5_P_Nested	[62]_TCAATAACCTTTGCCGAAACTG
	Msg5_P_Rv	[62]_gaatgcacaggtacacttgtttGGATCCCTTGGCGATCTAGTGAGTCAA
	Msg5_T_Fwd	[62]_taggggctgtataggtctcgGGATCCCCAAGGGAAGAAGTACGACAA
	Msg5_T_Nested	[62]_TGGAAAGAAGAAGGGCAGCAA
	Msg5_T_Rv	[62]_GCGGGAATCTATGCTTCATTG
neo	NeoF (gpdA9)	[62]_ccgcttgagcagacatcacaATGGGATCGGCCATTGAACAA
	NeoR (TrpC1)	[64]_cccgcggtcggcatctactTCAGAAGAACTCGTCAAGAAGG
	NeoG	[62]_TGCCCTGAATGAACTGCAAGA
	NeoY	[62]_CCAAGTTCTTCAGCAATATCAC
pacC	pacC-1F	[62]_CTCGGCGTTCTTATTTTCCTC
	pacC-1N	[62]_GCAGTAAACGGCAGTGAAAAG
	pacC-1R	[62]_tttacccagaatgcacaggtacacttgtttGACGGGAATAGAAGAGAATGC
	pacC-2F	[62]_tggtcgttgtaggggctgtattaggtctcgAGCTGCTGGTTTGGCTGTAC
	pacC-2N	[62]_AGGGAACTTACGAGAAACTGG
	pacC-2R	[62]_TAGGGGTAGATGGATTTGGTG
palH	palH-1F	[64]_AGTGCGGATGGCTGAGGTTC
	palH-1N	[64]_GCAACCGATGAACCGATGAAC
	palH-1R	[64]_tttacccagaatgcacaggtacacttgtttGAGGCAACACGCAACAGTATG
	palH-2F	[62]_tggtcgttgtaggggctgtattaggtctcgACTTAGCGAGGCGTTGTTTTC
	palH-2N	[62]_TGGGAAATATGGGGGACTTAC
	palH-2R	[62]_CTGATCGTTTGCCGTGTTTAG
pGEMT	M13F	[62]_CGCCAGGGTTTTCCCAGTCACGAC
	M13R	[62]_AGCGGATAACAATTTCACACAGGA
pHluorin	pHl Fwd ATG	[62]_ATGAGTAAAGGAGAAGAACTTTTC
	pHl TAA	[62]_tttacccagatgcacaggtacacttgtttTTATTTGTATAGTTCATCCATGCC
ptk2	Ptk2_1F	[62]_AGTATCTCGGGCTGTCCATC
	Ptk2_1N	[62]_AGTTTTTGGCGTTGTGTATCTG
	Ptk2_1R	[62]_tttacccagaatgcacaggtacacttgtttAAGTCGGGTGCTGAGAAATAG
	Ptk2_2F	[62]_tggtcgttgtaggggctgtattaggtctcgGATTGTGCGCCTATAACTTTTG
	Ptk2_2N	[62]_CACGCCCTTCTCTCATTCAC
	Ptk2_2R	[62]_AATCAGCCCTCCTACCTCTC
snf7	Snf7_P_Fwd	[62]_AACTTCCATTTCCACCTCAGC
	Snf7_P_Nested	[62]_ACAAGGAATTCGACACTGGAC
	Snf7_P_Rv	[62]_gaatgcacaggtacacttgtttGGATCCCTGATCGGTGAAGATTGGGG
	Snf7_T_Fwd	[62]_taggggctgtattaggtctcgGGATCCGCATTTAGTTGGTAGGGACTG

	Snf7_T_Nested	[62]_ACAGAGGATACGACAGAGGAA
	Snf7_T_Rv	[62]_GATAGTGAGATAAGTAGGATGG
vma7	Vma7_1F	[64]_TAAAGGGGATTCAGGGTGTTCT
	Vma7_1N	[64]_GATGTCCCAGTTGATGTGTAG
	Vma7_1R	[64]_tttacccagaatgcacaggtacacttgtttGTCCCTCTTGTTGTTGTTGATG
	Vma7-2F	[64]_tggtcgttgtaggggctgtattaggtctcgTGGAGCGAGCATGGTATAGAG
	Vma7-2N	[64]_CGAAGGACAATAGAGAGTAGAG
	Vma7_2R	[64]_CTATCGGCAAAGGTCAGCATG

3.5.2.4. Precipitation of DNA fragments and Southern blot probes

To purify and concentrate PCR products, these were routinely precipitated with ammonium acetate. Briefly, 1/10 volume of 3 M sodium acetate was added and carefully mixed. Two volumes of 100% cold-ethanol were added and samples were incubated at -20ºC for one hour. Precipitated DNA was then centrifuged at 13400 rpm for 30 minutes at RT. Pelleted DNA was washed with ethanol 70%, dried and finally resuspended with sterile ultrapure water.

DNA probes for Southern blot were precipitated with lithium chloride (LiCl). To 25 µl PCR product, 1/10 part of LiCl 8 M was added and carefully mixed. DNA was precipitated by adding 100% ice cold-ethanol (75 µl) and incubated 30 minutes at -20ºC. Precipitated DNA was then centrifuged at 13400 rpm for 30 minutes at 4ºC. Pelleted DNA was washed with ethanol 70%, dried and finally resuspended in 11 µl of sterile ultrapure water.

3.6 GENETIC TRANSFORMATION

3.6.1. Generation of *E. coli* transformants

3.6.1.1. Generation of competent cells

For preparation of *E. coli* DH5α competent cells, bacterial cells were streaked on LA plates and grown O.N. at 37°C. A single colony was then inoculated into 5 ml of PSI-b[4] medium and grown O.N. at 37°C with orbital shaking of 250 rpm. Grown culture was then used to inoculate 100 ml of fresh PSI-b (previously

warmed at 37°C). Cells were grown at 37°C with orbital shaking of 250 rpm, until reach an OD_{550} of 0.48. The culture was transferred to a centrifuge bottle, placed on ice for 5 minutes and centrifuged at 6000 rpm for 10 minutes at 4ºC. The supernatant was poured off and the pellet resuspended in 40 ml of cold Tfb-1[(5)] buffer. The centrifuge tubes were incubated on ice for 5 minutes and then centrifuged at 6000 rpm for 10 minutes at 4ºC. The pellet was finally resuspended in 4 ml of cold Tfb-2[(6)] solution and aliquots of 100 µl of cells prepared and stored at -80°C.

[(4)] PSI-b: 5 g/l yeast extract, 20 g/l bactopeptone and 5 g/l $MgSO_4.7H_2O$. Adjust the pH to 7.6 with KOH.
[(5)] Tfb-1: 30 mM potassium acetate pH 6.9, 50 mM $MnCl_2$, 100 mM KCl, 10 mM $CaCl_2$ and 15% glycerol (v/v).
[(6)] Tfb-2: 10 mM MOPS pH 7.0, 75 mM $CaCl_2$, 10 mM KCl and 15% glycerol (v/v).

3.6.1.2. Transformation of *E. coli*

For transformation of *E. coli*, 50 µl competent cells were combined with 10-100 ng of plasmid DNA. The mix was incubated on ice for 30 minutes, placed in a water bath at 42°C for 2 minutes and incubated again on ice for 5 minutes. Then, cells were incubated 10 minutes at RT and for selection of recombinants, cells were spread onto LA plates containing the appropriate antibiotics and incubated at 37°C O.N. For cells transformed with the pGEMT vector, the LA medium was supplemented with 134 µM isopropyl β-D-1-thiogalactopyranoside (IPTG; Apollo) and 0.005% (w/v) 5-bromo-4-chloro-3-indolyl β-D-galactorpyranoside (X-Gal; Sigma Aldrich) allowing the selection of ampicillin resistant strains, through the blue/white colonies.

3.6.2. Generation of *S. cerevisiae* transformants

3.6.2.1. Generation of yeast competent cells

Yeast competent cells were prepared following the instructions of the Yeastmaker™ Yeast Transformation System 2 manual (Clontech, USA), with few modifications. Briefly, a YPDA plate was streaked with the chosen yeast strain from a frozen yeast stock. The plate was incubated at 30ºC until isolated colonies appear (approximately 3 days). A single colony was inoculated in 3 ml YPD and incubated at 30°C with shaking at 200 rpm for 8 hours. 5 µl of this pre-culture was then transferred into 50 ml YPD and incubated on a shaker at 30°C O.N. (14-16 hours). When the OD_{600} reached 0.4-0.5, 50 ml culture were divided into two 50 ml sterile Falcon conical tubes and cells were centrifuged for 5 minutes at 3500 rpm at RT and each pellet resuspended with 8 ml of sterile water. Cells were centrifuged again and the pellet resuspended in 750 µl of fresh prepared 1.1xTE/LiAc[(7)] solution, split into two Eppendorf centrifuge tube, and centrifuged 15 seconds at 13400 rpm. Supernatants were discarded and each pellet was resuspended in 350 µl of 1.1xTE/LiAc solution and incubated on ice until transformation.

[(7)] 1.1xTE/LiAc solution: 1.1 ml of 10x TE buffer and 1.1 ml of 1M LiAc (10x), add sterile ultrapure water until 10 ml.

3.6.2.2. Transformation of yeast competent cells

Yeast transformation was performed accordingly with the instructions of the Yeastmaker™ Yeast Transformation System 2 manual (Clontech, USA), with few modifications. Briefly, in a pre-chilled Eppendorf tube was combined: plasmid DNA (approximately 100 ng), denatured carrier DNA (50 µg) and ultrapure sterile water for a final volume of 10 µl. Fresh prepared competent yeast cells (50 µl) were added and gently mixed by pipetting. Then, 450 µl of PEG/LiAc[(8)] were added, gently mixed with the cells, and incubated at 30ºC for 30 minutes, vortexing the samples every 10 minutes. Cells were treated with 20 µl of DMSO and incubated for 15 minutes more at 42ºC, mixing cells by vortexing every 5 minutes. Cells were

then centrifuged for 15 seconds at 13400 rpm at RT, and the pellet resuspended in 500 µl of ultrapure sterile water. 100 µl and 1/10 dilution of the transformation mix were spread on the appropriate selection media and incubated upside down at 30°C until colonies appear.

---

(8) PEG/LiAc solution: mix 8 ml of 50 % PEG 3350 with 1 ml 10x TE buffer and 1ml of 1M LiAc (10x).

3.6.3. Generation of *F. oxysporum* transformants

3.6.3.1. Generation of *F. oxysporum* protoplasts

Protoplasts were obtained following the protocol described by (Powell and Kistler, 1990), with minor modifications. Briefly, $5x10^8$ microconidia were inoculated in 200 ml of PDB for 14 hours at 28ºC and orbital shaking at 170 rpm. After O.N. incubation, germlings were harvested by filtration with a Monodur and carefully washed with OM(9). Washed germlings were then transferred to a sterile 50 ml Falcon tube, containing 0.5% (w/v) of the enzyme Glucanex® (Novozymes) dissolved in OM. The mix of germlings and enzyme was incubated for, at least, 1 hour at 30ºC with slow shaking (60 rpm). Protoplasts generation were monitored every 15 minutes, 45 minutes after start the incubation, in a microscope. When a high number of protoplasts was achieved, the reaction was stopped by adding ice-cold STC(10) solution to the 50 ml Falcon tube. Protoplasts were filtered through a double layer of Monodur filters and washed with 200 ml of STC. The flow-through containing the protoplasts was collected in pre-chilled Corex (Pyrex) centrifuge tubes. Samples were centrifuged at 3000 rpm for 15 minutes at 4ºC. Pelleted protoplasts were then carefully resuspended in 1 ml STC and counted. The protoplast suspension was adjusted to a final concentration of $3x10^8$ protoplasts/ml and stored as 100 µl aliquots in Eppendorf tubes to be used for transformation. For long-term storage at -80ºC, 10% of PEG(11) (v/v) and 1% DMSO (v/v) were added.

---

(9) OM: 1.2 M $MgSO_4$, 10 mM Na_2HPO_4, pH 5.8 adjusted with orthophosphoric acid.
(10) STC: 0.8 M sorbitol, 50 mM $CaCl_2$ and 50 mM Tris-HCl pH 7.5.
(11) PEG: 60% polyethylene glycol 4000 (p/v) in 0.6 M MOPS.

3.6.3.2. Transformation of *F. oxysporum* protoplasts

Transformation was performed as described (Malardier *et al*., 1989), with minor modifications. Briefly, in a pre-chilled Eppendorf tube were combined: transforming DNA (approximately 2 µg), aurintricarboxylic acid (ATA; Sigma Aldrich) (10 µl of a 0.1 M stock) and TEC[(12)] for a final volume of 60 µl. A control without DNA was also performed. Eppendorf tubes were incubated on ice for 20 minutes. In simultaneous, 100 µl protoplasts ($3x10^7$) were incubated on ice. Next, protoplasts and DNA were carefully mixed and incubated on ice for 20 minutes more. Finally, 160 µl of PEG were added, mixed carefully, and the mix was incubated for 15 minutes at RT. STC (1 ml) was added to the transformed cells and samples were centrifuged 5 minutes at 3000 rpm. Protoplasts were then resuspended in 200 µl of STC and 50 µl aliquots were mixed with 3 ml of top agar[(13)] and spread onto plates containing 25 ml of solid regeneration MM. Plates were incubated at 28ºC for 14 hours before addition of 3 ml of top agar containing 200 µg of hygromycin B or 100 µg of geneticin, respectively. Plates were then incubated until transformant colonies became visible which was in most cases achieved in 4-5 days. Colonies were transferred to PDA plates supplemented with the respective selective marker, and transformants were submitted to two consecutive rounds of single monoconidial purification on selective PDA plates.

---

(12) TEC: 10 mM Tris-HCl pH 7.5, 1 mM EDTA pH 8.0 and 40 mM $CaCl_2$.
(13) Top agar: 0.4% agar (Oxoid) (w/v) in regeneration MM.

3.6.3.3. Gene deletion mutant confirmation

For the confirmation of correct insertion of the deletion alleles constructed into the genome, genomic DNA of each transformant was extracted and analyzed by PCR and Southern blot. PCR was performed using pairs of primers located inside the selective marker and upstream or downstream of the insert. Southern blot analysis with gene-specific probes was performed as described (Di Pietro and Roncero, 1998) using the non-isotopic digoxigenin labelling kit for DNA labeling and detection (Roche Life Sciences).

3.7. WESTERN BLOT

3.7.1. Protein extraction and quantification in *S. cerevisiae*

For western blot analysis in *S. cerevisiae*, cells were grown O.N. in YPD medium at 30ºC and 200 rpm. Exponentially grown yeast cells were then washed and transferred to KSU buffer at pH 6.5. Cells were incubated at 30°C or 34°C, 200 rpm for one hour, and samples collected immediately after this period (time zero) and at different times after treatment. For western blot analysis, aliquots of 25 ml yeast culture were collected from each time-point. Samples were quenched by adding TCA (2% (v/v) final) and immediately chilled on ice. Quenched samples were harvested by centrifugation (5 minutes, 5000 rpm at RT) and resuspended in 1 ml of 10 mM sodium azide. Yeast cells were centrifuged again, the supernatant was removed and pellets were frozen at -80°C.

For protein extraction, frozen yeast pellets were thawed on ice and combined with 500 µl of ice-cold TCA buffer[14]. One half of the total volume of 0.5 mm glass beads (Sigma Aldrich) was added to each tube and cell membranes were disrupted by vortex mixing of the samples for 3 cycles of 1.5 minutes vortex and 0.5 minutes break on ice. Extracts were then incubated for 10 minutes on ice and precipitated proteins harvested by centrifugation at 13400 rpm for 10 minutes at 4°C. The supernatant was removed and the pellet resuspended in 75 µl of resuspension buffer[15], and heated to 95°C for 5 minutes. The denatured protein extracts were then centrifuged at 13400 rpm, 10 minutes to remove cellular debris, and the supernatants were transferred to a clean Eppendorf tube. The protein concentration in each protein extract was determined with the Bio-Rad *DC*™ Protein assay (Bio-Rad), using bovine serum albumin (BSA) as standard and following the instructions of the manufacturer.

---

[14] TCA buffer: 10 mM Tris pH 8.0, 10% (v/v) TCA, 25 mM NH_4OAc, 1 mM Na_2EDTA.
[15] Resuspension buffer: 100 mM Tris, 3% SDS and adjust the pH to 11.0 with 10 N NaOH.

3.7.2. Protein extraction and determination in *F. oxysporum*

For western blot analysis in *F. oxysporum*, $2.5x10^6$ spores/ml were germinated in YPD medium at pH 8.0 supplemented with 20 mM of HEPES pH 7.4, for 15 hours. Germinated microconidia were then washed, transferred to KSU buffer at pH 6.0 and incubated for one hour at 28ºC, 170 rpm. At the indicated time-points, samples of 10 ml ($2.5x10^7$ germlings) were quickly harvested by filtration through a Monodur in a vacuum filter system, and immediately chilled in liquid nitrogen. Frozen mycelia were thawed on ice and combined with 1 ml of fresh prepared lysis buffer[16]. Simultaneously to alkaline lysis, cellular disruption was achieved by mechanical homogenization using a T10 Ultra-Turrax (IKA). TCA (75 µl) was added to each sample to precipitate proteins, and samples were thoroughly mixed with the micropipette. Extracts were incubated for 10 minutes on ice, and precipitated proteins harvested by centrifugation at 13400 rpm for 5 minutes at 4°C. The supernatant was removed and the pellet resuspended in 100 µl of Tris-base 1 M and 200 µl 2X loading buffer[17]. Samples were heated at 95°C for 5 minutes and 10 µl of each sample was loaded into a Coomassie gel for determination of protein amounts.

---

[16] Lysis buffer: 200 µM NaOH 10 N and 0.2 % β-mercaptoethanol (v/v).
[17] Loading buffer: 20 mM Tris-HCl pH 6.8, 8% glycerol (v/v), 1.6 % SDS (w/v), 4% β-mercaptoethanol (v/v) and 0.1 % bromophenol blue (w/v).

3.7.3. Western blot

For western blot analysis in yeast, 40 µg protein was resuspended in protein loading buffer. For *F. oxysporum* extracts, the volume to load was determined by Coomassie gel. In both cases, proteins were separated in 10% Bis-Tris acrylamide[18] gels at 80 mV during the initial 40 minutes and 180 mV for one hour more, using Tris-HCl/glycine/SDS as running buffer[19]. The proteins in the gel were transferred to a nitrocellulose membrane (Bio-Rad) using the Trans-Blot® Turbo™ Transfer System RTA Transfer Kit (Bio-Rad) according to the instructions of the manufacturer. Membranes were blocked for 45 minutes in TBS-T[20] supplemented with 5% skim milk (w/v). Then membranes were incubated O.N. at 4ºC with the respective primary antibody. Membranes were washed three times with TBS-T for 10 minutes and incubated with the secondary antibody for 1 hour at RT. Membranes were washed three times more with TBS-T for 10 minutes. Proteins of interest were detected by chemioluminescence in a FujiFilm LAS 3000, after membrane staining with the ECL Select™ Western blotting Detection reagent (GE Healthcare, Amersham™).

Primary and secondary antibodies were prepared in TBS-T conjugated with 1% (w/v) BSA or 5% (w/v) skim milk, respectively. The primary and secondary antibodies used in this work as well as the concentration of antibodies and manufacturers are shown in [Table 8].

---

[18] 10% Bis-Tris acrylamide 1.0 mm gel (1 gel): Resolving gel is prepared by mixing: 4.25 ml deionized water, 2 ml LGB (1.5 M Trizma base and 0.4% SDS, dissolved in water and adjusted the pH to 8.8), 1.75 ml acrylamide (40%; 37.5:1), 10 µl tetramethylethylenediamine (TEMED) and 40 µl ammonium persulfate (APS) 10%. Stacking gel contains 3.25 ml deionized water, 1.25 ml UGB (0.5 M Trizma base and 0.4% SDS, dissolved in water and adjusted the pH to 6.8), 0.5 ml acrylamide (40%; 37.5:1), 10 µl TEMED and 30 µl APS 10%.

[19] Running buffer: 250 mM Trizma base, 1.92 M glycine and 1% (w/v) SDS.

[20] TBS-T: 202 mM Trizma base, 137 mM NaCl and 0.1% (v/v) Tween 20. Adjust the pH to 7.6.

Table 8 - List of antibodies and respective concentrations used in this study

ANTIBODY	ISOTYPE	DILUTION	MANUFACTURE (product code)
Anti-phospho-p44/42 (Thr202/Tyr204)	Rabbit IgG	1:3000	Cell Signaling (#4370)
Anti-phospho-p38 (Thr180/Tyr182)	Rabbit IgG	1:3000	Cell Signaling (#9211)
Anti-Mpk1 (yN-19)	Goat IgG	1:1500	Santa Cruz Biotechnology (SC-6802)
Anti-Fus3 (yN-19)	Goat IgG	1:1000	Santa Cruz Biotechnology (SC-6772)
Anti-*c*-Myc (9E10)	Mouse IgG	1:1000	Santa Cruz Biotechnology (SC-40)
Anti-α-tubulin	Mouse IgG	1:5000	Sigma Aldrich (T9026)
Anti-G6PDH	Rabbit IgG	1:50000	Cell Signaling (#A9521)
Anti-rabbit, HRP-linked	-	1:5000	Cell Signaling (#7074)
Donkey anti-goat, HRP-linked	-	1:5000	Santa Cruz Biotechnology (SC-2020)
Anti-mouse, HRP-linked	-	1:5000	Cell Signaling (#7076)

3.7.4. Western blot band intensity analysis

Protein hybridization band intensity was quantified with the Image J Software. Intensity of each band was normalized to the loading control, α-tubulin in *F. oxysporum* and G6PDH in yeast. For time-course analysis, band intensity was normalized to the time-point zero. For analysis of yeast Mpk1/Slt2 MAPK phosphorylation levels in acid-sensitive mutants, the ratio between time-point 20 min and zero (T20/T0) after Diethylstilbestrol (DES; Code: D4628; Sigma Aldrich) treatment was calculated. Yeast mutants with a ratio lower than 1.25 were considered to maintain phosphorylation of Mpk1 constant after DES treatment. Mutants with band intensities higher than 40000 at T0, were classified as hyperphosphorylated.

3.8. *IN VIVO* DETERMINATION OF INTRACELLULAR PH THROUGH THE GENETICALLY ENCODED PH SENSOR PHLUORIN

Yeast cells or *F. oxysporum* germlings were identically prepared for the determination of intracellular pH (pH_i). A calibration curve was obtained by incubating cells in different pH calibration buffers[21] ranging from 5.0 to 8.5, supplemented with freshly prepared nigericin (37 mg/ml; Sigma Aldrich) to permeabilize cells. 100 µl of permeabilized cells were added, in triplicate for each strain (expressing or not pHluorin), to wells in one half of a 96-well Microtiter™ Microplate. For pH_i analysis, test cells resuspended in 100 µl of KSU buffer were added in triplicate, for each strain (expressing or not pHluorin), to the wells in the other one half of the 96-well Microtiter™ Microplate, according to the scheme in [Figure 8].

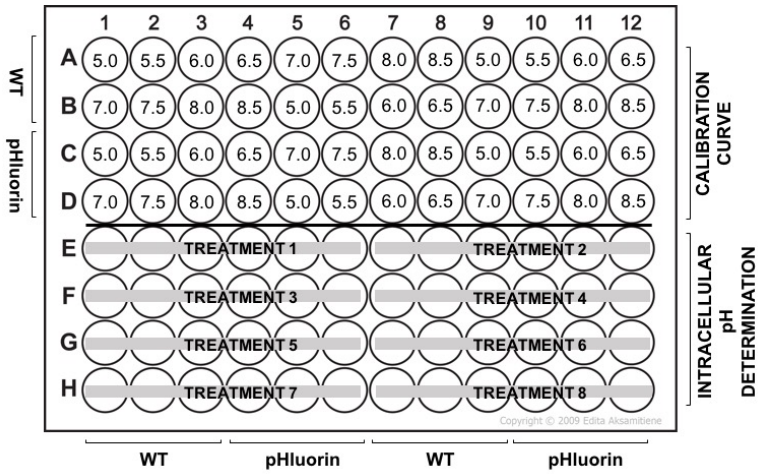

Figure 8 - Scheme of the cells distribution in a 96-well microtiter microplate for intracelular pH determination.

The plate was incubated for 30 minutes to allow nigericin to equilibrate the intra- and extracellular pH for the calibration curve and cells to adapt to the KSU buffer for analysis of pH_i. Fluorescence intensities after excitation at 395 and 475 nm on a spectrofluorometer (Infinite M200 PRO, TECAN Life Sciences, Switzerland) were recorded every 5 minutes for 30 minutes. After treatment with different compounds, fluorescence in cells incubated in KSU buffer was recorded for at least one hour

more. Ratios (395/475 nm) were calculated by first subtracting the background (wild type strain not expressing pHluorin) from each fluorescence value obtained in the wild type strain expressing pHluorin, as described in equation 1:

$$R_i\ (395/475) = (F_{395\ i} - F_{395\ background})/(F_{475\ i} - F_{475\ background})$$

R_i is the emission ratio at a given pH, F_{395nm} and F_{475nm} are the fluorescence intensities for a given pH, and $F_{405nm\ background}$ and $F_{475nm\ background}$ are average background fluorescence intensities for a given pH.

The ratio of fluorescence intensities was converted to pH_i values by fitting the following equation to the calibration curve:

$$pH = pK_a - \log_{10}\left[(R_i - R_{min})/(R_{max} - R_i)\right]$$

R_{max} and R_{min} are the limiting values for the ratio at the extreme acid (pH 5.0) and alkaline (pH 8.5) pH values, respectively, and pK_a the apparent pK_a value of the pHluorin fluorophore. All data are shown as the mean and standard deviation from at least three independent experiments, with three replicates each.

---

(21) Calibration buffer: 50 mM HEPES, 50 mM MES, 50 mM KCl, 50 mM NaCl, 0.2M $C_2H_7NO_2$, 10 mM NaN_3. Adjust the pH from 5.0 to 8.5, with 0.5 pH units steps.

3.8.1. Determination and manipulation of intracellular pH in yeast cells

To measure pH_i in *S. cerevisiae*, the wild type yeast strain was transformed with the pYEplac181 plasmid (2μ, amp^R, $LEU2^+$) containing the *pHluorin* gene under control of a *TEF1* promoter (a gift from Henrik G. Dohlman, University of North Carolina, USA). For pH_i analysis, the untransformed wild type and the wild type transformed with the pYEplac181 plasmid strains were grown in YPD at 30°C, with orbital shaking at 200 rpm O.N. until reaching an OD_{640} of 0.9. Cells were aliquoted to different Eppendorf tubes, collected by centrifugation at 5000 rpm for 5 minutes at RT and resuspended in KSU buffer at pH 6.5 or in the calibration curve buffers.

100 µl of cells were aliquoted into a 96-well Microtiter™ Microplate. The plate was pre-incubated 30 minutes at 30ºC and thereafter fluorescence intensities were measured as described above. After an additional 30 minutes, cells were treated with different chemical compounds and fluorescence was monitored for at least one hour more. For all pH measurements, the reported pH values correspond to the mean and standard deviation of at least three independent experiments, with three technical replicates each. In yeast, the effect of external pH on pH_i dynamics was tested by treating the cells with 21.7 mM hydrochloric acid (HCl) or $6x10^{-3}$ N sodium hydroxide (NaOH), which resulted in a change of pH of the buffer from 6.5 to 3.0 or 9.0, respectively. Pharmacological inhibition of Pma1 was achieved by treating cells with 25 µM DES, obtained by adding 0.25 µl of a 10 mM stock solution to each well. The solvent methanol was used as negative control.

3.8.2. Determination and manipulation of intracellular pH in *F. oxysporum*

For analysis of pH_i in *F. oxysporum*, the untransformed wild type strain and the wild type strain expressing the pH sensor pHluorin (Serrano, 2014), were used for background subtraction and pH_i determination, respectively. $2.5x10^6$ spores/ml were germinated in YPD medium at pH 8.0, supplemented with 20 mM HEPES pH 7.4, for 15 hours. Cultures were incubated at 28ºC, with orbital shaking at 170 rpm. Germinated microconidia were washed and resuspended in KSU buffer at pH 6.0, resulting in a concentration of approximately five times. A 96-well Microtiter™ Microplate was prepared by dispensing 80 µl of each calibration buffer, in triplicate. For the wells predetermined for pH_i determination, 80 µl of KSU pH 6.0 was added in triplicate. To each well, 20 µl of germlings of the untransformed wild type or the wild type expressing pHluorin were added in triplicate for each calibration buffer or experimental condition. Cell concentration in each well was adjusted to OD_{640} 0.5-0.7 in both strains before the start of the experiment. Cells in each well were resuspended by pipetting, and the plate was pre-incubated 30 minutes at 28ºC, 170 rpm. After that time, the fluorescence intensities were measured every 5 minutes for 30 minutes. After this time, cells were treated with different chemical compounds

and fluorescence was monitored for at least one hour more. For all pH_i measurements, the reported pH_i values correspond to the mean and standard deviation of at least three independent experiments with three technical replicates each. All chemicals tested were prepared as 10x stock solutions in sterile ultrapure water. Cells were treated with 0.25 µl of DES 200 mM (0.5 mM final concentration in the well) and a 372.8 mM stock of DES was prepared by dissolving it with methanol. The carbonyl cyanide-p-trifluoromethoxyphenylhydrazone (FCCP) (Code: S20357; Sigma Aldrich) was prepared at 1 mM concentration by dissolving it in DMSO and cells were treated with 6 µl (60 µM final concentration in the well). Cells were treated with methanol or DMSO as control. The external pH was changed by applying different concentrations of HCl or NaOH, as shown in [Table 9].

Table 9 – Concentrations of HCl and NaOH used to change the pH of KSU buffer in a microwell

Final pHex (from 6.0)	Stock solution	Final concentration
2.0	HCl 1.21 M	24.12 mM
3.0	HCl 0.12 M	19.3 mM
4.0	HCl 0.12 M	12.1 mM
5.0	HCl 0.12 M	4.8 mM
7.0	NaOH 0.1 N	$5x10^{-3}$ N
8.0	NaOH 0.1 N	$9x10^{-3}$ N
9.0	NaOH 0.1 N	$10x10^{-3}$ N

3.9. EXTRACELLULAR PH MEASUREMENTS

The fluctuations of the external pH were analyzed in the wild type strain of *F. oxysporum*. The pH was recorded every 30 seconds, using a conventional pH meter (HI2002-01; Hanna Instruments) coupled to a computer (kindly provided by Prof. José Ramos Ruiz, Department of Microbiology, University of Córdoba, Spain).

3.10. MEMBRANE ISOLATION FOR MEASUREMENT OF PMA1 ACTIVITY IN *F. OXYSPORUM*

The activity of the PM H^+-ATPase Pma1 was measured in the wild type strain of *F. oxysporum*, following a protocol based on phosphate generation by the ATPase hydrolytic activity, previously described in yeast cells (Kahm *et al.*, 2012) with minor modifications. For these experiments, $2.5x10^6$ spores/ml were germinated in YPD medium at pH 8.0, supplemented with 20 mM HEPES pH 7.4 for 15 hours. Germinated microconidia were washed and transferred to KSU buffer at pH 6.0 and incubated for one hour at 28ºC, 170 rpm. For each time-point of analysis, samples of 10 ml ($2.5x10^7$ germlings) were quickly harvested by filtration through a Monodur in a vacuum filter system, and immediately frozen in liquid nitrogen. For crude membrane purification, frozen mycelia were thawed on ice and combined with 250 µl KSU pH 6.0 and 250 µl of extraction buffer[22]. One half volume of 0.5 mm glass beads (Sigma Aldrich) was added and cells were broken by vortexing the Eppendorf tubes for three cycles of 2.5 minutes vortexing and 30 seconds break on ice. 900 µl of GTED20 buffer[23] were added to the crude extract, which was then centrifuged at 4ºC for 20 minutes at 2000 rpm. The supernatant of each sample was transferred to a new Eppendorf tube and centrifuged for an additional 20 minutes at 13400 rpm, 4ºC. The resulting pellet was resuspended in 75 µl GTED20 buffer and the samples were stored at -80ºC until protein determination. The protein concentration in each extract was determined with the Bio-Rad *DC*™ Protein assay (Bio-Rad), using BSA as standard and following the instructions of the manufacturer. Samples were adjusted to obtain 2 mg protein/ml. Activity assays were conducted in triplicate in a 96-well Microtiter™ Microplate. 3 µl of sample (6 µg total protein) was assayed in the presence of 1 µl methanol (solvent control) or 1 µl DES 0.8 mM (final concentration 0.2 mM). The plate was pre-incubated for 30 minutes at RT to allow DES inhibition of Pma1 activity. The reaction was then started by adding 65 µl of reaction buffer[24] to each well, followed by incubation for 40 minutes at 30ºC. The reaction was stopped by adding 130 µl of detection solution[25], and the plate was incubated at RT for 20 minutes before reading

absorbance at 750 nm in a spectrofluorometer (Infinite M200 PRO, TECAN Life Sciences, Switzerland). A calibration curve with serial dilutions of Na_2HPO_4 was performed in parallel. To calculate the specific Pma1 activity, the residual activity value obtained in the presence of DES (presumably corresponding to additional non-plasma membrane H^+-ATPases which are not inhibited by DES) was subtracted from the total activity (methanol). Pma1 activity was expressed in mmol/min/g protein assayed and was normalized to time-point zero in the time-course analysis.

---

(22) Extraction buffer: 0.3 M Tris-HCl pH 8.0, 180 mM KCl, 30 mM EDTA, 6 mM DTT (Sigma Aldrich) and Protease Inhibitor Cocktail (Roche Life Sciences).
(23) GTED20: 20% (v/v) glycerol, 10 mM Tris-HCl pH 7.6, 1 mM EDTA and 1 mM DTT (Sigma Aldrich).
(24) Reaction buffer: 50 mM MES-Tris pH 5.7, 5 mM $MgSO_4$, 50 mM KNO_3, 5 mM Na Azide, 0.3 mM ammonium molybdate (Sigma Aldrich), 2 mM ATP (Sigma Aldrich).
(25) Detection solution: 2% (v/v) sulphuric acid, 0.5% (w/v) ammonium molybdate (Sigma Aldrich), 0.5% (w/v) SDS, 0.1% (w/v) ascorbic acid.

3.11. VEGETATIVE GROWTH ASSAY

For phenotypic analysis of colony growth, drops of 2 µl of water containing $1x10^5$, $1x10^4$ or $1x10^3$ microconidia were spotted onto YPDA plates. The medium was buffered to pH 4.0 with 30.7 mM citric acid and 38.6 mM dibasic sodium phosphate; to pH 6.0 with 17.9 mM citric acid and 64.2 mM dibasic sodium phosphate and to pH 8.0 with 6 mM monobasic dihydrogen phosphate and 94 mM dibasic monohydrogen phosphate. For analysis of different hyperosmotic or cell wall stress, YPDA plates were supplemented with 0.6 M NaCl or 40 µg/ml CFW (Sigma), respectively. YPDA plates with CFW were buffered to pH 6.5 with 1% (w/v) MES. Plates were incubated at 28°C for 2 days and then imaged. All experiments included three replicates.

3.12. CELLOPHANE PENETRATION

The cellophane penetration assay was performed as previously described (Prados Rosales and Di Pietro, 2008). Cellophane sheets with the same size of a Petri dish

were cut, autoclaved in deionized water and placed on the center of PDA or Puhalla's MM plates buffered to pH 5.0 or 7.0 with 2% (w/v) of MES, avoiding the presence of bubbles. Drops of 5 µl of water containing $5x10^4$ microconidia were spotted onto the center of the plates, and plates were incubated at 28ºC for 2 or 3 days, respectively, for PDA or Puhalla's MM. Then, the cellophane sheet with the fungal colony was carefully removed and the plates incubated for more 24 hours at 28ºC. Plates were imaged before and after removal of the cellophane. All experiments included three replicates and were performed twice.

3.1.3. TOMATO ROOT INFECTION

Tomato root infection assays were performed in a growth chamber as described (Di Pietro and Roncero, 1998), using the susceptible cultivar Monika. Briefly, 2-week-old tomato seedlings were inoculated with *F. oxysporum* strains by immersing the roots in a microconidial suspension containing $5x10^6$ spores/ml, planted in vermiculite, and maintained in a growth chamber. Ten days after inoculation, the severity of disease symptoms and percentage survival were recorded daily for 30 days as previously described (López-Berges *et al*., 2012). Ten plants were used for each treatment. Survival was estimated by the Kaplan-Meier method and compared among groups using the log-rank test. Results were analyzed with the software GraphPad Prism 6.0.

3.14. CELL STAINING WTH FLUORESCENT DYES

For vacuolar pH determination in *F. oxysporum*, a similar protocol to the pH_i determination was established using the vacuole-specific dye BCECF-AM (2',7'-Bis-(2-Carboxyethyl)-5-(and-6)-Carboxyfluorescein, Acetoxymethyl Esther; SC Biotech). Briefly, microconidia were germinated for 15 hours and stained with 5 µM BCECF-AM (stock prepared at 1 mg/ml in DMSO) for 15 minutes in the dark with orbital shaking (170 rpm) at 28ºC. Unstained cells were also incubated and

used as control. Cells were then washed and resuspended in KSU buffer to remove the excess of dye, and incubated for one more hour at 28ºC. A calibration curve was obtained by incubating cells in different pH calibration buffers ranging from 5.0 to 8.5, supplemented with freshly prepared nigericin to permeabilize cells, as described in section 3.8 for pH_i determination. Vacuolar pH was determined by measuring fluorescence intensity after excitation at 440 and 490 nm (535 nm emission) in a spectrofluorometer and calculating the ratio of intensities at 490/440 nm. Ratios (490/440 nm) were calculated by first subtracting the background (unstained cells) from each fluorescence value obtained in stained cells with BCECF-AM and then by fitting the values to the standard curve to determine the vacuolar pH values, as described for the pH_i. Stained cells with BCECF-AM were also inspected by fluorescence microscopy to confirm BCECF vacuolar localization.

3.15.FLUORESCENCE MICROSCOPY

Wide-field fluorescence imaging was performed using a Zeiss Axio Imager M2 microscope equipped with a Photometrics Evolve EMCCD camera. To visualize fluorescence localization in the *F. oxysporum* wild type strain expressing pHluorin, samples were observed at different times of germination in YPD medium buffered to pH 7.4 with 20 mM HEPES. Vacuolar localization of BCECF-AM was verified in cells incubated in KSU buffer.

3.16.BIOINFORMATIC ANALYSIS

3.16.1. Sequence retrieval

The *F. oxysporum* orthologs of yeast proteins were identified by BLASTp search in FungiDB (The Fungal and Oomycete Genomics Resource, http://fungidb.org/fungidb/) using the *S. cerevisiae* protein sequences obtained from the Saccharomyces Genome Database (http://www.yeastgenome.org). Hits were considered putative orthologs when a score higher than 100 was obtained.

3.16.2. Protein alignment and sequence domains

Proteins alignment was made using the ClustalOmega software (http://www.ebi.ac.uk). Protein domains prediction was made using the Prosite database (ExPASy; http://prosite.expasy.org) and the SMART-EMBL website (http://smart.embl-heidelber.de). PEST domains were identified using the epestfind online software (http://emboss.bioinformatics.nl/cgi-bin/emboss/epestfind). Potential PEST domains were considered when a positive PEST score was obtained.

3.17.SOFTWARE AND ONLINE TOOLS

Data management and processing was performed using the following software products listed in [Table 10].

Table 10 – List of software and online tools used in this study

Program	**Application**
BioEdit	Multiple sequence alignment
Carl Zeiss Vision (AxioVision 4.7)	Microscope imaging and analysis
Endnote	Bibliography editing
Epson Scan	Image scanning
Fujifilm Image Reader	Chemiluminescence image acquisition
Image J	Image processing/ Western blot bands quantification
Kodak 1D Image Analysis	DNA gel imaging
Oligo 7	Synthetic oligonucleotides synthesis
GraphPad Prism Version 6.0	Graph creating and statistical analysis
OmniGraffle	Image illustration
SnapGene	Sequence editor
Online Software	**Application**
ClustalOmega	Multiple Sequence alignment
Epestfind	PEST domains
NCBI https://www.ncbi.nlm.nih.gov	BLAST: Sequence alignment Genome database: Retrieval of gene and protein sequences
SMART-EMBL	Protein domains search

4

RESULTS

INTRACELLULAR pH DYNAMICS AND HOMEOSTASIS IN *FUSARIUM OXYSPORUM*
INTRACELLULAR pH ACTS AS A SECOND MESSENGER FOR MAPK SIGNALLING IN *FUSARIUM OXYSPORUM*
ROLE OF KEY REGULATORS OF pH HOMEOSTASIS ON MAPK SIGNALING IN *F. OXYSPORUM*
YEAST AS A MODEL SYSTEM TO STUDY pH-INDUCED MAPK REGULATION IN *FUSARIUM OXYSPORUM*
COMPARATIVE ANALYSIS OF DES-TRIGGERED MAPK SIGNALING IN *FUSARIUM OXYSPORUM* AND *SACCHAROMYCES CEREVISIAE*

RESULTS

4.1. INTRACELLULAR PH DYNAMICS AND HOMEOSTASIS IN *FUSARIUM OXYSPORUM*

4.1.1. Fluorescence level analysis of the pH-sensor pHluorin in *F. oxysporum*

For measuring pH_i in living cells of *F. oxysporum*, the pH-sensitive variant of GFP, pHluorin was employed. Previously a wild-type strain expressing pHluorin was obtained in our group by co-transformation of protoplasts of the wild type strain of *F. oxysporum* f. sp. *lycopersici* 4287 with a cassette expressing the *pHluorin* gene under control of the strong constitutive *A. nidulans gpdA* promoter and the *trpC* terminator, and the *hygromycin* resistance (Hyg^R) cassette (Serrano, 2014). Hyg^R transformants were then screened by fluorescence microscopy for the fluorescence level of pHluorin, and a transformant (transformant #9) which presented the highest fluorescence intensity was selected for further studies. *In vivo* calibration demonstrated pH sensitivity and spectral characteristics, allowing the determination of pH_i in this transformant strain (Serrano, 2014).

We initially attempted to express the *pHluorin* gene in other *F. oxysporum* strains, such as isogenic deletion mutants. To this aim, protoplasts of these strains were transformed following the same experimental conditions as before (co-transformation of *pHluorin* and Hyg^R cassettes). However, we failed to obtain transformants with the same high intensity of fluorescence as observed in transformant #9. Similarly, co-transformation of the wild type strain with *pHluorin* and the *phleomycin* resistance ($Phleo^R$) cassettes also failed to produce transformants with the same high intensity of fluorescence as observed in transformant #9. Finally, we attempted a new approach in which the *pHluorin* gene was placed under control of the strong elongation factor 1-alpha (*tef-1*) promoter from *Neurospora crassa*. Fusion PCR of the *pHluorin* cassette with Hyg^R were performed, and the *pHluorin-*Hyg^R construct was specifically directed to a non-coding region of the genome of *F. oxysporum*. However, the fluorescence level of

the obtained transformants was still significantly lower than that in transformant #9. The low fluorescence level prevented to acquire a reliable calibration curve and, consequently, to determine the pH_i in the transformants. In an attempt to understand the low levels of fluorescence in the newly obtained transformants compared to transformant #9, a Southern blot was performed to determine the number of copies of the *pHluorin* gene in these strains. This revealed that transformant #9 carries more than one copy of the gene oppositely to a single copy in the other transformants, which explains the high level of fluorescence observed in this strain (data not shown). Therefore transformant #9 was used in the subsequent experiments for quantification of pH_i in *F. oxysporum*.

Time-lapse microscopy analyses revealed that pHluorin distribution inside the cells changed significantly during germination of microconidia and hyphal growth. In conidia and young hypha with 3-7 hours of germination, fluorescence was mainly detected in spherical structures, but largely absent from the cytosol [Figure 9]. By contrast, in hyphae germinated for 15 hours, fluorescence was mainly localized in the cytosol. We thus decided to use 15-hours-old hyphae for all subsequent experiments of pH_i measurements with transformant #9.

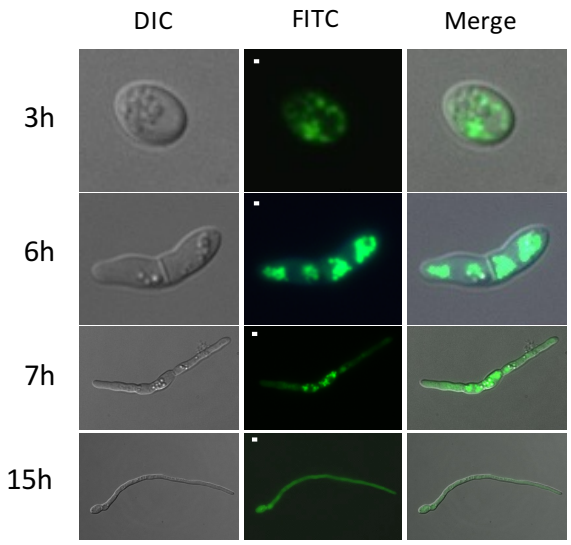

Figure 9 – Age-dependent distribution of pHluorin in *F. oxysporum* hyphae.
Microconidia of *F. oxysporum* expressing pHluorin were germinated in YPD medium and imaged by fluorescence microscope 3, 6, 7 and 15 hours after germination. Fluorescence localizes to spherical structures in young hyphae and to the cytosol in older hyphae. Bar, 10 μm.

4.1.2. *In vivo* calibration for determination of intracellular pH

After validation of pHluorin localization, pH_i measurements were made using a microwell reader coupled to a spectrofluorometer. This experimental approach allowed to simultaneously measure the fluorescence of 10^5 germlings per well and thus to follow rapid fluctuations of pH_i in the cell population. To obtain a pH_i calibration curve, cells were permeabilized with nigericin in the presence of buffers adjusted to different pH values. Fluorescence was measured and ratios of emission intensities were calculated after excitation at 395 nm and 475 nm. The obtained calibration curve displayed a linear response to pH values between 5.5 and 8.0 [Figure 10A]. The calculated pK_a of pHluorin was 6.9±0.1 [Figure 10B].

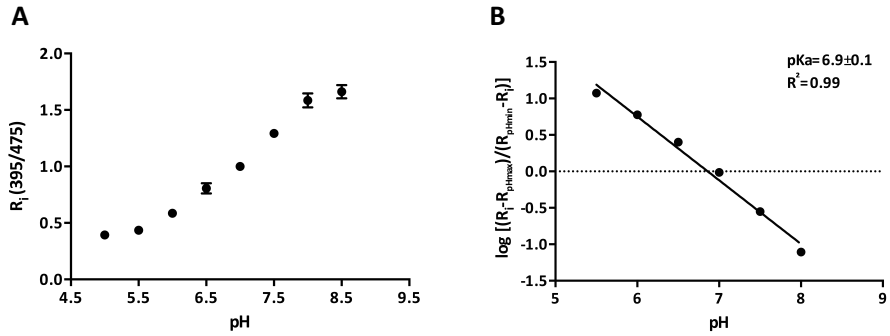

Figure 10 – *In vivo* calibration of pHluorin.
(A) Plot of the fluorescence excitation ratio (R_i) *versus* buffer pH. Fifteen-hour germinated microconidia of *F. oxysporum* expressing pHluorin were washed and suspended in pH-adjusted buffers, ranging from 5.0 to 8.5, containing nigericin to equalize the extracellular pH with the pH_i. Excitation at 395 nm and 475 nm was measured in a spectrofluorometer and the ratio between the two emission intensities collected both at 510 nm was calculated. All data are shown as mean and standard deviation from at least three independent experiments, with three independent replicates for each condition. **(B)** Logarithmic plot of the fluorescence excitation ratio *versus* buffer pH for determination of the constant pKa. R_{max} and R_{min} are the limiting values for the ratio at the extreme acid (pH 5.0) and alkaline (pH 8.5) conditions. R_i is the ratio determined in (A) for each pH.

4.1.3. Intracellular pH recovers rapidly in response to sudden shifts in external pH

To explore the effect of extracellular pH on pH_i dynamics, cells were initially maintained at pH 6.0, and then subjected to a sudden shift in extracellular pH ranging from a final value of 2.0 to 9.0 by adding different concentrations of diluted HCl or NaOH, respectively. Cells exposed to acidic pH shifts showed a rapid and transient acidification of the cytosol, while those subjected to extracellular alkalinization displayed a rapid and transitory increase of pH_i [Figure 11A]. In almost all tested conditions, the maximum fluctuation of pH_i was observed 6 minutes after the change in the external pH. Cells exposed to maximum external acidification (pH 2.0) showed a drop in pH_i of about one pH unit, while cells exposed to the most extreme alkaline condition (pH 9.0) displayed a rise in pH_i of approximately 0.5 units. These results demonstrated, that in response to extreme shifts in extracellular pH, the pH_i fluctuates within a range between 6.38±0.02 at pH

2.0 and 7.81±0.16 at pH 9.0 [Figure 11B]. Interestingly, one hour after the initial shift in external pH, pH_i had returned to homeostatic values ranging between 6.9 and 7.3. These results reveal the existence of a robust mechanism of pH_i homeostasis control in *F. oxysporum*, and suggest that the pH_i homeostasis is unaffected even after prolonged exposure of cells to extreme external pH [Figure 11C].

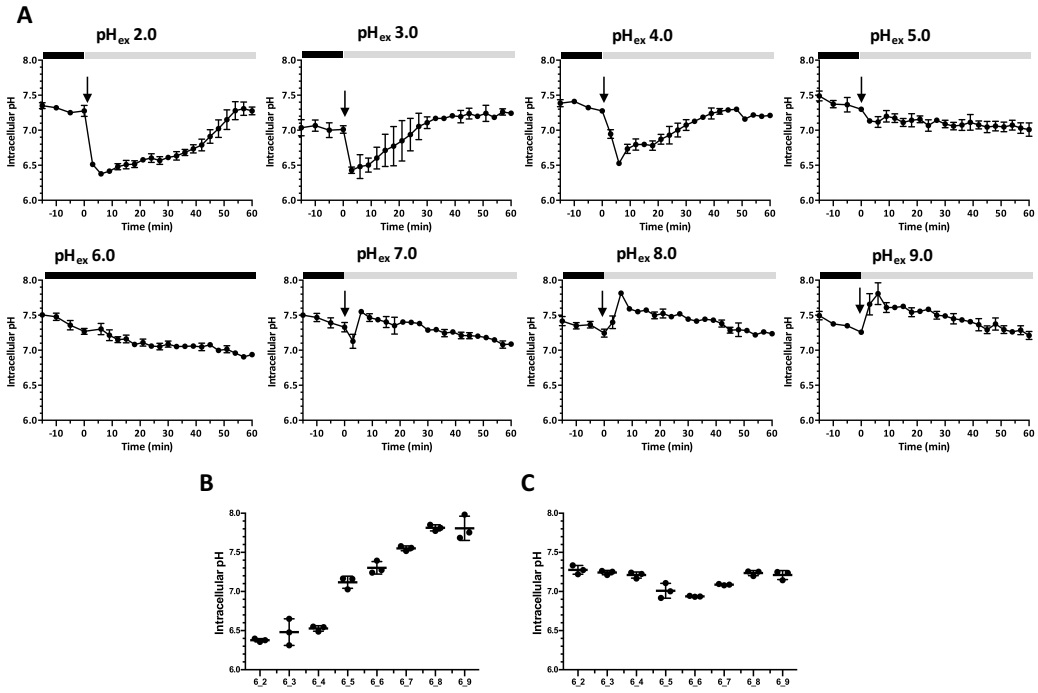

Figure 11 - Response of intracellular pH to sudden shifts in extracellular pH.
(A) Time course of pH_i after a sudden shift in extracellular pH. Fifteen-hour germinated microconidia were washed and suspended in KSU buffer at pH 6.0 and pre-incubated for 45 minutes at 28ºC. pH_i measurements were initiated 15 minutes before treatment. Extracellular pH in each well was subjected to sudden shifts ranging from a final value of 2.0 to 9.0 by adding different concentrations of diluted HCl or NaOH, respectively. pH_i was monitored every 3 minutes for 1 hour. For pH_i determination, the ratio between the emission intensities (collected at 510 nm) after excitation at 395 nm and 475 nm was calculated. Data shown represent the mean and standard deviation of one of three independent experiments, with three independent replicates for each condition. **(B)** pH_i values measured 6 minutes after the shift in extracellular pH are shown for each pH condition of (A), coinciding with the maximum amplitude of pH_i variation. **(C)** pH_i values measured one hour after the shift in extracellular pH are shown for each pH condition of (A). Note the remarkable capacity of pH_i homeostasis in *F. oxysporum*.

4.1.4. Carbon sources trigger intracellular pH fluctuations

In *S. cerevisiae,* an effect of glucose metabolism on pH_i dynamics has been described (Dechant *et al*., 2010; Isom *et al*., 2013). Moreover, 10 mM ammonium chloride also triggered changes in pH_i (Maresová *et al*., 2010). In *F. oxysporum*, directed hyphal growth towards carbon or nitrogen sources such as glucose or amino acids was reported, and was found to depend on the IG MAPK cascade (Turrà *et al*., 2015). Here we investigated the effect of different carbon and nitrogen sources on pH_i of *F. oxysporum*. We found that addition of 110 mM glucose to the medium induced a rapid drop in pH_i of approximately 0.8 units, followed by a partial recovery. Other sugars such as galactose, fructose or xylose, also induced a decrease of pH_i, followed by partial recovery and stabilization at approximately 7.0. Glucose induced a stronger acidification of the cytosol (to approximately 6.5) compared to the other sugars tested. Moreover, glucose-treated cells showed the fastest recovery of pH_i starting after 3 minutes, while cells treated with galactose, fructose or xylose needed at least 9 minutes [Figure 12A]. Inorganic nitrogen sources such as ammonium chloride, sodium nitrate and ammonium nitrate at 10 mM failed to show a significant effect on pH_i dynamics [Figure 12B]. However, amino acids such as sodium glutamate or sodium aspartate induced a rapid drop on pH_i of approximately 0.8 units [Figure 12C]. Importantly, addition of these compounds did not trigger a significant change in the extracellular pH (data not shown).

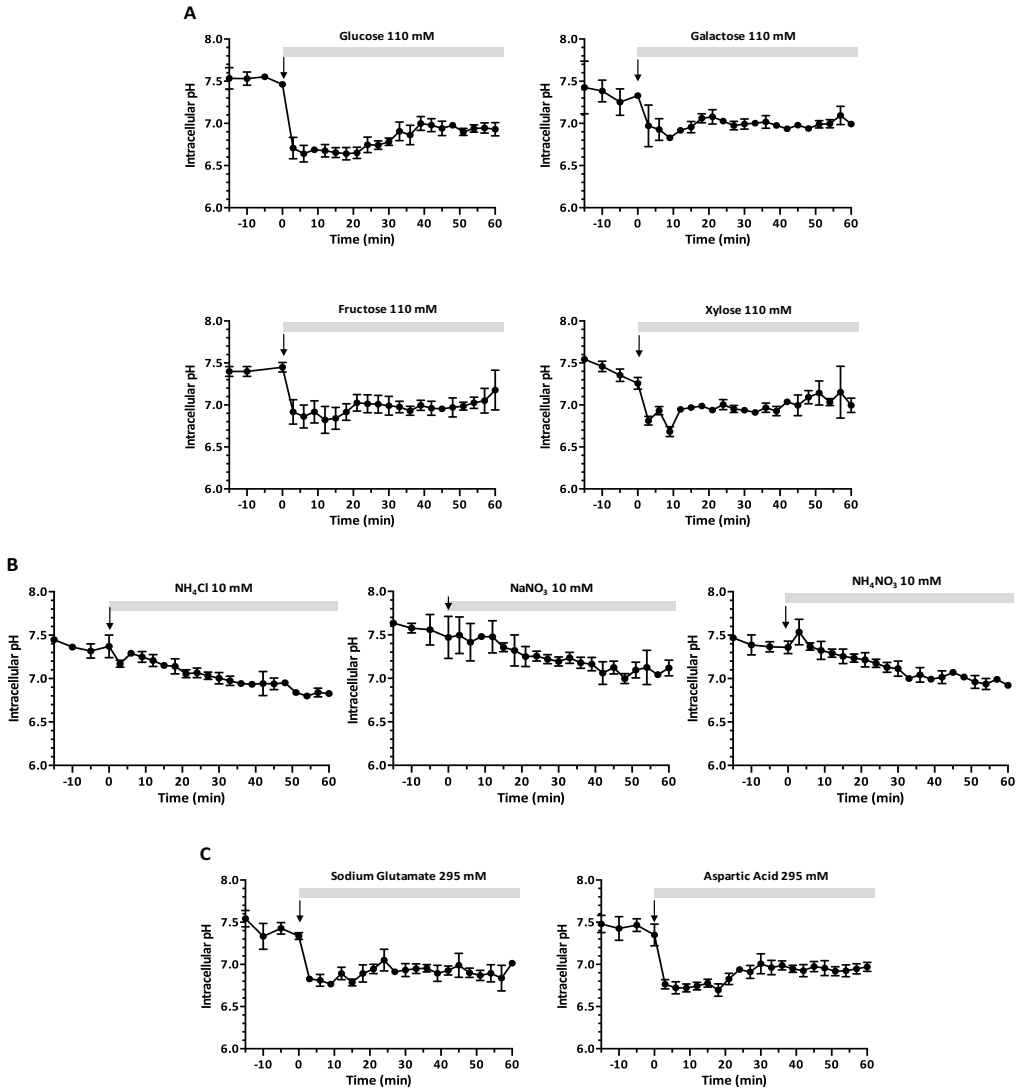

Figure 12 – Effect of carbon and nitrogen sources in intracellular pH.
(A) Fifteen-hour germinated microconidia were washed and suspended in KSU buffer at pH 6.0 and pre-incubated for 45 minutes at 28ºC. pH_i measurements were initiated 15 minutes before treatment. At time 0, different sugars **(A)**, inorganic nitrogen sources **(B)**, or amino acids **(C)** were added and pH_i was monitored every 3 minutes for 1 hour. For pH_i determination, the ratio between the emission intensities (collected at 510 nm) after excitation at 395 nm and 475 nm was calculated. Data shown represent the mean and standard deviation of one of three independent experiments, with three independent replicates for each condition.

4.2. INTRACELLULAR PH ACTS A SECOND MESSENGER FOR MAPK SIGNALING IN *FUSARIUM OXYSPORUM*

4.2.1. Extracellular pH affects MAPK phosphorylation status in *Fusarium oxysporum*

External pH governs infectious growth in the plant pathogen *F. oxysporum* by reprogramming the phosphorylation level of the MAPK Fmk1 (Masachis *et al.*, 2016). Previous results in our group indicated that external pH also affects phosphorylation status of the two other MAPKs identified in *F. oxysporum,* Mpk1 and Hog1 (Segorbe, 2014). Because in the present study a new experimental approach had been designed for measurement of pH_i, we decided to re-evaluate the impact of extracellular pH on MAPK phosphorylation under the new experimental conditions. We found that Fmk1 was rapidly phosphorylated when pH increased to a value higher than 6.0, and dephosphorylated when pH decreased below 6.0. Conversely, Mpk1 was rapidly phosphorylated upon extracellular acidification and dephosphorylated upon alkalinization [Figure 13]. These results confirmed those obtained in previous experiments (Segorbe, 2014) and suggested that, independently of the experimental condition, extracellular pH regulates MAPK activity in *F. oxysporum*.

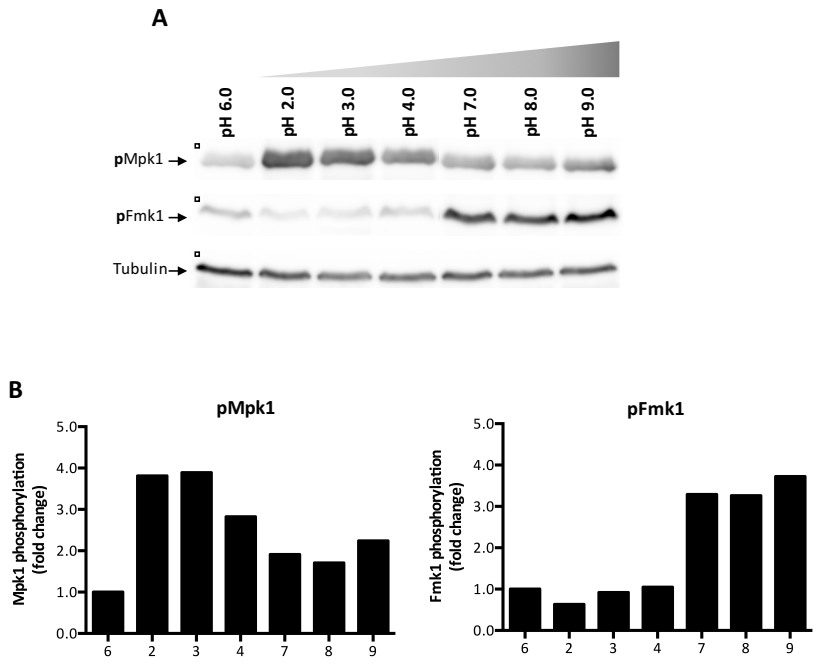

Figure 13 - MAPK phosphorylation is affected by shifts in ambient pH.
(A) Mpk1 phosphorylation is induced at acidic pH while the Fmk1 phosphorylation is induced at neutral or alkaline pH. *F. oxysporum* conidia were germinated in YPD medium for 15 hours, collected, washed and resuspended in KSU buffer at pH 6.0. Ambient pH was subjected to a sudden downshift to a final value of 2, 3 or 4, or a sudden upshift to 7, 8 or 9 by adding different concentrations of diluted HCl or NaOH, respectively. Total protein extracts collected before (control at pH 6.0) or 5 minutes after the pH shift were subjected to immunoblot analysis with anti-phospho-p44/42 MAPK antibodies for pMpk1 and pFmk1 detection. Anti-tubulin antibody was used as loading control. **(B)** Graphs show the ratio of pMpk1 or pFmk1 band intensity normalized to tubulin and expressed as fold response compared with control at pH 6.0.

4.2.2. Establishment of an experimental system to change intracellular pH through a mechanism independent of extracellular pH

The molecular events underlying the regulation of MAPK activity in response to ambient pH are currently unknown. Because our previous data revealed that ambient pH affects pH_i homeostasis in a rapid and transitory way (see Figure 11), we asked whether pH_i could act as a second messenger for MAPK activity. To test this idea, we set out to design an experimental system allowing manipulation of pH_i independently of extracellular pH. In another study, chemical inhibition of the plasma membrane (PM) H^+-ATPase or depolarization of the plasma membrane had been used successfully to manipulate pH_i in fungi (Bagar *et al*., 2009).

4.2.2.1. DES, a specific inhibitor of plasma membrane H^+-ATPase (Pma1), induces prolonged intracellular acidification

The PM H^+-ATPase (Pma1) has been described as the main regulator of pH_i in fungi (Kane, 2016). Exogenous application of DES, a specific inhibitor of Pma1, was previously reported in *Saccharomyces cerevisiae* (Kahm *et al*., 2012; Moskvina *et al*., 1999). Here we tested the effect of different concentrations of DES, ranging from 0.25 to 2.5 mM, on pH_i of *F. oxysporum*. Addition of DES to the germlings induced a rapid and sustained intracellular acidification. With all concentrations, the pH_i dropped from 7.20±0.13 to 6.37±0.05 in only 15 minutes, with the major part of the drop occurring within the first 5 minutes. No recovery of pH_i to the baseline was observed during one hour [Figure 14A]. This suggests that DES is highly effective in *F. oxysporum* Pma1 inhibition, and that Pma1 acts as a major regulator of pH_i homeostasis in this species [Figure 14A]. Importantly, addition of methanol (the solvent of DES) had no effect on pH_i (data not shown). To confirm that the observed drop in pH_i was not a consequence of external pH change, we monitored the effect of DES on extracellular pH, with measurements taken every 30 seconds.

We saw that DES addition to the medium made the extracellular pH constant [Figure 14B].

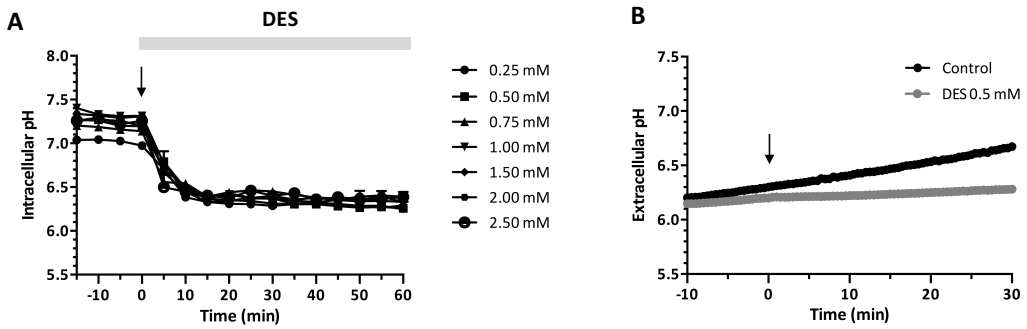

Figure 14 – The Pma1 inhibitor DES triggers rapid and sustained intracellular acidification.
Fifteen-hour germinated microconidia were washed and suspended in KSU buffer at pH 6.0 and pre-incubated for 45 minutes at 28ºC. **(A)** pH_i measurements were initiated 15 minutes before treatment. At time 0, DES was added at the indicated concentrations and fluorescence was measured every 5 minutes for 1 hour. For pH_i determination, the ratio between the emission intensities (collected at 510 nm) after excitation at 395 nm and 475 nm was calculated. Data shown represent the mean and standard deviations of one of three independent experiments, with three independent replicates. **(B)** Extracellular pH was measured over time in the absence (control) or presence of 0.5 mM DES.

4.2.2.2. The membrane uncoupler FCCP equilibrates pH gradients across plasma membrane and causes a rapid decrease of intracellular pH

As a second approach to manipulate pH_i independent of extracellular pH changes, we tested different concentrations of FCCP, a protonophore which has been described to act as an uncoupler of oxidative phosphorylation (Bagar *et al*., 2009). A rapid and dose-dependent effect on pH_i was observed for FCCP, but not for DMSO (the solvent of FCCP) [Figure 15A]. At the highest concentration tested (60 µM), pH_i decreased from 7.2 to approximately 6.0, which equals the pH of the external KSU buffer medium [Figure 15A]. As with DES, no recovery of pH_i homeostasis was observed within 1 hour of treatment. Moreover, no effect of FCCP on extracellular pH was detected when compared with the control [Figure 15B].

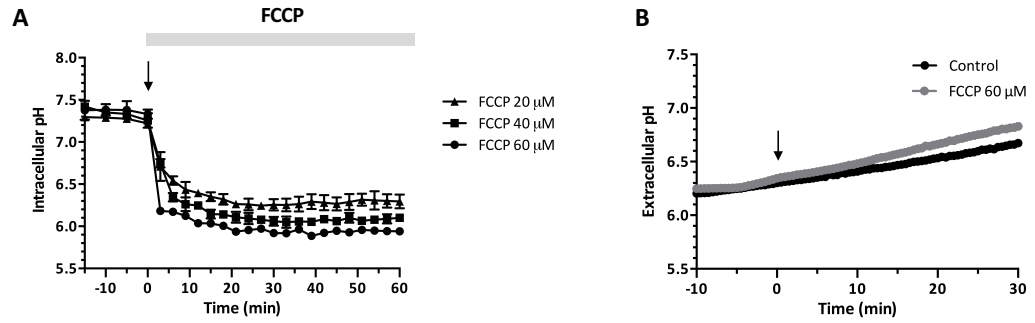

Figure 15 – The membrane uncoupler FCCP applied in KSU triggers rapid and sustained intracellular acidification.
Fifteen-hour germinated microconidia were washed and suspended in KSU buffer at pH 6.0 and pre-incubated for 45 minutes at 28ºC. **(A)** pH_i measurements were initiated 15 minutes before treatment. At time 0, FCCP was added at the indicated concentrations and fluorescence was measured every 5 minutes for 1 hour. For pH_i determination, the ratio between the emission intensities (collected at 510 nm) after excitation at 395 nm and 475 nm was calculated. Data shown represent the mean and standard deviations of one of three independent experiments, with three independent replicates. **(B)** Extracellular pH was measured over time in the absence (control) or presence of FCCP 60 µM.

4.2.3. Pma1 activity controls intracellular pH in *Fusarium oxysporum*

DES has been described as a specific inhibitor of Pma1 in *S. cerevisiae* (Kahm *et al.*, 2012; Moskvina *et al.*, 1999). However, no studies in filamentous fungi have been performed so far using this compound. The rapid intracellular acidification induced by DES suggested that it also inhibits Pma1 in *F. oxysporum*. To confirm this, we measured the ATPase activity of Pma1 in this fungus using a method previously established for *S. cerevisiae* (Kahm *et al.*, 2012), with few modifications. Briefly, ATPase hydrolytic activity of Pma1 was determined by subtracting the activity obtained in the presence of DES (presumably corresponding to additional non-plasma membrane H^+-ATPases which are not inhibited by DES) from total activity.

4.2.3.1. DES induces intracellular acidification through complete inhibition of the activity of Pma1

To explore the effect of DES on Pma1 activity, membranes were isolated from 15 hours germinated microconidia before and at different times after treatment with 0.5 mM DES. Samples were collected every 5 minutes during 15 minutes, and ATPase activity was measured. DES caused a drastic inhibition of Pma1 activity in *F. oxysporum* [Figure 16]. In membranes isolated 5 minutes after DES treatment, Pma1 activity was almost null, showing a drop from 1 (time-point zero) to 0.085±0.014. The activity of Pma1 did not recover during the 15 min of the experiment, and a slight decrease in the last time-point analyzed (0.036±0.021) was even detected. Importantly, the solvent control (methanol) had no significant effect on Pma1 activity [Figure 16].

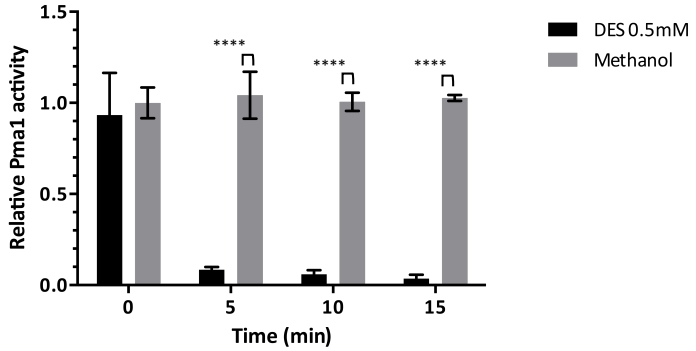

Figure 16 – DES inhibits the activity of the plasma membrane H^+-ATPase Pma1.
Time-course analysis of Pma1 activity in the presence of 0.5 mM DES or methanol (solvent of DES used as control). ATPase activity was assayed in total membranes isolated from 15-hours germinated microconidia of *F. oxysporum*. Activity was normalized to that of the time-point zero. Results represent the average and standard deviation of three independent measurements at each time-point and essentially identical results were observed in three separate experiments. ****p<0.0001, DES *versus* methanol, according to two-way ANOVA and Bonferroni Test.

4.2.3.2. FCCP does not affect the activity of Pma1

To investigate the effect of FCCP on Pma1 activity, membranes were isolated before and after FCCP treatment and ATPase activity was determined. In the presence of 60 µM FCCP the activity of Pma1 was not affected suggesting that the effect of FCCP on proton conductivity of the PM does not affect the activity of Pma1 [Figure 17].

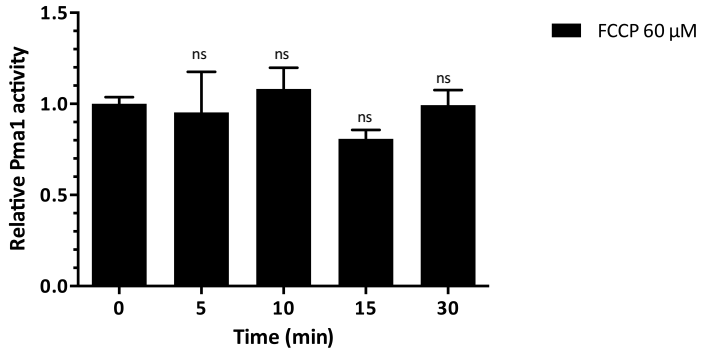

Figure 17 – The membrane uncoupler FCCP has no direct effect on the activity of Pma1.
Activity of Pma1 was assayed in total membranes isolated from 15-hours germinated microconidia of *F. oxysporum*. Time-course analysis of ATPase activity in the presence of 60 µM FCCP. Activity was normalized to that of time-point zero. Results represent the average and standard deviation of three independent measurements at each time-point, and essentially identical results were observed in three separate experiments. ns = non-significant, $p<0.001$; *versus* T0 according to one-way ANOVA and Bonferroni Test.

4.2.3.3. Extracellular pH and glucose regulate Pma1 activity

Our previous data showed that sudden changes in extracellular pH or addition of sugars such as glucose trigger rapid and transitory fluctuations in pH_i (see Figure 11 and 12). The mechanism underlying these pH_i variations is not understood. Here we examined the effect of extracellular pH shifts or glucose addition on Pma1 activity. When the pH of the buffer medium was dropped from 7.0 to 5.0, Pma1 activity decreased drastically 15 minutes after extracellular acidification and only recovered slightly after 30 minutes [Figure 18A]. When the extracellular pH was shifted back

from 5.0 to 7.0, the activity of Pma1 increased and reached 0.860±0.071, almost the same as before the external acidification [Figure 18A].

Glucose treatment first triggered a rapid reduction of Pma1 activity of about 50%, followed by a recovery after 10 minutes, reaching the initial activity after 30 minutes [Figure 18B]. Altogether, these results demonstrate that pH_i dynamics mirrors, at least in part, the activity of Pma1, suggesting a key role for this proton pump on pH_i homeostasis control.

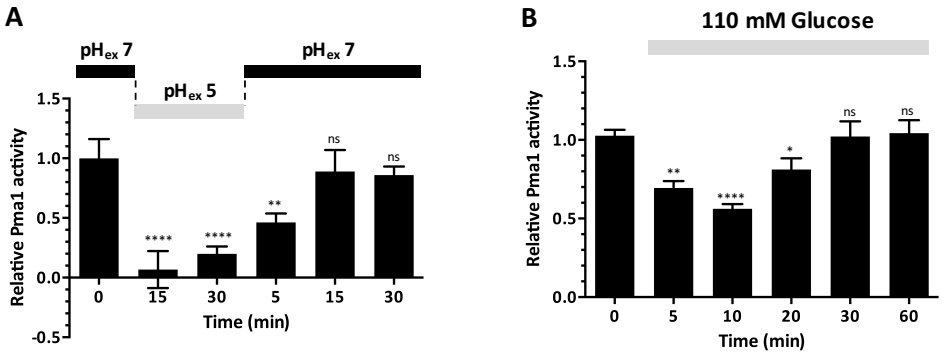

Figure 18 – Shifts in extracellular pH and addition of glucose impact Pma1 activity. Activity of Pma1 was assayed in total membranes isolated from 15-hours germinated microconidia of the wild type strain of *F. oxysporum*. **(A)** Time-course analysis of Pma1 activity upon a shift in extracellular pH from 7.0 to 5.0 and back to 7.0. ATPase activity was determined at the indicated times. **(B)** Time-course analysis of Pma1 activity before and after addition of 110 mM glucose. **(A, B)** The graphs show the activity of Pma1 normalized to that of the time 0. Results represent the average and standard deviation of three independent measurements at each time-point. ns = non-significant $p<0.001$; **** $p<0.0001$; ** $p<0.01$; * $p<0.05$; *versus* T0 according to one-way ANOVA and Bonferroni Test.

4.2.4. DES- and FCCP-triggered intracellular acidification affects MAPK phosphorylation in *F. oxysporum*

In order to understand the role of pH_i in regulation of MAPK activity, MAPK phosphorylation was analyzed by western blot after treatment of germlings with DES or FCCP to induce a drop in pH_i. We found that DES triggered a marked increase (more than 8 times) in the phosphorylation levels of Mpk1 and Hog1. By contrast, the phosphorylation level of Fmk1 decreased approximately 30% upon DES treatment [Figure 19].

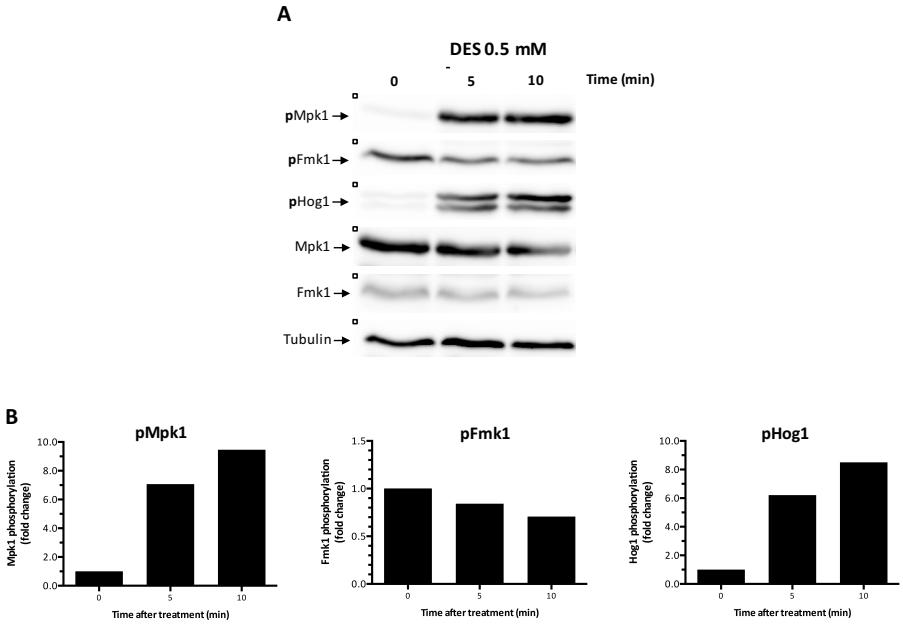

Figure 19 - DES-triggered intracellular acidification activates Mpk1 and Hog1 and inhibits Fmk1.
(**A**) Fifteen-hour germinated microconidia were washed and resuspended in KSU buffer at pH 6.0 and pre-incubated for 1 hour at 28ºC. At time 0, 0.5 mM DES was added to the buffer. Protein extracts collected before (time 0) and 5 or 10 minutes after DES treatment were subjected to immunoblot analysis with anti-phospho-p44/42 MAPK or anti-phosho-p38 MAPK antibodies, for pMpk1 and pFmk1, or pHog1 detection, respectively. Anti-Mpk1 and anti-Fus3 (Fmk1) antibodies were used for MAPK loading control, and anti-tubulin antibody was used as total extract loading control. **(B)** Graphs show the ratio of pMpk1, pFmk1 or pHog1 band intensity normalized to tubulin and expressed as fold response compared with untreated cells (time zero).

Likewise, FCCP triggered rapid phosphorylation of Mpk1 and Hog1 and dephosphorylation of Fmk1 [Figure 20]. In all cases, the pattern of MAPK phosphorylation in response to DES- and FCCP-induced intracellular acidification was consistent with that triggered by extracellular acidification. These results suggest that changes in pH_i directly affect MAPK activity in *F. oxysporum*.

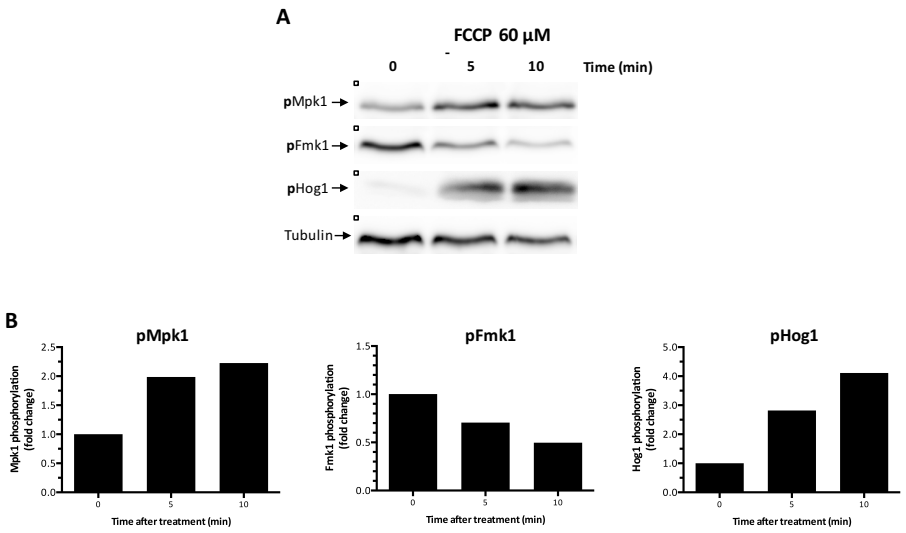

Figure 20 – The membrane uncoupler FCCP applied in KSU activates Mpk1 and Hog1 and inhibits Fmk1.
(A) Fifteen-hour germinated microconidia were washed and resuspended in KSU buffer at pH 6.0 and pre-incubated for 1 hour at 28ºC. At time 0, 60 µM FCCP was added to the buffer. Protein extracts collected before (time 0) and 5 or 10 minutes after FCCP treatment were subjected to immunoblot analysis with anti-phospho-p44/42 MAPK or anti-phosho-p38 MAPK antibodies, for pMpk1 and pFmk1, or pHog1 detection, respectively. Anti-tubulin antibody was used as total extract loading control. **(B)** Graphs show the ratio of pMpk1, pFmk1 or pHog1 band intensity normalized to tubulin and expressed as fold response compared with untreated cells (time zero).

4.3. ROLE OF KEY REGULATORS OF PH HOMEOSTASIS ON MAPK SIGNALING IN *F. OXYSPORUM*

Our previous results demonstrated that pH_i acts as a second messenger for MAPK signaling in *F. oxysporum*. First, we found that a shift in the external pH triggers a rapid and transient change in the pH_i. Further, we found that DES induced sustained drop in pH_i is accompanied by changes in MAPK phosphorylation, supporting the idea that pH_i acts as a key switch controlling MAPK activity. Expecting that defects on pH_i homeostasis control will impact MAPK signaling, we generated knockout mutant strains of possibly relevant regulators of pH_i homeostasis in *F. oxysporum*. Targeted deletion of the PM pH-sensor PalH and of the transcription factor PacC, components of the alkaline pH-response Pal/Rim pathway, as well as of Ptk2, a kinase that promotes Pma1 activation in response to glucose, were generated in *F. oxysporum*. With this approach, we aimed to genetically validate the role of pH_i in MAPK signaling regulation.

4.3.1. Generation of deletion mutants

4.3.1.1. Targeted deletion of *pacC* and *palH*, two key components of the Pal pathway in *F. oxysporum*

The Pal/Rim pathway is arguably the best-studied mechanism of environmental pH sensing and response in fungi. Neutral-alkaline pH is sensed by the seven-transmembrane-domain receptor PalH/Rim21 located at the PM. This results in activation of the downstream signaling pathway which culminates with the proteolytic activation of the transcription factor PacC/Rim101 and its translocation to the nucleus where it governs transcriptional changes that promote neutral-alkaline pH-dependent responses (Peñalva *et al*., 2008). Although Pal/Rim pathway has been extensively described for fungal response to external pH changes, a role of this pathway in pH_i homeostasis control has not been reported so far.

PacC of *F. oxysporum* (FOXG_02222) was previously identified and a PacC loss-of-function mutant constructed (Caracuel *et al*., 2013). Here, to investigate in more detail the role of PacC in pH_i homeostasis control in *F. oxysporum*, we generated a Δ*pacC* allele by replacing the complete ORF with the Hyg^R resistance cassette [Figure 21A]. The two split-marker deletion constructs obtained by fusion PCR were used to co-transform protoplasts of the *F. oxysporum* wild type strain. Transformants carrying a homologous insertion at the *pacC* locus were initially identified by PCR analyses using two pairs of primers that hybridize outside of the fragments used for transformation and inside of the resistance cassette [Figure 21B]. Further analysis of the selected candidate transformants was performed by Southern blot to verify the correct insertion of a single copy into the genome. We identified three transformants in which the 9.5 Kb hybridizing *Nde*I fragment corresponding to the wild type *pacC* allele had been replaced by a hybridizing fragment of the expected size of 4.3 Kb, consistent with homologous insertion of the deletion construct in these transformants [Figure 21C].

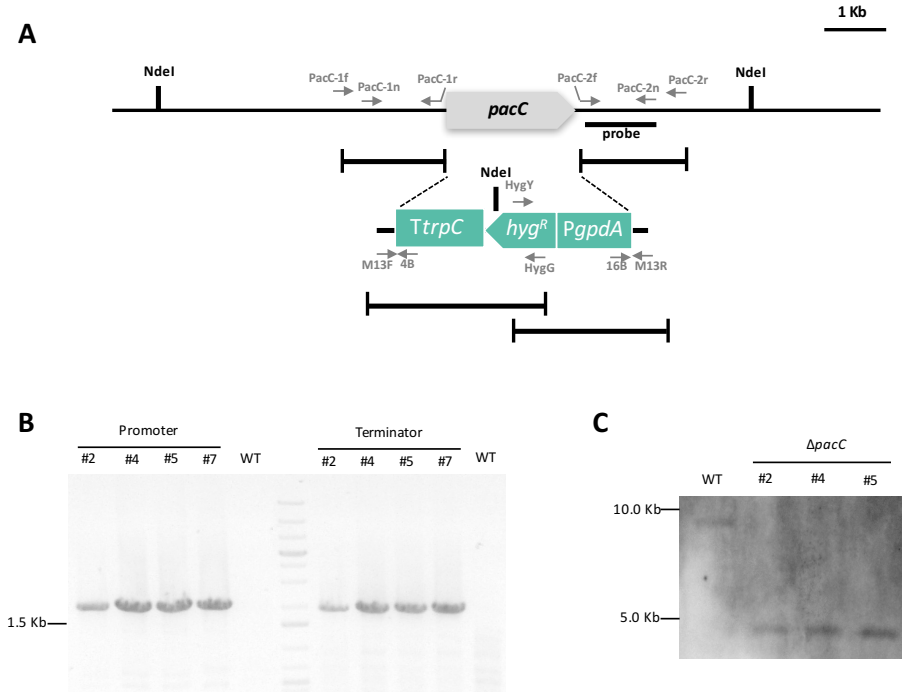

Figure 21 – Targeted deletion of the *F. oxysporum pacC* gene.
(A) Physical maps of the *pacC* locus and the split-marker gene replacement construct obtained by fusion PCR (Δ*pacC* allele). Relative positions of the primers used for generation of the gene disruption construct and PCR analyses of the transformants, as well as the probe used for Southern blot are indicated. **(B)** PCR analyses for homologous integration of the gene disruption construct into the genome of the transformants. Genomic DNA of the wild type strain (negative control) and transformants was amplified using the pairs of primers: PacC-1f/TrpC-4B (promoter region) and GpdA16B/PacC-2r (terminator region). **(C)** Southern blot hybridization analysis of the wild type strain 4287 and the different Δ*pacC* transformants. Genomic DNA treated with *Nde*I was hybridized with the probe indicated in (A).

A BLASTp search of the *F. oxysporum* genome sequence with the *S. cerevisiae* Rim21 sequence identified a single PalH ortholog (FOXG_09368). The *F. oxysporum* PalH is a predicted protein of 779 amino acids which exhibits 24% identity with yeast Rim21 and more than 50% with PalH proteins from the filamentous ascomycetes *N. crassa* (NCU_0007), *M. oryzae* (MGG_06440) or *A. nidulans* (AN_6886).

To investigate the biological relevance of PalH in *F. oxysporum*, we generated a Δ*palH* allele by replacing the complete ORF with the *Hyg*^{R} resistance cassette [Figure 22A]. The two split-marker deletion constructs obtained by fusion PCR

were used to co-transform protoplasts of the *F. oxysporum* wild type strain. Transformants carrying a homologous insertion at the *palH* locus were initially identified by PCR analyses using two pairs of primers that hybridize outside of the fragments used for transformation and inside of the resistance cassette [Figure 22B]. Further analysis of the selected candidate transformants was performed by Southern blot to verify the correct insertion of a single copy into the genome. We identified two transformants in which the 2.4 Kb hybridizing *Xho*I fragment corresponding to the wild type *palH* allele had been replaced by a hybridizing fragment of the expected size of 5.7 Kb, consistent with homologous insertion of the deletion construct in these transformants [Figure 22C].

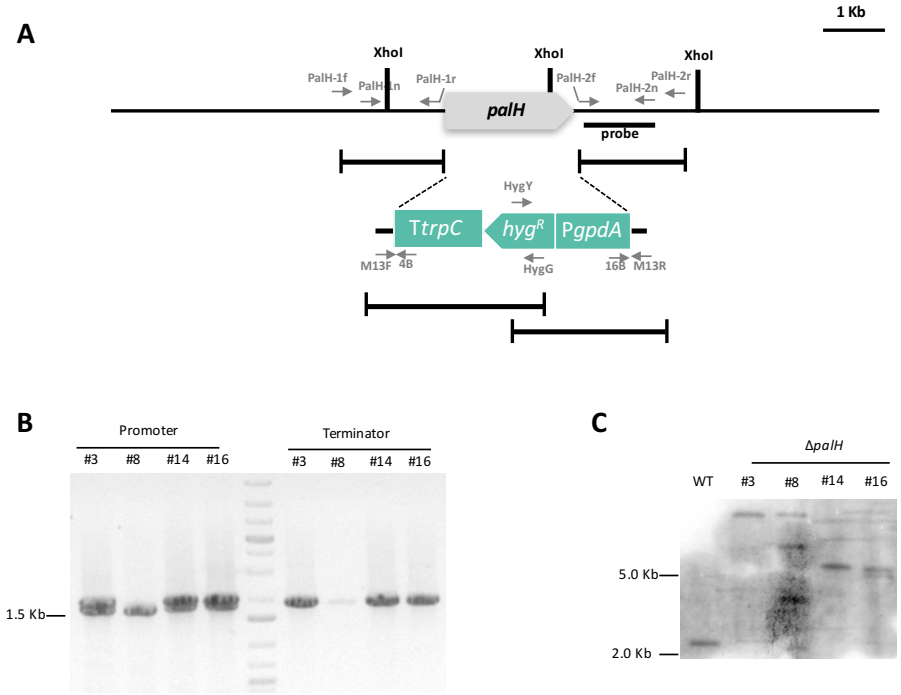

Figure 22 - Targeted deletion of the *F. oxysporum palH* gene.
(A) Physical maps of the *palH* locus and the split-marker gene replacement construct obtained by fusion PCR (Δ*palH* allele). Relative positions of the primers used for generation of the gene disruption construct and PCR analyses of the transformants, as well as the probe used for Southern blot are indicated. **(B)** PCR analyses for homologous integration of the gene disruption construct into the genome of the transformants. Genomic DNA of the transformants was amplified using the pairs of primers: PalH-1f/TrpC-4B (promoter region) and GpdA16B/PalH-2r (terminator region). **(C)** Southern blot hybridization analysis of the wild type strain 4287 and the different Δ*palH* transformants. Genomic DNA treated with *Xho*I was hybridized with the probe

indicated in (A).

4.3.1.2. Targeted deletion of *ptk2* in *F. oxysporum*

In *S. cerevisiae*, the protein kinase Ptk2, a member of the NPR/HAL5 family, is located at the PM and phosphorylates Pma1 at S899 during glucose activation (Eraso *et al.*, 2006; Moskvina *et al.*, 1999).

A BLASTp search of the *F. oxysporum* genome sequence with the *S. cerevisiae* Ptk2 sequence identified with close and relative low score more than one putative Ptk2 orthologs. A BLASTp search of the genome sequence of other ascomycetes revealed a similar result. Therefore, the sequence with highest score (FOXG_03632) was considered to generate a Δ*ptk2* allele in *F. oxysporum*.

As previously described for the Pal/Rim pathway deletion mutants, a Δ*ptk2* allele was generated by replacing the complete ORF with the Hyg^R resistance cassette [Figure 23A]. The two split-marker deletion constructs obtained by fusion PCR were used to co-transform protoplasts of the *F. oxysporum* wild type strain. Transformants carrying a homologous insertion at the *ptk2* locus were initially identified by PCR analyses using two pairs of primers that hybridize outside of the fragments used for transformation and inside of the resistance cassette [Figure 23B]. Further analysis of the selected candidate transformants was performed by Southern blot to verify the correct insertion of a single copy into the genome. We identified two transformants in which the 2.5 Kb hybridizing *Hind*III fragment corresponding to the wild type *ptk2* allele had been replaced by a hybridizing fragment of the expected size of 6.0 Kb, consistent with homologous insertion of the deletion construct in these transformants [Figure 23C].

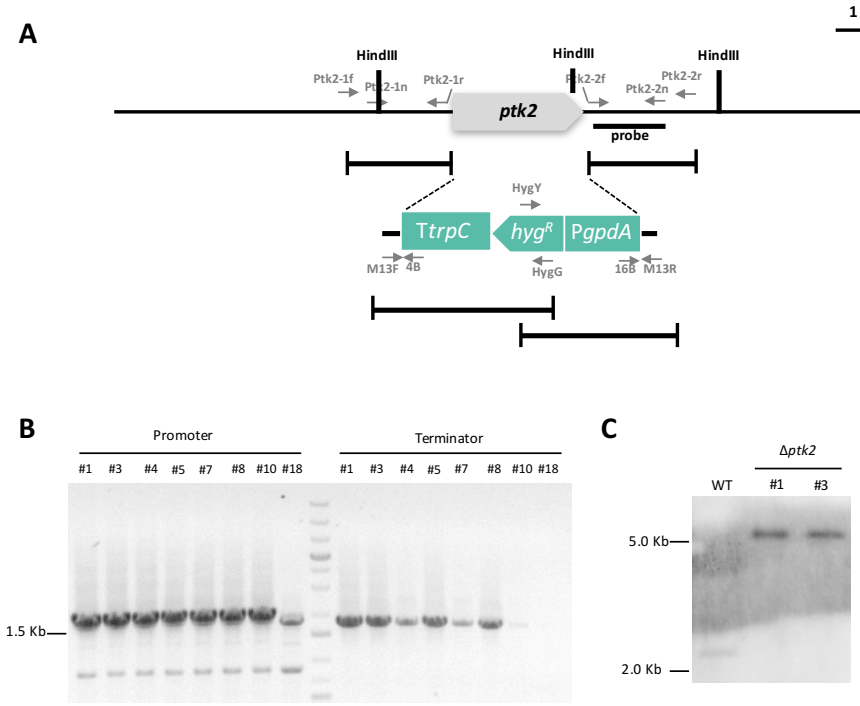

Figure 23 - Targeted deletion of the *F. oxysporum ptk2* gene.
(A) Physical maps of the *ptk2* locus and the split-marker gene replacement construct obtained by fusion PCR (Δ*ptk2* allele). Relative position of the primers used for generation of the gene disruption construct and PCR analyses of the transformants, as well as the probe used for Southern blot are indicated. **(B)** PCR analyses of homologous integration of the gene disruption construct into the genome of the transformants. Genomic DNA of the transformants was amplified using the pairs of primers: Ptk2-1f/TrpC-4B (promoter region) and GpdA16B/Ptk2-2r (terminator region). **(C)** Southern blot hybridization analysis of the wild type strain 4287 and the two Δ*ptk2* transformants. Genomic DNA treated with *Hind*III was hybridized with the probe indicated in (A).

4.3.2. Phenotype of *ΔpalH*, Δ*pacC* and Δ*ptk2* mutants under pH, hyperosmotic and cell wall stress

We examined the growth of the generated deletion mutants in YPD medium buffered to pH 4, 6 and 8, or supplemented with 0.6 M NaCl (hyperosmotic stress) or 40 μg/ml CFW (cell wall stress). The Δ*pacC and* Δ*palH* mutants exhibited a complete absence of growth at alkaline pH and a significant reduction at pH 6 and in the presence of hyperosmotic stress, compared to the wild type [Figure 24].

On the other hand, the Δ*ptk2* mutants only showed a slight reduction of growth at acidic pH and in the presence of CFW [Figure 24].

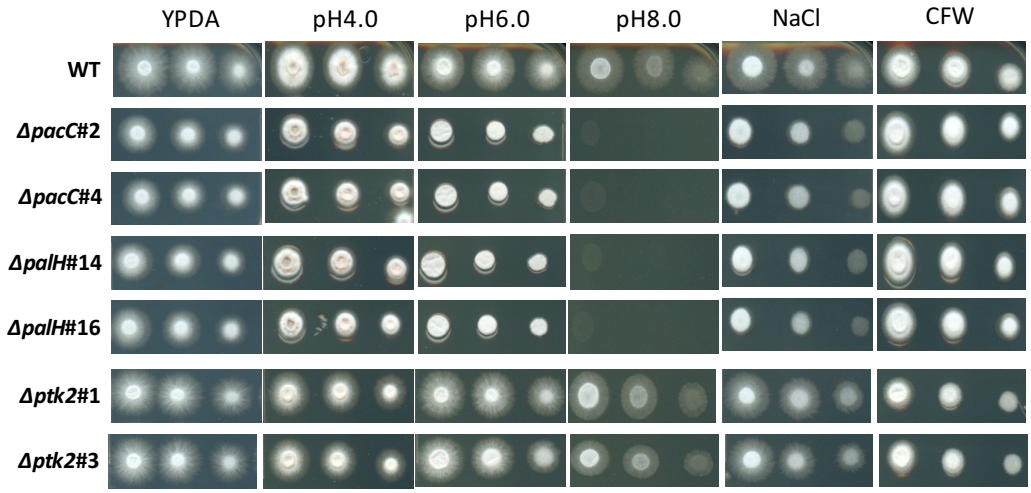

Figure 24 – The Pal pathway is required for growth at alkaline pH, while Ptk2 is dispensable for pH, osmotic and cell wall stress responses.
Colony phenotype of the indicated strains grown on YPDA, YPDA buffered at the indicated pH or YPDA supplemented with 0.6 M NaCl or 40 μg/ml CFW. Plates were spot-inoculated with 10^5, 10^4 and 10^3 microconidia, incubated for 2 days at 28ºC and scanned.

4.3.3. The Pal pathway regulates vacuolar pH but is not required for pH homeostasis of the cytosol

Although the Pal pathway has been demonstrated to be fundamental for the alkaline pH response, its role in pH_i homeostasis control has not been reported so far. Therefore, we compared the vacuolar and cytosolic pH of the Δ*pacC* and Δ*palH* mutants with that of the wild type strain. We also included a *F. oxysporum* strain carrying a truncated, dominant activating $pacC^c$ allele (Caracuel *et al.*, 2003).

For measurement of pH_v, cells were stained with the ratiometric dye BCECF-AM as previously described for *S. cerevisiae* (Diakov and Kane, 2010). For pH_v analysis, strains stained and unstained (control) with BCECF-AM were used. To obtain a pH_v calibration curve, cells were permeabilized with nigericin in the presence of buffers adjusted to different pH values, similarly to that described for pH_i determination. Fluorescence was measured and ratios of emission intensities were calculated after excitation at 490 nm and 440 nm.

To confirm that BCECF also localizes to the vacuole in *F. oxysporum*, we performed fluorescence microscopy of the wild type hyphae stained with 5 μM BCECF-AM and observed fluorescence localizing mostly in vacuole-like structures [Figure 25A]. Moreover, addition of Concanamycin A, a specific inhibitor of the vacuolar H^+-ATPase, induced an increase of pH_v by 0.3 units [Figure 25B]. Based on these to results, we concluded that BCECF-AM staining constitutes a valid experimental approach for measuring pH_v in *F. oxysporum*.

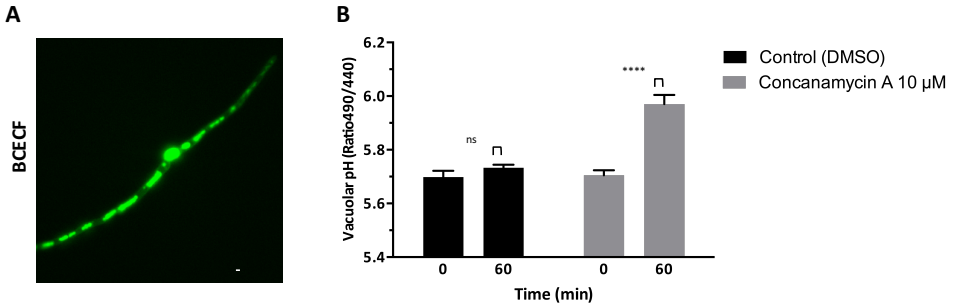

Figure 25 – The dye BCECF-AM localizes to vacuoles in *F. oxysporum*.
Fifteen-hour germinated microconidia of *F. oxysporum* in KSU buffer at pH 6.0 were stained with 5 µM BCECF-AM for 15 minutes at 28ºC, 170 rpm. Cells were then washed with KSU pH 6.0 to remove the excess of dye and incubated for one more hour at 28ºC. **(A)** Vacuolar localization of the dye was assessed by fluorescence microscopy. Bar 20 µm. **(B)** Fluorescence intensities were recorded after excitation at 490 nm and 440 nm in a spectrofluorometer. For determination of vacuolar pH (pH_v) the ratio between the emission intensities (collected at 535 nm) was calculated. pH_v was determined every 5 minutes for 1 hour. Bars represent pH_v at time zero and one hour after treatment of cells with 10 µM Concanamycin A or the solvent DMSO (control). Data shown represent the mean and standard deviations of three technical replicates. ns = non-significant $p<0.001$; **** $p<0.0001$; *versus* T0 according to two-way ANOVA and Bonferroni Test.

Next, pH_v was determined in the wild type strain and in the different deletion mutants exposed to different extracellular pH environments. In all strains tested, pH_v increased at higher external pH [Figure 26]. For example, in the wild type strain pH_v increased from 5.57±0.024 at external pH 4 to 6.04±0.022 at external pH 7. Interestingly, at acidic environmental pH (4.0 or 5.0), the Δ*pacC* and Δ*palH* mutants showed a significantly more acidic pH_v than the wild type strain. However, at near to neutral or neutral pH, no differences in pH_v were observed between the strains [Figure 26].

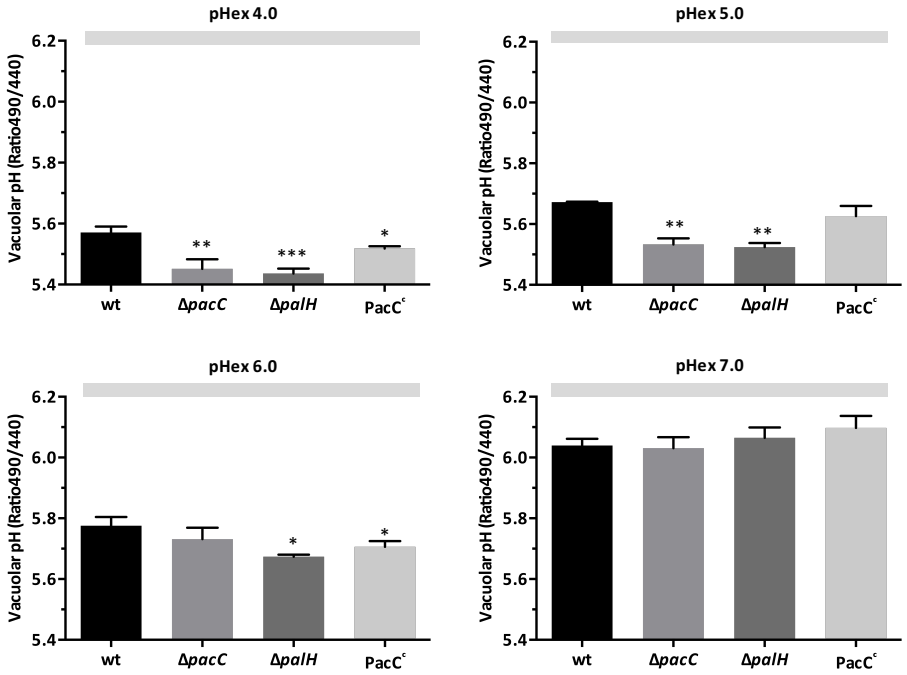

Figure 26 – Pal mutants have a lower vacuolar pH in acidic environments than the wild type strain.

Fifteen-hour germinated microconidia of *F. oxysporum* wild type, Δ*pacC*, Δ*palH* and PacC^c strains in KSU buffer at pH 6.0 were stained with 5 µM BCECF-AM for 15 minutes at 28ºC, 170 rpm. Cells were then washed and incubated in KSU at pH 4.0, 5.0, 6.0 or 7.0. After one hour at 28ºC, excitation at 440 nm and 490 nm was measured and the ratio between the emission intensities collected at 535 nm was calculated. Bars show pH_v values one hour after incubation at different pH buffers. Data shown represent the mean and standard deviations of one of two independent experiments, with three technical replicates. ns = non-significant $p<0.001$; *** $p<0.001$; ** $p<0.01$; * $p<0.05$; *versus* WT. Student t-test.

To test the effect of the Δ*pacC* and Δ*palH* mutations on cytosolic pH, the deletion alleles were generated in the genetic background of transformant #9 expressing high levels pHluorin, by replacing the *pacC* or *palH* coding region with the *Neo*^{R} resistance cassette using the split-marker protocol. The final deletion constructs were obtained by fusion PCR and used to co-transform protoplasts of *F. oxysporum* pHluorin-expressing transformant #9. Southern blot analysis identified two Δ*pacC* transformants in which the 4.8 Kb hybridizing *Pvu*II fragment corresponding to the

wild type *pacC* allele had been replaced by the expected 5.8 Kb fragment [Figure 27].

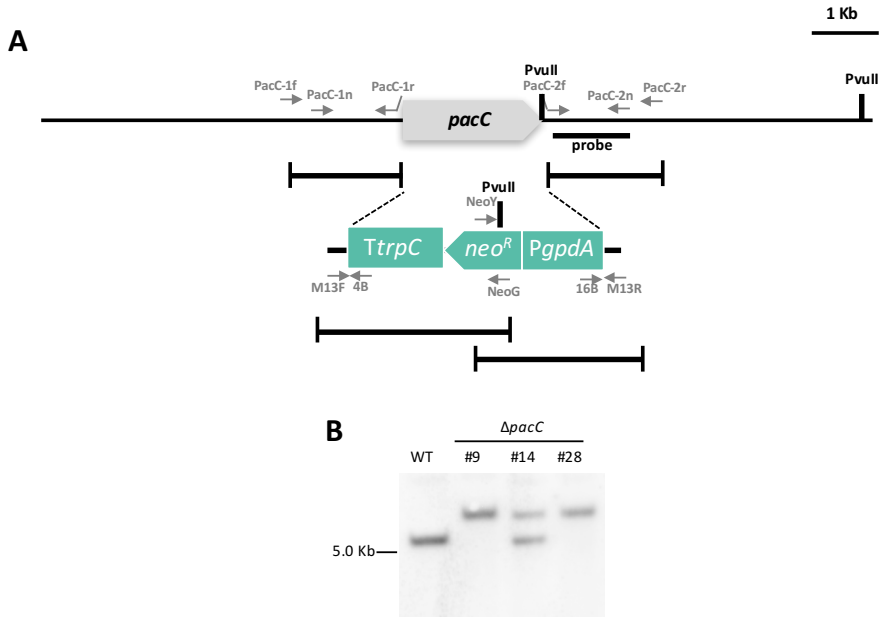

Figure 27 - Targeted disruption of the *pacC* gene in the *F. oxysporum* strain expressing pHluorin.
(**A**) Physical maps of the *pacC* locus and the split-marker gene replacement construct obtained by fusion PCR (Δ*pacC* allele). Relative positions of the primers used for generation of the gene disruption construct and PCR analysis of the transformants, as well as the probe used for Southern blot are indicated. (**B**) Southern blot hybridization analysis of the wild type strain 4287 and the different Δ*pacC* transformants. Genomic DNA treated with *Pvu*II was hybridized with the probe indicated in (A).

Moreover, three Δ*palH* transformants were identified in which the 2.4 Kb hybridizing *Xho*I corresponding to the wild type allele was replaced by a 5.7 Kb fragment, revealing homologous insertion in these transformants [Figure 28]. Fluorescence levels in all the generated mutants were comparable to those of the original transformant #9 expressing pHluorin (data not shown).

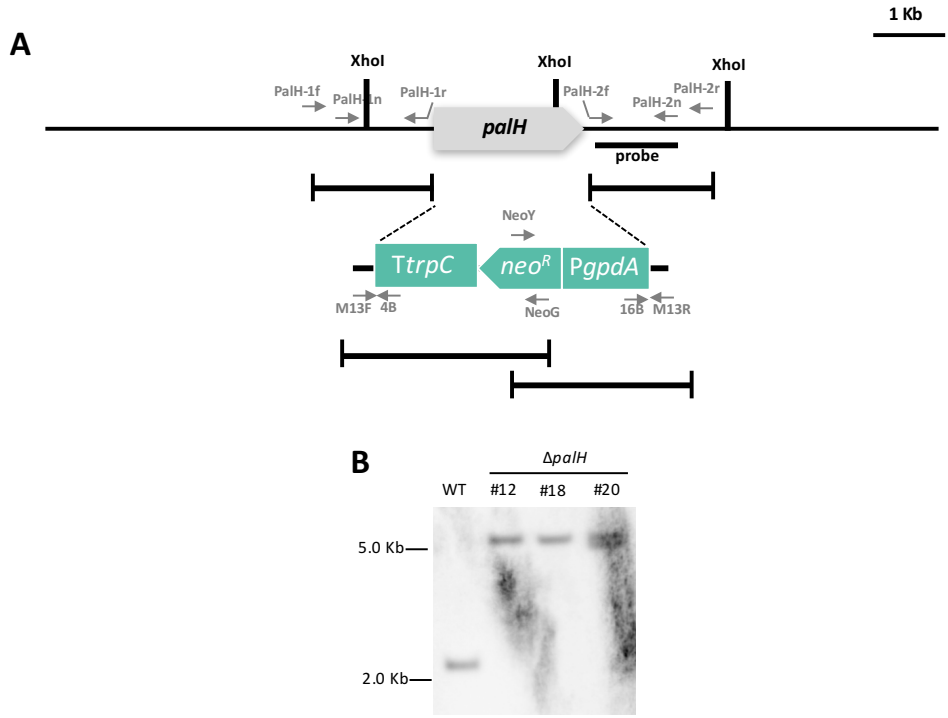

Figure 28 - Targeted disruption of the *palH* gene in the *F. oxysporum* strain expressing pHluorin.
(A) Physical maps of the *palH* locus and the split-marker gene replacement construct obtained by fusion PCR (Δ*palH* allele). Relative positions of the primers used for generation of the gene disruption construct and PCR analysis of the transformants, as well as the probe used for Southern blot are indicated. **(B)** Southern blot hybridization analysis of the wild type strain 4287 and the different Δ*palH* transformants. Genomic DNA treated with *Xho*I was hybridized with the probe indicated in (A).

To explore the role of the Pal pathway in pH_i homeostasis, we measured steady state pH_i in the Δ*pacC and* Δ*palH* mutants maintained for 2 hours in KSU buffer at pH 6.0 (control condition). Our results revealed no significant differences in pH_i between the Δ*pacC* and Δ*palH* mutants and the wild type strain [Figure 29A]. We next tested whether rapid pH_i fluctuations could be affected in these mutants. To this aim extra- or intracellular acidification was induced, by adding diluted HCl or DES, respectively. The effect of extracellular acidification on pH_i was evaluated in two independent mutants for each gene, and no significant differences to the wild type were detected [Figure 29B]. Similarly, the sustained acidification of the cytosol induced by DES was almost identical in the Δ*pacC and* Δ*palH* mutants and

the wild type strain [Figure 29C]. These results suggest that the Pal pathway does not play a major role in pH_i homeostasis, at least under the conditions tested here.

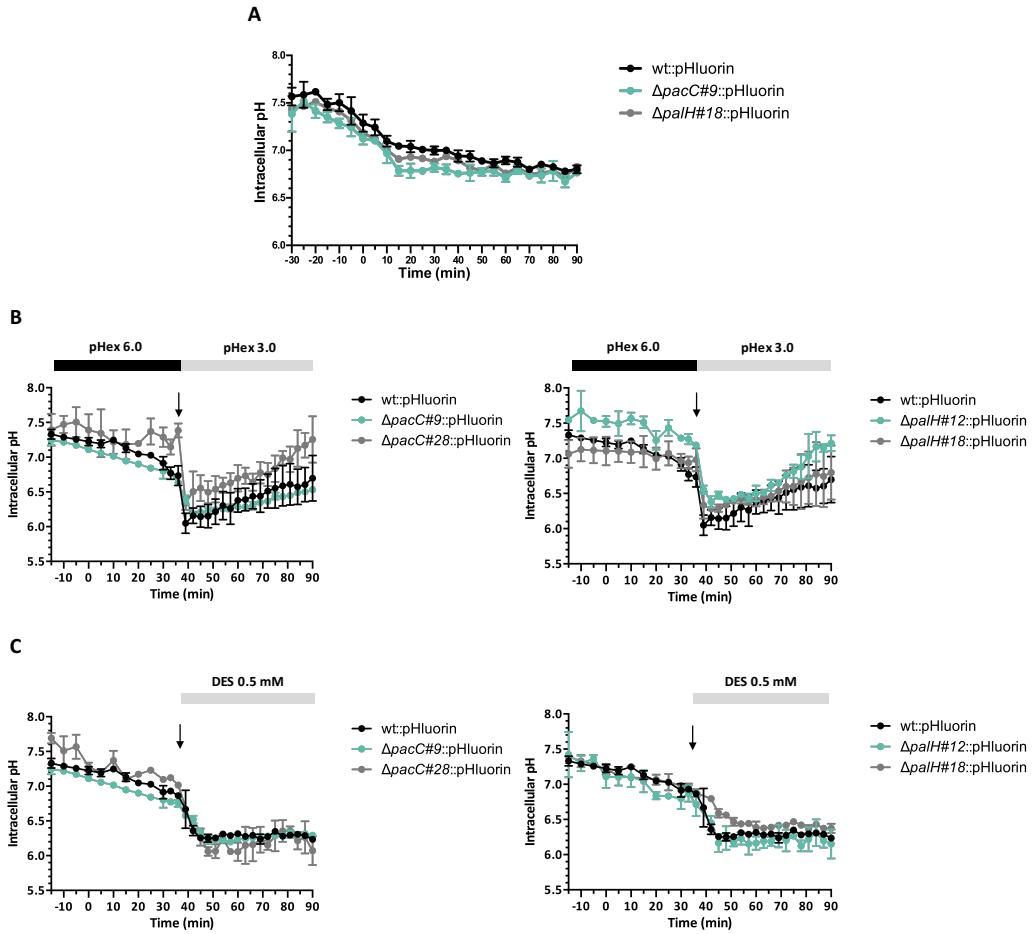

Figure 29 - Δ*pacC* and Δ*palH* mutants are not affected in pH_i homeostasis.
Fifteen-hour germinated microconidia of the *F. oxysporum* wild type, Δ*pacC* and Δ*palH* strains expressing pHluorin were washed and suspended in KSU buffer at pH 6.0 and pre-incubated for 45 minutes at 28ºC. **(A)** pH_i in the indicated strains was measured every 5 minutes for 2 hours. **(B, C)** pH_i measurements were initiated 15 minutes before time zero and 30 minutes later diluted HCl was added to change extracellular pH to 3.0 **(B)**, or 0.5 mM DES was added **(C),** and pH_i was measured every 3 minutes for one more hour. For pH_i determination, the ratio between the emission intensities (collected at 510 nm) after excitation at 395 nm and 475 nm was calculated. Data shown represent the mean and standard deviations of three independent replicates for each strain.

4.3.4. The Pal pathway contributes to rapid activation of Mpk1 in response to pH_i acidification

We previously observed that phosphorylation of the CWI MAPK Mpk1 is rapidly induced in response to extra- or intracellular acidification. To test the role of the Pal pathway in this rapid response, we followed the phosphorylation level of Mpk1 in the Δ*pacC and* Δ*palH* mutants treated with diluted HCl. We found that both Δ*pacC* and Δ*palH* exhibited a delay in Mpk1 phosphorylation in response to extracellular acidification compared to the wild type strain, whereas the concomitant dephosphorylation of Fmk1 was unaffected in these mutants [Figure 30].

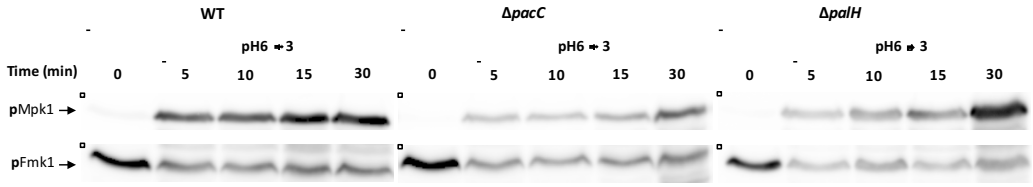

Figure 30 – Pacc and Palh contribute to the rapid activation of Mpk1 in response to extracellular acidification.
Fifteen-hour germinated microconidia of the *F. oxysporum* wild type, Δ*pacC* and Δ*palH* strains were washed and resuspended in KSU buffer at pH 6.0 and pre-incubated for 1 hour at 28ºC. At time 0, diluted HCl was added to change the pH of the buffer from 6.0 to 3.0. Protein extracts collected before (time 0) and 5, 10, 15 or 30 minutes after acidification were subjected to immunoblot analysis with anti-phospho-p44/42 MAPK antibody for pMpk1 and pFmk1 detection.

A similar delay in Mpk1 phosphorylation was observed in the Δ*pacC* mutant upon DES-triggered intracellular acidification [Figure 31]. Interestingly, the dominant activating $PacC^{c}$ mutant exhibited a faster Mpk1 phosphorylation in response to DES than the wild type. Collectively, these results indicate that the Pal pathway contributes to acid pH-triggered Mpk1 activation.

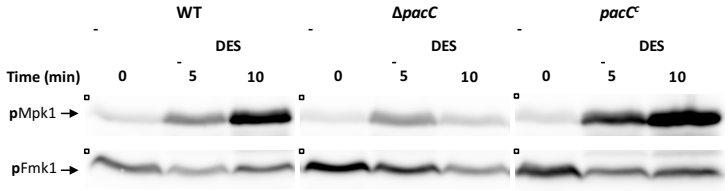

Figure 31 – PacC contributes to the rapid activation of Mpk1 in response to intracellular acidification.
Fifteen-hour germinated microconidia of the *F. oxysporum* wild type, Δ*pacC* and Δ*palH* strains were washed and resuspended in KSU buffer at pH 6.0 and pre-incubated for 1 hour at 28ºC. At time 0, 0.5 mM DES was added to the buffer. Protein extracts collected before (time 0) and 5 or 10 minutes after DES were subjected to immunoblot analysis with anti-phospho-p44/42 MAPK antibody for pMpk1 and pFmk1 detection.

We next evaluated the role of the protein kinase Ptk2 in MAPK phosphorylation responses to extracellular pH changes. Our results showed a very similar phosphorylation pattern of the Mpk1 and Fmk1 MAPK cascades in the Δ*ptk2* mutant as in the wild type strain. Mpk1 MAPK was phosphorylated at pH 5.0 and dephosphorylated at 7.0, while Fmk1 follows an opposite pattern [Figure 32] (compare with Figure 4B).

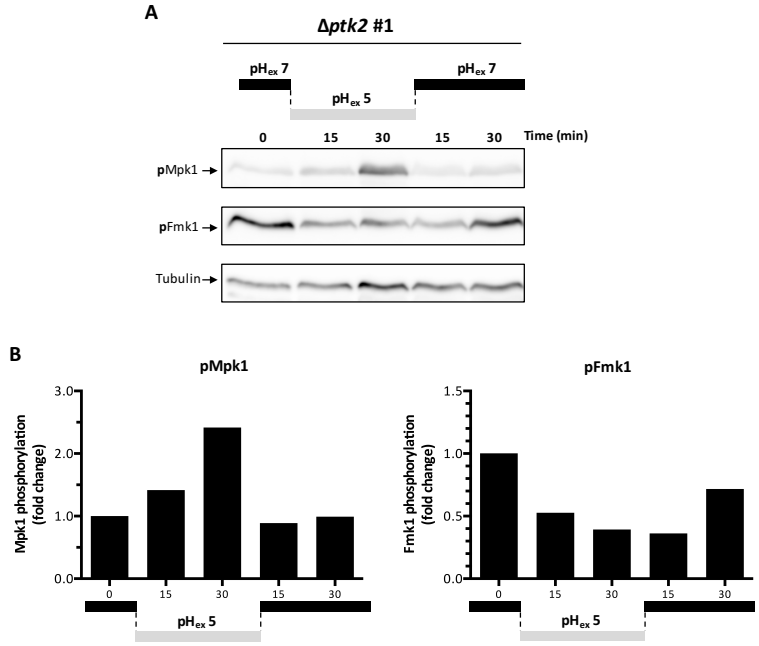

Figure 32 – Ptk2 is not required for MAPK regulation by extracellular pH.
(A) Fifteen-hour germinated microconidia of the *F. oxysporum* Δ*ptk2* strain were washed and resuspended in KSU buffer at pH 7.0 and pre-incubated for 1 hour at 28ºC. The pH of the buffer was then shifted from 7.0 to 5.0 and back to 7.0, by adding diluted HCl or NaOH, respectively. Protein extracts collected before (control at pH 7.0) and 15 or 30 minutes after each pH shift were subjected to immunoblot analysis with anti-phospho-p44/42 MAPK antibodies for pMpk1 and pFmk1 detection. Anti-tubulin antibody was used as loading control. **(B)** Graphs show the ratio of pMpk1 or pFmk1 band intensity normalized to tubulin and expressed as fold response compared with time zero (control at pH 7.0).

4.3.5. The Pal pathway and Ptk2 are not required for virulence of *F. oxysporum* on tomato plants

To test the role of the Pal pathway and of Ptk2 in virulence of *F. oxysporum* on tomato plants, roots were inoculated with microconidia of the different strains, and plant survival was followed. No significant differences in mortality rates were observed between the mutants and the wild type strain [Figure 33]. Interestingly, the wilt symptoms appeared earlier in the plants inoculated with the Δ*pacC* mutant, although the difference was not statistical significant. These results are consistent

with those obtained in a previous study using a PacC loss-of-function mutant (Caracuel *et al*., 2003). Moreover, the Δ*ptk2* appeared to cause slightly less mortality, although again the difference was not statistical significant. Collectively, these results indicate that the Pal pathway and Ptk2 are not essential for plant infection in this fungal pathogen.

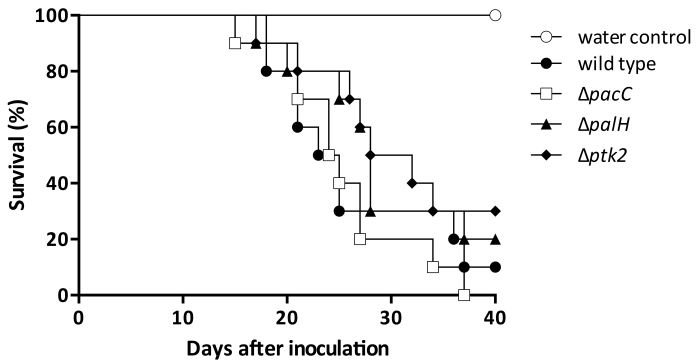

Figure 33 – The Pal pathway and Ptk2 are not required for virulence of *F. oxysporum* on tomato plants.
Kaplan–Meier plot of survival of tomato plants infected with the indicated *F. oxysporum* strains. Mortality significance was evaluated through the log-rank test. Data are from one representative experiment.

4.4. YEAST AS A MODEL SYSTEM TO STUDY pH_i-INDUCED MAPK REGULATION IN *FUSARIUM OXYSPORUM*

We previously found that pH_i acts as second messenger for the activity of the MAPK signaling in *F. oxysporum*. However, the molecular mechanisms underlying this response are unknown. The identification of new components regulating pH_i-mediated MAPK signaling is one of the steps towards such a goal. However, it requires a broad approach where hundreds of mutants could be assayed and in *F. oxysporum* although an efficient gene targeting protocol has been developed over the last years, a complete mutant library is not still available for this organism. On the other hand, the budding yeast *S. cerevisiae* (hereafter called "yeast") has been widely used as a model organism for studying eukaryotic cellular processes, mainly through genome-wide analysis of biological functions. There are many advantages to working with yeast. It shares a high level of conservation of essential cellular processes with more complex eukaryotes and it is easy to grow in the laboratory and genetically tractable. Therefore, the yeast versatility makes it a useful model to investigate new components regulating pH_i-mediated MAPK signaling.

4.4.1. Intracellular pH also acts as a second messenger for MAPK signaling in yeast

4.4.1.1. Ambient pH impacts intracellular pH homeostasis and MAPK signaling

We first examined the pH_i dynamics in *S. cerevisiae* upon extracellular pH change, using a yeast strain transformed with the pYEplac181 plasmid containing the *pHluorin* gene under control of a *TEF1* promoter (a gift from Henrik G. Dohlman, University of North Carolina, USA). As for *F. oxysporum*, pH_i measurements in yeast cells were performed using a microwell reader coupled to a spectrofluorometer. For pH_i analyses, the yeast wild type and the wild type expressing *pHluorin* strains were used. To obtain a pH calibration curve, yeast cells

were permeabilized with nigericin in the presence of buffers adjusted to different pH values. Fluorescence was measured and ratios of emission intensities were calculated after excitation at 395 nm and 475 nm. Determination of pH_i revealed that steady state pH_i under these conditions is more acidic in yeast than in *F. oxysporum* (6.61±0.05 *versus* 7.45±0.13, respectively) [Figure 34]. After a sudden shift in extracellular from pH 6.5 to 3.0, a rapid acidification of the cytosol by 0.7 pH units was detected in 20 minutes. After one hour, the pH_i almost returned to the initial value [Figure 34A]. On the other hand, external alkalinization triggered an even faster increase of 1.38 units, followed by a complete recovery to the initial value after 25-30 minutes [Figure 34B]. These pH_i responses resemble those previously observed in *F. oxysporum* (see Figure 11A).

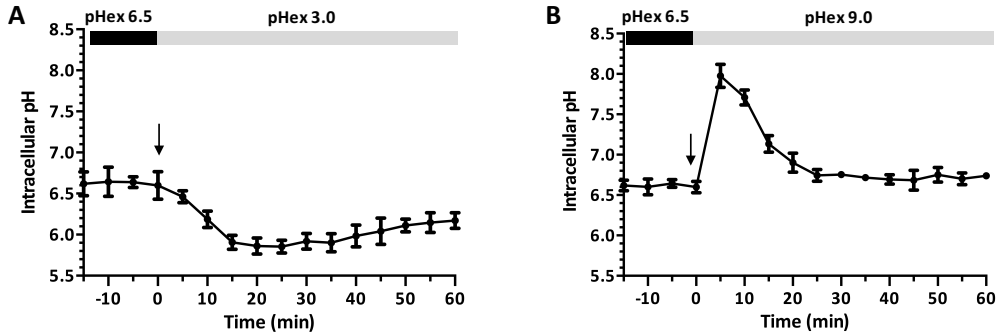

Figure 34 – Extracellular pH shifts induce a rapid and transitory change of intracellular pH in yeast.
Exponentially growing cells of the *S. cerevisiae* wild type strain were washed and resuspended in KSU buffer at pH 6.5, and pre-incubated for 45 minutes at 30ºC. pH_i measurements were initiated 15 minutes before treatment. Extracellular pH in each well was subjected to sudden shift to 3.0 **(A)** or 9.0 **(B)** by adding diluted HCl or NaOH, respectively. pH_i was monitored every 5 minutes for 1 hour. For pH_i determination, the ratio between the emission intensities (collected at 510 nm) after excitation at 395 nm and 475 nm was calculated. Data shown represent the mean and standard deviations of one of three independent experiments, with three independent replicates.

Western blot analysis of MAPK phosphorylation patterns in the same experimental conditions revealed that a shift in extracellular pH from 6.5 to 3.0 induced rapid phosphorylation of Mpk1/Slt2 and Hog1 and a slight dephosphorylation of the

Fmk1 ortholog Fus3 [Figure 35]. These responses display the same trend as previously observed in *F. oxysporum*. Similarly, when the extracellular pH was rapidly shifted from 6.5 to 9.0 a marked dephosphorylation of Mpk1 and Hog1 was observed, again mirroring the results obtained in *F. oxysporum*. However, in contrast to *F. oxysporum*, phosphorylation levels of Fmk1 orthologs Fus3 and Kss1 did not increase upon alkalinization [Figure 35]. Intrigued by this difference we determined the phosphorylation patterns of Fus3 and Kss1 at different pH conditions ranging from 6.0 to 9.0, and we found that both MAPKs display pH-dependent phosphorylation levels with a peak at pH 6.5 [Figure 36]. As expected, Mpk1 and Hog1 phosphorylation levels decreased progressively as extracellular pH increased.

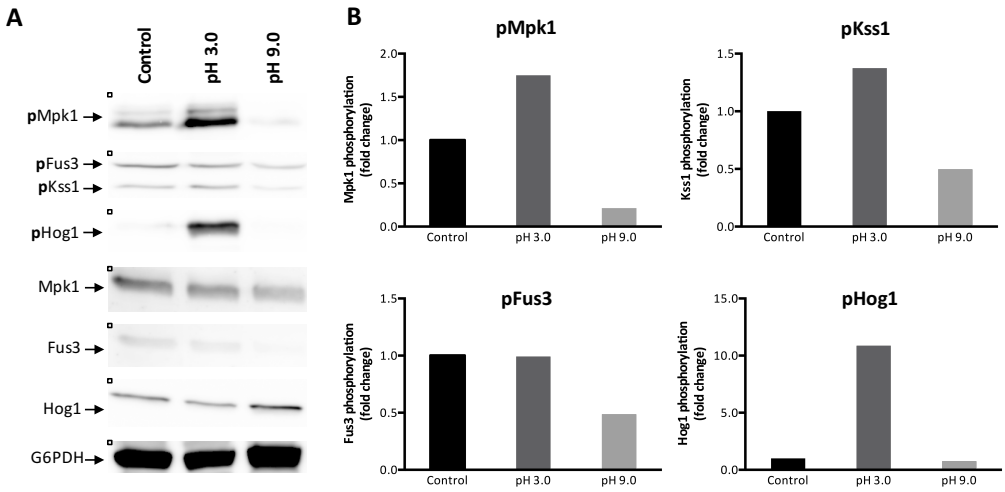

Figure 35 – Effect of ambient pH on MAPK phosphorylation in yeast.
(A) Exponentially growing cells of the *S. cerevisiae* wild type strain were washed and resuspended in KSU buffer at pH 6.0 and incubated for 1 hour at 30ºC. After this hour, the pH of the buffer was suddenly shifted to 3.0 or to 9.0, with diluted HCl or NaOH, respectively. Proteins extracts collected before (control pH 6.0) and 5 minutes after pH change were subjected to immunoblot analysis with anti-phospho-p44/42 MAPK or anti-phosho-p38 MAPK antibodies, for pMpk1, pFus3 and pKss1, or pHog1 detection, respectively. Anti-Mpk1, anti-Fus3 and anti-Hog1 antibodies were used for MAPK loading control. Anti-G6PDH antibody was used as total extract loading control. **(B)** Graphs show the ratio of pMpk1, pFus3, pKss1 or pHog1 band intensity normalized to G6PDH and expressed as fold response compared with control (pH 6.0).

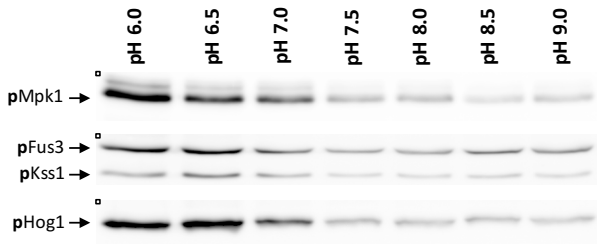

Figure 36 – MAPK phosphorylation in yeast is regulated by ambient pH.
(A) Exponentially growing cells of the *S. cerevisiae* wild type strain were washed and resuspended in KSU buffer at different pH values, ranging from 6.0 to 9.0, and incubated for 1 hour at 30ºC. Proteins extracts collected after this hour were subjected to immunoblot analysis with anti-phospho-p44/42 MAPK or anti-phosho-p38 MAPK antibodies, for pMpk1, pFus3 and pKss1, or pHog1 detection, respectively. Anti-G6PDH antibody was used as total extract loading control. **(B)** Graphs show the ratio of pMpk1, pFus3, pKss1 or pHog1 band intensity normalized to G6PDH and expressed as fold response compared with control (pH 6.0).

4.4.1.2. DES-triggered intracellular acidification activates Mpk1 phosphorylation and inhibits Fus3 and Kss1 phosphorylation in yeast

Taken together, our previous results suggest that MAPK signaling in yeast is regulated by external pH in a similar way as in *F. oxysporum*. To examine whether pH_i also acts as a second messenger in this process, yeast cells were treated with the Pma1-specific inhibitor DES. Among different concentrations tested, 25 μM DES induced maximum levels of Mpk1 phosphorylation [Figure 37]. With this concentration, Hog1 also became phosphorylated. The phosphorylation level of Fus3 and Kss1 is apparently highly sensitive to DES, since a dephosphorylation was perceptible even with the lower concentration of DES tested (to compare with the phosphorylation level at pH 6.5/control condition see Figure 35) suggesting that these MAPKs are rapidly dephosphorylated in response to DES treatment.

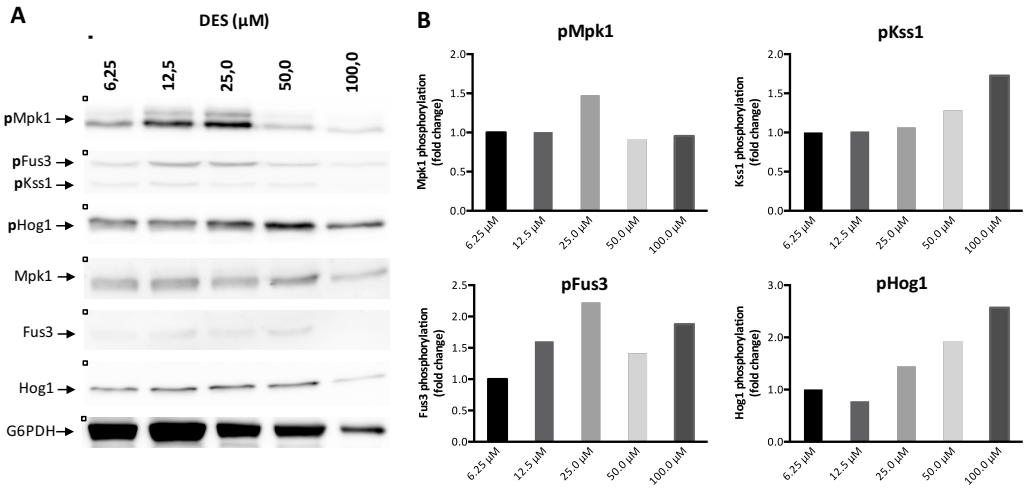

Figure 37 – DES treatment of yeast cells leads to changes in MAPK phosphorylation.

(A) Exponentially growing cells of the *S. cerevisiae* wild type strain were washed and resuspended in KSU buffer at pH 6.5 and incubated for 1 hour at 30ºC. After this hour, DES at different concentrations was added to the buffer. Proteins extracts collected 5 minutes after DES treatment were subjected to immunoblot analysis with anti-phospho-p44/42 MAPK or anti-phosho-p38 MAPK antibodies, for pMpk1, pFus3 and pKss1, or pHog1 detection, respectively. Anti-Mpk1, anti-Fus3 and anti-Hog1 antibodies were used for MAPK loading control. Anti-G6PDH antibody was used as total extract loading control. **(B)** Graphs show the ratio of pMpk1, pFus3, pKss1 or pHog1 band intensity normalized to G6PDH and expressed as fold response compared with lower concentration of DES assayed (6.25 µM).

We next followed pH_i dynamics in yeast cells after treatment with 25 µM DES. A decrease of pH_i by 0.4 units was observed 20 minutes after DES treatment, which was not detected with the solvent control [Figure 38A]. A gradual recovery of pH_i started 25 minutes after DES treatment. In accordance with these results, western blot revealed a maximum induction of Mpk1 phosphorylation after 20 minutes, followed by a progressive decrease [Figure 38B]. The phosphorylation levels of Fus3 and Kss1 decreased over the entire period of the experiment. Collectively, these results reveal that in yeast, MAPK phosphorylation is regulated by pH_i, suggesting that pH_i acts as a second messenger in this process.

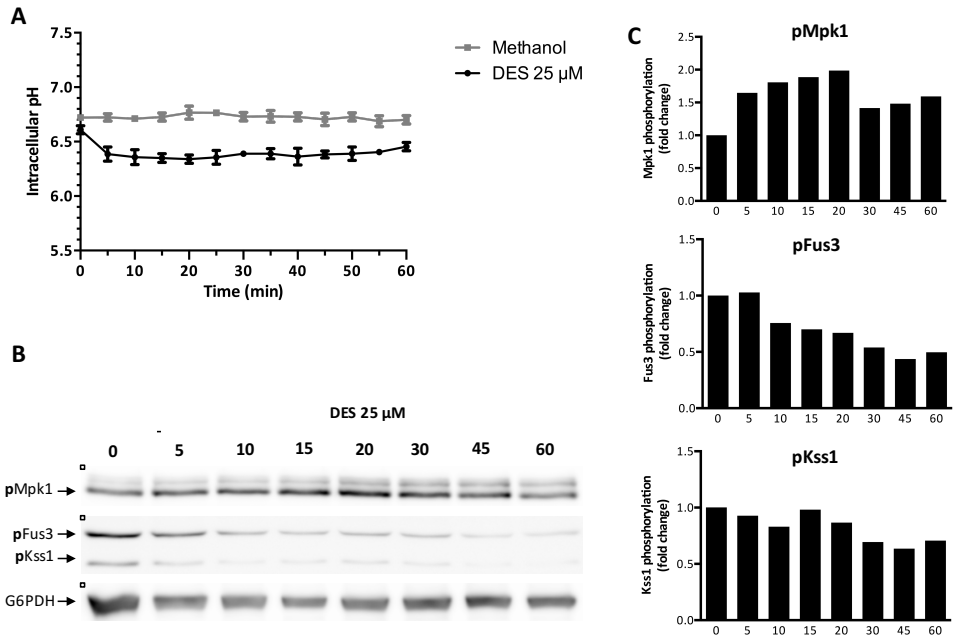

Figure 38 – DES-triggered intracellular acidification regulates MAPK signaling in yeast.
Exponentially growing cells of the *S. cerevisiae* wild type strain were washed and resuspended in KSU buffer at pH 6.5 and incubated for 1 hour at 30ºC. At time 0, 25 µM DES or methanol (solvent control) were added to the buffer. **(A)** pH_i was monitored every 5 minutes for 1 hour. For pH_i determination, the ratio between the emission intensities (collected at 510 nm) after excitation at 395 nm and 475 nm was calculated. Data shown represent the mean and standard deviations of three independent replicates. **(B)** Protein extracts collected before (time 0) and 5 to 60 minutes after DES were subjected to immunoblot analysis with anti-phospho-p44/42 MAPK antibody for pMpk1, pFus3 and pKss1 detection. Anti-G6PDH antibody was used as total extract loading control. **(C)** Graphs show the ratio of pMpk1, pFus3 or pKss1 band intensity normalized to G6PDH and expressed as fold response compared with control.

4.4.2. Understanding the molecular mechanism of Mpk1 activation by intracellular acidification

Our results from *F. oxysporum* and yeast suggest that the role of pH_i in regulation of MAPK signaling is conserved among fungi. The molecular bases of this process are currently unknown. In an attempt to understand the mechanism of pH_i-triggered Mpk1 activation, we approached the question from three experimental angles using the genetically tractable yeast model: 1) role of known upstream regulators of the Mpk1 cascade; 2) role of Hog1 cascade; 3) role of known MAPK phosphatases; 4)

selection of mutants affected in pH_i-mediated MAPK signaling from known acid-sensitive mutants.

4.4.2.1. Role of known upstream regulators of the Mpk1 cascade

The yeast Slt2/Mpk1 MAPK pathway ensures cell wall integrity and is crucial for the response to environmental stresses such as low osmolarity, high temperature, or nutrient limitation. Stress signals are sensed by three plasma membrane receptors, Wsc1, Mid2 and Mtl1, depending on the nature of the stimulus. The signal is then transmitted to Rom2, a guanine exchange factor of the GTP-binding protein Rho1. Rho1 then activates Pkc1 which in turn activates the three-tiered MAPK module Bck1-Mkk1/Mkk2-Mpk1 [Figure 39] (Levin, 2011)

In addition to the canonical CWI upstream pathway, recent studies had demonstrated that Mpk1 activation can also be promoted by the yeast AGC kinase orthologs Ypk1 and Ypk2 that control important cellular functions such as endocytosis and sphingolipids metabolism (deHart *et al*., 2002). The full activation of the redundant Ypk1/2 is complex and appears to require a multi-step process. First, sphingolipid depletion triggers Ypk1/2 localization at the PM (Luo *et al*., 2008; Niles *et al*., 2012; Niles and Powers, 2012). Second, Ypk1/2 are phosphorylated by TORC2 at two different sites located at its C-terminal regulatory domain, possibility increasing its competence to be additionally phosphorylated (Niles et al 2012). Third, Pkh1/2 phosphorylate Ypk1/2 within the activation loop of their kinase domain in order to be fully activated (deHart *et al*., 2002; Niles *et al*., 2012; Roelants *et al*., 2002). In the final, the activation of the Pkh-Ypk module leads to an induction of sphingolipids synthesis. The exact mechanism by which the Ypk1/2 modulate the CWI MAPK pathway is not still completely understood. Recently it was demonstrated that Ypk1 kinase regulates the Pkc1 activity through proper localization of Rom2 at the PM (Niles and Powers, 2014). More studies are still required to fully understand this process [Figure 39].

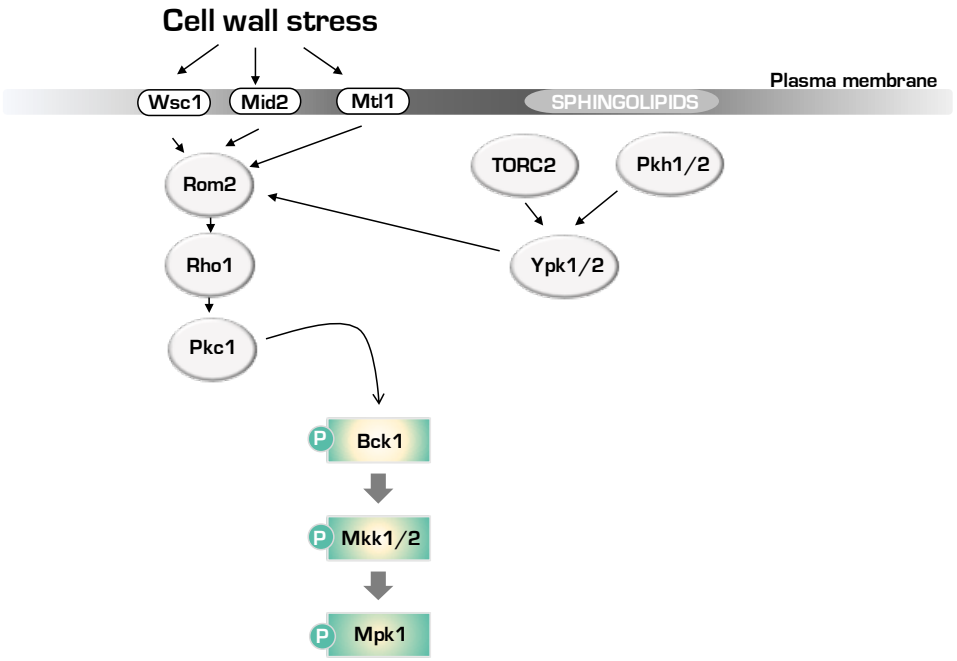

Figure 39 – Schematic diagram of the CWI MAPK signaling pathway in *S. cerevisiae*.
Cell wall stress conditions stimulate the CWI MAPK signaling pathway through the stress sensors located at the PM. The stress sensors Wsc1, Mid2 or Mtl1 sense cell wall perturbing conditions and transmit it to Rom2 that activates Rho1. Rho1 then activates Pkc1 which in turn activates the MAPK module Bck1-Mkk1/2-Mpk1. The redundant kinases Ypk1/2, which are activated by TORC2 and Pkh1/2, can also activate the CWI pathway through proper localization of Rom2 at the PM (Adapted from (Levin, 2011)).

The finding that DES-triggered cytosolic acidification induces phosphorylation of Mpk1 prompted us to test the role of known upstream components in this response. As shown in [Figure 40], mutants lacking *wsc1*, *mid2*, *mtl1* or *rom2* showed an increase in Mpk1 phosphorylation and a decrease in Fus3 and Kss1phosphorylation after DES treatment, similar to that of the wild type strain. We conclude that these components are not required for pH_i-mediated MAPK signaling.

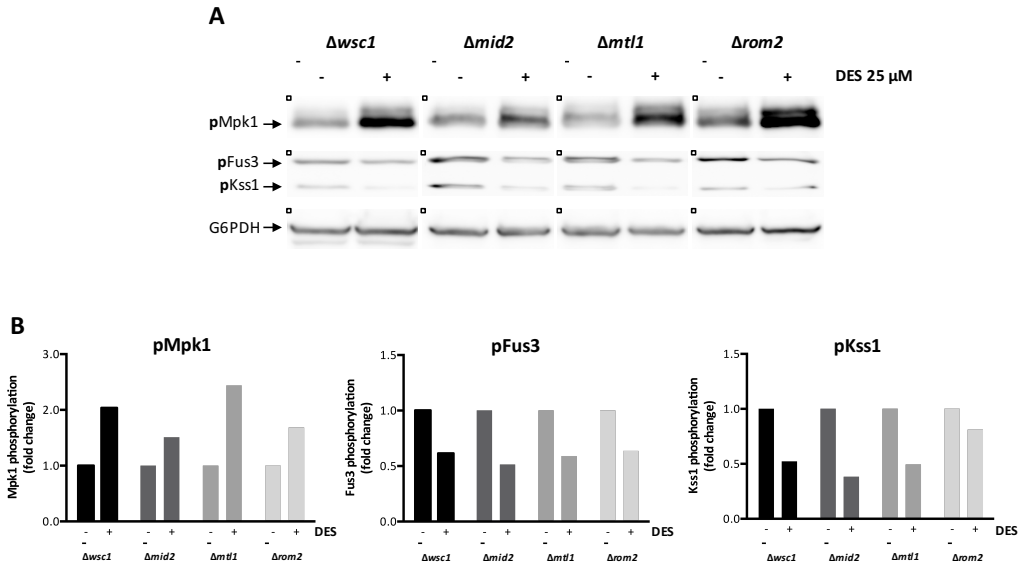

Figure 40 – Upstream regulators Wsc1, Mid2, Mtl1 and Rom2 are not required for DES-triggered Mpk1 activation.
(A) Exponentially growing cells of the *S. cerevisiae* Δ*wsc1*, Δ*mid2*, Δ*mtl1*and Δ*rom2* strains were washed and resuspended in KSU buffer at pH 6.5 and incubated for 1 hour at 30ºC. At time 0, 25 µM DES was added to the buffer. Protein extracts collected at time zero (-) and 20 minutes after (+) DES treatment were subjected to immunoblot analysis with anti-phospho-p44/42 MAPK for pMpk1, pFus3 and pKss1 detection. Anti-G6PDH antibody was used as total extract loading control. **(B)** Graphs show the ratio of pMpk1, pFus3 or pKss1 band intensity normalized to G6PDH and expressed as fold response compared with control (time zero; -).

Because Rho1 and Pkc1 are essential for cell survival, we used mutants carrying temperature-sensitive alleles to study their involvement in DES-triggered Mpk1 activation. Since these mutants had been generated in a background different from BY4741, the respective wild type strains were also included in the experiment. After O.N. growth at permissive temperature (25°C), cells were shifted for one hour to restrictive temperature conditions (34°C) before treatment with 25 µM DES. The *rho1-ts* strain showed a reduced level of Mpk1 phosphorylation even before DES treatment, reflecting the crucial role of this GTP-binding protein in the CWI MAPK cascade activity [Figure 41]. Nevertheless, DES-triggered cytosolic acidification still induced a clear increase of Mpk1 phosphorylation in the *rho1-ts* strain, suggesting that this response is not mediated by Rho1. The *pkc1-ts* strain displayed

an even more drastic reduction of baseline Mpk1 phosphorylation than the *rho1-ts* strain, confirming that Pkc1 is essential even for basal Mpk1 activity. In contrast to the *rho1-ts* strain, no induction of Mpk1 phosphorylation upon DES treatment was detected in the *pkc1-ts* strain, even with high exposition times. Importantly, the respective wild type strains presented the same MAPK phosphorylation phenotype previously described for the BY4741 strain.

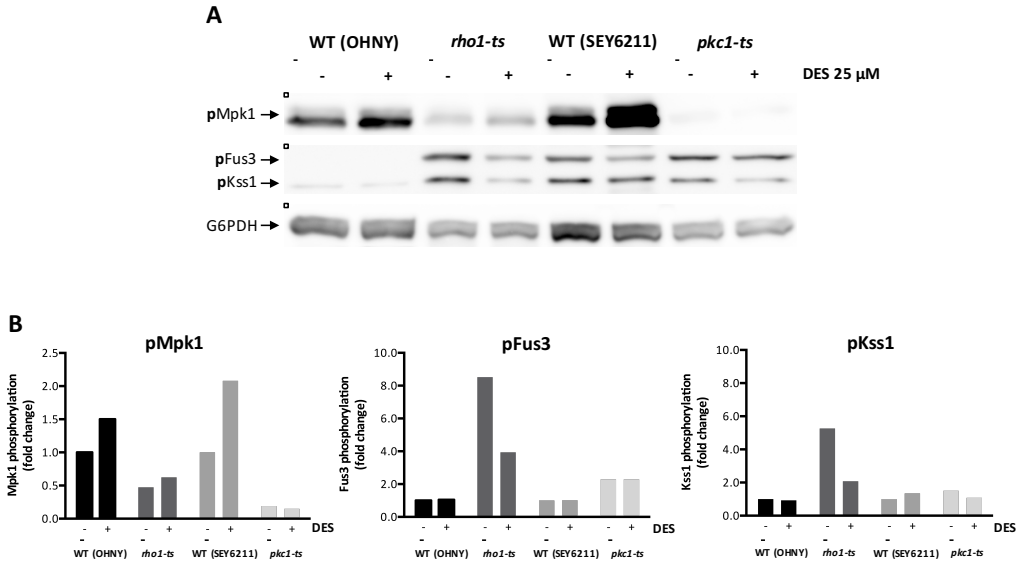

Figure 41 – Pkc1, but not Rho1, is essential for DES-triggered Mpk1 activation.
(**A**) Exponentially growing cells of the *S. cerevisiae rho1-ts* and *pkc1-ts* strains, and respective OHNY and SEY6211 wild type strains, were washed and resuspended in KSU buffer at pH 6.5 and incubated for 1 hour at 34ºC. At time 0, 25 µM DES was added to the buffer. Protein extracts collected at time zero (-) and 20 minutes after (+) DES treatment were subjected to immunoblot analysis with anti-phospho-p44/42 MAPK for pMpk1, pFus3 and pKss1 detection. Anti-G6PDH antibody was used as total extract loading control. **(B)** Graphs show the ratio of pMpk1, pFus3 or pKss1 band intensity normalized to G6PDH and expressed as fold response compared with control (time zero; -).

The finding that Pkc1, but not its canonical upstream component Rho1, is required for DES-triggered Mpk1 activation [Figure 42], prompted us to evaluate the role of the alternative Pkh-Ypk branch in this process. When single mutants were analyzed, we found that loss of Pkh1, Pkh2, Ypk1 or Ypk2 did not affect DES-triggered

induction of Mpk1 phosphorylation or Fus3 and Kss1 dephosphorylation [Figure 42].

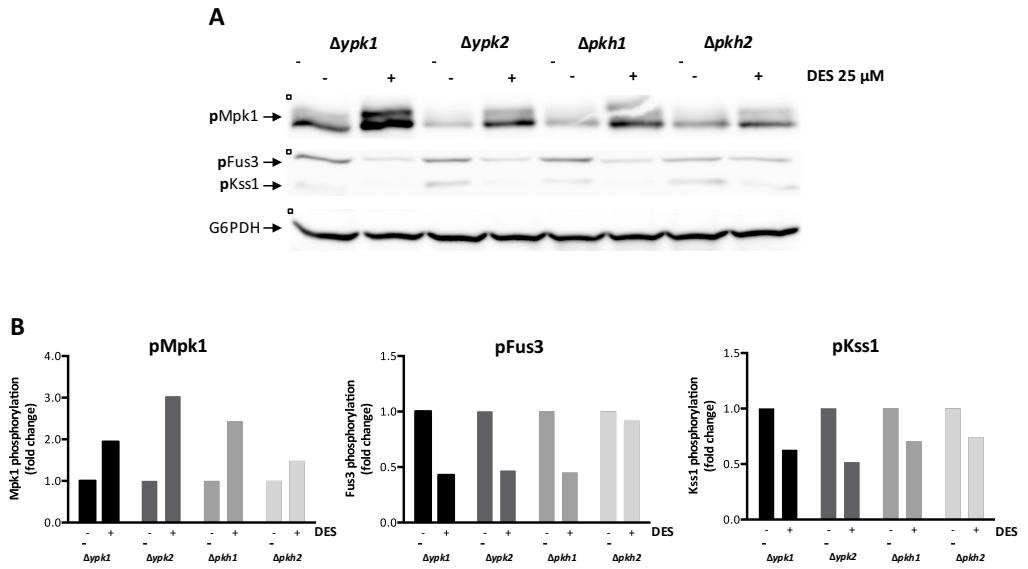

Figure 42 – Single mutants in Pkh1/2 or Ypk1/2 are not affected in DES-triggered Mpk1 activation.

(A) Exponentially growing cells of the *S. cerevisiae* Δ*ypk1*, Δ*ypk2*, Δ*pkh1* and Δ*pkh2* strains were washed and resuspended in KSU buffer at pH 6.5 and incubated for 1 hour at 30ºC. At time 0, 25 µM DES was added to the buffer. Protein extracts collected at time zero (-) and 20 minutes after (+) DES treatment were subjected to immunoblot analysis with anti-phospho-p44/42 MAPK for pMpk1, pFus3 and pKss1 detection. Anti-G6PDH antibody was used as total extract loading control. **(B)** Graphs show the ratio of pMpk1, pFus3 or pKss1 band intensity normalized to G6PDH and expressed as fold response compared with control (time zero; -).

However, since Pkh1/2, as well as Ypk1/2 were previously shown to be functionally redundant, we checked the double mutants lacking both *ypk1* and *ypk2*. Because these double mutants are inviable (indicating that the duplicated genes share an essential function), we again employed temperature-sensitive *ypk1-ts*/Δ*ypk2* strain. After O.N. growth at permissive temperature (25°C), cells were shifted for one hour to restrictive temperature conditions (34°C), before treatment with 25 µM DES. Interestingly, in contrast to the corresponding wild type strain the *ypk1-ts*/Δ*ypk2* mutant failed to induce activation of Mpk1 upon DES treatment [Figure 43].

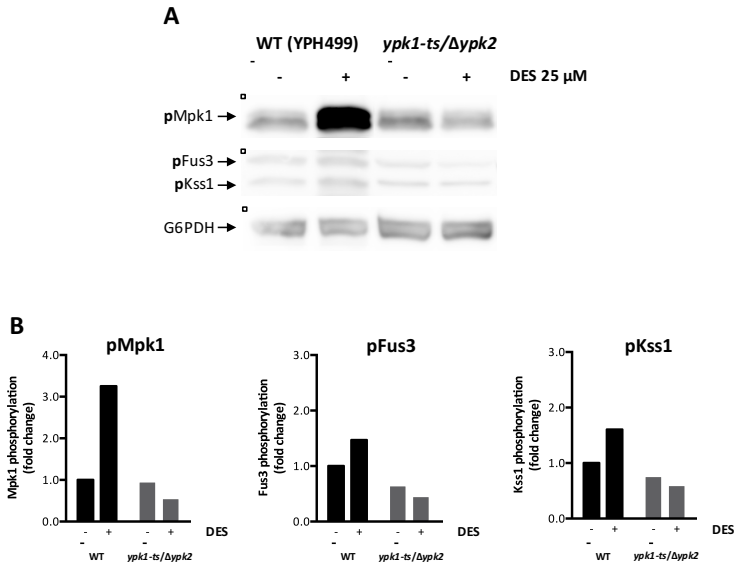

Figure 43 – Ypk1/Ypk2 have important but redundant roles in DES-triggered Mpk1 activation.

(A) Exponentially growing cells of the *S. cerevisiae* wild type YPH499 and *ypk1-ts*/Δ*ypk2* mutant strains were washed and resuspended in KSU buffer at pH 6.5 and incubated for 1 hour at 34ºC. At time 0, 25 μM DES was added to the buffer. Protein extracts collected at time zero (-) and 20 minutes after (+) DES treatment were subjected to immunoblot analysis with anti-phospho-p44/42 MAPK for pMpk1, pFus3 and pKss1 detection. Anti-G6PDH antibody was used as total extract loading control. **(B)** Graphs show the ratio of pMpk1, pFus3 or pKss1 band intensity normalized to G6PDH and expressed as fold response compared with control (wild type untreated cells; -).

Finally, we also monitored the phosphorylation response in mutants lacking either the MAPKKK Bck1 or the MAPK Mpk1 itself. As expected, Bck1 was essential for basal Mpk1 phosphorylation, but interestingly DES-triggered dephosphorylation of Fus3 and Kss1 was still functional in this mutant. Thus, Mpk1 phosphorylation is apparently not required for DES-triggered dephosphorylation of Fus3 and Kss1. Strikingly, in the Δ*mpk1* mutant Fus3 and Kss1 were not dephosphorylated upon DES-treatment suggesting a phosphorylation-independent role of Mpk1 in this process [Figure 44].

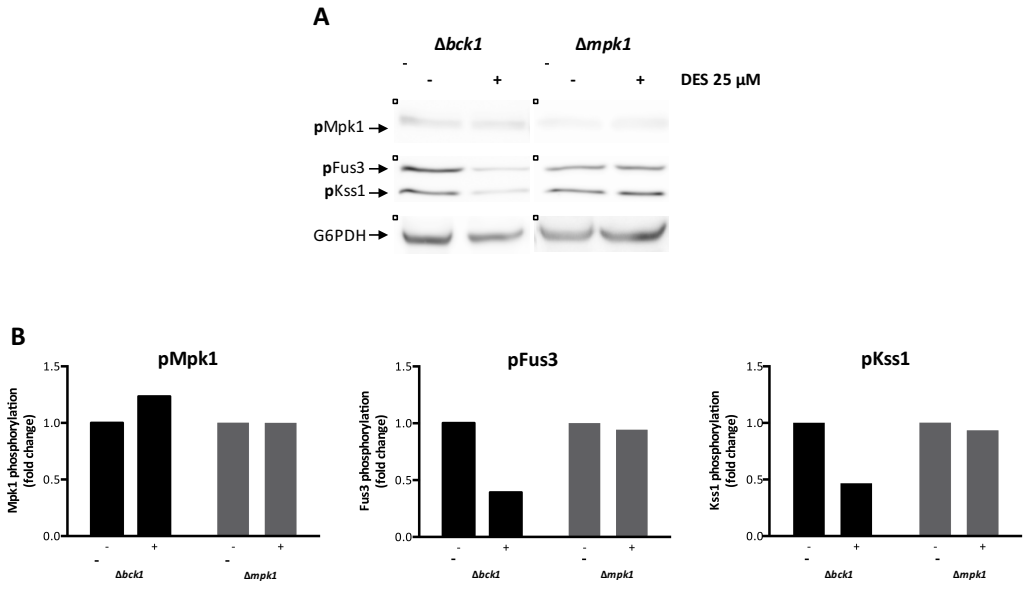

Figure 44 – Evidence for a phosphorylation-independent role of Mpk1 in DES-triggered Fus3 and Kss1 dephosphorylation.
(A) Exponentially growing cells of the *S. cerevisiae Δbck1* and *Δmpk1* strains were washed and resuspended in KSU buffer at pH 6.5 and incubated for 1 hour at 30ºC. At time 0, 25 µM DES was added to the buffer. Protein extracts collected at time zero (-) and 20 minutes after (+) DES treatment were subjected to immunoblot analysis with anti-phospho-p44/42 MAPK for pMpk1, pFus3 and pKss1 detection. Anti-G6PDH antibody was used as total extract loading control. **(B)** Graphs show the ratio of pMpk1, pFus3 or pKss1 band intensity normalized to G6PDH and expressed as fold response compared with control (time zero; -).

4.4.2.2. Role of the Hog1 cascade in DES-triggered Mpk1 activation

The Hog1 MAPK cascade is crucial for fungal growth under hyperosmotic conditions and appears also to have a role in the low temperature response in yeast (Hohmann *et al*., 2007; Panadero *et al*., 2006). The Pbs2-Hog1 MAPK module can be activated by two upstream branches [Figure 45]. The first involves the redundant MAPKKKs Ssk2/Ssk22 and a two-component histidine kinase phospho-relay module comprised of Sln1, Ypd1, and Ssk1. The other branch involves the MAPKKK Ste11, which functions downstream of the membrane sensors Sho1 and Msb2 (Saito and Posas, 2012).

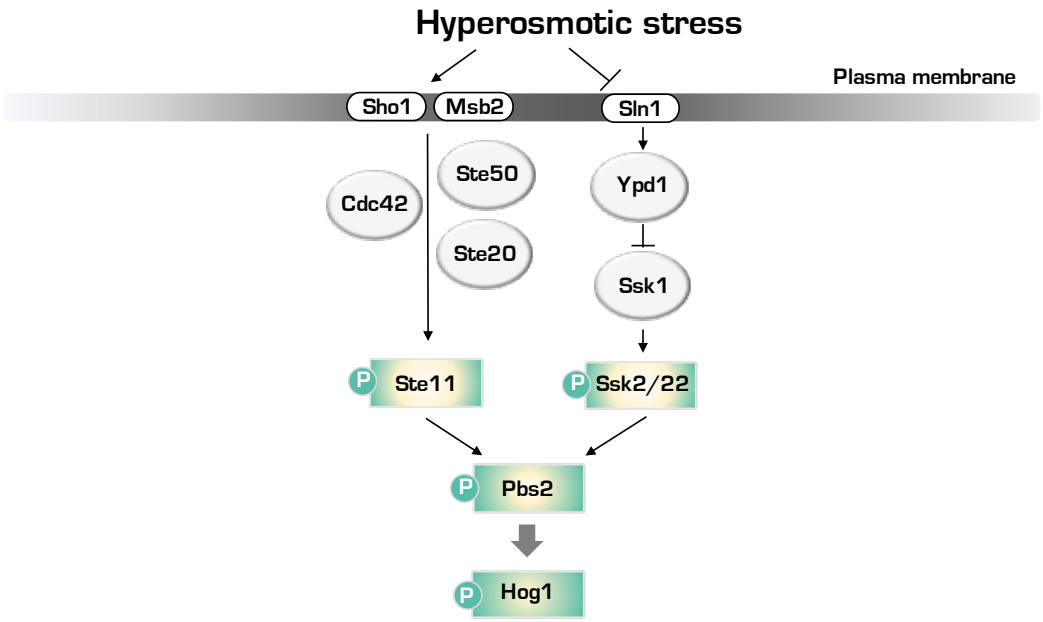

Figure 45 - Schematic Diagram of the hyperosmotic stress Hog1 MAPK signaling pathway in *S. cerevisiae*.
The Pb2-Hog1 MAPK module can be activated by two different upstream branches. One involves the MAPKKK Ste11 which is activated by membrane sensors as Sho1 or Msb2. The other involves the redundant MAPKKKs Ssk2/Ssk22 and a two-component histidine kinase phospho-relay module comprised of Sln1, Ypd1 and Ssk1 (Adapted from (Saito and Posas, 2012)).

We previously found that Hog1 is also phosphorylated upon DES-triggered intracellular acidification, in parallel with Mpk1 (see Figure 37). Western blot analysis of selected deletion mutants in the Hog1 pathway revealed that the Δ*sho1* mutant displayed the same Hog1 phosphorylation response as the wild type, while the Δ*ssk1* mutant failed to activate Hog1 upon DES treatment [Figure 46]. This suggests that Hog1 activation in response to intracellular acidification is mediated by the Sln1-Ssk1 branch, while the Sho1-Ste11 branch is dispensable for this process. As expected, we failed to detect any Hog1 phosphorylation signal in the Δ*pbs2* and Δ*hog1* mutants. Interestingly, the Mpk1 phosphorylation levels before DES treatment appeared to be higher in the Δ*ssk1*, Δ*pbs2* and Δ*hog1* mutants compared to those observed in previous experiments in the wild type strain.

Furthermore, Mpk1 phosphorylation was not induced in these mutants after DES treatment. However, DES-triggered Fus3 and Kss1 dephosphorylation was not affected in any of the Hog1 pathway mutants.

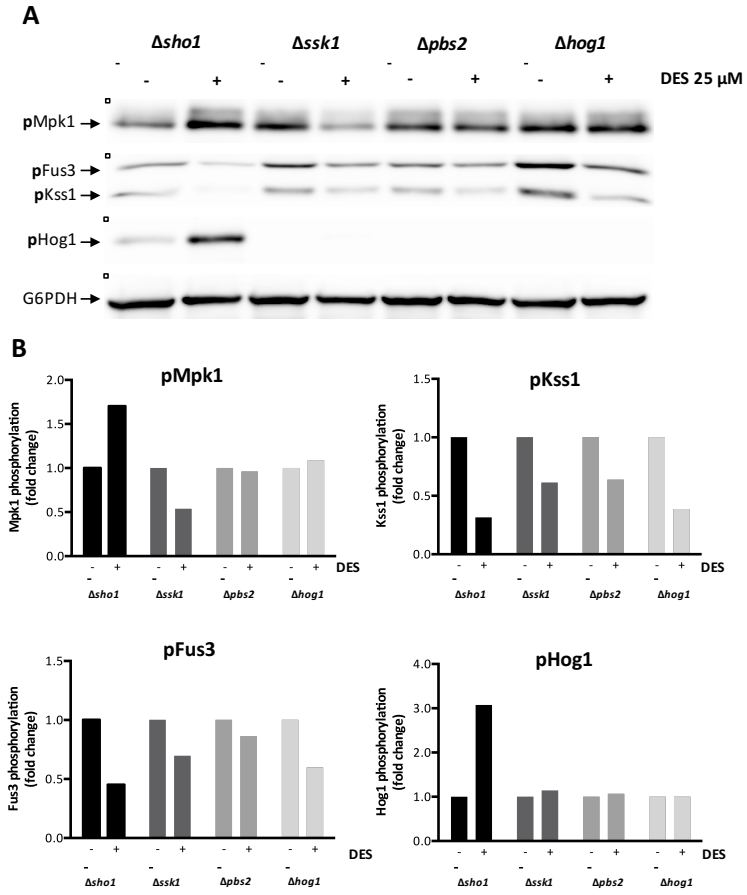

Figure 46 – Role of the Hog1 pathway in DES-mediated Mpk1 activation.
(A) Exponentially growing cells of the *S. cerevisiae* Δ*sho1*, Δ*ssk1*, Δ*pbs2* and Δ*hog1* strains were washed and resuspended in KSU buffer at pH 6.5 and incubated for 1 hour at 30ºC. At time 0, 25 µM DES was added to the buffer. Protein extracts collected at time zero (-) and 20 minutes after (+) DES treatment were subjected to immunoblot analysis with anti-phospho-p44/42 MAPK or anti-phosho-p38 MAPK antibodies, for pMpk1, pFus3 and pKss1, or pHog1 detection, respectively. Anti-G6PDH antibody was used as total extract loading control. **(B)** Graphs show the ratio of pMpk1, pFus3, pKss1 or pHog1 band intensity normalized to G6PDH and expressed as fold response compared with control (time zero; -).

4.4.2.3. Role of known MAPK phosphatases in DES-triggered Mpk1 activation

Proper activation of the MAPK Mpk1 is crucial for maintenance of cell wall integrity in different environmental conditions. However, hyperactivation of this MAPK cascade, as well as of any other MAPK cascade, can be lethal for the cell. Therefore, cells have developed mechanisms for controlling the magnitude and duration of MAPK activation. Phosphorylation of both threonine and tyrosine within the activation loop is required for MAPK activity, and dephosphorylation of either residue is sufficient for MAPK inactivation. Protein phosphatases are able to downregulate MAPK signaling by removing the phosphate from the tyrosine, threonine or from both residues. At present, three classes of protein phosphatases have been described: protein tyrosine phosphatases (PTPs), serine/threonine protein phosphatases and dual-specificity protein phosphatases (DSPs) (Martín *et al*., 2005) [Figure 47].

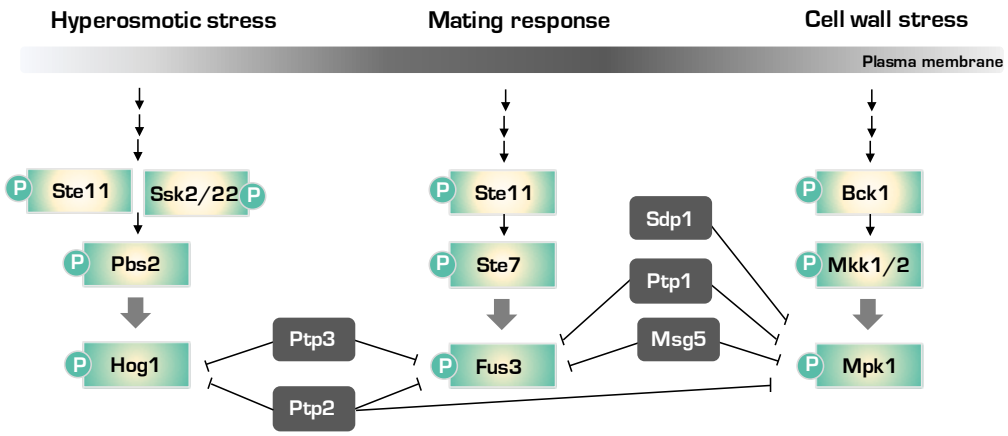

Figure 47 – Schematic diagram of the known MAPK phosphatases inhibiting MAPK signaling in *S. cerevisiae*.
The specificity of the protein tyrosine phosphatases (PTPs) Ptp1, Ptp2 and Ptp3, as well as of the dual-specificity protein phosphatase (DSPs) Sdp1 and Msg5 is indicated in the figure (Adapted from (Martín *et al*., 2005)).

Because protein phosphatases act as negative regulators of MAPK phosphorylation, we reasoned that they might contribute to pH_i-mediated regulation of MAPK activity. We thus decided to explore the role of known MAPK phosphatases, including the PTPs Ptp1, Ptp2 and Ptp3, as well as the DSPs Spd1 and Msg5 [Figure 47], using yeast deletion mutants. We found that DES-triggered induction of Mpk1 was still functional in the Δ*ptp1*, Δ*sdp1*, Δ*ptp2* and Δ*ptp3* mutants [Figure 48]. Interestingly, the Δ*ptp2* mutant strain appeared to have a stronger increase of Mpk1 phosphorylation than previously observed in the wild type strain. Strikingly, the Δ*msg5* mutant showed no apparent induction of Mpk1 phosphorylation upon DES-induced intracellular acidification. Moreover, the baseline phosphorylation level of Mpk1 before DES treatment was increased in the Δ*msg5* mutant.

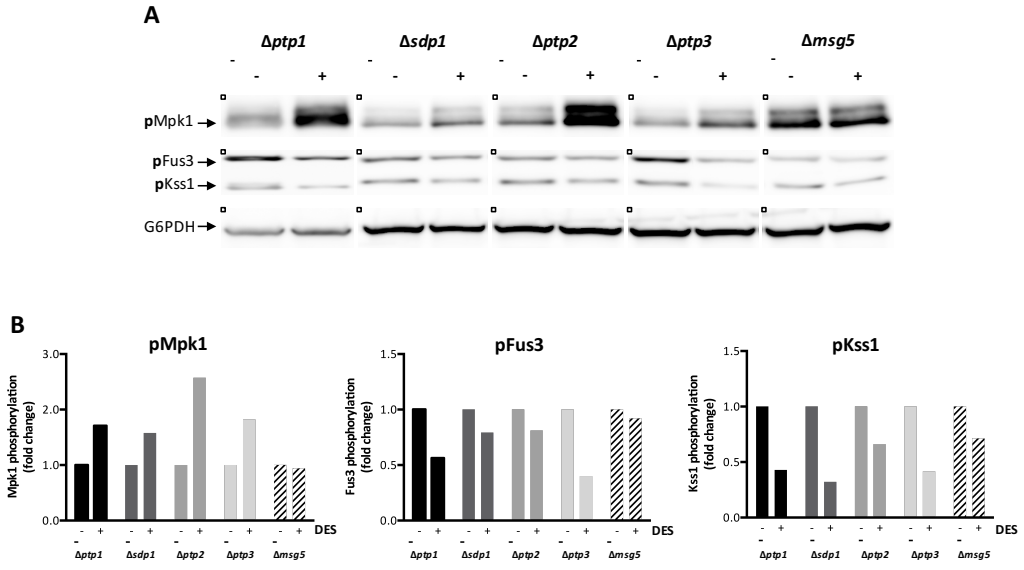

Figure 48 – The dual-specificity protein phosphatase Msg5 regulates pH-triggered Mpk1 phosphorylation in yeast.

(A) Exponentially growing cells of the *S. cerevisiae* Δ*ptp1*, Δ*sdp1*, Δ*ptp2*, Δ*ptp3* and Δ*msg5* strains were washed and resuspended in KSU buffer at pH 6.5 and incubated for 1 hour at 30ºC. At time 0, 25 µM DES was added to the buffer. Protein extracts collected at time zero (-) and 20 minutes after (+) DES treatment were subjected to immunoblot analysis with anti-phospho-p44/42 MAPK for pMpk1, pFus3 and pKss1 detection. Anti-G6PDH antibody was used as total extract loading control. **(B)** Graphs show the ratio of pMpk1, pFus3 or pKss1 band intensity normalized to G6PDH and expressed as fold response compared with control (time zero; -).

4.4.2.3.1. Msg5 is a key regulator of Mpk1 activity

To further investigate the role of Msg5 in pH_i-mediated regulation of Mpk1 activity, a time-course analysis of Mpk1 phosphorylation was performed in the wild type and *Δmsg5* mutant strains after DES-induced intracellular acidification. In the wild type strain, as previously observed, Mpk1 became rapidly phosphorylated while Fus3/Kss1 became dephosphorylated [Figure 49]. In the *Δmsg5* mutant, the Mpk1 phosphorylation level at time 0 was three times higher than in the wild type, but still increased after DES-triggered intracellular acidification, although less than in the wild type strain. Fus3 and Kss1 MAPKs dephosphorylation was apparently not affected by the loss of Msg5 [Figure 49].

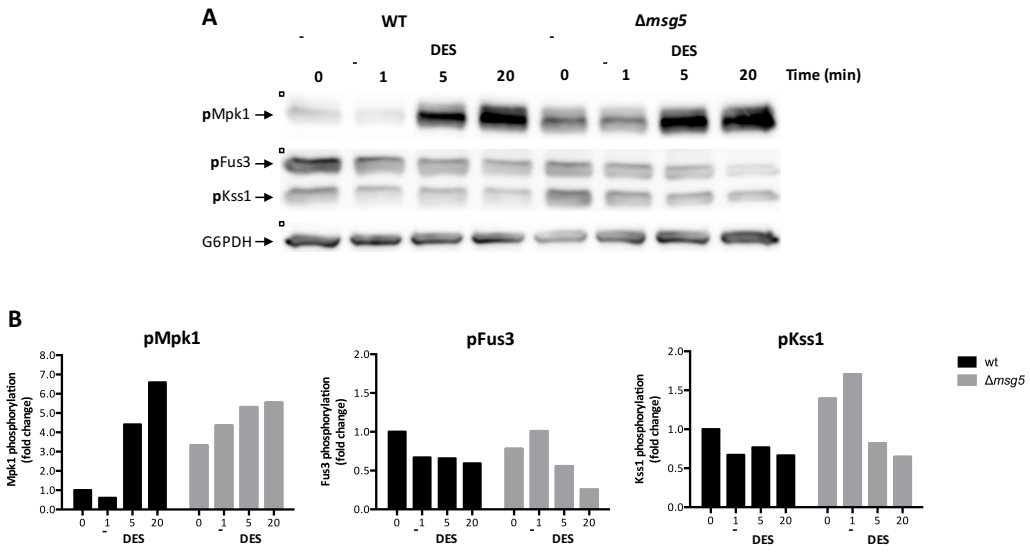

Figure 49 – Msg5 inhibits Mpk1 phosphorylation in no-treated yeast cells.
(A) Exponentially growing cells of the *S. cerevisiae* wild type and Δ*msg5* strains were washed and resuspended in KSU buffer at pH 6.5 and incubated for 1 hour at 30ºC. At time 0, 25 μM DES was added to the buffer. Protein extracts collected before (time zero) and 1, 5 or 20 minutes after DES treatment were subjected to immunoblot analysis with anti-phospho-p44/42 MAPK for pMpk1, pFus3 and pKss1 detection. Anti-G6PDH antibody was used as total extract loading control. **(B)** Graphs show the ratio of pMpk1, pFus3 or pKss1 band intensity normalized to G6PDH and expressed as fold response compared with wild type at time zero.

So far, our data suggest that Msg5 is a major regulator of Mpk1 activity, and that it limits the phosphorylation of this MAPK to baseline level at time 0. But does Msg5 have a role in the rapid activation of Mpk1 upon DES-triggered intracellular acidification? One hypothetical mechanism for such a role would be a reduced interaction between Msg5 and Mpk1, which should prevent dephosphorylation of the MAPK and therefore result in its activation. Reduced Msg5-Mpk1 interaction could occur either as a consequence of reduced affinity of Msg5 or due to higher instability and rapid decrease of Msg5 protein levels in the cell. To test the latter hypothesis, we monitored the abundance of Msg5 after DES treatment in a yeast strain carrying a *msg5-Myc*$_6$ allele integrated into the *msg5* locus (Flández *et al.*, 2004). Detection of Myc-tagged protein was carried out by western blot with a commercial anti-*c*-Myc antibody. These experiments revealed that the level of Msg5 decreased by approximately 40%, twenty minutes after DES-induced intracellular acidification [Figure 50]. This result provides a first evidence suggesting that intracellular acidification triggers a decrease in Msg5 protein levels, which should result in higher levels of phosphorylated Mpk1 protein.

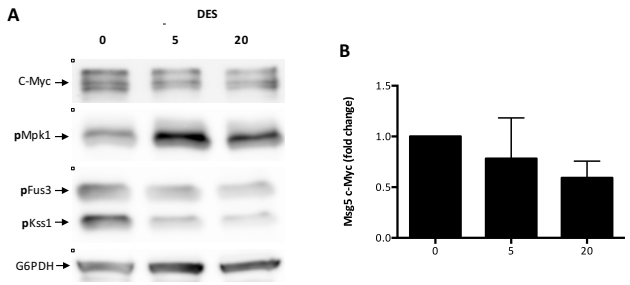

Figure 50 – The level of the Msg5 phosphatase is affected by intracellular acidification.

(A) Time-course analysis of Msg5 level in the YMF1 yeast strain carrying a *c*-Myc tagged Msg5 protein. Exponentially growing cells were washed and resuspended in KSU buffer at pH 6.5 and incubated for 1 hour at 30ºC. At time 0, 25 µM DES was added to the buffer. Protein extracts collected before (time zero) and 5 or 20 minutes after DES treatment were subjected to immunoblot analysis with anti-phospho-p44/42 MAPK or anti-*c*-Myc antibodies for pMpk1, pFus3 and pKss1 or *c*-Myc detection, respectively. Anti-G6PDH antibody was used as total extract loading control. **(B)** Graphs show the ratio of *c*-Myc band intensity normalized to G6PDH and expressed as fold response compared with control (time zero). Data shown represent the mean and standard deviations of three independent replicates.

4.4.2.4. Identification of fungal genes regulating pH_i-triggered Mpk1 activation

4.4.2.4.1. Design of a general strategy to identify new regulators of DES-triggered Mpk1 activation using yeast deletion mutants

Our results obtained so far established that pH_i acts as a key regulator of MAPK phosphorylation, both in *F. oxysporum* and in yeast. Moreover, the finding that the Mpk1 MAPK cascade is activated in response to extra- and intracellular acidification suggests that this pathway must be important for cell survival at acidic conditions. In line with this idea, previous screens for acid-sensitive deletion mutants in yeast identified Mpk1 and several upstream regulators of the CWI MAPK cascade (Kawahata *et al.*, 2006; Schüller *et al.*, 2004). We thus hypothesized that at least some of the acid-sensitive mutants identified in these previous studies should also be affected in pH_i-mediated MAPK regulation. If this is the case, the available list of acid-sensitive mutants could be used as a starting point for the identification of new components regulating pH_i-mediated Mpk1 activation in fungi, using our well-established western blot protocol after DES-treatment.

Based on this idea, we designed the following general strategy:

1) Select a subset of the acid-sensitive yeast mutants identified in the studies by (Kawahata *et al.*, 2006; Schüller *et al.*, 2004) from the EUROSCARF haploid knockout strain collection. A preselection was necessary, because the high investment of time and cost associated with the western blot protocol would only allow us to screen approximately one hundred candidate mutants.

2) Analyze the selected subset of acid-sensitive mutants for DES-triggered phosphorylation of Mpk1 in comparison with the wild type strain, using our established western blot protocol and two time-points, 0 and 20 min (T0, T20).

3) Identify the mutants affected in the phosphorylation response and classify the proteins encoded by the deleted genes according to their cellular functions.

4) Subject the most interesting candidates to additional analysis, including phosphorylation of other MAPKs or presence of potential orthologs in *Fusarium oxysporum*.

4.4.2.4.2. Criteria for the preselection of a subset of the acid-sensitive yeast mutants for analysis of DES-triggered Mpk1 phosphorylation

The following criteria were established to preselect a subset of acid-sensitive mutants from the EUROSCARF haploid knockout strain collection. First, only HCl-sensitive mutants (as opposed to mutants sensitive to other acids such as acetic or sorbic acid) were selected, since HCl had been used consistently for acidification in our experiments. Second, after clustering the mutants into functional categories according to Gene Ontology in the Saccharomyces Genome Database (SGD), all downstream components of the Mpk1 cascade which are mostly associated with gene expression or translational control, were excluded. Application of these two selection criteria yielded a total of 106 haploid mutant strains to be submitted to analysis of DES-triggered Mpk1 activation [Table 11].

Table 11 – List of acid-sensitive yeast mutant strains preselected for analysis in this study, clustered into functional categories.

GENE	ORF	GENE	ORF
METABOLISM			
Amino acid metabolism			
ARO1	YDR127W	HOM3	YER052C
ARO2	YGL148W	ILV1	YER086W
FUR4	YBR021C	THR1	YHR025W
GLY1	YEL046C	TYR1	YBR166C
HOM2	YDR158W		
Lipid, fatty acid and isoprenoid metabolism			
ARG82	YDR173C	ERG6	YML008C
CSG2	YBR036C	KCS1	YDR017C
ERG24	YNL280C	SAC1	YKL212C
ERG28	YER044C	SKM1	YOL113W
ERG3	YLR056W	SUR1	YPLL057C
ERG4	YGL012W		
CELLULAR TRAFFICKING			

BST1	YFL025C	SNF7	YLR025W
CLC1	YGR167W	TLG2	YOL018C
CSF1	YLR087C	VPS1	YKR001C
DID4	YKL002W	VPS15	YBR097W
DRS2	YAL026C	VPS17	YOR132W
GYP1	YOR070C	VPS20	YMR077C
KRE11	YGR166W	VPS24	YKL041W
PEP3	YLR148W	VPS25	YJR102C
PEP5	YMR231W	VPS29	YHR012W
PEP7	YDR323C	VPS45	YGL095C
PEP8	YJL053W	VPS5	YOR069W
RMD7	YER083C	VPS51	YKR020W
SLA2	YBL007C	VPS9	YML097C
REGULATION OF INTERACTION WITH CELLULAR ENVIRONMENT			
Ion homeostasis			
CCH1	YGR217W	VMA16	YHR026W
CUP5	YEL027W	VMA2	YBR127C
ECM7	YLR443W	VMA21	YGR105W
ICS3	YJL077C	VMA4	YOR332W
MID1	YNL291C	VMA5	YKL080W
TRK1	YJL129C	VMA7	YGR020C
VMA1	YDL185W	VMA8	YEL051W
VMA11	YPL234C	VPH2	YKL119C
VMA13	YPR036W	VPS3	YDR495C
Cellular sensing and response / signal transduction pathways			
ASC1	YMR116C	RGD1	YBR260C
CCS1	YMR038C	SCP160	YJL080C
CNB1	YKL190W	SOD1	YJR104C
NBP2	YDR162C		
CONTROL OF CELLULAR ORGANIZATION			
Cell wall			
CWH41	YGL027C	KRE1	YGL203C
DCW1	YKL046C	KRE6	YPR159W
FLC1	YPL221W	ROT2	YBR229C
GAS1	YMR307W	SMI1	YGR229C
Cytoskeleton and cell polarity			
BEM2	YER155C	SHE4	YOR035C
CDC10	YCR002C	SPC72	YAL047C
RBL2	YOR265W	SRV2	YNL138W
PROTEIN FATE (FOLDING, MODIFICATION AND FATE)			
ALG5	YPL227C	MOT2	YER068W
ALG6	YOR002W	OCH1	YGL038C
ALG8	YOR067C	OST4	YDL232W
DIE2	YGR227W	PER1	YCR044C

GUP1	YGL084C	RHK1	YBL082C
CELL CYCLE			
HSL1	YKL101W		
SIT4	YDL047W		
GENE EXPRESSION			
BUD32	YGR262C		
SPT3	YDR392W		
TRANSLATION REGULATION			
MTQ2	YDR140W		
RNY1	YPL123C		
SSD1	YDR293C		
OTHERS			
ATG14	YBR127C		
HUR1	YGL168W		
KEX1	YGL203C		
VAM10	YOR068C		

4.4.2.4.3. Analysis of Mpk1 activation in the pre-selected acid-sensitive mutants

Mutant strains were grown until an OD_{640} of 0.9, washed and incubated in KSU buffer medium at pH 6.5, for one hour. Afterwards, samples were collected before (T0) and 20 minutes (T20) after DES addition to the buffer. The amount of protein was determined in each sample using the Bradford assay and western blot analysis performed in all selected mutants as described above [Figure 51].

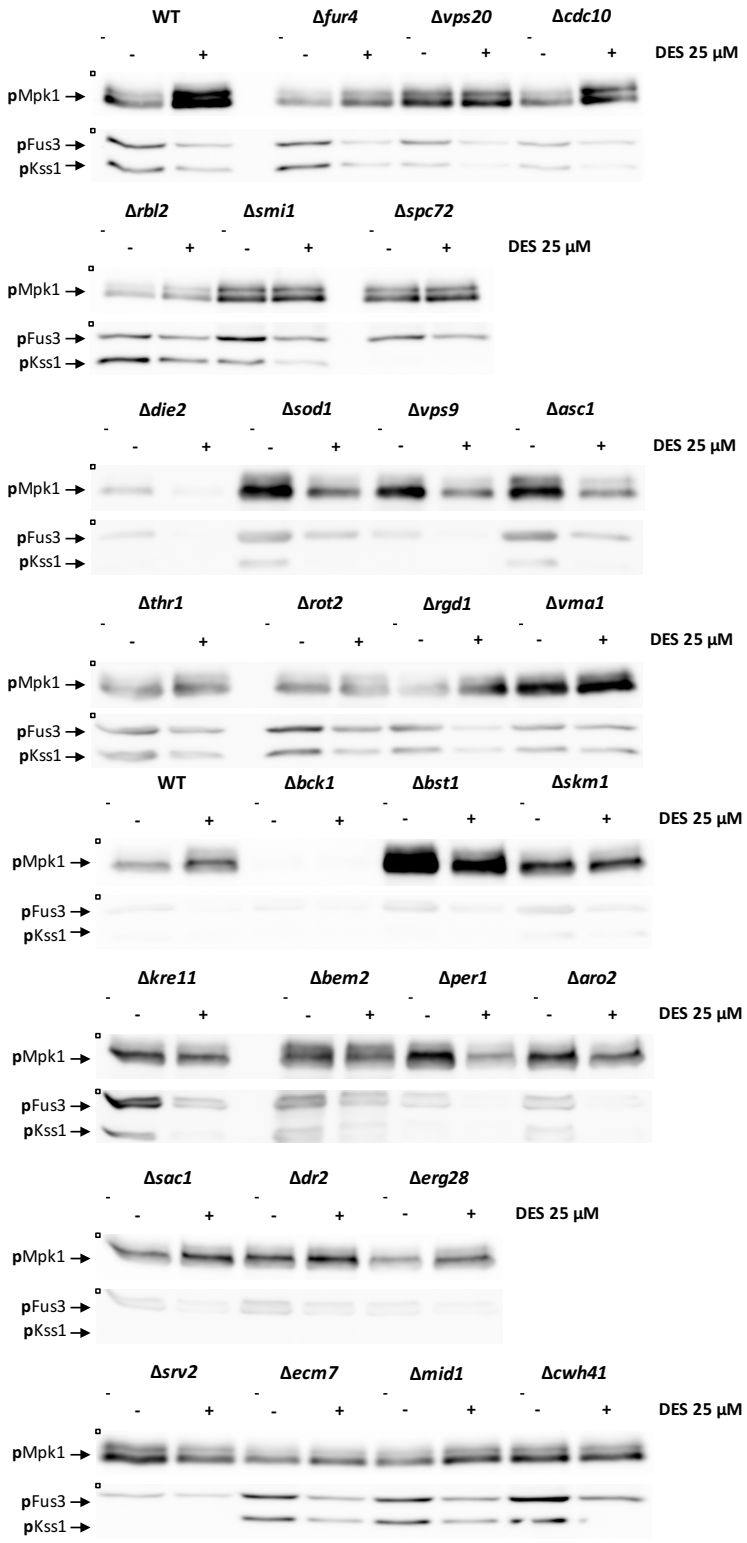
WT
Δfur4
Δvps20
Δcdc10
DES 25 µM
pMpk1
pFus3
pKss1
Δrbl2
Δsmi1
Δspc72
DES 25 µM
pMpk1
pFus3
pKss1
Δdie2
Δsod1
Δvps9
Δasc1
DES 25 µM
pMpk1
pFus3
pKss1
Δthr1
Δrot2
Δrgd1
Δvma1
DES 25 µM
pMpk1
pFus3
pKss1
WT
Δbck1
Δbst1
Δskm1
DES 25 µM
pMpk1
pFus3
pKss1
Δkre11
Δbem2
Δper1
Δaro2
DES 25 µM
pMpk1
pFus3
pKss1
Δsac1
Δdr2
Δerg28
DES 25 µM
pMpk1
pFus3
pKss1
Δsrv2
Δecm7
Δmid1
Δcwh41
DES 25 µM
pMpk1
pFus3
pKss1

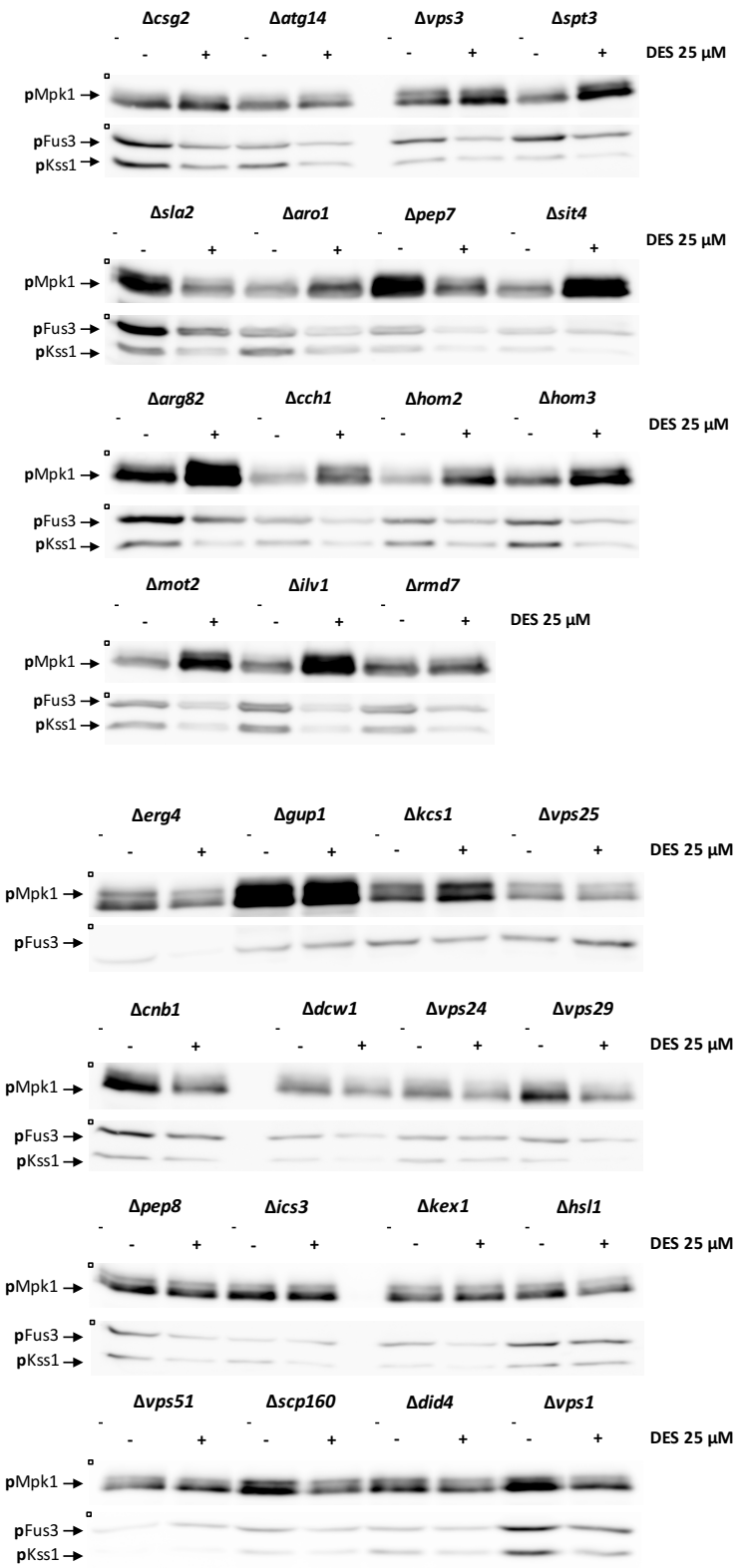
Δcsg2
Δatg14
Δvps3
Δspt3
DES 25 µM
pMpk1
pFus3
pKss1
Δsla2
Δaro1
Δpep7
Δsit4
DES 25 µM
pMpk1
pFus3
pKss1
Δarg82
Δcch1
Δhom2
Δhom3
DES 25 µM
pMpk1
pFus3
pKss1
Δmot2
Δilv1
Δrmd7
DES 25 µM
pMpk1
pFus3
pKss1
Δerg4
Δgup1
Δkcs1
Δvps25
DES 25 µM
pMpk1
pFus3
Δcnb1
Δdcw1
Δvps24
Δvps29
DES 25 µM
pMpk1
pFus3
pKss1
Δpep8
Δics3
Δkex1
Δhsl1
DES 25 µM
pMpk1
pFus3
pKss1
Δvps51
Δscp160
Δdid4
Δvps1
DES 25 µM
pMpk1
pFus3
pKss1

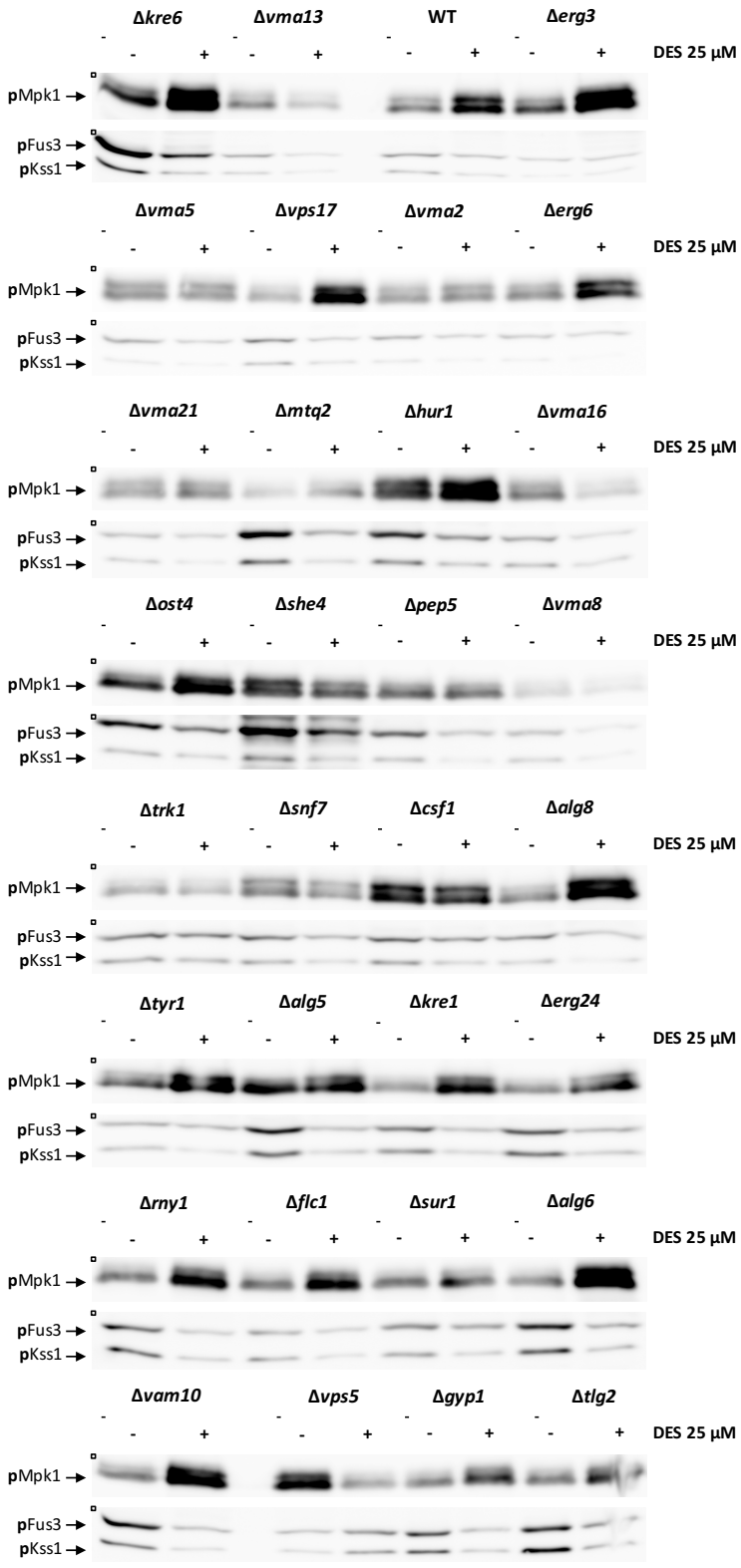
Δkre6
Δvma13
WT
Δerg3
DES 25 µM
pMpk1
pFus3
pKss1
Δvma5
Δvps17
Δvma2
Δerg6
Δvma21
Δmtq2
Δhur1
Δvma16
Δost4
Δshe4
Δpep5
Δvma8
Δtrk1
Δsnf7
Δcsf1
Δalg8
Δtyr1
Δalg5
Δkre1
Δerg24
Δrny1
Δflc1
Δsur1
Δalg6
Δvam10
Δvps5
Δgyp1
Δtlg2

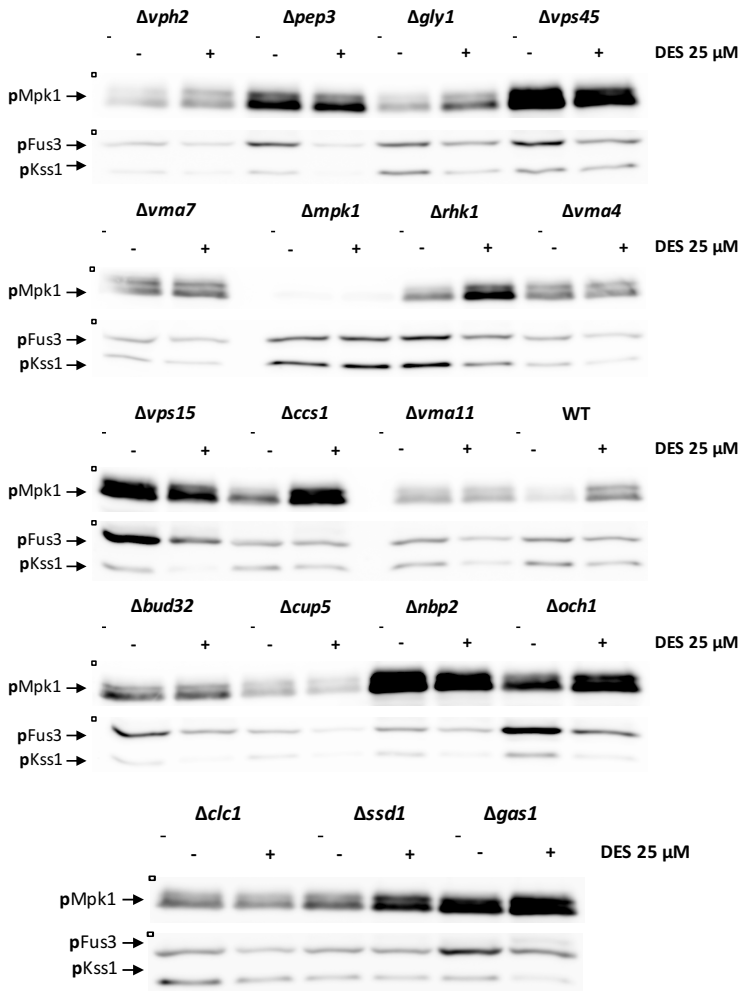

Figure 51 – Identification of acid-sensitive mutants involved on DES-triggered Mpk1 activation.

Exponentially growing cells of the *S. cerevisiae* acid-sensitive mutant strains were washed and resuspended in KSU buffer at pH 6.5 and incubated for 1 hour at 30ºC. At time 0, 25 µM DES was added to the buffer. Protein extracts collected at time zero (-) and 20 minutes after (+) DES treatment were subjected to immunoblot analysis with anti-phospho-p44/42 MAPK for pMpk1, pFus3 and pKss1 detection.

4.4.2.4.4. Criteria for the identification of candidate regulators of DES-triggered Mpk1 phosphorylation

To identify mutants affected in DES-triggered Mpk1 activation two selection criteria were established, both based on phosphorylation levels of Mpk1 before (T0) and 20 min after DES treatment (T20). In previous experiments with the wild type strain, Mpk1 phosphorylation level at T0 was 14543±4980 (arbitrary units provided by the ImageJ software) while those at T20 was 32111±12060. This corresponds to a T20/T0 ratio of 2.19±0.23, or an approximately two-fold induction of Mpk1 phosphorylation. We thus quantified the intensity of Mpk1 phosphorylation in the analyzed mutant strains at T0 and T20, and calculated the T20/T0 ratio. First, mutants with a ratio <1.25 were considered to present no significant increase in Mpk1 phosphorylation. Second, mutants with an intensity of at T0 >40000 (twice the wild type at T0) were considered to exhibit constitutive hyperphosphorylation of Mpk1. After applying these two criteria, we identified three different categories of mutants:

1) low initial phosphorylation levels, DES-triggered induction (similar to the wild type): T0<40000, T20/T0>1.25.

2) low initial phosphorylation levels, no DES-triggered induction: T0<40000, T20/T0<1.25.

3) constitutive hyperphosphorylation, no DES-triggered induction: T0>40000, T20/T0<1.25.

From all acid-sensitive yeast mutants analyzed (106 in the total), we identified 39 mutants in the category 1 presenting an induction similar to the wild type. From the mutants exhibiting no DES-triggered induction of Mpk1, 59 mutants showed a similar phosphorylation at T0 to the wild type (category 2), while 8 mutant strains showed constitutive hyperphosphorylation at T0 (category 3). An example of mutant exhibiting the features of each category is showed in [Figure 52].

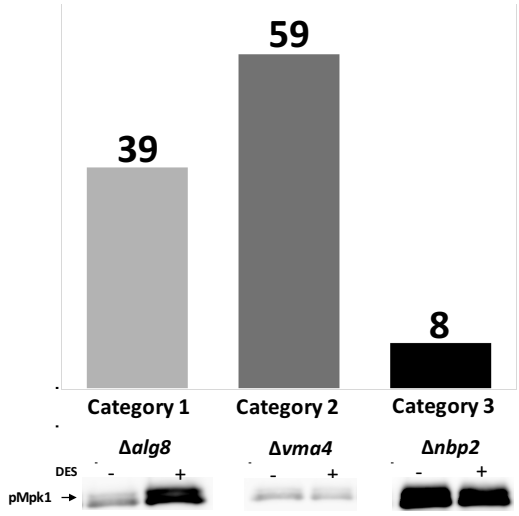

Figure 52 - Result of the analysis of 106 pre-selected acid-sensitive mutants for DES-triggered Mpk1 phosphorylation.
Western blotting analysis was performed in 106 haploid mutant strains of *S. cerevisiae*. Exponentially growing cells were washed and resuspended in KSU buffer at pH 6.5 and incubated for 1 hour at 30ºC. At time 0, 25 µM DES was added to the buffer. Protein extracts collected at time zero (-) and 20 minutes after (+) DES treatment were subjected to immunoblot analysis with anti-phospho-p44/42 MAPK for pMpk1 detection. Each mutant was grouped in Category 1, 2 or 3, accordingly with the level of phosphorylation at T0 and ratio T20/T0. Mutants in Category 1 presented an induction similar to the wild type strain. Category 2 and 3 include mutants in which no induction of Mpk1 was observed. Category 3 differ from Category 2 by presenting mutants with constitutive hyperphosphorylation of Mpk1 at T0. An example for each category is exhibited.

Mutants affected in DES-triggered Mpk1 activation (T20/T0 <1.25; Category 2 and 3) were classified into functional categories according to their biological function [Table 12]. In addition, the fold change of Mpk1 phosphorylation (T20/T0), as well as the absolute Mpk1 phosphorylation level at T0 (Mpk1-P T0) are indicated in the table.

Table 12 - Classification of mutants impaired in DES-triggered Mpk1 phosphorylation according to biological function. Mutants with Mpk1-P level T0>40000 are in bold

GENE	T20/T0	Mpk1-P level T0	CELLULAR FUNCTION
METABOLISM			
Amino acid metabolism			
ARO2	0,71	20004	Bifunctional chorismate synthase and flavin reductase; catalyzes the conversion of 5-enolpyruvylshikimate 3-phosphate (EPSP) to chorismate
Lipid, fatty acid and isoprenoid metabolism			
CSG2	1,13	21382	ER membrane protein; required for mannosylation of inositolphosphorylceramide and for growth at high calcium concentrations
ERG28	0,71	27527	ER membrane protein; may facilitate interactions between the Erg26 dehydrogenase and the Erg27 3-ketoreductase
ERG4	0,62	23309	C-24(28) sterol reductase; catalyzes the final step in ergosterol biosynthesis
SAC1	0,57	24200	Phosphatidylinositol phosphate (PtdInsP) phosphatase regulates PtdIns[4]P hydrolysis; involved in protein trafficking and processing, secretion, and cell wall maintenance; regulates sphingolipid biosynthesis (through PtdIns(4)P metabolism)
SKM1	0,89	26950	Predicted serine/threonine kinase similar to Ste20 and Cla4; involved in negative regulation of sterol import
SUR1	1,22	12536	Mannosylinositol phosphorylceramide (MIPC) synthase catalytic subunit; forms a complex with regulatory subunit Csg2; function in sphingolipid biosynthesis
CELLULAR TRAFFICKING			
BST1	0,80	**45800**	GPI inositol deacylase of the ER; negatively regulates COPII vesicle formation; prevents production of vesicles with defective subunits; required for proper discrimination between resident ER proteins and Golgi-bound cargo molecules
CLC1	0,74	19909	Structural light chain protein component of clathrin vesicle coats; required for proper trimerization of clathrin heavy chains; positively regulates endocytosis
CSF1	0,87	30316	Protein plays a role in the maturation of secretory proteins
DID4	0,77	26729	Class E Vps protein of the ESCRT-III complex; required for sorting of integral membrane proteins into lumenal vesicles of multivesicular bodies (MVB), and for delivery of newly synthesized vacuolar enzymes to the vacuole, involved in endocytosis
DRS2	0,91	28881	Subunit of the Cdc50-Drs2 aminophospholipid flippase complex; maintains membrane lipid asymmetry in post-Golgi secretory vesicles; contributes to clathrin-coated

			vesicle formation, endocytosis, protein trafficking between the Golgi and endosomal system and the cellular response to mating pheromone
KRE11	0,83	17685	Component of transport protein particle (TRAPP) complex II; TRAPPII is a multimeric guanine nucleotide-exchange factor for the GTPase Ypt1, regulating intra-Golgi and endosome-Golgi traffic; role in cell wall beta-glucan biosynthesis
PEP3	0,86	34646	Component of CORVET membrane tethering complex; vacuolar peripheral membrane protein that promotes vesicular fusion reactions in conjunction with SNARE proteins, required for vacuolar biogenesis
PEP5	0,90	26397	Histone E3 ligase, component of CORVET membrane tethering complex; peripheral vacuolar membrane protein required for protein trafficking and vacuole biogenesis; interacts with Pep7; involved in ubiquitination and degradation of excess histones
PEP7	0,47	**40032**	Adaptor protein involved in vesicle-mediated vacuolar protein sorting; ensures high-fidelity vesicle docking and fusion, essential for targeting vesicles to the endosome
PEP8	0,88	26037	Vacuolar protein that forms part of the multimeric membrane-associated retromer complex involved in vacuolar protein sorting along with Vps35, Vps29, Vps17, and Vps5; essential for endosome-to-Golgi retrograde protein transport
RMD7	1,09	21019	Subunit of the GET complex; involved in insertion of proteins into the ER membrane
SLA2	0,41	33212	Adaptor protein that links actin to clathrin and endocytosis; involved in membrane cytoskeleton assembly and cell polarization
SNF7	0,72	15191	Subunit of the ESCRT-III complex; involved in the sorting of transmembrane proteins into the MVB pathway; recruited from the cytoplasm to endosomal membranes
VPS1	0,68	30940	Dynamin-like GTPase required for vacuolar sorting; involved in cytoskeleton organization, endocytosis, late Golgi-retention of some proteins
VPS15	0,75	**44558**	Serine/threonine protein kinase involved in vacuolar protein sorting; function as a membrane-associated complex with Vps34; active form recruits Vps34 to the Golgi; interacts with the GDP-bound form of Gpa1
VPS20	1,03	28059	Myristoylated subunit of the ESCRT-III complex; cytoplasmic protein recruited to endosomal membranes
VPS24	0,72	17410	Subunit of the ESCRT-III complex; forms a subcomplex with Did4; involved in the sorting of transmembrane proteins into the multivesicular body (MVB) pathway

VPS25	0,84	13696	Component of the ESCRT-II complex; ESCRT-II is involved in ubiquitin-dependent sorting of proteins into the endosome
VPS29	0,49	28070	Subunit of the membrane-associated retromer complex; essential for endosome-to-Golgi retrograde transport; forms a subcomplex with Vps35 and Vps26
VPS45	0,91	**49232**	Protein of the Sec1/Munc-18 family; required for the function of Pep12 and Tlg2; essential for fusion of Golgi-derived vesicles with the prevacuolar compartment
VPS5	0,28	32077	Component of prevacuolar/late endosomal compartment back to late Golgi; forms a retromer subcomplex with Vps17
VPS51	1,20	16358	One of four components of the GARP (Golgi-associated retrograde protein) complex, required for the recycling of proteins from endosomes to the late Golgi
VPS9	0,48	23066	Guanine nucleotide exchange factor (GEF) and ubiquitin receptor; involved in Golgi-endosome trafficking and sorting through the MVB; required for localization of the CORVET complex to endosomes

REGULATION OF INTERACTION WITH CELLULAR ENVIRONMENT

Ion homeostasis

CUP5	0,76	9163	Proteolipid subunit c of the V0 domain of V-ATPase; required for vacuolar acidification and important for copper and iron metal ion homeostasis
ECM7	1,16	13197	Putative integral membrane protein with a role in calcium uptake
ICS3	0,99	24781	Protein with a role in copper homeostasis; possible role in vacuolar sorting and processing of secretory proteins
TRK1	0,81	7045	Component of the Trk1-Trk2 potassium transport system
VMA1	1,13	25577	Subunit A of the V1 peripheral membrane domain of V-ATPase
VMA11	0,91	11355	V-ATPase V0 domain subunit c’
VMA13	0,47	10864	Subunit H of the V1 peripheral membrane domain of V-ATPase
VMA16	0,34	14419	Subunit c’’ of the V-ATPase V0 domain
VMA2	1,16	14085	Subunit B of V1 peripheral membrane domain of the V-ATPase
VMA21	1,08	10978	Integral membrane protein required for V-ATPase function; not an actual component of the V-ATPase; functions in the assembly of the V-ATPase
VMA4	0,86	18409	Subunit E of the V1 domain of the V-ATPase
VMA5	0,83	19199	Subunit C of the V1 peripheral membrane domain of V-ATPase
VMA7	1,19	16480	Subunit F of the V1 peripheral membrane domain of V-ATPase

VMA8	0,58	6727	Subunit D of the V1 peripheral membrane domain of V-ATPase
VPS3	1,24	24118	Component of CORVET complex; required for the sorting and processing of soluble vacuolar proteins, and assembly of the V-ATPase
Cellular sensing and response / signal transduction pathways			
ASC1	0,39	28257	G-protein beta subunit and guanine dissociation inhibitor for Gpa2; core component of the small (40S) ribosomal subunit; required to prevent frameshifting at ribosomes stalled at repeated CGA codons; represses Gcn4 in the absence of amino acid starvation
CNB1	0,53	37201	Regulatory subunit of calcineurin, a Ca^{2+}/calmodulin-regulated type 2B protein phosphatase that regulates the stress-response transcription factor Crz1
NBP2	0,88	**46603**	Protein involved in the HOG pathway; negatively regulates Hog1 by recruitment of phosphatase Ptc1 to the Pbs2p-Hog1 complex; interacts with Bck1 and down regulates the CWI pathway
SCP160	0,65	30448	Essential RNA-binding G protein effector of mating response pathway; ligand-activated RNA-binding protein that delivers RNAs involved in polarization and perpetualizing mating signal to shmoo tip during pheromone signaling; Scp160p-mediated RNA trafficking essential for chemotropism and successful mating
SOD1	0,47	31083	Cytosolic copper-zinc superoxide dismutase, that detoxifies superoxide
CONTROL OF CELLULAR ORGANIZATION			
Cell wall			
CWH41	0,90	24428	Processing alpha glucosidase I; ER type II integral membrane N-glycoprotein involved in assembly of cell wall beta 1,6 glucan and asparagine-linked protein glycosylation.
DCW1	0,72	16836	Putative mannosidase; GPI-anchored membrane protein required for cell wall biosynthesis in bud formation.
GAS1	1,15	**45247**	Beta-1,3-glucanosyltransferase; required for cell wall assembly; localizes to cell surface via a GPI anchor
ROT2	0,88	9738	Glucosidase II catalytic subunit; required to trim the final glucose in N-linked glycans; required for normal cell wall synthesis
SMI1	1,04	23853	Protein involved in the regulation of cell wall synthesis; proposed to be involved in coordinating cell cycle progression with cell wall integrity
Cytoskeleton and cell polarity			
BEM2	0,83	23010	Rho GTPase activating protein (RhoGAP); involved in the control of cytoskeleton organization and cellular

			morphogenesis
SHE4	0,72	**44701**	Binds to myosin motor domains to regulate myosin function; involved in endocytosis and polarization of the actin cytoskeleton
SPC72	1,12	21275	Gamma-tubulin small complex (gamma-TuSC) receptor; recruits the gamma-TuSC complex to the cytoplasmic side of the Spindle pole body (SPB); involved in astral microtubule formation and stabilization
SRV2	0,67	28372	CAP (cyclase-associated protein); N-terminus binds adenylate cyclase and facilitates activation by RAS; N-terminus forms novel hexameric star-shaped shuriken structures that directly catalyze cofilin-mediated severing of actin filaments; C-terminus binds and recycles cofilin bound, ADP-actin monomers, facilitating regulation of actin dynamics and cell morphogenesis
PROTEIN FATE (FOLDING, MODIFICATION AND FATE)			
ALG5	1,12	26235	UDP-glucose:dolichyl-phosphate glucosyltransferase; involved in asparagine-linked glycosylation in the ER
DIE2	0,46	3657	Dolichyl-phosphoglucose-dependent alpha-1,2-glucosyltransferase; functions in pathway that synthesizes the dolichol-linked oligosaccharide precursor for N-linked protein glycosylation in the ER
GUP1	0,96	**50805**	Plasma membrane protein involved in remodeling GPI anchors; member of the MBOAT family of putative membrane-bound O-acyltransferases; role in misfolded protein quality control
PER1	0,41	23652	Protein of the ER required for GPI-phospholipase A2 activity that remodels the GPI anchor as a prerequisite for association of GPI-anchored proteins with lipid rafts
CELL CYCLE			
HSL1	0,77	21880	Septin-binding kinase that localizes to the bud neck septin ring and regulates the morphogenesis checkpoint
GENE EXPRESSION			
BUD32	0,91	19292	Protein kinase; component of the EKC/KEOPS complex with Kae1, Cgi121, Pcc1, and Gon7; EKC/KEOPS complex is required for t6A tRNA modification and telomeric TG1-3 recombination; may have role in transcription
OTHERS			
KEX1	0,99	22204	Cell death protease essential for hypochlorite-induced apoptosis; involved in the processing of killer toxin and alpha factor precursor
ATG14	0,94	16647	Autophagy-specific subunit of phosphatidylinositol 3-kinase complex I; Atg14 targets complex I to the phagophore assembly site (PAS)

The classification into functional categories allowed us to gain an understanding of the main cellular functions involved in pH_i-mediated Mpk1 activation. It is important to note, however, that the representation of the functional categories may partly reflect the differential abundance in the pre-selected acid-sensitive mutants in [Table 11]. To account for this, the number of mutants with loss of DES-triggered Mpk1 phosphorylation (Mpk1 phosphorylation level at T0<40000 and T20/T0<1.25; Category 2 in the Figure 52) in a given functional category was considered as a function of the total number of mutants analyzed for this category [Figure 53A]. Therefore, the most relevant cellular functions for pH_i-triggered Mpk1 activation were identified [Figure 53B]. The biological processes "Cellular Trafficking", "Ion homeostasis", "Cellular sensing and response" and "Cell Wall" were particularly represented, since >50% of the mutants tested in these categories were impaired in DES-triggered Mpk1 activation. The "Cellular Trafficking" category contains a significant number of proteins with a role in endocytosis, sorting into multivesicular bodies (MVB) and vacuole sorting for protein degradation, as well as, in endosome-to-Golgi retrograde transport for recycling. Importantly, all tested mutants with a function in V-ATPase activity (classified in the "Ion homeostasis" category) were affected in pH_i-mediated Mpk1 activation. Copper and potassium cellular homeostasis also appears to be important for this process, while only one of the mutants with a role in calcium uptake, Δ*ecm7,* was affected in Mpk1 phosphorylation. The "Cellular sensing and response" category encompassed proteins with different functions including detoxification of superoxide (Sod1) or effectors of the mating response pathway, among others [Table 12]. In addition, other categories such as "Lipid, fatty acid and isoprenoid metabolism" and "Cytoskeleton and cell polarity" also contained a substantial number of genes whose deletion abrogated Mpk1 activation. By contrast, the categories "Amino acid metabolism" or "Protein fate" were apparently not relevant for this process, since only a low number of the mutants analyzed were affected in Mpk1 phosphorylation [Figure 53A].

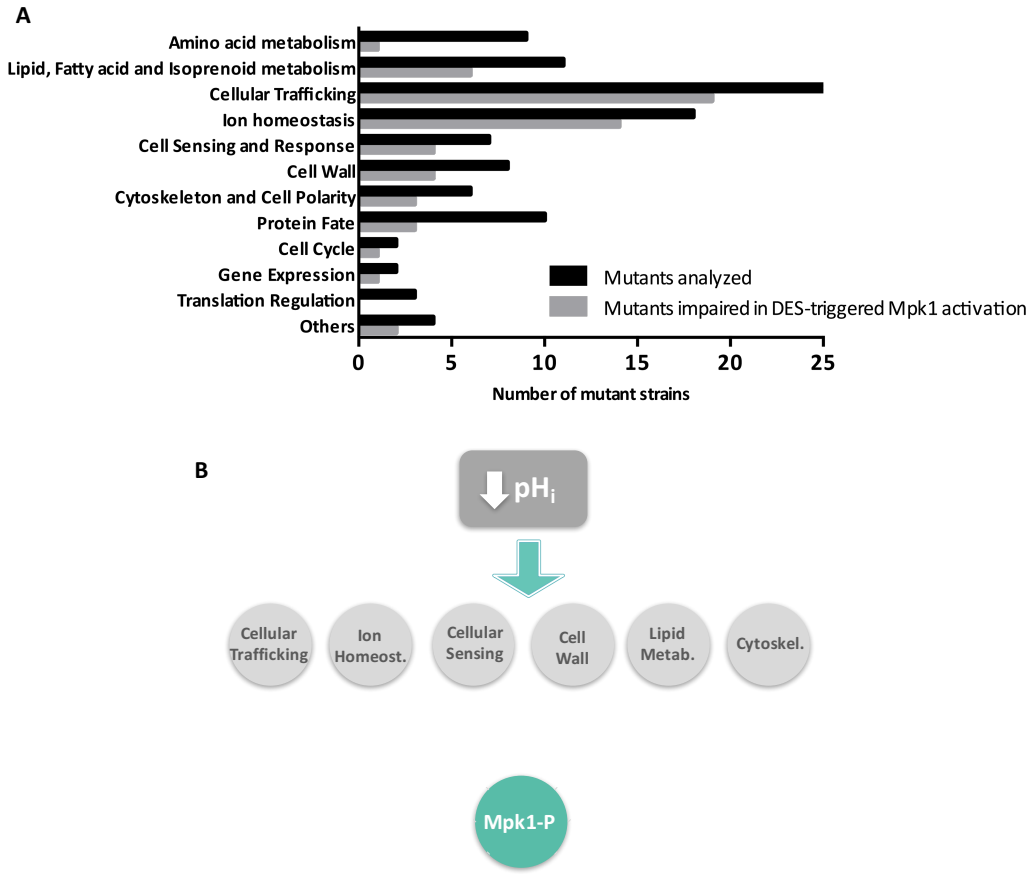

Figure 53 – Most represented biological functions among the identified mutants affected in pH_i-mediated Mpk1 activation.
(**A**) Representation of the number of mutants impaired in DES-triggered Mpk1 activation (Mpk1 phosphorylation level at T0<40000 and T20/T0<1.25; Category 2 in the Figure 52) among the total number of mutants analyzed in each category. (**B**) Schematic representation of the most relevant biological functions, with > 50% of the mutants analyzed with impaired activation of Mpk1. Abbreviations: Ion Homeost. = Ion Homeostasis; Lipid Metab. = Lipid, fatty acid and isoprenoid metabolism; Cytoskel. = Cytoskeleton and Cell Polarity.

Among the categories of genes whose deletion resulted in constitutive hyperphosphorylation of Mpk1 at T0, "Cellular Trafficking" was the most representative, containing half (4 of 8) of the identified mutants. The presence of mutants in *bst1* and *pep7*, which regulate vesicle production and docking/fusion, respectively, suggest that endocytosis may have a role in preventing inappropriate activation of the Mpk1 signaling cascade [Table 12].

4.4.2.4.5. Identification of common pH_i-mediated activators of the Mpk1 and Hog1 MAPKs

We had previously found that DES-induced intracellular acidification triggers activation of both Mpk1 and Hog1 (see Figure 37). To further investigate the mechanism of pH_i-mediated Hog1 activation, we first asked whether the Mpk1 cascade could function upstream of Hog1. However, we observed that Δ*mpk1*, Δ*bck1* and Δ*rom2* mutants exhibited a similar level of Hog1 phosphorylation as the wild type strain, suggesting that the CWI pathway is not required for DES-triggered Hog1 activation [Figure 54, first panel]. We next tested the different phosphatase mutants and found that only Sdp1 appeared to be involved in Hog1 activation [Figure 54, second panel]. To test whether the most relevant functional categories involved in pH_i-mediated Mpk1 activation are also required for Hog1 activation, representative mutants were analyzed for DES-triggered Hog1 activation [Figure 54, third panel]. The V-ATPase function appeared to be dispensable for Hog1 activation, while the Δ*trk1*, both in the "Ion homeostasis" category, showed no induction of Hog1 activation. Interestingly, the lack of Hog1 activation in the Δ*snf7* and Δ*vps24* mutants, both in the "Cellular Trafficking" category, suggests that the ESCRT-III complex, which mediates the sorting of transmembrane proteins to the MVB pathway, is also important for Hog1 activation. Moreover, the results obtained with the Δ*sod1*, Δ*die2* and Δ*hsl1* mutants point towards a role of oxidative stress response, N-linked protein glycosylation and cell cycle control, respectively, in Hog1 activation. Interestingly, the two negative regulators of Mpk1 phosphorylation tested (mutants from the Category 3 in the Figure 52; Mpk1 phosphorylation level at T0>40000 and T20/T0<1.25), Δ*bst1* and Δ*gup1* mutants, did not show an increased baseline Hog1 phosphorylation.

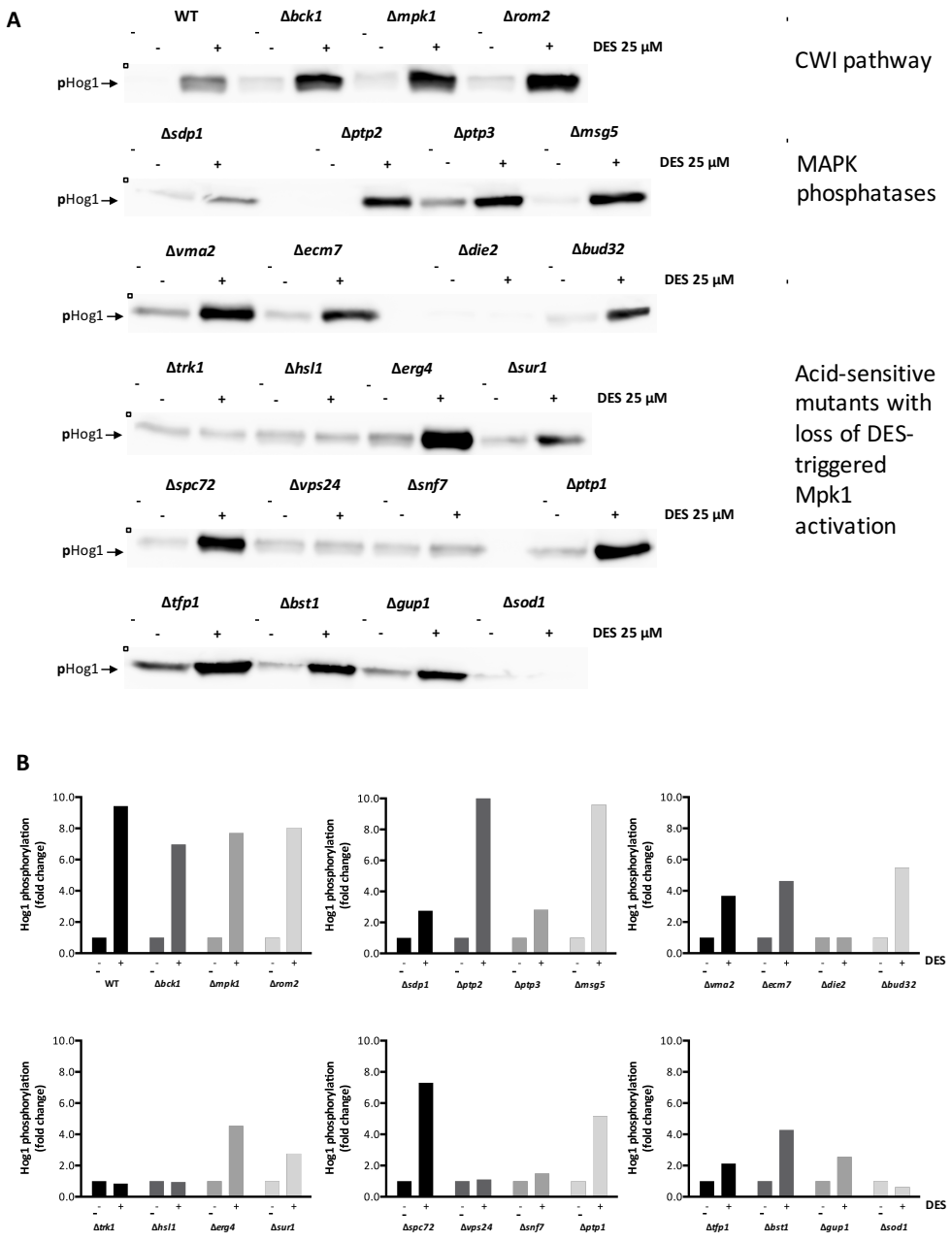

Figure 54 – Analysis of DES-triggered Hog1 phosphorylation in representative mutants of the CWI pathway, MAPK phosphatases and acid-sensitive mutants with loss of DES-triggered Mpk1 activation.

Western blotting analysis in the indicated *S. cerevisiae* strains. (**A**) Exponentially growing cells were washed and resuspended in KSU buffer at pH 6.5, and incubated for 1 hour at 30ºC. At time 0, 25 µM DES was added to the buffer. Protein extracts collected at time zero (-) and 20 minutes after (+) DES treatment were subjected to immunoblot analysis with anti-phospho-p38 MAPK for pHog1 detection. (**B**) Graphs show pHog1 band intensity expressed as fold response compared with control (time zero; -).

Although only a limited number of mutants was analyzed, our data appears to indicate that some biological processes are involved in pH_i-triggered activation of both Mpk1 and Hog1. These include "Cellular Trafficking", "Cellular Sensing", "Protein glycosylation" and "Cell cycle" [Figure 55].

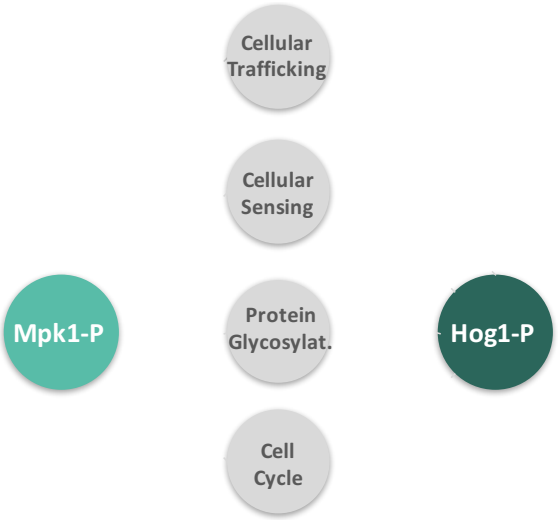

Figure 55 – Schematic diagram of the biological functions relevant for pH_i-triggered Mpk1 and Hog1 activation.
Protein Glycosylat. = Protein Glycosylation.

4.5. COMPARATIVE ANALYSIS OF DES-TRIGGERED MAPK SIGNALING IN *FUSARIUM OXYSPORUM* AND *SACCHAROMYCES CEREVISIAE*

The results obtained in *S. cerevisiae* revealed a number of biological processes involved in pH_i-mediated Mpk1 activation. These findings help to clarify the main intermediates of this process and shed light on possible molecular mechanisms regulating Mpk1 MAPK signaling. We next asked whether the role of key mediators of pH_i-mediated MAPK regulation in yeast is also conserved in *F. oxysporum*.

4.5.1. As in *S. cerevisiae*, Rho1 is not involved in DES-triggered Mpk1 activation in *F. oxysporum*

To explore the role of Mpk1 upstream regulators in pH_i-triggered activation of Mpk1 and Hog1, we analyzed mutant strains in the small GTPase Rho1 or the MAPKKK Bck1 previously generated in our group (Martinez-Rocha *et al*., 2008; Turrà *et al*., 2015). In the *F. oxysporum* Δ*rho1* mutant, Mpk1 and Hog1 MAPK were phosphorylated, while Fmk1 was dephosphorylated [Figure 56]. As expected, Mpk1 remained completely dephosphorylated in the absence of the MAPKKK Bck1. However, Hog1 was still activated and Fmk1 dephosphorylated in this mutant, similar to the wild type. In line with *S. cerevisiae*, these results indicate that DES treatment regulates Mpk1 phosphorylation independently of Rho1 and that these upstream components of the Mpk1 MAPK cascade are not involved in pH_i-mediated control of Fmk1 and Hog1 MAPK cascades.

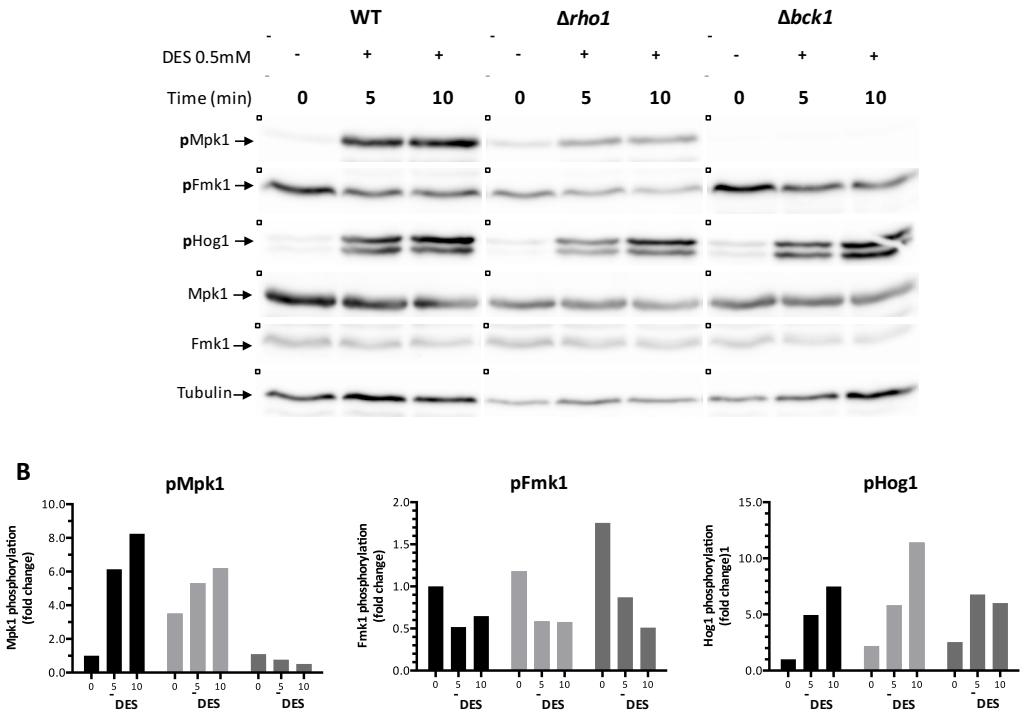

Figure 56 – Rho1 is not required for DES-triggered phosphorylation of Mpk1 and Hog1 or dephosphorylation of Fmk1 in *F. oxysporum*.

(A) Fifteen-hours germinated microconidia of the *F. oxysporum* wild type, Δ*rho1* and Δ*bck1* strains were washed and resuspended in KSU buffer at pH 6.0 and pre-incubated for 1 hour at 28ºC. At time 0, 0.5 mM DES was added to the buffer. Protein extracts collected before (time 0) and 5 or 10 minutes after DES treatment were subjected to immunoblot analysis with anti-phospho-p44/42 MAPK or anti-phosho-p38 MAPK antibodies, for pMpk1 and pFmk1, or pHog1 detection, respectively. Anti-Mpk1 and anti-Fus3 (Fmk1) antibodies were used as MAPK loading control. Anti-tubulin antibody was used as total extract loading control. **(B)** Graphs show the ratio of pMpk1, pFmk1 or pHog1 band intensity normalized to tubulin and expressed as fold response compared with untreated wild type cells (time zero).

4.5.2. Role of the phosphatase Msg5 in regulation of Mpk1 phosphorylation

In this study we found that the dual-specificity MAPK phosphatase Msg5 functions as a major regulator of Mpk1 phosphorylation status in *S. cerevisiae*, as reported previously (Sacristán-Reviriego *et al.*, 2015). Therefore, the role of Msg5 in *F. oxysporum* was explored.

4.5.2.1. Targeted deletion of *msg5* in *F. oxysporum*

A BLASTp search of the *F. oxysporum* genome with the *S. cerevisiae* Msg5 sequence identified a putative ortholog, FOXG_01836, a predicted protein of 788 amino acids. Amino acid sequence alignment of the predicted *F. oxysporum* Msg5 with orthologs in other fungal species revealed 97%, 56% and 38% identity with dual-specificity MAPK phosphatases from *F. fujikuroi*, *Trichoderma reesei* and *A. nidulans*, respectively. The predicted active site ($HC(X)_5RS$) showed perfect amino acid identity to Msg5 from *S. cerevisiae* (YNL053W) [Figure 57A]. However, *F. oxysporum* Msg5 contains a N-terminal extension of about 150 amino acids which is lacking in *S. cerevisiae* Msg5. The presence of a PEST sequence suggests that this region could hypothetically affect stability of *F. oxysporum* Msg5 [Figure 57B].

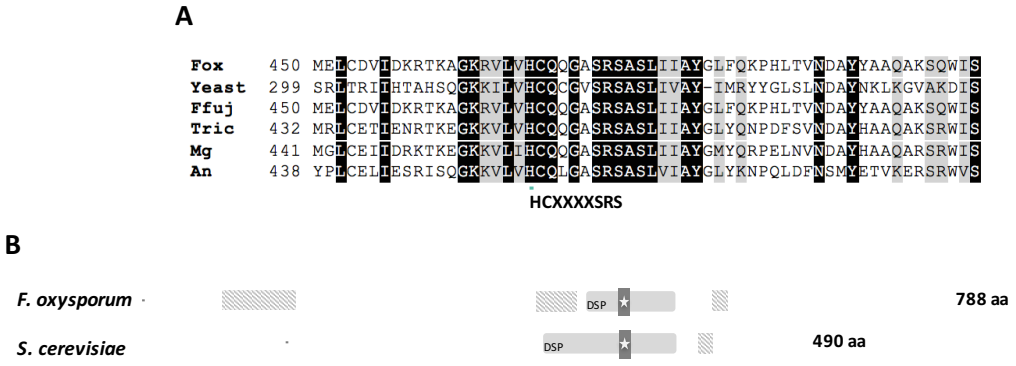

Figure 57 – Sequence alignment of fungal Msg5 proteins.
(A) Amino acid sequence alignments of DSP active sites of the predicted Msg5 proteins from *F. oxysporum*, *S. cerevisiae*, *F. fujikuroi*, *T. reesei*, *M. oryzae* and *A. nidulans*. The green bar indicates the highly-conserved $HC(X)_5RS$ DSP motif. Protein alignment was performed with the ClustalOmega Software. **(B)** Schematic representation of the domain structure of *F. oxysporum* and *S. cerevisiae* Msg5 proteins. The DSP domain is depicted as a grey box and the active site by a dark grey box with a star. Predicted PEST domains are shown as hatched boxes. Total number of amino acids (aa) is indicated on the right.

To investigate the biological role of Msg5 in *F. oxysporum*, we generated a Δ*msg5* allele by replacing the ORF with the *Hyg*^{R} resistance cassette [Figure 58A]. Two split-marker deletion constructs obtained by fusion PCR were used to co-transform protoplasts of the *F. oxysporum* wild type strain. Transformants carrying a homologous insertion at the *msg5* locus were identified first by PCR analysis and then by Southern blot. We identified three transformants in which a 4.8 Kb hybridizing *Hind*III fragment corresponding to the wild type *msg5* allele had been replaced by a fragment of the expected size of 11.4 Kb, consistent with a single homologous insertion of the deletion construct in these transformants [Figure 58B].

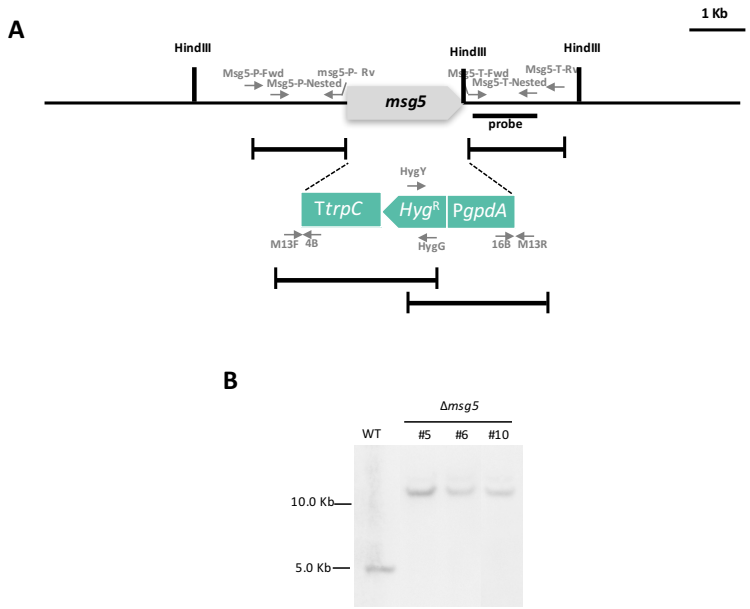

Figure 58 - Targeted deletion of the *F. oxysporum msg5* gene.
(A) Physical maps of the *msg5* locus and the split-marker gene replacement construct obtained by fusion PCR (Δ*msg5* allele). Relative positions of the primers used for generation of the gene deletion construct and PCR analysis of the transformants, as well as of the probe used for Southern blot are indicated. **(B)** Southern blot hybridization analysis of the wild type strain 4287 and the different Δ*msg5* transformants. Genomic DNA treated with *Hind*III was hybridized with the probe indicated in (A).

4.5.2.2. *Fusarium oxysporum* Msg5 is a key regulator of Mpk1 activity

To investigate the role of *F. oxysporum* Msg5 in regulation of Mpk1 activity, a time-course western blot analysis of Mpk1 phosphorylation upon DES-triggered intracellular acidification was performed in the wild type and three Δ*msg5* mutant strains, Δ*msg5*#5, Δ*msg5*#6 and Δ*msg5*#10. In all mutants, the Mpk1 phosphorylation level at T0 was increased up to three times compared to the wild type strain [Figure 59]. Moreover, DES-triggered Mpk1 activation was abolished in the Δ*msg5* mutants. Thus, *F. oxysporum* Msg5 has an important role as a negative regulator of Mpk1 phosphorylation. As in the wild type strain, Fmk1 was dephosphorylated in the Δ*msg5* mutants after DES-triggered intracellular acidification.

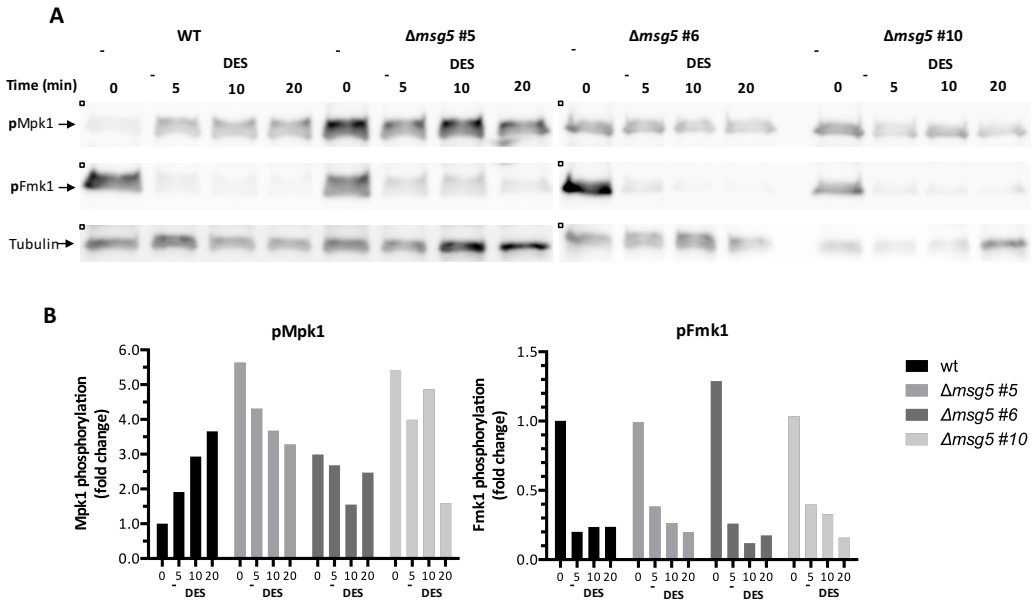

Figure 59 – *F. oxysporum* Msg5 negatively regulates Mpk1 phosphorylation and is required for DES-triggered Mpk1 activation.
(**A**) Fifteen-hour germinated microconidia of F. oxysporum wild type and three different Δ*msg5* mutant strains were washed and resuspended in KSU buffer at pH 6.0 and pre-incubated for 1 hour at 28ºC. At time 0, 0.5 mM DES was added to the buffer. Protein extracts collected before (time 0) and 5, 10 or 20 minutes after DES treatment were subjected to immunoblot analysis with anti-phospho-p44/42 MAPK antibody for pMpk1 and pFmk1 detection. Anti-tubulin antibody was used as total extract loading control. **(B)** Graphs show the ratio of pMpk1 or pFmk1 band intensity normalized to tubulin and expressed as fold response compared with untreated wild type cells (time zero).

4.5.3. Analysis of *F. oxysporum* candidate genes involved in pH_i-triggered Mpk1 activation

Our previous analysis of a sub-set of acid-sensitive *S. cerevisiae* mutants identified 59 proteins required for DES-triggered Mpk1 activation. The amino acid sequences were used for BLASTp searches in FungiDB to identify predicted gene orthologs in *F. oxysporum*. Using the criteria described on Material and Methods we found clear orthologs for 37 of the 59 yeast proteins in *F. oxysporum* [Table 13].

Table 13 – *F. oxysporum* orthologs of *S. cerevisiae* proteins mediating pH_i-triggered Mpk1 activation identified by Blastp analysis.

Yeast protein	Function	Ortholog in *Fox*	AA identity (%)	Predicted function in *Fox*
METABOLISM				
Amino acid metabolism				
ARO2	Chorismate synthase and flavin reductase	FOXG_11059	61	Chorismate synthase
Lipid, fatty acid and isoprenoid metabolism				
ERG4	C-24(28) sterol reductase	FOXG_05355	51	Delta24(24(1))-sterol reductase
SAC1	Phosphatidylinositol phosphatase	FOXG_01012	40	Hypothetical protein
SUR1	Mannosylinositol phosphorylceramide synthase catalytic subunit	FOXG_16891	31	Hypothetical protein
CELLULAR TRAFFICKING				
CSF1	Protein plays a role in the maturation of secretory proteins	FOXG_06277	31	Hypothetical protein
DID4	Class E Vps protein: ESCRT-III complex	FOXG_11524	53	Hypothetical protein
DRS2	Aminophospholipid flippase complex	FOXG_02086	60	Phospholipid-translocating ATPase
PEP3	CORVET membrane tethering complex	FOXG_09431	24	Hypothetical protein
PEP5	Histone E3 ligase, component of CORVET	FOXG_11089	26	Hypothetical protein
PEP8	Vacuolar protein;	FOXG_00236	64	Hypothetical

	multimeric membrane-associated retromer complex			protein
SLA2	Adaptor protein; links actin to clathrin and endocytosis	FOXG_03618	53	Hypothetical protein
SNF7	Subunit of the ESCRT-III complex	FOXG_05316	45	Vacuolar-sorting protein SNF7
VPS1	Dynamin-like GTPase required for vacuolar sorting	FOXG_01628	61	Vacuolar sorting-associated protein 1
VPS29	Membrane-associated retromer complex	FOXG_11158	43	Hypothetical protein
VPS5	Component of retromer complex	FOXG_04343	34	Hypothetical protein
VPS9	Guanine nucleotide exchange factor (GEF) and ubiquitin receptor	FOXG_00470	33	Hypothetical protein
REGULATION OF INTERACTION WITH CELLULAR ENVIRONMENT				
Ion homeostasis				
VMA1	Subunit A of the V1 of V-ATPase	FOXG_01804	69	V-ATPase catalytic subunit A
VMA13	Subunit H of the V1 of V-ATPase	FOXG_00239	34	V-ATPase 54 kDa subunit
VMA16	Subunit c'' of the V-ATPase V0 domain	FOXG_06367	67	V-ATPase 21 kDa subunit
VMA2	Subunit B of V1 of the V-ATPase	FOXG_00954	83	V-ATPase catalytic subunit B
VMA4	Subunit E of the V1 of V-ATPase	FOXG_03408	45	V-ATPase catalytic subunit E
VMA5	Subunit C of the V1 of V-ATPase	FOXG_00056	35	Hypothetical protein
VMA7	Subunit F of the V1 of V-ATPase	FOXG_06289	62	V-ATPase catalytic subunit F
VMA8	Subunit D of the V1 of V-ATPase	FOXG_14288	77	V-ATPase catalytic subunit D
Cellular sensing and response / signal transduction pathways				
ASC1	G-protein beta subunit and guanine dissociation inhibitor for Gpa2	FOXG_05557	59	Guanine nucleotide-binding protein subunit beta-like protein
CNB1	Regulatory subunit of calcineurin	FOXG_01489	63	Calcineurin subunit B
SCP160	Essential RNA-binding G	FOXG_06187	25	Hypothetical

	protein effector of mating response pathway			protein
SOD1	Cooper-zinc superoxide dismutase	FOXG_03076	74	Superoxide dismutase
CONTROL OF CELLULAR ORGANIZATION				
Cell wall				
CWH41	Processing alpha glucosidase I	FOXG_07965	38	Mannosyl-oligosaccharide glucosidase
ROT2	Glucosidase II catalytic subunit	FOXG_07678	39	alpha 1,3-glucosidase
SMI1	Cell wall synthesis; coordinated cell cycle with cell wall integrity	FOXG_01811	36	Hypothetical protein
Cytoskeleton and cell polarity				
SRV2	CAP (cyclase-associated protein)	FOXG_04210	38	Hypothetical protein
PROTEIN FATE (FOLDING, MODIFICATION AND FATE)				
ALG5	UDP-glucose:dolichyl-phosphate glucosyltransferase	FOXG_08496	38	Dolichyl-phosphate beta-glucosyltransferase
PER1	Protein of the ER required for GPI-phospholipase A2 activity	FOXG_00251	34	Hypothetical protein
GENE EXPRESSION				
BUD32	Protein kinase; component of the EKC/KEOPS complex	FOXG_05368	40	BUD32 protein kinase
OTHERS				
KEX1	Cell death protease essential for hypochlorite-induced apoptosis	FOXG_05262	39	Carboxypeptidase D

We detected orthologs in *F. oxysporum* of almost all subunits of the V-ATPase complex, one of the key components involved in DES-triggered Mpk1 activation. To understand the role of this conserved proton pump in MAPK signaling of *F. oxysporum*, we decided to generate Δ*vma7* mutant strains in a component of the V1 subcomplex of the V-ATPase. However, we were unable to isolate genetically purified transformants with a replacement of the *vma7* allele. A similar result was

previously obtained in an independent study for the *vma2* and *vma5* genes, which also encode components of the V1 subcomplex (Segorbe *et al*., unpublished). Taken together, these results suggest that the V1 complex of V-ATPase might be essential for growth of *F. oxysporum* under the conditions used in this study.

Among the identified yeast proteins with a crucial role in pH_i-triggered Mpk1 activation, Snf7, a subunit of the ESCRT-III complex involved in the control of endocytosis and protein sorting to the MVB pathway, has a clear ortholog in *F. oxysporum*. However, generation of a Δ*snf7* mutant in *F. oxysporum* was also unsuccessful. Although PCR analysis revealed replacement of the *snf7* allele by *Hyg* in 11 of the obtained transformants, we noted a low level of DNA amplification suggesting that they are heterokaryons carrying a high proportion of wild type nuclei. Indeed, Southern blot analysis of two transformants exhibiting a 4.6 Kb *SacI* hybridizing fragment corresponding to the Δ*snf7* allele also revealed the presence of a second hybridizing 6.7 Kb *SacI* fragment corresponding to the wild type allele. Although *snf7* is a non-essential gene in *S. cerevisiae*, our results strongly suggest that *snf7* might be essential in *F. oxysporum*, as previously described in the yeast *Yarrowia lipolytica* (Blanchin-Roland *et al*., 2005).

5

DISCUSSION

INTRACELLULAR PH GOVERNS MAPK PHOSPHORYLATION

ROLE OF DIFFERENT SIGNAL TRANSDUCTION PATHWAYS IN PHI-INDUCED MPK1 ACTIVATION

A ROLE OF PHI IN MAPK PHOSPHATASE STABILITY?

CELLULAR TRAFFICKING AND ION HOMEOSTAIS AS REGULATORS MAPK SIGNALING

CELLULAR FUNCTIONS INVOLVED IN BOTH MPK1 AND HOG1 CASCADE ACTIVATION

PMA1 AND V-ATPASE FUNCTIONS AID TO DISTRIBUTE CELLULAR FUNCTIONS ACCORDINGLY WITH THEIR INVOLVEMENT ON MPK1 OR HOG1 MAPKS ACTIVATION

DISCUSSION

Previous studies demonstrated that ambient pH acts as a key regulator of pathogenicity in *F. oxysporum* by modulating the activity of the IG MAPK Fmk1 (Masachis *et al*., 2016). Moreover, a shift in external pH triggers rapid changes in the phosphorylation status of Mpk1 and Hog1, in a way opposite to Fmk1 (Segorbe, 2014). However, the molecular events underlying MAPK regulation by pH were not known. Here, we present evidence suggesting that pH_i acts as a key regulator of MAPK signaling, both in *F. oxysporum* and *S. cerevisiae*. Experimentally induced acidification of the cytosol through pharmacological inhibition of Pma1 activates both Mpk1 and Hog1, and inactivate Fmk1. Because previous results had suggested that Mpk1 is required for Fmk1 dephosphorylation at acid pH (Segorbe, 2014), we decided to investigate in more detail the mechanism of pH_i-induced Mpk1 activation. Because the identification of new components involved in this process requires the screening of hundreds of mutants, we decided to use the model organism *S. cerevisiae* where a knockout library is available. Analysis of a subset of yeast mutants suggests that the sphingolipid-regulated Ypk1/2 upstream branch as well as the Sln1 upstream branch of the Hog1 MAPK cascade contribute to Mpk1 phosphorylation by acidic pH. In addition, proteins functioning in cellular trafficking and ion homeostasis (mainly V-ATPase function) and lipid metabolism, most of which have orthologs in *F. oxysporum*, are also fundamental for DES-triggered Mpk1 activation.

5.1.INTRACELLULAR PH GOVERNS MAPK PHOSPHORYLATION

Although tightly regulated, pH_i is affected by changes in external pH. The finding that pH_i is a regulator of a broad range processes in the cell have given rise to new approaches to evaluate pH_i dynamics and to understand the precise mechanisms of its regulation. The genetically encoded pH-sensitive probe pHluorin has proven exceptionally valuable for studies on pH_i, in yeast (Dechant *et al*., 2010; Hughes

and Gottschling, 2012; Isom *et al*., 2013; Peters *et al*., 2013; Young *et al*., 2010), filamentous fungi (Bagar *et al*., 2009; Valkonen *et al*., 2014) and higher eukaryotes (Rathje *et al*., 2013). In yeast cells, different approaches for *in vivo* monitoring of pH_i in pHluorin expressing strains have been developed. Fluorescence microscopy is the most commonly used approach, since it allows studies of pH_i compartmentalization within the cell and offers spatial and temporal insights into population variability (Bagar *et al*., 2009; Orij *et al*., 2009). Ratiometric flow cytometry analysis of pHluorin expressing cells has also emerged as an efficient approach, since it combines high-throughput analysis at the single-cell level with monitoring of pH_i distribution within cell populations (Valkonen *et al*., 2014; Valli *et al*., 2005; Weigert *et al*., 2009). In addition, analysis of pH_i in a microwell reader coupled to a spectrofluorometer has proven useful for high-throughput analysis combining fast data acquisition with the possibility to simultaneously assay different experimental conditions (Isom *et al*., 2013). Considering our aim of evaluating the effect of different external pH conditions on pH_i dynamics, we established the spectrofluorometer approach to measure pH_i in *F. oxysporum*. To our knowledge, this is the first description of pHluorin-based pH_i analysis in filamentous fungi using an approach other than fluorescence microscopy. Importantly, our pH_i measurements in *F. oxysporum* provided values that are close to those described in other filamentous fungi such as *A. niger* (Bagar *et al*., 2009), validating the accuracy of our experimental approach.

As described in other organisms (Orij *et al*., 2009; Valkonen *et al*., 2014), we found that *F. oxysporum* exhibits a huge capacity of pH_i homeostasis. Even upon extreme shifts in external pH followed by a rapid oscillation in pH_i, the value returned to homeostatic level after one hour, suggesting the presence of an efficient cellular mechanism of pH_i buffering. This is of biological relevance, since fungal pathogens are constantly exposed to oscillations in the pH of the surrounding medium. Therefore, these organisms require a robust homeostatic mechanism to maintain pH_i at constant levels in order to survive, proliferate and invade the host. Intriguingly,

we observed a difference in the amplitude of pH_i fluctuation in response to external acidification or alkalinization in *F. oxysporum*, similarly to the findings reported in *A. niger* (Bagar *et al.*, 2009). Our results demonstrated that a shift in the external pH from 6.0 to pH 2.0 triggered a drop in pH_i of about 1 unit of pH, while an external increase of pH from 6.0 to 9.0 induced a rise in pH_i of approximately 0.5 units. Although more studies are required, we speculate that the higher fluctuation of pH_i in response to external acidification might be of relevance considering the acidic pH of the roots encountered by *F. oxysporum* during infection.

In this study we observed that the activity of Pma1 governs fluctuations in pH_i. Our data suggest that a decrease of Pma1 activity in response to extracellular acidification is, at least in part, responsible for the observed acidification of the cytosol, while a rise in Pma1 activity occurs after external alkalinization, increasing pH_i (see Figure 18). In agreement with these results, studies in yeast revealed that the activity of Pma1 is markedly inhibited by acidification of the medium (Simkovic *et al.*, 2007; Stratford *et al.*, 2013; Trushina *et al.*, 2013). Furthermore, the yeast *pma1-007* strain whose Pma1 activity is reduced by >50%, showed a more severe decrease of pH_i upon external acidification than the wild type (Porat *et al.*, 2005; Young *et al.*, 2010). The lack of recovery of pH_i to the baseline upon pharmacological inhibition of Pma1 by DES reinforces the idea that its activity is of major importance for pH_i homeostasis in *F. oxysporum*. To better characterize and genetically elucidate for the role of Pma1 in this process, a transformant expressing *pma1* under control of an inducible promoter was recently obtained in our group (Franco, 2017).

Our results demonstrated that pH_i is affected by glucose and other carbon sources. Various studies in yeast cells treated with glucose described a rapid and transient intracellular acidification, followed by alkalinization (Orij *et al.*, 2009; Ullah *et al.*, 2013; Valkonen *et al.*, 2014). The initial decrease of pH_i appears to be a consequence of rapid proton influx during the uptake of the sugar (Guimarães *et al.*, 2008), while the increased generation of ATP during glycolysis was shown to

increase the activity of Pma1 and trigger intracellular alkalinization (Cyert and Philpott, 2013). However, we failed to observe a net increase of Pma1 activity upon glucose treatment, which is in line with the lack of intracellular alkalinization. It is possible that the KSU buffer used in our experiments may be responsible for the lack of such a response. While Pma1 was reported to normally export protons from the cytoplasm with a stoichiometry of one proton ejected per ATP (Cid *et al*., 1987), this value was found to decline to 0.1 proton per ATP in starved cells (Venema and Palmgren, 1995). KSU buffer is a nutrient poor medium, and the constant acidification of the cytosol observed in the wild type strain under control condition suggests that Pma1 activity might be decreasing throughout the experiment as consequence of nutrient deprivation.

Although pH_i is a tightly regulated physiological parameter in *F. oxysporum*, we found that shifts in external pH transitorily affect pH_i dynamics. The timing and magnitude of pH_i fluctuations resembles the behavior of well-known second messengers such as cAMP or calcium. It is increasingly appreciated that pH_i acts as a second messenger in a variety of cellular functions, such as cell growth (Orij *et al*., 2009), life span (Hughes and Gottschling, 2012) and glucose response (Dechant *et al*., 2010). Here we provide evidence that pH_i acts as a second messenger for MAPK signaling, both in yeast and in *F. oxysporum*. Some differences between these two organisms were found in pH_i regulation of MAPK activity. For example, in *F. oxysporum* the Fmk1 MAPK phosphorylation status responded in an almost linear fashion to extracellular pH variations, while in yeast Fus3 and Kss1 showed maximal phosphorylation at pH 6.5. A similar effect of pH in the control of Fus3 phosphorylation level was previously described (Isom *et al*., 2013).

Although pH_i fluctuations have been reported to regulate important cellular processes, less is known about the mechanism of pH_i sensing. One of the big challenges has been to identify the cellular components able to detect changes in pH_i and transmit the signal to the cellular machinery. In yeast, so far the V-ATPase, phosphatidic acid and Gα subunits have been identified as potential pH_i sensors.

However, there are still mistakes in the *in vitro* analysis and *in vivo* experimental reports. For example, the Gα protein Gpa1 was shown to respond to pH variations *in vitro* through networks of pH-sensing sidechains that promote a conformational change after a proton binding (Isom *et al*., 2013). However, the authors failed to demonstrate a direct connection between Gpa1 protonation and activation of the downstream MAPK cascades. Furthermore, they were able to show Fus3 and Kss1 MAPK activation in response to pH_i in cells treated with acetic acid or α-pheromone, but not with the tetracycline-dependent Pma1 repression system used to demonstrate pH_i-dependent Gpa1 phosphorylation (Isom *et al*., 2013).

As shown for V-ATPase activity (Dechant *et al*., 2010), we found that Pma1 activity is regulated by environmental pH. However, Pma1 itself is unlikely to act as a pH_i sensor, because instead of sensing fluctuations of pH_i Pma1 is creating them. In addition, our results with the membrane uncoupler FCCP which perturbs pH_i in a mechanism independent of Pma1 activity, also support the idea that this proton pump is not directly regulating MAPK signaling, but that it is the Pma1-induced pH_i change that functions as a signal for the MAPK response.

Uncovering the mechanism by which pH_i governs MAPK signaling is a complex task that needs to be addressed in the future. A huge number of proteins can bind or release protons, but few have been confirmed as bona fine pH_i sensors. A hypothetical pH_i sensor must couple physiological changes in pH_i to regulation of MAPK signaling. In this work, we attempted to identify cellular processes involved in pH_i-induced MAPK regulation. The results bring us closer to the mechanisms that mediate MAPK activity in response to changes in pH_i.

5.2. ROLE OF DIFFERENT SIGNAL TRANSDUCTION PATHWAYS IN PH_I-INDUCED MPK1 ACTIVATION

In fungi, the Pal/Rim signaling pathway is arguably the best-studied mechanism of sensing and response to external alkalinization (Peñalva *et al*., 2014). Since Pal and MAPK signaling pathways are both regulated by ambient pH, we wondered whether the Pal pathway could directly regulate MAPK activity. Our studies with the *F. oxysporum* Δ*pacC* and Δ *palH* mutants revealed a delay in Mpk1 phosphorylation pattern after DES-induced intracellular acidification, but failed to detect significant defects in Fmk1 dephosphorylation. Interestingly, the Pal/Rim pathway was reported to be required for yeast adaptation and resistance to acids (Mira *et al*., 2009). Thus, even if not essential for activation of the Mpk1 cascade, our data suggest that the Pal pathway might be important for a rapid activation of the CWI MAPK pathway. Interestingly, when the extracellular pH acidified, the Δ*pacC* and Δ*palH* mutants displayed a more acidic vacuolar pH but a similar pH_i compared to the wild type strain. This suggests that the Pal pathway regulates rapid Mpk1 phosphorylation downstream of pH_i acidification. In summary, our results suggest that the Pal pathway is not a major regulator of MAPK activity in *F. oxysporum*.

Preliminary results from our group suggested that Mpk1 activation is required for Fmk1 dephosphorylation at acidic external pH (Segorbe, 2014). It is likely that Mpk1-mediated inactivation of Fmk1 determines the reduced virulence of *F. oxysporum* in acidic environments (Masachis *et al*., 2016). Here we show that in *S. cerevisiae* the Δ*mpk1* mutant also fails to dephosphorylate the orthologous Fus3 and Kss1 MAPKs in response to intracellular acidification. Although these results still need to be corroborated in *F. oxysporum*, our overall results indicate that inhibition of Fmk1 activity at acidic pH is dependent on Mpk1 activation. Thus, our attention then focused on the mechanism of Mpk1 activation at acidic conditions.

pH_i governs MAPK signaling both in *Fusarium* and in yeast, suggesting that the mechanism is conserved in fungi. To comprehensively characterize the cellular functions involved in pH_i-mediated MAPK responses, we screened a subset of acid sensitive yeast mutants for loss of DES-triggered Mpk1 activation. We found a significant enrichment of GO biological process terms related to cellular sensing and response/signal transduction pathways, including components of the calcineurin-Crz1 pathway or of the oxidative stress response. The calcineurin-Crz1 pathway has been reported to be important for resistance to high temperature or to cell wall stress (Cruz *et al*., 2001; Odom *et al*., 1997), both stimuli that promote the activation of the CWI pathway. However, it was not established so far whether the calcium responsive pathway regulates the activity of the CWI pathway or whether both pathways act in parallel in response to cell wall stress conditions. Regarding to oxidative stress, an activation of the CWI pathway has been reported in response to different oxidizing agents such as linoleic acid hydroperoxide, diamide and hydrogen peroxide, both in yeast and in human fungal pathogens (Alic *et al*., 2003; Gerik *et al*., 2008; Staleva *et al*., 2004). These data suggest that the activation of the CWI pathway in response to oxidative stress is a common stage of agents operating on different targets, and that the activation of CWI pathway must be fundamental for an effective response to oxidative stress. Our results appear to indicate that intracellular acidification may trigger an oxidative stress in the cell that is important for efficiently signal for the Mpk1 activation. Overall, our results suggest that the interplay between different signaling pathways is required for fully activate the Mpk1 MAPK in response to intracellular acidification.

We found that like Mpk1, Hog1 is activated in response to intracellular acidification, both in *Fusarium* and in yeast. In a previous study, the Δ*hog1* mutant was identified in a screen for acid-sensitive yeast mutants (Kawahata *et al*., 2006), supporting the relevance of this pathway in the acid pH response. Importantly, the Pbs2 MAPKK and the Hog1 MAPK, as well as the Ssk1 upstream regulator of the Ssk2 MAPKKK, showed high phosphorylation level of Mpk1 at baseline and loss

of DES-triggered Mpk1 activation, suggesting that Hog1 may function upstream of Mpk1 activation in response to pH_i decrease. A similar effect of Hog1-dependent activation of Mpk1 MAPK was also reported in response to other stimuli. For instance, in *C. albicans* the activation of the Mpk1 ortholog Mkc1 in response to oxidative stress showed to be also Pbs2 and Hog1 dependent (Arana *et al.*, 2005). Further, in the yeast *S. cerevisiae* the activation of Mpk1 after treatment with the cell wall perturbing agent Zymolyase also showed to be Hog1 dependent (Bermejo *et al.*, 2008; Garcia *et al.*, 2009). Importantly, Bermejo *et al.*, 2008 showed that Zymolyase-mediated Mpk1 activation was also independent of the upstream GTPase Rom2 or of the stress sensors Mid2 and Wsc1 (Bermejo *et al.*, 2008), suggesting that Mpk1 activation by the Hog1 pathway could be highly relevant when the regulation is independent of the classical upstream components of the Mpk1 MAPK module. In summary, our results suggest that pH_i-triggered Mpk1 activation is, at least in part, mediated by the Hog1 pathway.

We also explored a direct role of upstream regulators of the CWI pathway in pH_i -mediated Mpk1 activation. While none of the three classical sensors of the CWI pathway, Wsc1, Mid2 or Mtl1, was required for Mpk1 activation in response to intracellular acidification, our data appear to indicate that the Ypk1/2 branch acts upstream of Mpk1 activation upon DES treatment. Although Ypk1/2 were recently suggested to act via Rom2 (Niles and Powers, 2014), we show here that this GDP/GTP exchange factor for Rho1 and Rho2 is dispensable for pH_i-mediated Mpk1 activation in yeast. While Rho1-deficient mutants in yeast and *F. oxysporum* showed a low level of Mpk1 phosphorylation at baseline, in both species an induction of Mpk1 phosphorylation was still observed after DES treatment. Thus, components downstream of Rho1 must be mediating Mpk1 activation in our experimental conditions. On the other hand, Pkc1, the upstream protein kinase of the Mpk1 MAPK module, was required for DES-triggered Mpk1 activation. While Pkc1 activation was mainly shown to depend on its association at the PM with Rho1 in its GTP-bound form, there is also evidence for Pkc1 activation via the two

redundant Pkh1/2 kinases upstream of Ypk1/2 (Inagaki *et al*., 1999; Roelants *et al*., 2004). Our results suggest that DES-triggered Mpk1 activation is mediated by Pkc1, whose activation likely depends of the AGC upstream kinases Ypk1/2.

Interestingly, the Ypk1/2-mediated signaling was previously shown to be activated in response to acetic acid, and its phosphorylation and activation was strictly required for acid tolerance (Guerreiro *et al*., 2016; Mira *et al*., 2010). Acid-triggered Ypk1/2 activation appears to be mediated by sphingolipid depletion at the PM (Roelants *et al*., 2011). In this process, the final effectors of Ypk1/2 regulate *de novo* synthesis of sphingolipids through phosphorylation of Orm1 and Orm2, two inhibitors of the L-serine:palmitoyl-CoA acyltransferase (SPT), the enzyme complex that catalyzes the first step in sphingolipid biosynthesis (Breslow *et al*., 2010), or by activation of Lac1 and Lag1, the catalytic subunits of the ceramide synthase complex (Muir *et al*., 2014). Thus, the Ypk1/2-mediated signaling is part of a homeostatic mechanism whose activation by PM stress mediates compensatory changes in cellular lipid synthesis to improve stress tolerance (Guerreiro *et al*., 2016; Niles and Powers, 2014). It is interesting to note that our screen of acid-sensitive yeast mutants detected sphingolipid synthesis as a mechanism for pH_i-mediated Mpk1 activation, since mutants in the *sac1*, *sur1* or *csg2* genes encoding enzymes involved in sphingolipid biosynthesis, failed to activate Mpk1. Altogether, these data suggest that sphingolipid levels and composition may regulate Mpk1 activation via Ypk1/2. If sphingolipid depletion is the signal for Ypk1/2 activation after DES-triggered Pma1 inhibition, it is reasonable that sphingolipid-deficient strains should lose the ability to activate the Mpk1 cascade. In yeast, the transmembrane protein Nce102 has been described as a sensor of sphingolipid levels and to regulate the activity of Ypk1/2 (Frohlich *et al*., 2009; García-Marqués *et al*., 2016). Therefore, it will be interesting to test whether the distribution and level of sphingolipids at the PM and Nce102 translocation are regulated by pH_i and whether it could modulate the activity of the Mpk1 MAPK cascade.

Our results suggest that the levels of ergosterol in the PM also regulate Mpk1

activity, since the Δ*erg28* and Δ*erg4* mutants lose the ability to activate this MAPK. Sphingolipids, along with ergosterol, are critical for the formation of microdomains at the PM that have been referred to as lipid rafts. Interestingly, mutants in both types of lipids show hypersensitivity to different cell wall perturbing agents (García *et al*., 2015), suggesting that they could regulate the CWI MAPK pathway in a different context of pH_i decrease.

5.3.A ROLE OF PHI IN MAPK PHOSPHATASE STABILITY?

MAPKs are activated through phosphorylation of conserved threonine and tyrosine residues in their phosphorylation loop by the specific upstream MAPKK. While the lack of signaling through MAPK pathways leads to a defective cellular response to the corresponding stimulus, inappropriate hyperactivation of MAPK routes also results in deleterious effects. Therefore, the duration and extent of MAPK activation is tightly regulated through the balance of upstream kinases and protein phosphatases. Apart of their importance in desensitization and adaptation to external signals, MAPK phosphatases are fundamental for keeping the adequate level of phosphorylated MAPK protein both at basal and stimulating conditions (Martín *et al*., 2005).

The aim of this work was to characterize the molecular mechanism underlying Mpk1 activation in response to pH_i decrease. Much attention in yeast has focused on the components that transfer signals to activate MAPK cascades, while knowledge on the MAPK phosphatases that act as negative regulators to inactive the phosphorylated elements is more limited. Here we analyzed the role of known MAPK phosphatases in DES-triggered Mpk1 activation. Our results confirm that the DSP Msg5 and the tyrosine phosphatase Ptp2 are important regulators of the Mpk1 phosphorylation level. Ptp2 appears to be relevant for regulation of Mpk1 phosphorylated level after intracellular acidification, as previously described for cell wall stress conditions such as high temperature or CR (Flández *et al*., 2004; Marín *et al*., 2009; Sacristán-Reviriego *et al*., 2015). However, in *F. graminearum* Ptp2

had no influence on sensitivity to CR, indicating that its function in this fungus may not be associated with the CWI MAPK pathway or may be redundant (Yun *et al*., 2015). Therefore, we decided to explore the role of Msg5 in Mpk1 regulation in *F. oxysporum*. The Msg5 ortholog was identified by its homology to the Msg5 protein from *S. cerevisiae*. Although the amino acid sequence identity between the two Msg5 proteins is relatively low, several lines of evidence suggest that they are structural orthologous. Both *F. oxysporum* and yeast Msg5 have dual specificity phosphatase and PEST domains and contain a highly conserved active site. Moreover, in both species Msg5 is fundamental for inhibition of Mpk1 phosphorylation at basal conditions.

In *S. cerevisiae*, Msg5 is essential to regulate the level of Mpk1 phosphorylation after CR treatment, since a Δ*msg5* mutant showed higher level of Mpk1 activation than the wild type (Sacristán-Reviriego *et al*., 2015). However, in our experiments the yeast Δ*msg5* mutant showed no increased activation of Mpk1 after intracellular acidification (see Figure 49), suggesting that Msg5 is not fundamental for Mpk1 downregulation after pH_i decrease. Oppositely to yeast cells, in all *F. oxysporum* Δ*msg5* mutants analyzed the activation of Mpk1 after DES-triggered pH_i decrease was abolished (see Figure 59), suggesting that Msg5 is important for this process.

A hypothesis can be drawn to explain the differences in the results obtained with the Δ*msg5* mutants of *S. cerevisiae* and *F. oxysporum*. The mechanism of Mpk1 downregulation might be more complex in yeast cells. It has been well established that MAPK phosphatases show redundancy and promiscuity, since more than one phosphatase can regulate the same MAPK in yeast cells. Therefore, the existence of parallel mechanisms acting on Mpk1 phosphorylation under stimulating conditions could explain the lack of effect in the Δ*msg5* mutant. On the other hand, our results in *F. oxysporum* suggest that it is more sensitive to *msg5* loss. The lack of induction of Mpk1 phosphorylation indicates that Msg5 is important in this process. However, the hyperphosphorylation of Mpk1 at basal conditions could affect its response to pH_i decrease, and might be deleterious for this fungus. A viability assay needs to be

performed in the future to elucidate the relationship between loss of pH_i triggered CWI response and cell survival in this mutant.

In the yeast Msg5 it was shown that the motif $I^{102}YT^{104}$ is required for its binding to Mpk1 (Palacios *et al*., 2011). However, since this domain is not conserved in *F. oxysporum* Msg5 we speculate that Msg5 may have distinct mechanisms of Mpk1 regulation, explaining the different degree of inhibition in these fungal species. MAPK phosphatases and MAPKKs compete for the same binding site within the MAPK. Thus, the increase of Mpk1 phosphorylation levels in the absence of Msg5 could be the result of reduced dephosphorylation by this phosphatase as well as a higher phosphorylation rate by the upstream MAPKK (Andersson *et al*., 2004).

Both the yeast and *F. oxysporum* Msg5 proteins present PEST domains, which are characteristic of rapidly degraded proteins and have been suggested to mediate proteolysis. Since the presence of PEST sequences predicts that Msg5 could be unstable, we asked whether DES-triggered intracellular acidification affects the stability of this phosphatase [Figure 60A]. This hypothesis was experimentally confirmed using a yeast strain expressing a *c*-Myc-tagged Msg5 version, in which Msg5 protein levels decreased by approximately 40% after DES treatment. Previous studies in animal cells showed that degradation of the MAPK phosphatases MKP-1 and MKP-7 which inhibit phosphorylation of the ERK1/2 and p38 MAPKs, respectively, was induced by inhibitors of the ubiquitin-directed proteasome complex (Katagiri *et al*., 2005; Lin *et al*., 2003). Our results suggest that Msg5 degradation could, at least in part, be responsible for the acid-induced increase of Mpk1 phosphorylation [Figure 60A]. In addition, Msg5 degradation could explain the lack of effect of Msg5 on pH_i-stimulated Mpk1 activation.

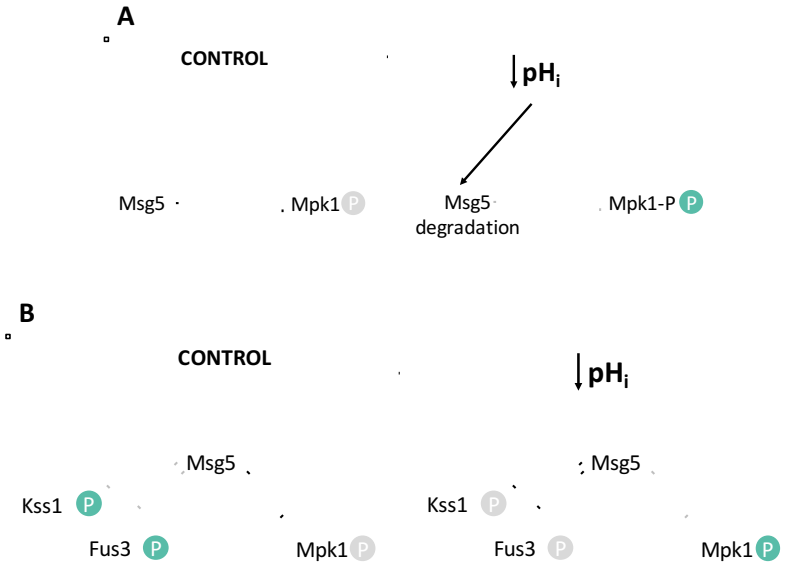

Figure 60 – Two models summarizing how Msg5 could affect pH$_i$-mediated MAPK signaling.
(A) Model 1: Intracellular acidification affects Msg5 stability. In normal conditions (control; left panel) Msg5 inhibits Mpk1 activation, while intracellular decrease of pH (right panel) induces Msg5 degradation reducing the negative effect on Mpk1. Consequently, Mpk1 is activated by upstream positive regulators and an increase of phosphorylation is observed. **(B)** Model 2: Intracellular acidification negatively affects Msg5-Mpk1 binding while simultaneously promoting Msg5-Fus3/Kss1 interaction. In normal conditions (control; left panel), Msg5 inhibits Mpk1 activation and has no effect on Fus3/Kss1 MAPKs that are phosphorylated. Intracellular acidification (right panel) promotes Msg5 binding to Fu3/Kss1 leading to their inactivation and, loss of interaction with Mpk1 allows its activation by upstream positive regulators. Green circles containing the letter P denote phosphorylated amino acid residues, while grey circles denote no-activated MAPKs.

In yeast, the DSP Msg5 regulates both Mpk1 and Fus3/Kss1 phosphorylation (Palacios *et al*., 2011). We therefore hypothesized that in our experimental conditions, DES-triggered pH$_i$ decrease could negatively affect Msg5-Mpk1 binding while simultaneously promoting Msg5-Fus3/Kss1 interaction [Figure 60B]. A pH$_i$-dependent switch in MAPK affinity of Msg5 would readily explain the observed effects on MAPK phosphorylation status. However, in our experiments phosphorylation of Fus3/Kss1 or Fmk1 in yeast and *F. oxysporum*, respectively, appeared to be unaffected by loss of Msg5. Thus, other mechanism(s) could mediate acid-induced downregulation of the IG MAPK cascade.

In summary, we propose that DES-triggered Mpk1 activation is the result of a synergetic effect between increased phosphorylation by the upstream MAPKK and a decrease of inhibition by MAPK phosphatases [Figure 61].

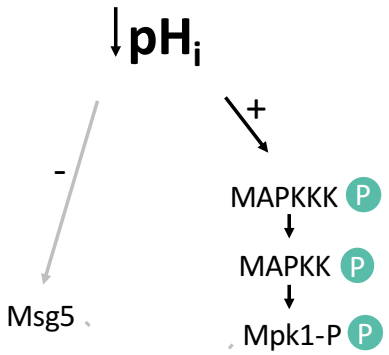

Figure 61 – Intracellular acidification triggers Mpk1 activation through a negative effect in Msg5 stability.
DES-triggered intracellular acidification affects Msg5 stability promoting degradation of this phosphatase. Activation of Mpk1 is the result of a synergetic effect between increased phosphorylation by upstream MAPKK and a decrease of inhibition by Msg5.

5.4.CELLULAR TRAFFICKING AND ION HOMEOSTASIS AS REGULATORS OF MAPK SIGNALING

The process of protein synthesis, modification and intracellular transport is complex and highly conserved in eukaryotic cells. During their synthesis, proteins are translocated to the endoplasmic reticulum (ER) and directed to the correct target compartment in order to fulfill their specific function, undergo modifications, or be degraded. From the Golgi apparatus, newly synthesized proteins are either sorted to the PM, outside the cell (secretory or SEC pathway) or to the vacuole (vacuolar sorting or VPS pathway) through the endosomes [Figure 62]. PM proteins can be internalized by endocytosis (END) and transported to the endosomes where they are either targeted for vacuolar degradation (VPS pathway) or redirected to the Golgi where they enter the secretory pathway to be readdressed to the PM (recycling or RCY pathway). In our yeast mutant screen we identified almost all these processes

as essential for DES-triggered Mpk1 activation [Figure 62], suggesting that cellular trafficking has an important role in regulation of Mpk1 activity. This is further supported by the discovery of "cytoskeleton and cell polarity" as another highly represented category involved in DES-triggered Mpk1 activation, considering the close relation of these two processes with endocytosis. Indeed, the actin cytoskeleton contributes to the formation of endocytic vesicles by stimulating actin depolymerization at the site of the vesicle budding. Interestingly, the requirement of endocytosis for CWI MAPK activity is not exclusive of the pH response, since mutants of *S. cerevisiae* and *C. albicans* affected in cellular trafficking showed an increased sensitivity to cell wall perturbing agents (Cornet *et al.*, 2006; García *et al.*, 2015).

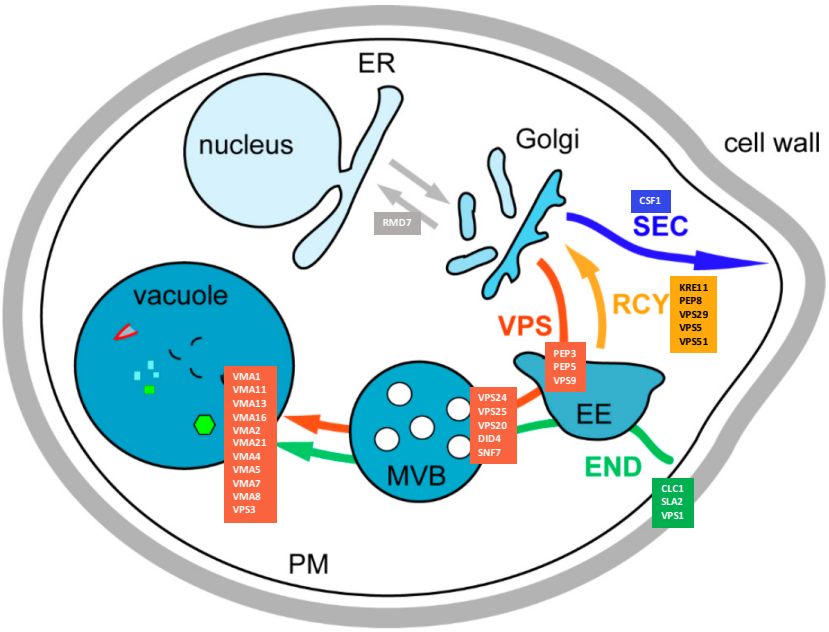

Figure 62 – Membrane trafficking pathways in yeast.
Schematic representation of the most relevant membrane trafficking pathways in yeast. Different trafficking steps shown to affect pH_i-induced Mpk1 activation include the secretory (SEC), recycling (RCY), endocytic (END) and vacuolar protein sorting (VPS) pathways. Proteins identified in each step are highlighted with the same color as the respective pathway. Scheme adapted from Feyder *et al.*, 2015.

The mechanism(s) by which cellular trafficking affects MAPK signaling appear to be complex. Recent studies in mammalian cells have focused on the interplay between endocytosis and cellular signaling. One of the most extensively described functions of endocytosis is the downregulation of signaling pathways by removing activated receptors at the PM and sending them to degradation in the vacuole. However, it is becoming increasingly clear that the output of a signaling process depends not only on the activation of the signaling molecules, but also on the propagation and amplification of the signal (Kholodenko, 2006; Sorkin and von Zastrow, 2009). Indeed, most of the signaling pathways, including ERK-type MAPKs in mammals and fungi are activated at the PM, and the signal needs to be propagated through the cell to its target via endocytosis. In addition, endocytosis could regulate MAPK signaling through the localization of proteins at the endosomal membranes or through direct interaction of activated signaling molecules with critical components in the endosomes such as phosphoinositols, whose synthesis is regulated by cellular trafficking. Furthermore, it has been also proposed that signaling can be mediated at the endosomal membranes. In yeast, it was recently demonstrated that the activation of the CWI pathway can be triggered at the post-Golgi endosomes, where Pkc1 protein kinase upstream of the Mpk1 MAPK module and Wsc1, Rho1 and Rom2 co-localize in this compartment to activate Mpk1 (Fernandez-Acero *et al*., 2015). In summary, our exciting new findings together with those of other groups suggest that the importance of cellular trafficking in signaling goes well beyond its conventional role in cargo degradation, and that these processes contribute in a fundamental manner to MAPK regulation.

Our set of yeast mutants showing impaired activation of Mpk1 in response to cytosolic acidification was also enriched for subunits of the V-ATPase complex. V-ATPase is a highly conserved proton pump that resides at the membrane of organelles such as the vacuole, Golgi apparatus and endosomes, where it mediates intraluminal acidification in an ATP-dependent manner. Interestingly, mutants in cellular trafficking tend to have an increased compartmental pH (Sambade *et al*.,

2005). This suggests that the lack of Mpk1 activation in cellular trafficking mutants could be a consequence of impaired V-ATPase activity.

V-ATPase is an important regulator of the pH_i homeostasis and *vma* mutants exhibit a more acidic cytosolic pH (Dechant *et al*., 2010; Martínez-Muñoz and Kane, 2008). Trk1, a K^+ transporter at the PM, also controls pH_i homeostasis through activation of Pma1 (Rodríguez-Navarro, 2000). Therefore, it is likely that Δ*trk1* mutant has a more acidic cytosol, as previously described (Young *et al*., 2010). In this work, we found evidences showing that both V-ATPase and Trk1 are involved in DES-triggered Mpk1 activation. Our results suggest that a functional machinery controlling pH_i is fundamental for MAPK signaling regulation. Further, the observed enrichment of mutants affected in pH_i homeostasis control reinforces the importance of pH_i in regulation of MAPK signaling.

We also obtained some controversial results. Given that *vma* and Δ*trk1* mutants should likely present a more acidic cytosol, we would expect a higher level of Mpk1 phosphorylation after DES treatment, or even at T0. There are a number of hypotheses to explain this: (1) since the mutants are hypersensitive to acid, as described (Milgrom *et al*., 2007), they may not survive the strong DES-induced intracellular acidification and thus no induction of Mpk1 is seen; (2) a relative decrease of pH_i similar to that observed in the wild type strain is required for Mpk1 activation; therefore mutants with a constitutively acidic cytosol are unable to signal Mpk1 activation; (3) the V-ATPase complex itself, independent of its function in pH_i homeostasis, is fundamental for Mpk1 activation.

So far we have no data on cell survival or baseline pH_i in the mutants analyzed, therefore we cannot confirm or exclude these hypotheses. Nevertheless, we did observe that the DES-triggered decrease in pH_i in the yeast wild type strain leads to an increase in vacuolar pH (data not shown), suggesting that V-ATPase is inhibited by a drop in pH_i, as previously described (Martínez-Muñoz and Kane, 2008). Thus, an intriguing question is how V-ATPase mediates Mpk1 activation while its activity

is inhibited. Dechant *et al*., 2010 demonstrated that alkalinization of the cytosol as a result of glucose addition to starved cells, promotes V-ATPase assembly, and that this process positively regulates the cAMP-dependent PKA pathway in yeast (Dechant *et al*., 2010). More recently, the authors demonstrated that GTPases which mediate activation of the PKA pathway interact with the V-ATPase complex (Dechant *et al*., 2014). Interestingly, in mammalian cells V-ATPase was also found to regulate ERK MAPK signaling. It was reported that the B2 subunit of the V-ATPase complex, which has no apparent structural ortholog in ascomycetes, can stimulate ERK signaling through direct interaction with important upstream activators of this pathway. These results suggest that protein-protein interaction rather than V-ATPase activity itself mediates V-ATPase triggered ERK activation (Li *et al*., 2006; Liu *et al*., 2016). If pH_i decrease also mediates V-ATPase disassembly in our experimental conditions, it is possible that the inability of *vma* mutants to dissociate the V-ATPase complex in response to pH, prevents them from activating MAPK signaling.

In *F. oxysporum* we made every effort to create knockout mutants in components of the V-ATPase complex, by targeting subunits *b* (Vma2), *c* (Vma5) and *f* (Vma7) from the V1 domain. Unfortunately, however, we failed to observe single homologous recombination events in the obtained transformants. This suggests that the function of the V-ATPase is essential in this phytopathogen. However, Chen *et al* 2013 performed targeted gene disruption of *vma11*, encoding the c' subunit of the V0 domain of the V-ATPase of *M. oryzae*, to show that the vacuolar H^+-ATPase complex is fundamental for pathogenicity in this fungus. Interestingly, they found that the Δ*vma11* mutant exhibits cell wall defects, reinforcing the idea that the V-ATPase has a regulatory role in the CWI MAPK pathway (Chen *et al*., 2013).

Our results obtained in the yeast mutant screen pave the way for further studies in *F. oxysporum*. A subunit of the V0 domain of V-ATPase will likely be the next target for gene disruption. Moreover, since recent data demonstrated that V-ATPase regulates various cellular signaling pathways by recruitment of small GTPases

(Dechant *et al*., 2014; Hurtado-Lorenzo *et al*., 2006; Zoncu *et al*., 2011) we should consider investigating the physical interaction between upstream regulators of the CWI pathway and the V-ATPase subunits, in response to pH_i decrease.

5.5. CELLULAR FUNCTIONS INVOLVED IN BOTH MPK1 AND HOG1 CASCADE ACTIVATION

In this work we discovered a new role of pH_i as a regulator for MAPK signaling in *S. cerevisiae* and *F. oxysporum*. In addition to Mpk1, Hog1 was also induced by a decrease in pH_i. To find out whether the conserved cellular functions mediate activation of both acid-induced MAPK cascades, we tested key mutants from each of the most enriched categories required for the Mpk1 activation, for loss of pH_i-mediated Hog1 activation. First, we found that the components of the Mpk1 cascade are not involved in Hog1 activation. On the other hand, the Mpk1 phosphorylation levels before DES treatment appeared to be higher in the Δ*ssk1,* Δ*pbs2* and Δ*hog1* mutants compared to those observed in previous experiments in the wild type strain. Furthermore, Mpk1 phosphorylation was not induced in Hog1 MAPK component mutants after DES treatment, suggesting that Hog1 is upstream of Mpk1 activation in response to pH_i decrease. A preliminary analysis revealed that cellular trafficking is fundamental for Hog1 activation. In yeast cells, Hog1 activation has been related to acid stress-induced endocytosis of the aquaglycerolporin Fps1 (Mollapour and Piper, 2007). However, a link between cellular trafficking and regulation of Hog1 was not reported so far. We also found that Trk1 and V-ATPase, both key regulators of pH_i homeostasis, have different roles in Hog1 activation. While the Δ*trk1* mutant failed to activate Hog1, the *vma* mutants were not affected, in line with a recent publication placing the V-ATPase complex downstream of Hog1 (Li *et al*., 2012). Thus, additional mechanisms besides pH_i are likely involved in Hog1 activation. Finally, sphingolipids or ergosterol deficiency had no major effect on pH_i-mediated Hog1 activation. This contrasts with a report by Tanigawa *et al*., 2012, who described that different mutants in sphingolipid synthesis presented

hyper-phosphorylation of Hog1. Thus, future experiments need to validate whether, depending on the sphingolipid species, lipid metabolism controls exclusively Mpk1 or both MAPK cascades in response to pH_i.

5.6. PMA1 AND V-ATPASE FUNCTIONS AID TO DISTRIBUTE CELLULAR FUNCTIONS ACCORDINGLY WITH THEIR INVOLVEMENT ON MPK1 OR HOG1 MAPKS ACTIVATION

Pma1 is the most abundant protein in the yeast PM and the main player in fungal pH_i homeostasis (Kane, 2016). Although the activity of Pma1 is strictly regulated, different processes in the cell had been described to impact its function. These include lipids or the transport of ions throughout the PM as well as the activity of the vacuolar H^+-ATPase.

Sphingolipids and ergosterol, which are critical for the formation of microdomains in membranes commonly known as lipid rafts (Grossmann *et al.*, 2007), are vital for sorting and delivery, as well as maintaining of Pma1 at the PM (Czyz *et al.*, 2013; Permyakov *et al.*, 2012). Therefore, alterations in membrane lipid composition can strongly impact Pma1 activity.

The uptake of potassium through Trk1 has been shown to induce a difference on PM potential that promotes the activity of Pma1. Importantly, the described intracellular acidification in Δ*trk1* mutants is thought to be mainly a consequence of loss of activity of Pma1.

The activity of V-ATPase has also been demonstrated to affect the activity of Pma1. Yeast *vma* mutants target Pma1 to the vacuoles through endocytosis for degradation, leading to lower levels of Pma1 at the PM (Martínez-Muñoz and Kane, 2008).

Our results obtained in the yeast mutant screen revealed that sphingolipids and ergosterol, as well as Trk1 and V-ATPase are fundamental for pH_i-mediated Mpk1

activation. Considering that mutants in all these cellular functions could have defects in Pma1 activity, we consider that the compromised activation of Mpk1 in acidic pH_i could be caused by Pma1. But how does reduced Pma1 activity block DES-mediated Mpk1 activation? We speculate that mutants with less Pma1 at the PM might be more sensitive to certain stresses impacting on pH_i homeostasis than the wild type strain. This would lead to loss of viability upon strong intracellular acidification induced by DES. On the other hand, lower levels of Pma1 at the PM could also lead to a less efficient inhibition by DES and a less pronounced decrease of pH_i, thus reducing Mpk1 activation.

However, it is likely that Pma1 is not the only factor responsible for the observed phenotypes. Analysis of Hog1 phosphorylation in mutants lacking DES-triggered Mpk1 activation allowed to differentiate between those cellular functions that are specifically required for activation of only one, or both MAPKs. Through an unknown mechanism, Hog1 appears to inhibit Mpk1 under non-induced conditions, while promoting its activation upon pH_i decrease. On the other hand, Trk1 is essential for both Mpk1 and Hog1 activation, while V-ATPase is only required for Mpk1 activation. This suggests that the role of V-ATPase in Mpk1 phosphorylation could be independent of pH_i control. Reinforcing this idea, cellular trafficking that should affect compartmental pH, functions in both MAPK signaling cascades. This suggests that lack of Mpk1 activation in these mutants is not a consequence of V-ATPase function.

In summary, our data suggest a model in which DES-triggered pH_i decrease affects both Hog1 and Mpk1, with Hog1 functioning upstream of Mpk1 [Figure 63]. Cellular trafficking is relevant for signal propagation and duration, affecting both MAPK cascades either through an interdependent or an independent mechanism. Sphingolipids and ergosterol appear to function exclusively in Mpk1 activation, most likely via Ypk1/2. Finally, V-ATPase mediate specifically Mpk1 activation, possibly by protein-protein interaction with important intermediates of the CWI

MAPK pathway. Integration of these different cellular processes will thus lead collectively to Mpk1 activation in response to intracellular acidification [Figure 63].

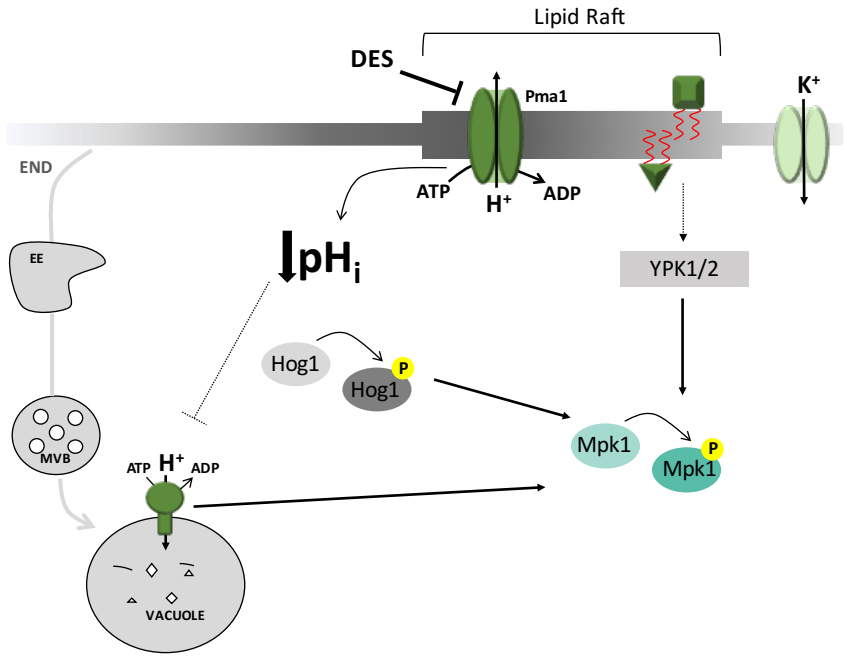

Figure 63 – Schematic model of the proposed mechanisms whereby DES-triggered intracellular acidification triggers Mpk1 activation.
In response to DES-triggered intracellular acidification, Hog1 pathway functions upstream of Mpk1 activation. Mpk1 is also activated by an alternative upstream branch involving Ypk1/2, likely through a lipids-mediated signaling. Biological processes as cellular trafficking or ion homeostasis affect both pH_i-induced Hog1 and Mpk1 activation. On the other hand, V-ATPase function, which is partially inhibited by intracellular acidification, is only relevant for Mpk1 activation. Green triangle and square at the PM represents sphingolipids and ergosterol. END means endocytosis and is presented as representative of the Cellular Trafficking category.

A major goal in future studies will be to elucidate the mechanism of acid pH_i-mediated Fmk1 inactivation. Our data in yeast and *F. oxysporum* suggest that this process depends on Mpk1, but is independent of Msg5. More efforts are needed to understand how pH_i can differently regulate MAPK signaling in fungi. Finally, a key goal is to further dissect the identified mechanisms, particularly lipids and the V-ATPase complex, to elucidate the pH sensing mechanism that transmits the changes in pH_i to the MAPK signaling machinery.

6

CONCLUSIONES
CONCLUSIONS

CONCLUSIONES

- Los cambios en el pH extracelular inducen fluctuaciones rápidas y transitorias en el pH intracelular (pH_i).
- La H^+-ATPasa de la membrana plasmática Pma1, un regulador importante de la homeostasis del pH_i en *Fusarium oxysporum*, controla las fluctuaciones en repuesta a nutrientes y a cambios del pH extracelular.
- El pH_i actúa como un señal para la regulación de las rutas MAPK en *F. oxysporum*.
- La ruta MAPK Mpk1, que regula la respuesta a estreses de pared, es activada por una bajada del pH_i. Esta respuesta esta conservada entre *Fusarium oxysporum* y *Saccharomyces cerevisiae*.
- En levadura, la ruta mediada por la quinasa Ypk1/2 y la rama Sln1 de la ruta Hog1 funcionan aguas arriba de Mpk1 tras la acidificación del citoplasma.
- La fosfatasa Msg5 es un regulador negativo de Mpk1 y su abundancia se ve afectada por el pH_i.
- Distintas funciones celulares como el tráfico celular, la homeostasis de iones y el metabolismo de lípidos estan implicadas en la activación de Mpk1 en respuesta a una bajada del pH_i.

CONCLUSIONS

- Extracellular pH changes induce rapid and transitory fluctuations in the intracellular pH (pH_i).
- The PM H^+-ATPase Pma1 is a major determinant of pH_i homeostasis in *Fusarium oxysporum*, regulating pH_i fluctuations in response to nutrients and external pH changes.
- pH_i acts as a signal for the regulation of MAPK cascades in the fungal plant pathogen *F. oxysporum*.
- The CWI Mpk1 MAPK is rapidly activated by a decrease in pH_i. This response is conserved between *F. oxysporum* and *Saccharomyces cerevisiae*.
- In yeast, the Ypk1/2 branch of the CWI pathway and the Sln1 branch of the Hog1 pathway function upstream of Mpk1 in response to pH_i decrease.
- The phosphatase Msg5 acts as a negative regulator of Mpk1 and its abundance is affected by pH_i.
- Several cellular functions such as cellular trafficking, ion homeostasis and lipid metabolism are involved in pH_i-mediated Mpk1 activation.

7

REFERENCES

REFERENCES

Agrios, G. N. (2005). *Plant Pathology*. St. Louis: MO: Academic Press.

Alic, N., Higgins, V. J., Pichova, A., Breitenbach, M., Dawes, I. W. (2003). Lipid hydroperoxides activate the mitogen-activated protein kinase Mpk1p in *Saccharomyces cerevisiae*. *J Biol Chem, 278*(43), 41849-41855.

Alkan, N., Davydov, O., Sagi, M., Fluhr, R., Prusky, D. (2009). Ammonium secretion by *Colletotrichum coccodes* activates host NADPH oxidase activity enhancing host cell death and fungal virulence in tomato fruits. *Mol Plant Microbe Interact, 22*(12), 1484-1491.

Alkan, N., Espeso, E. A., Prusky, D. (2013). Virulence regulation of phytopathogenic fungi by pH. *Antioxid Redox Signal, 19*(9), 1012-1025.

Andersson, J., Simpson, D. M., Qi, M., Wang, Y., Elion, E. A. (2004). Differential input by Ste5 scaffold and Msg5 phosphatase route a MAPK cascade to multiple outcomes. *The EMBO Journal, 23*(13), 2564-2576.

Arana, D. M., Nombela, C., Alonso-Monge, R., Pla, J. (2005). The Pbs2 MAP kinase kinase is essential for the oxidative-stress response in the fungal pathogen *Candida albicans*. *Microbiology, 151*(4), 1033-1049.

Armstrong, G. M., Armstrong, J. K. (1981). *Formae speciales and races of Fusarium oxysporum causing wilt diseases*. University Park, PA: Penn State University Press.

Bagar, T., Altenbach, K., Read, N. D., Bencina, M. (2009). Live-Cell imaging and measurement of intracellular pH in filamentous fungi using a genetically encoded ratiometric probe. *Eukaryot Cell, 8*(5), 703-712.

Bais, H. P., Weir, T. L., Perry, L. G., Gilroy, S., Vivanco, J. M. (2006). The role of root exudates in rhizosphere interactions with plants and other organisms. *Annu Rev Plant Biol, 57*, 233-266.

Barad, S., Espeso, E. A., Sherman, A., Prusky, D. (2016). Ammonia activates pacC and patulin accumulation in an acidic environment during apple colonization by *Penicillium expansum*. *Mol Plant Pathol, 17*(5), 727-740.

Bermejo, C., Rodriguez, E., Garcia, R., Rodriguez-Pena, J. M., Rodriguez de la Concepcion, M. L., Rivas, C., Arias, P., Nombela, C., Posas, F., Arroyo, J. (2008). The

sequential activation of the yeast HOG and SLT2 pathways is required for cell survival to cell wall stress. *Mol Biol Cell, 19*(3), 1113-1124.

Bertuzzi, M., Schrettl, M., Alcazar-Fuoli, L., Cairns, T. C., Muñoz, A., Walker, L. A., Herbst, S., Safari, M., Cheverton, A. M., Chen, D., Liu, H., Saijo, S., Fedorova, N. D., Armstrong-James, D., Munro, C. A., Read, N. D., Filler, S. G., Espeso, E. A., Nierman, W. C., Haas, H., Bignell, E. M. (2015). Correction: The pH-Responsive PacC Transcription Factor of *Aspergillus fumigatus* Governs Epithelial Entry and Tissue Invasion during Pulmonary Aspergillosis. *PLoS Pathog, 11*(6), e1004943.

Bi, F., Barad, S., Ment, D., Luria, N., Dubey, A., Casado, V., Glam, N., Minguez, J. D., Espeso, E. A., Fluhr, R., Prusky, D. (2016). Carbon regulation of environmental pH by secreted small molecules that modulate pathogenicity in phytopathogenic fungi. *Mol Plant Pathol, 17*(8), 1178-1195.

Bignell, E., Negrete-Urtasun, S., Calcagno, A. M., Haynes, K., Arst, H. N., Jr., Rogers, T. (2005). The *Aspergillus* pH-responsive transcription factor PacC regulates virulence. *Mol Microbiol, 55*(4), 1072-1084.

Blanchin-Roland, S., Da Costa, G., Gaillardin, C. (2005). ESCRT-I components of the endocytic machinery are required for Rim101-dependent ambient pH regulation in the yeast *Yarrowia lipolytica*. *Microbiology, 151*(11), 3627-3637.

Breslow, D. K., Collins, S. R., Bodenmiller, B., Aebersold, R., Simons, K., Shevchenko, A., Ejsing, C. S., Weissman, J. S. (2010). Orm family proteins mediate sphingolipid homeostasis. *Nature, 463*(7284), 1048-1053.

Brown, A. J., Budge, S., Kaloriti, D., Tillmann, A., Jacobsen, M. D., Yin, Z., Ene, I. V., Bohovych, I., Sandai, D., Kastora, S., Potrykus, J., Ballou, E. R., Childers, D. S., Shahana, S., Leach, M. D. (2014). Stress adaptation in a pathogenic fungus. *J Exp Biol, 217*(1), 144-155.

Burgaud, G., Le Calvez, T., Arzur, D., Vandenkoornhuyse, P., Barbier, G. (2009). Diversity of culturable marine filamentous fungi from deep-sea hydrothermal vents. *Environ Microbiol, 11*(6), 1588-1600.

Caracuel, Z., Roncero, M. I., Espeso, E. A., Gonzalez-Verdejo, C. I., Garcia-Maceira, F. I., Di Pietro, A. (2003). The pH signalling transcription factor PacC controls virulence in the plant pathogen *Fusarium oxysporum*. *Mol Microbiol, 48*(3), 765-779.

Carman, G. M., Han, G.-S. (2011). Regulation of Phospholipid Synthesis in the Yeast *Saccharomyces cerevisiae*. *Annual review of biochemistry, 80*, 859-883.

Casamayor, A., Torrance, P. D., Kobayashi, T., Thorner, J., Alessi, D. R. (1999). Functional counterparts of mammalian protein kinases PDK1 and SGK in budding yeast. *Curr Biol, 9*(4), 186-197.

Cessna, S. G., Sears, V. E., Dickman, M. B., Low, P. S. (2000). Oxalic acid, a pathogenicity factor for *Sclerotinia sclerotiorum*, suppresses the oxidative burst of the host plant. *Plant Cell, 12*(11), 2191-2200.

Chen, G., Liu, X., Zhang, L., Cao, H., Lu, J., Lin, F. (2013). Involvement of MoVMA11, a Putative Vacuolar ATPase c' Subunit, in Vacuolar Acidification and Infection-Related Morphogenesis of *Magnaporthe oryzae*. *PLoS One, 8*(6), e67804.

Chen, R. E., Thorner, J. (2007). Function and regulation in MAPK signaling pathways: lessons learned from the yeast *Saccharomyces cerevisiae*. *Biochim Biophys Acta, 1773*(8), 1311-1340.

Chinnici, J. L., Fu, C., Caccamise, L. M., Arnold, J. W., Free, S. J. (2014). *Neurospora crassa* female development requires the PACC and other signal transduction pathways, transcription factors, chromatin remodeling, cell-to-cell fusion, and autophagy. *PLoS One, 9*(10), e110603.

Cid, A., Perona, R., Serrano, R. (1987). Replacement of the promoter of the yeast plasma membrane ATPase gene by a galactose-dependent promoter and its physiological consequences. *Curr Genet, 12*(2), 105-110.

Collins, M. K., Furlong, I. J., Malde, P., Ascaso, R., Oliver, J., Lopez Rivas, A. (1996). An apoptotic endonuclease activated either by decreasing pH or by increasing calcium. *J Cell Sci, 109 (Pt 9)*, 2393-2399.

Cornet, M., Gaillardin, C., Richard, M. L. (2006). Deletions of the Endocytic Components VPS28 and VPS32 in *Candida albicans* Lead to Echinocandin and Azole Hypersensitivity. *Antimicrobial Agents and Chemotherapy, 50*(10), 3492-3495.

Cruz, M. C., Fox, D. S., Heitman, J. (2001). Calcineurin is required for hyphal elongation during mating and haploid fruiting in *Cryptococcus neoformans*. *EMBO J, 20*(5), 1020-1032.

Cyert, M. S., Philpott, C. C. (2013). Regulation of cation balance in *Saccharomyces cerevisiae*. *Genetics, 193*(3), 677-713.

Czyz, O., Bitew, T., Cuesta-Marbán, A., McMaster, C. R., Mollinedo, F., Zaremberg, V. (2013). Alteration of Plasma Membrane Organization by an Anticancer Lysophosphatidylcholine Analogue Induces Intracellular Acidification and

Internalization of Plasma Membrane Transporters in Yeast. *J Biol Chem, 288*(12), 8419-8432.

Danhof, H. A., Lorenz, M. C. (2015). The *Candida albicans* ATO Gene Family Promotes Neutralization of the Macrophage Phagolysosome. *Infect Immun, 83*(11), 4416-4426.

Davidzon, M., Alkan, N., Kobiler, I., Prusky, D. (2010). Acidification by gluconic acid of mango fruit tissue during colonization via stem end infection by *Phomopsis mangiferae*. *Postharvest Biology and Technology, 55*(2), 71-77.

Davis, D. A. (2009). How human pathogenic fungi sense and adapt to pH: the link to virulence. *Curr Opin Microbiol, 12*(4), 365-370.

De Bernardis, F., Muhlschlegel, F. A., Cassone, A., Fonzi, W. A. (1998). The pH of the host niche controls gene expression in and virulence of *Candida albicans*. *Infect Immun, 66*(7), 3317-3325.

Dean, R., Van Kan, J. A., Pretorius, Z. A., Hammond-Kosack, K. E., Di Pietro, A., Spanu, P. D., Rudd, J. J., Dickman, M., Kahmann, R., Ellis, J., Foster, G. D. (2012). The Top 10 fungal pathogens in molecular plant pathology. *Mol Plant Pathol, 13*(4), 414-430.

Dechant, R., Binda, M., Lee, S. S., Pelet, S., Winderickx, J., Peter, M. (2010). Cytosolic pH is a second messenger for glucose and regulates the PKA pathway through V-ATPase. *EMBO J, 29*(15), 2515-2526.

Dechant, R., Saad, S., Ibáñez, A. J., Peter, M. (2014). Cytosolic pH regulates cell growth through distinct GTPases, Arf1 and Gtr1, to promote Ras/PKA and TORC1 activity. *Mol Cell, 55*(3), 409-421.

deHart, A. K., Schnell, J. D., Allen, D. A., Hicke, L. (2002). The conserved Pkh-Ypk kinase cascade is required for endocytosis in yeast. *J Cell Biol, 156*(2), 241-248.

Di Pietro, A., Garcia-MacEira, F. I., Meglecz, E., Roncero, M. I. (2001). A MAP kinase of the vascular wilt fungus *Fusarium oxysporum* is essential for root penetration and pathogenesis. *Mol Microbiol, 39*(5), 1140-1152.

Di Pietro, A., Roncero, M. I. (1998). Cloning, expression, and role in pathogenicity of pg1 encoding the major extracellular endopolygalacturonase of the vascular wilt pathogen *Fusarium oxysporum*. *Mol Plant Microbe Interact, 11*(2), 91-98.

Diakov, T. T., Kane, P. M. (2010). Regulation of vacuolar proton-translocating ATPase activity and assembly by extracellular pH. *J Biol Chem, 285*(31), 23771-23778.

Eraso, P., Mazón, M. J., Portillo, F. (2006). Yeast protein kinase Ptk2 localizes at the plasma membrane and phosphorylates in vitro the C-terminal peptide of the H+-ATPase. *Biochimica et Biophysica Acta (BBA) - Biomembranes, 1758*(2), 164-170.

Fernandes, T. R., Segorbe, D., Prusky, D., Di Pietro, A. (2017). How Alkalinization drives fungal pathogenicity. *PLoS Pathog (accepted)*.

Fernandez-Acero, T., Rodriguez-Escudero, I., Molina, M., Cid, V. J. (2015). The yeast cell wall integrity pathway signals from recycling endosomes upon elimination of phosphatidylinositol (4,5)-bisphosphate by mammalian phosphatidylinositol 3-kinase. *Cell Signal, 27*(11), 2272-2284.

Flández, M., Cosano, I. C., Nombela, C., Martín, H., Molína, M. (2004). Reciprocal regulation between Slt2 MAPK and isoforms of Msg5 dual-specificity protein phosphatase modulates the yeast cell integrity pathway. *J Biol Chem, 279*(12), 11027-11034.

Franco, M. (2017). *Análisis genético y bioquímico de la H+-ATPasa Pma1 en el hongo patógeno Fusarium oxysporum*. (Master Thesis), Universidad de Córdoba, Spain.

Frohlich, F., Moreira, K., Aguilar, P. S., Hubner, N. C., Mann, M., Walter, P., Walther, T. C. (2009). A genome-wide screen for genes affecting eisosomes reveals Nce102 function in sphingolipid signaling. *J Cell Biol, 185*(7), 1227-1242.

García, R., Botet, J., Rodriguez-Pena, J. M., Bermejo, C., Ribas, J. C., Revuelta, J. L., Nombela, C., Arroyo, J. (2015). Genomic profiling of fungal cell wall-interfering compounds: identification of a common gene signature. *BMC Genomics, 16*, 683.

Garcia, R., Rodriguez-Pena, J. M., Bermejo, C., Nombela, C., Arroyo, J. (2009). The high osmotic response and cell wall integrity pathways cooperate to regulate transcriptional responses to zymolyase-induced cell wall stress in *Saccharomyces cerevisiae*. *J Biol Chem, 284*(16), 10901-10911.

García-Marqués, S., Randez-Gil, F., Dupont, S., Garre, E., Prieto, J. A. (2016). Sng1 associates with Nce102 to regulate the yeast Pkh-Ypk signalling module in response to sphingolipid status. *Biochim Biophys Acta, 1863*(6), 1319-1333.

Gerik, K. J., Bhimireddy, S. R., Ryerse, J. S., Specht, C. A., Lodge, J. K. (2008). PKC1 is essential for protection against both oxidative and nitrosative stresses, cell integrity,

and normal manifestation of virulence factors in the pathogenic fungus *Cryptococcus neoformans*. *Eukaryot Cell, 7*(10), 1685-1698.

Gonçalves, V. N., Cantrell, C. L., Wedge, D. E., Ferreira, M. C., Soares, M. A., Jacob, M. R., Oliveira, F. S., Galante, D., Rodrigues, F., Alves, T. M., Zani, C. L., Junior, P. A., Murta, S., Romanha, A. J., Barbosa, E. C., Kroon, E. G., Oliveira, J. G., Gomez-Silva, B., Galetovic, A., Rosa, C. A., Rosa, L. H. (2016). Fungi associated with rocks of the Atacama Desert: taxonomy, distribution, diversity, ecology and bioprospection for bioactive compounds. *Environ Microbiol, 18*(1), 232-245.

Grossmann, G., Opekarova, M., Malinsky, J., Weig-Meckl, I., Tanner, W. (2007). Membrane potential governs lateral segregation of plasma membrane proteins and lipids in yeast. *EMBO J, 26*(1), 1-8.

Guerreiro, J. F., Muir, A., Ramachandran, S., Thorner, J., Sa-Correia, I. (2016). Sphingolipid biosynthesis upregulation by TOR complex 2-Ypk1 signaling during yeast adaptive response to acetic acid stress. *Biochem J, 473*(23), 4311-4325.

Guimarães, P. M., Multanen, J. P., Domingues, L., Teixeira, J. A., Londesborough, J. (2008). Stimulation of zero-trans rates of lactose and maltose uptake into yeasts by preincubation with hexose to increase the adenylate energy charge. *Appl Environ Microbiol, 74*(10), 3076-3084.

Haruta, M., Sabat, G., Stecker, K., Minkoff, B. B., Sussman, M. R. (2014). A peptide hormone and its receptor protein kinase regulate plant cell expansion. *Science, 343*(6169), 408-411.

Heo, W. D., Inoue, T., Park, W. S., Kim, M. L., Park, B. O., Wandless, T. J., Meyer, T. (2006). PI(3,4,5)P and PI(4,5)P Lipids Target Proteins with Polybasic Clusters to the Plasma Membrane. *Science, 314*(5804), 1458.

Hohmann, S., Krantz, M., Nordlander, B. (2007). Yeast osmoregulation. *Methods Enzymol, 428*, 29-45.

Hughes, A. L., Gottschling, D. E. (2012). An early age increase in vacuolar pH limits mitochondrial function and lifespan in yeast. *Nature, 492*(7428), 261-265.

Hurtado-Lorenzo, A., Skinner, M., El Annan, J., Futai, M., Sun-Wada, G. H., Bourgoin, S., Casanova, J., Wildeman, A., Bechoua, S., Ausiello, D. A., Brown, D., Marshansky, V. (2006). V-ATPase interacts with ARNO and Arf6 in early endosomes and regulates the protein degradative pathway. *Nat Cell Biol, 8*(2), 124-136.

Igbaria, A., Lev, S., Rose, M. S., Lee, B. N., Hadar, R., Degani, O., Horwitz, B. A. (2008). Distinct and combined roles of the MAP kinases of *Cochliobolus heterostrophus* in virulence and stress responses. *Mol Plant Microbe Interact, 21*(6), 769-780.

Inagaki, M., Schmelzle, T., Yamaguchi, K., Irie, K., Hall, M. N., Matsumoto, K. (1999). PDK1 Homologs Activate the Pkc1–Mitogen-Activated Protein Kinase Pathway in Yeast. *Mol Cell Biol, 19*(12), 8344-8352.

Isom, D. G., Sridharan, V., Baker, R., Clement, S. T., Smalley, D. M., Dohlman, H. G. (2013). Protons as second messenger regulators of G protein signaling. *Molecular cell, 51*(4), 531-538.

Jennings, D. (1989). "Some perspectives on nitrogen and phosphorus metabolism in fungi". In R. M. L. Boddy, D. J. Read. (Ed.), *Nitrogen, Phosphorus and Sulphur Utilization by Fungi*. (pp. 1-31): Cambridge: Cambridge University Press.

Kahm, M., Navarrete, C., Llopis-Torregrosa, V., Herrera, R., Barreto, L., Yenush, L., Ariño, J., Ramos, J., Kschischo, M. (2012). Potassium starvation in yeast: mechanisms of homeostasis revealed by mathematical modeling. *PLoS Comput Biol, 8*(6), e1002548.

Kamoun, S., Zipfel, C. (2016). Fungal pathogenesis: Host modulation every which way. *Nat Microbiol, 1*(6), 16075.

Kane, P. M. (2016). Proton Transport and pH Control in Fungi. *Adv Exp Med Biol, 892*, 33-68.

Katagiri, C., Masuda, K., Urano, T., Yamashita, K., Araki, Y., Kikuchi, K., Shima, H. (2005). Phosphorylation of Ser-446 determines stability of MKP-7. *J Biol Chem, 280*(15), 14716-14722.

Kawahata, M., Masaki, K., Fujii, T., Iefuji, H. (2006). Yeast genes involved in response to lactic acid and acetic acid: acidic conditions caused by the organic acids in *Saccharomyces cerevisiae* cultures induce expression of intracellular metal metabolism genes regulated by Aft1p. *FEMS Yeast Res, 6*(6), 924-936.

Kholodenko, B. N. (2006). CELL SIGNALLING DYNAMICS IN TIME AND SPACE. *Nature reviews. Molecular cell biology, 7*(3), 165-176.

Kim, J. Y. (2016). Human fungal pathogens: Why should we learn? *J Microbiol, 54*(3), 145-148.

Kojima, K., Kikuchi, T., Takano, Y., Oshiro, E., Okuno, T. (2002). The mitogen-activated protein kinase gene MAF1 is essential for the early differentiation phase of appressorium formation in *Colletotrichum lagenarium*. *Mol Plant Microbe Interact, 15*(12), 1268-1276.

Kondo, A., Yamamoto, S., Nakaki, R., Shimamura, T., Hamakubo, T., Sakai, J., Kodama, T., Yoshida, T., Aburatani, H., Osawa, T. (2017). Extracellular Acidic pH Activates the Sterol Regulatory Element-Binding Protein 2 to Promote Tumor Progression. *Cell Rep, 18*(9), 2228-2242.

Kraus, P. R., Fox, D. S., Cox, G. M., Heitman, J. (2003). The *Cryptococcus neoformans* MAP kinase Mpk1 regulates cell integrity in response to antifungal drugs and loss of calcineurin function. *Mol Microbiol, 48*(5), 1377-1387.

Lagadic-Gossmann, D., Huc, L., Lecureur, V. (2004). Alterations of intracellular pH homeostasis in apoptosis: origins and roles. *Cell Death Differ, 11*(9), 953-961.

Lecchi, S., Nelson, C. J., Allen, K. E., Swaney, D. L., Thompson, K. L., Coon, J. J., Sussman, M. R., Slayman, C. W. (2007). Tandem phosphorylation of Ser-911 and Thr-912 at the C terminus of yeast plasma membrane H+-ATPase leads to glucose-dependent activation. *J Biol Chem, 282*(49), 35471-35481.

Lengeler, K. B., Davidson, R. C., D'souza, C., Harashima, T., Shen, W. C., Wang, P., Pan, X., Waugh, M., Heitman, J. (2000). Signal transduction cascades regulating fungal development and virulence. *Microbiol Mol Biol Rev, 64*(4), 746-785.

Levin, D. E. (2011). Regulation of cell wall biogenesis in *Saccharomyces cerevisiae*: the cell wall integrity signaling pathway. *Genetics, 189*(4), 1145-1175.

Li, G., Yang, Q., Krishnan, S., Alexander, E. A., Borkan, S. C., Schwartz, J. H. (2006). A novel cellular survival factor - the B2 subunit of vacuolar H+-ATPase inhibits apoptosis. *Cell Death Differ, 13*(12), 2109-2117.

Li, S. C., Diakov, T. T., Rizzo, J. M., Kane, P. M. (2012). Vacuolar H+-ATPase works in parallel with the HOG pathway to adapt *Saccharomyces cerevisiae* cells to osmotic stress. *Eukaryot Cell, 11*(3), 282-291.

Lin, Y. W., Chuang, S. M., Yang, J. L. (2003). ERK1/2 achieves sustained activation by stimulating MAPK phosphatase-1 degradation via the ubiquitin-proteasome pathway. *J Biol Chem, 278*(24), 21534-21541.

Liu, Y., Zuo, S., Li, X., Fan, J., Cao, X., Yu, X., Yang, Q. (2016). Interaction between V-ATPase B2 and (Pro) renin Receptors in Promoting the progression of Renal Tubulointerstitial Fibrosis. *Sci Rep, 6*, 25035.

López-Berges, M. S., Capilla, J., Turrà, D., Schafferer, L., Matthijs, S., Jöchl, C., Cornelis, P., Guarro, J., Haas, H., Di Pietro, A. (2012). HapX-Mediated Iron Homeostasis Is Essential for Rhizosphere Competence and Virulence of the Soilborne Pathogen *Fusarium oxysporum*. *Plant Cell, 24*(9), 3805-3822.

Luo, G., Gruhler, A., Liu, Y., Jensen, O. N., Dickson, R. C. (2008). The sphingolipid long-chain base-Pkh1/2-Ypk1/2 signaling pathway regulates eisosome assembly and turnover. *J Biol Chem, 283*(16), 10433-10444.

Lyakh, S. P., Kozlova, T. M., Salivonik, S. M. (1983). Effect of periodic freezing and thawing on cells of the Antarctic black yeast *nadsoniella-nigra* var *hesuelica*. *Microbiology, 52*, 486–491.

Ma, L. J., van der Does, H. C., Borkovich, K. A., Coleman, J. J., Daboussi, M. J., Di Pietro, A., Dufresne, M., Freitag, M., Grabherr, M., Henrissat, B., Houterman, P. M., Kang, S., Shim, W. B., Woloshuk, C., Xie, X., Xu, J. R., Antoniw, J., Baker, S. E., Bluhm, B. H., Breakspear, A., Brown, D. W., Butchko, R. A., Chapman, S., Coulson, R., Coutinho, P. M., Danchin, E. G., Diener, A., Gale, L. R., Gardiner, D. M., Goff, S., Hammond-Kosack, K. E., Hilburn, K., Hua-Van, A., Jonkers, W., Kazan, K., Kodira, C. D., Koehrsen, M., Kumar, L., Lee, Y. H., Li, L., Manners, J. M., Miranda-Saavedra, D., Mukherjee, M., Park, G., Park, J., Park, S. Y., Proctor, R. H., Regev, A., Ruiz-Roldan, M. C., Sain, D., Sakthikumar, S., Sykes, S., Schwartz, D. C., Turgeon, B. G., Wapinski, I., Yoder, O., Young, S., Zeng, Q., Zhou, S., Galagan, J., Cuomo, C. A., Kistler, H. C., Rep, M. (2010). Comparative genomics reveals mobile pathogenicity chromosomes in *Fusarium*. *Nature, 464*(7287), 367-373.

Malardier, L., Daboussi, M. J., Julien, J., Roussel, F., Scazzocchio, C., Brygoo, Y. (1989). Cloning of the nitrate reductase gene (niaD) of *Aspergillus nidulans* and its use for transformation of *Fusarium oxysporum*. *Gene, 78*(1), 147-156.

Manteau, S., Abouna, S., Lambert, B., Legendre, L. (2003). Differential regulation by ambient pH of putative virulence factor secretion by the phytopathogenic fungus *Botrytis cinerea*. *FEMS Microbiol Ecol, 43*(3), 359-366.

Maresová, L., Hosková, B., Urbanková, E., Chaloupka, R., Sychrová, H. (2010). New applications of pHluorin-measuring intracellular pH of prototrophic yeasts and determining changes in the buffering capacity of strains with affected potassium homeostasis. *Yeast, 27*(6), 317-325.

Marín, M. J., Flández, M., Bermejo, C., Arroyo, J., Martín, H., Molina, M. (2009). Different modulation of the outputs of yeast MAPK-mediated pathways by distinct stimuli and isoforms of the dual-specificity phosphatase Msg5. *Mol Genet Genomics, 281*(3), 345-359.

Martín, H., Flández, M., Nombela, C., Molina, M. (2005). Protein phosphatases in MAPK signalling: we keep learning from yeast. *Mol Microbiol, 58*(1), 6-16.

Martínez-Muñoz, G. A., Kane, P. (2008). Vacuolar and plasma membrane proton pumps collaborate to achieve cytosolic pH homeostasis in yeast. *J Biol Chem, 283*(29), 20309-20319.

Martinez-Rocha, A. L., Roncero, M. I., Lopez-Ramirez, A., Marine, M., Guarro, J., Martinez-Cadena, G., Di Pietro, A. (2008). Rho1 has distinct functions in morphogenesis, cell wall biosynthesis and virulence of *Fusarium oxysporum*. *Cell Microbiol, 10*(6), 1339-1351.

Masachis, S., Segorbe, D., Turrà, D., Leon-Ruiz, M., Furst, U., El Ghalid, M., Leonard, G., López-Berges, M. S., Richards, T. A., Felix, G., Di Pietro, A. (2016). A fungal pathogen secretes plant alkalinizing peptides to increase infection. *Nat Microbiol, 1*(6), 16043.

Matsuyama, S., Llopis, J., Deveraux, Q. L., Tsien, R. Y., Reed, J. C. (2000). Changes in intramitochondrial and cytosolic pH: early events that modulate caspase activation during apoptosis. *Nat Cell Biol, 2*(6), 318-325.

Mehrabi, R., Van der Lee, T., Waalwijk, C., Gert, H. J. (2006). MgSlt2, a cellular integrity MAP kinase gene of the fungal wheat pathogen *Mycosphaerella graminicola*, is dispensable for penetration but essential for invasive growth. *Mol Plant Microbe Interact, 19*(4), 389-398.

Mey, G., Held, K., Scheffer, J., Tenberge, K. B., Tudzynski, P. (2002). CPMK2, an SLT2-homologous mitogen-activated protein (MAP) kinase, is essential for pathogenesis of *Claviceps purpurea* on rye: evidence for a second conserved pathogenesis-related MAP kinase cascade in phytopathogenic fungi. *Mol Microbiol, 46*(2), 305-318.

Michielse, C. B., Rep, M. (2009). Pathogen profile update: *Fusarium oxysporum*. *Mol Plant Pathol, 10*(3), 311-324.

Milgrom, E., Diab, H., Middleton, F., Kane, P. M. (2007). Loss of vacuolar proton-translocating ATPase activity in yeast results in chronic oxidative stress. *J Biol Chem, 282*(10), 7125-7136.

Mira, N. P., Lourenco, A. B., Fernandes, A. R., Becker, J. D., Sá-Correia, I. (2009). The RIM101 pathway has a role in *Saccharomyces cerevisiae* adaptive response and resistance to propionic acid and other weak acids. *FEMS Yeast Res, 9*(2), 202-216.

Mira, N. P., Palma, M., Guerreiro, J. F., Sá-Correia, I. (2010). Genome-wide identification of *Saccharomyces cerevisiae* genes required for tolerance to acetic acid. *Microb Cell Fact, 9*, 79.

Miyara, I., Shafran, H., Davidzon, M., Sherman, A., Prusky, D. (2010). pH Regulation of ammonia secretion by *Colletotrichum gloeosporioides* and its effect on appressorium formation and pathogenicity. *Mol Plant Microbe Interact, 23*(3), 304-316.

Miyara, I., Shafran, H., Kramer Haimovich, H., Rollins, J., Sherman, A., Prusky, D. (2008). Multi-factor regulation of pectate lyase secretion by *Colletotrichum gloeosporioides* pathogenic on avocado fruits. *Mol Plant Pathol, 9*(3), 281-291.

Miyara, I., Shnaiderman, C., Meng, X., Vargas, W. A., Diaz-Minguez, J. M., Sherman, A., Thon, M., Prusky, D. (2012). Role of nitrogen-metabolism genes expressed during pathogenicity of the alkalinizing *Colletotrichum gloeosporioides* and their differential expression in acidifying pathogens. *Mol Plant Microbe Interact, 25*(9), 1251-1263.

Mollapour, M., Piper, P. W. (2007). Hog1 mitogen-activated protein kinase phosphorylation targets the yeast Fps1 aquaglyceroporin for endocytosis, thereby rendering cells resistant to acetic acid. *Mol Cell Biol, 27*(18), 6446-6456.

Moskvina, E., Imre, E. M., Ruis, H. (1999). Stress factors acting at the level of the plasma membrane induce transcription via the stress response element (STRE) of the yeast *Saccharomyces cerevisiae*. *Molecular Microbiology, 32*(6), 1263-1272.

Muir, A., Ramachandran, S., Roelants, F. M., Timmons, G., Thorner, J. (2014). TORC2-dependent protein kinase Ypk1 phosphorylates ceramide synthase to stimulate synthesis of complex sphingolipids. *Elife, 3*.

Murray, M. G., Thompson, W. F. (1980). Rapid isolation of high molecular weight plant DNA. *Nucleic Acids Res, 8*(19), 4321-4325.

Niles, B. J., Mogri, H., Hill, A., Vlahakis, A., Powers, T. (2012). Plasma membrane recruitment and activation of the AGC kinase Ypk1 is mediated by target of rapamycin complex 2 (TORC2) and its effector proteins Slm1 and Slm2. *Proc Natl Acad Sci U S A, 109*(5), 1536-1541.

Niles, B. J., Powers, T. (2012). Plasma membrane proteins Slm1 and Slm2 mediate activation of the AGC kinase Ypk1 by TORC2 and sphingolipids in *S. cerevisiae*. *Cell Cycle, 11*(20), 3745-3749.

Niles, B. J., Powers, T. (2014). TOR complex 2–Ypk1 signaling regulates actin polarization via reactive oxygen species. *Molecular Biology of the Cell, 25*(24), 3962-3972.

Nishino, K., Obara, K., Kihara, A. (2015). The C-terminal Cytosolic Region of Rim21 Senses Alterations in Plasma Membrane Lipid Composition: INSIGHTS INTO SENSING MECHANISMS FOR PLASMA MEMBRANE LIPID ASYMMETRY. *J Biol Chem, 290*(52), 30797-30805.

Nobile, C. J., Solis, N., Myers, C. L., Fay, A. J., Deneault, J. S., Nantel, A., Mitchell, A. P., Filler, S. G. (2008). *Candida albicans* transcription factor Rim101 mediates pathogenic interactions through cell wall functions. *Cell Microbiol, 10*(11), 2180-2196.

Nucci, M., Anaissie, E. (2007). *Fusarium* Infections in Immunocompromised Patients. *Clinical Microbiology Reviews, 20*(4), 695-704.

O'Donnell, K., Sutton, D. A., Rinaldi, M. G., Magnon, K. C., Cox, P. A., Revankar, S. G., Sanche, S., Geiser, D. M., Juba, J. H., van Burik, J. A., Padhye, A., Anaissie, E. J., Francesconi, A., Walsh, T. J., Robinson, J. S. (2004). Genetic diversity of human pathogenic members of the *Fusarium oxysporum* complex inferred from multilocus DNA sequence data and amplified fragment length polymorphism analyses: evidence for the recent dispersion of a geographically widespread clonal lineage and nosocomial origin. *J Clin Microbiol, 42*(11), 5109-5120.

O'Meara, T. R., Holmer, S. M., Selvig, K., Dietrich, F., Alspaugh, J. A. (2013). *Cryptococcus neoformans* Rim101 is associated with cell wall remodeling and evasion of the host immune responses. *MBio, 4*(1).

Odom, A., Muir, S., Lim, E., Toffaletti, D. L., Perfect, J., Heitman, J. (1997). Calcineurin is required for virulence of *Cryptococcus neoformans*. *EMBO J, 16*(10), 2576-2589.

Orij, R., Brul, S., Smits, G. J. (2011). Intracellular pH is a tightly controlled signal in yeast. *Biochim Biophys Acta, 1810*(10), 933-944.

Orij, R., Postmus, J., Ter Beek, A., Brul, S., Smits, G. J. (2009). *In vivo* measurement of cytosolic and mitochondrial pH using a pH-sensitive GFP derivative in *Saccharomyces cerevisiae* reveals a relation between intracellular pH and growth. *Microbiology, 155*(1), 268-278.

Ortoneda, M., Guarro, J., Madrid, M. P., Caracuel, Z., Roncero, M. I., Mayayo, E., Di Pietro, A. (2004). *Fusarium oxysporum* as a multihost model for the genetic dissection of fungal virulence in plants and mammals. *Infect Immun, 72*(3), 1760-1766.

Ozaki, K., Tanaka, K., Imamura, H., Hihara, T., Kameyama, T., Nonaka, H., Hirano, H., Matsuura, Y., Takai, Y. (1996). Rom1p and Rom2p are GDP/GTP exchange proteins (GEPs) for the Rho1p small GTP binding protein in *Saccharomyces cerevisiae*. *EMBO J, 15*(9), 2196-2207.

Palacios, L., Dickinson, R. J., Sacristán-Reviriego, A., Didmon, M. P., Marín, M. J., Martin, H., Keyse, S. M., Molína, M. (2011). Distinct docking mechanisms mediate interactions between the Msg5 phosphatase and mating or cell integrity mitogen-activated protein kinases (MAPKs) in *Saccharomyces cerevisiae*. *J Biol Chem, 286*(49), 42037-42050.

Palková, Z., Devaux, F., Icicova, M., Minarikova, L., Le Crom, S., Jacq, C. (2002). Ammonia pulses and metabolic oscillations guide yeast colony development. *Mol Biol Cell, 13*(11), 3901-3914.

Panadero, J., Pallotti, C., Rodriguez-Vargas, S., Randez-Gil, F., Prieto, J. A. (2006). A downshift in temperature activates the high osmolarity glycerol (HOG) pathway, which determines freeze tolerance in *Saccharomyces cerevisiae*. *J Biol Chem, 281*(8), 4638-4645.

Paravicini, G., Cooper, M., Friedli, L., Smith, D. J., Carpentier, J. L., Klig, L. S., Payton, M. A. (1992). The osmotic integrity of the yeast cell requires a functional PKC1 gene product. *Mol Cell Biol, 12*(11), 4896-4905.

Pearce, G., Moura, D. S., Stratmann, J., Ryan, C. A., Jr. (2001). RALF, a 5-kDa ubiquitous polypeptide in plants, arrests root growth and development. *Proc Natl Acad Sci U S A, 98*(22), 12843-12847.

Peñalva, M. A., Lucena-Agell, D., Arst, H. N. J. (2014). Liaison alcaline: Pals entice non-endosomal ESCRTs to the plasma membrane for pH signaling. *Curr Opin Microbiol, 22*, 49-59.

Peñalva, M. A., Tilburn, J., Bignell, E., Arst, H. N. J. (2008). Ambient pH gene regulation in fungi: making connections. *Trends Microbiol, 16*(6), 291-300.

Pérez-Nadales, E., Di Pietro, A. (2011). The membrane mucin Msb2 regulates invasive growth and plant infection in *Fusarium oxysporum*. *Plant Cell, 23*(3), 1171-1185.

Perez-Nadales, E., Nogueira, M. F., Baldin, C., Castanheira, S., El Ghalid, M., Grund, E., Lengeler, K., Marchegiani, E., Mehrotra, P. V., Moretti, M., Naik, V., Oses-Ruiz, M., Oskarsson, T., Schafer, K., Wasserstrom, L., Brakhage, A. A., Gow, N. A., Kahmann, R., Lebrun, M. H., Perez-Martin, J., Di Pietro, A., Talbot, N. J., Toquin, V., Walther, A., Wendland, J. (2014). Fungal model systems and the elucidation of pathogenicity determinants. *Fungal Genet Biol, 70*, 42-67.

Permyakov, S., Suzina, N., Valiakhmetov, A. (2012). Activation of H+-ATPase of the plasma membrane of *Saccharomyces cerevisiae* by glucose: the role of sphingolipid and lateral enzyme mobility. *PLoS One, 7*(2), e30966.

Peters, L. Z., Hazan, R., Breker, M., Schuldiner, M., Ben-Aroya, S. (2013). Formation and dissociation of proteasome storage granules are regulated by cytosolic pH. *J Cell Biol, 201*(5), 663-671.

Porat, Z., Wender, N., Erez, O., Kahana, C. (2005). Mechanism of polyamine tolerance in yeast: novel regulators and insights. *Cell Mol Life Sci, 62*(24), 3106-3116.

Portillo, F., Eraso, P., Serrano, R. (1991). Analysis of the regulatory domain of yeast plasma membrane H+-ATPase by directed mutagenesis and intragenic suppression. *FEBS Lett, 287*(1-2), 71-74.

Powell, W. A., Kistler, H. C. (1990). *In vivo* rearrangement of foreign DNA by *Fusarium oxysporum* produces linear self-replicating plasmids. *Journal of Bacteriology, 172*(6), 3163-3171.

Prados Rosales, R. C., Di Pietro, A. (2008). Vegetative hyphal fusion is not essential for plant infection by *Fusarium oxysporum*. *Eukaryot Cell, 7*(1), 162-171.

Prusky, D., McEvoy, J. L., Leverentz, B., Conway, W. S. (2001). Local modulation of host pH by *Colletotrichum* species as a mechanism to increase virulence. *Mol Plant Microbe Interact, 14*(9), 1105-1113.

Prusky, D., Yakoby, N. (2003). Pathogenic fungi: leading or led by ambient pH? *Mol Plant Pathol, 4*(6), 509-516.

Punt, P. J., Oliver, R. P., Dingemanse, M. A., Pouwels, P. H., van den Hondel, C. A. (1987). Transformation of *Aspergillus* based on the *hygromycin B* resistance marker from *Escherichia coli*. *Gene, 56*(1), 117-124.

Ramamoorthy, V., Zhao, X., Snyder, A. K., Xu, J. R., Shah, D. M. (2007). Two mitogen-activated protein kinase signalling cascades mediate basal resistance to antifungal plant defensins in *Fusarium graminearum*. *Cell Microbiol, 9*(6), 1491-1506.

Rathje, M., Fang, H., Bachman, J. L., Anggono, V., Gether, U., Huganir, R. L., Madsen, K. L. (2013). AMPA receptor pHluorin-GluA2 reports NMDA receptor-induced intracellular acidification in hippocampal neurons. *Proc Natl Acad Sci U S A, 110*(35), 14426-14431.

Reshkin, S. J., Greco, M. R., Cardone, R. A. (2014). Role of pHi, and proton transporters in oncogene-driven neoplastic transformation. *Philos Trans R Soc Lond B Biol Sci, 369*(1638).

Rispail, N., Soanes, D. M., Ant, C., Czajkowski, R., Grunler, A., Huguet, R., Perez-Nadales, E., Poli, A., Sartorel, E., Valiante, V., Yang, M., Beffa, R., Brakhage, A. A., Gow, N. A., Kahmann, R., Lebrun, M. H., Lenasi, H., Perez-Martin, J., Talbot, N. J., Wendland, J., Di Pietro, A. (2009). Comparative genomics of MAP kinase and calcium-calcineurin signalling components in plant and human pathogenic fungi. *Fungal Genet Biol, 46*(4), 287-298.

Rodríguez-Navarro, A. (2000). Potassium transport in fungi and plants. *Biochimica et Biophysica Acta (BBA) - Reviews on Biomembranes, 1469*(1), 1-30.

Roelants, F. M., Breslow, D. K., Muir, A., Weissman, J. S., Thorner, J. (2011). Protein kinase Ypk1 phosphorylates regulatory proteins Orm1 and Orm2 to control sphingolipid homeostasis in *Saccharomyces cerevisiae*. *Proc Natl Acad Sci U S A, 108*(48), 19222-19227.

Roelants, F. M., Torrance, P. D., Bezman, N., Thorner, J. (2002). Pkh1 and Pkh2 differentially phosphorylate and activate Ypk1 and Ykr2 and define protein kinase modules required for maintenance of cell wall integrity. *Mol Biol Cell, 13*(9), 3005-3028.

Roelants, F. M., Torrance, P. D., Thorner, J. (2004). Differential roles of PDK1- and PDK2-phosphorylation sites in the yeast AGC kinases Ypk1, Pkc1 and Sch9. *Microbiology, 150*(10), 3289-3304.

Rollins, J. A. (2003). The *Sclerotinia sclerotiorum* pac1 gene is required for sclerotial development and virulence. *Mol Plant Microbe Interact, 16*(9), 785-795.

Sacristán-Reviriego, A., Martín, H., Molina, M. (2015). Identification of putative negative regulators of yeast signaling through a screening for protein phosphatases acting on cell wall integrity and mating MAPK pathways. *Fungal Genet Biol, 77*, 1-11.

Saito, H., Posas, F. (2012). Response to hyperosmotic stress. *Genetics, 192*(2), 289-318.

Sambade, M., Alba, M., Smardon, A. M., West, R. W., Kane, P. M. (2005). A Genomic Screen for Yeast Vacuolar Membrane ATPase Mutants. *Genetics, 170*(4), 1539-1551.

Scarborough, G. A. (2000). The plasma membrane proton-translocating ATPase. *Cellular and Molecular Life Sciences CMLS, 57*(6), 871-883.

Schelling, J. R., Abu Jawdeh, B. G. (2008). Regulation of cell survival by Na(+)/H(+) exchanger-1. *Am J Physiol Renal Physiol, 295*(3), F625-F632.

Schüller, C., Mamnun, Y. M., Mollapour, M., Krapf, G., Schuster, M., Bauer, B. E., Piper, P. W., Kuchler, K. (2004). Global Phenotypic Analysis and Transcriptional Profiling Defines the Weak Acid Stress Response Regulon in *Saccharomyces cerevisiae*. *Molecular Biology of the Cell, 15*(2), 706-720.

Segorbe, D. (2014). *Mecanismos de señalización por nitrógeno en el hongo fitopatógeno Fusarium oxysporum*. (PhD Thesis), Universidad de Córdoba, Spain.

Segorbe, D., Di Pietro, A., Peréz-Nadales, E., Turrà, D. (2017). Three *Fusarium oxysporum* mitogen-activated protein kinases (MAPKs) have distinct and complementary roles in stress adaptation and cross-kingdom pathogenicity. *Mol Plant Pathol, 18*(7), 912-924.

Serrano, A. (2014). *In vivo determination of intracellular pH using pHluorin proteins in Fusarium Oxysporum*. (Master Degree), Universidad de Córdoba, Spain.

Shigeto, J., Tsutsumi, Y. (2016). Diverse functions and reactions of class III peroxidases. *New Phytol, 209*(4), 1395-1402.

Shindia, A. A., El-Sherbeny, G. A., El-Esawy, A. E., Sheriff, Y. M. (2006). Production of gluconic acid by some local fungi. *Mycobiology, 34*(1), 22-29.

Sikorski, R. S., Hieter, P. (1989). A system of shuttle vectors and yeast host strains designed for efficient manipulation of DNA in *Saccharomyces cerevisiae*. *Genetics, 122*(1), 19-27.

Simkovic, M., Ditte, P., Chovanec, P., Varecka, L., Lakatos, B. (2007). Changes in growth competence of aged *Trichoderma viride* vegetative mycelia. *Antonie Van Leeuwenhoek, 91*(4), 407-416.

Sorkin, A., von Zastrow, M. (2009). Endocytosis and signalling: intertwining molecular networks. *Nature reviews. Molecular cell biology, 10*(9), 609-622.

Staleva, L., Hall, A., Orlow, S. J. (2004). Oxidative stress activates FUS1 and RLM1 transcription in the yeast *Saccharomyces cerevisiae* in an oxidant-dependent Manner. *Mol Biol Cell, 15*(12), 5574-5582.

Stratford, M., Nebe-von-Caron, G., Steels, H., Novodvorska, M., Ueckert, J., Archer, D. B. (2013). Weak-acid preservatives: pH and proton movements in the yeast *Saccharomyces cerevisiae*. *Int J Food Microbiol, 161*(3), 164-171.

Thynne, E., Saur, I. M. L., Simbaqueba, J., Ogilvie, H. A., Gonzalez-Cendales, Y., Mead, O., Taranto, A., Catanzariti, A. M., McDonald, M. C., Schwessinger, B., Jones, D. A., Rathjen, J. P., Solomon, P. S. (2017). Fungal phytopathogens encode functional homologues of plant rapid alkalinization factor (RALF) peptides. *Mol Plant Pathol, 18*(6), 811-824.

Torres, A. M., Weeden, N. F., Martín, A. (1993). Linkage among isozyme, RFLP and RAPD markers in *Vicia faba*. *Theoretical and applied genetics, 85*(8), 937-945.

Trushina, N., Levin, M., Mukherjee, P. K., Horwitz, B. A. (2013). PacC and pH-dependent transcriptome of the mycotrophic fungus *Trichoderma virens*. *BMC Genomics, 14*, 138.

Turrà, D., El Ghalid, M., Rossi, F., Di Pietro, A. (2015). Fungal pathogen uses sex pheromone receptor for chemotropic sensing of host plant signals. *Nature, 527*(7579), 521-524.

Turrà, D., Segorbe, D., Di Pietro, A. (2014). Protein kinases in plant-pathogenic fungi: conserved regulators of infection. *Annu Rev Phytopathol, 52*, 267-288.

Ullah, A., Lopes, M. I., Brul, S., Smits, G. J. (2013). Intracellular pH homeostasis in *Candida glabrata* in infection-associated conditions. *Microbiology, 159*(4), 803-813.

Valkonen, M., Penttila, M., Bencina, M. (2014). Intracellular pH responses in the industrially important fungus *Trichoderma reesei*. *Fungal Genet Biol, 70*, 86-93.

Valli, M., Sauer, M., Branduardi, P., Borth, N., Porro, D., Mattanovich, D. (2005). Intracellular pH distribution in *Saccharomyces cerevisiae* cell populations, analyzed by flow cytometry. *Appl Environ Microbiol, 71*(3), 1515-1521.

Venema, K., Palmgren, M. G. (1995). Metabolic modulation of transport coupling ratio in yeast plasma membrane H(+)-ATPase. *J Biol Chem, 270*(33), 19659-19667.

Villar, C. C., Kashleva, H., Nobile, C. J., Mitchell, A. P., Dongari-Bagtzoglou, A. (2007). Mucosal tissue invasion by *Candida albicans* is associated with E-cadherin degradation, mediated by transcription factor Rim101p and protease Sap5p. *Infect Immun, 75*(5), 2126-2135.

Vylkova, S. (2017). Environmental pH modulation by pathogenic fungi as a strategy to conquer the host. *PLoS Pathog, 13*(2), e1006149.

Vylkova, S., Carman, A. J., Danhof, H. A., Collette, J. R., Zhou, H., Lorenz, M. C. (2011). The fungal pathogen *Candida albicans* autoinduces hyphal morphogenesis by raising extracellular pH. *MBio, 2*(3), e00055-00011.

Vylkova, S., Lorenz, M. C. (2014). Modulation of phagosomal pH by *Candida albicans* promotes hyphal morphogenesis and requires Stp2p, a regulator of amino acid transport. *PLoS Pathog, 10*(3), e1003995.

Webb, B. A., Chimenti, M., Jacobson, M. P., Barber, D. L. (2011). Dysregulated pH: a perfect storm for cancer progression. *Nat Rev Cancer, 11*(9), 671-677.

Weigert, C., Steffler, F., Kurz, T., Shellhammer, T. H., Methner, F.-J. (2009). Application of a Short Intracellular pH Method to Flow Cytometry for Determining *Saccharomyces cerevisiae* Vitality. *Appl Environ Microbiol, 75*(17), 5615-5620.

Xu, J. R., Hamer, J. E. (1996). MAP kinase and cAMP signaling regulate infection structure formation and pathogenic growth in the rice blast fungus *Magnaporthe grisea*. *Genes Dev, 10*(21), 2696-2706.

Yang, L., Ukil, L., Osmani, A., Nahm, F., Davies, J., De Souza, C. P., Dou, X., Perez-Balaguer, A., Osmani, S. A. (2004). Rapid production of gene replacement constructs and generation of a green fluorescent protein-tagged centromeric marker in *Aspergillus nidulans*. *Eukaryot Cell, 3*(5), 1359-1362.

You, B., Chung, K. (2007). Phenotypic characterization of mutants of the citrus pathogen *Colletotrichum acutatum* defective in a PacC-mediated pH regulatory pathway. *FEMS Microbiol Lett, 277*(1), 107-114.

Young, B. P., Shin, J. J., Orij, R., Chao, J. T., Li, S. C., Guan, X. L., Khong, A., Jan, E., Wenk, M. R., Prinz, W. A., Smits, G. J., Loewen, C. J. (2010). Phosphatidic acid is a pH biosensor that links membrane biogenesis to metabolism. *Science, 329*(5995), 1085-1088.

Yun, Y., Liu, Z., Yin, Y., Jiang, J., Chen, Y., Xu, J. R., Ma, Z. (2015). Functional analysis of the *Fusarium graminearum* phosphatome. *New Phytol, 207*(1), 119-134.

Zoncu, R., Bar-Peled, L., Efeyan, A., Wang, S., Sancak, Y., Sabatini, D. M. (2011). mTORC1 senses lysosomal amino acids through an inside-out mechanism that requires the vacuolar H(+)-ATPase. *Science, 334*(6056), 678-683.